MEASUREMENTS ON THE ADDED MASSES OF A CLUSTER OF VIBRATING CYLINDERS IN FLUID

by

Chiang Chen

Under the supervision of Prof. M.P. Paidoussis

A Thesis Submitted to the Faculty of Graduate Studies and Research in Partial Fulfillment of the Requirements for the Degree of Master of Engineering

Department of Mechanical Engineering

McGill University

Montreal, Quebec, Canada

MEASUREMENTS ON THE ADDED MASSES OF VIBRATING CYLINDERS IN FLUID

ABSTRACT

This thesis deals with the hydrodynamic, or "added" masses of a cluster of cylinders vibrating in fluid (liquid) contained by a rectangular tank. The terms in the added mass coefficient matrix derived analytically by S. Suss, M.A. Pustejovsky and M.P. Paidoussis in 1976 were studied experimentally for a system of one, two and three cylinders.

The tests were conducted by oscillating one of the cylinders and measuring the fluctuating pressure field on the surface of the same or another cylinder, induced by the surrounding fluid. From the measured surface pressure distributions and the acceleration of the vibrating cylinder, the added mass coefficients can then be determined. Measurements were made for fifteen distinct configurations, with oscillating frequencies varying from 50 to 250 Hz, while the acceleration of the oscillating cylinder was kept constant, usually at 2 g. Results are discussed and compared with those obtained from a computer program based on the theoretical work referred to above.

SOMMAIRE

Cette thèse traite de la masse hydrodynamique ou "ajoutée" d'un faisceau de cylindres, oscillant dans un fluide (liquide) contenu dans un reservoir rectangulaire. Les termes de la matrice des coefficients de masse ajoutée, dérivés analytiquement par S. Suss, M.A. Pustejovsky et M.P. Paidoussis en 1976, ont été étudiés experimentalement pour des systèmes d'un, de deux et de trois cylindres.

Les essais furent effectués en faisant osciller un des cylindres et en mesurant le champ fluctuant de pression, en surface du même ou d'un autre cylindre, induit par le fluide environnant. A partir des distributions de pression en surface et de l'accélération du cylindre oscillant, on peut déterminer les coefficients de masse ajoutée. Des mesures ont été prises pour quinze configurations distinctes, les fréquences d'oscillation variant de 50 à 250 Hz et l'accélération du cylindre en oscillation étant maintenue constante, normalement à 2 g. Les résultats sont discutés et comparés à ceux obtenus à l'aide d'un programme d'ordinateur basé sur les travaux théoriques mentionnés ci-haut.

ACKNOWLEDGEMENTS

The author is very grateful for the indispensable guidance and encouragement offered by his supervisor Professor M.P. Paidoussis during the course of this work and deeply appreciates the typing of this thesis by Mrs. Assunta Cerrone-Mancini.

Sincere thanks are due to Mr. J. Gagnon for useful discussions concerning the use of certain pieces of apparatus and to Mr. Joe Dubik for his assistance in constructing the experimental accessories. Also, the moral support of Mrs. R. Gray was truly welcome.

The author would also like to acknowledge the financial support of Atomic Energy of Canada, Ltd. (AECL), the Natural Sciences and Engineering Research Council (NSERC), le Programme de Formation des Chercheurs et Action Concertée (FCAC) and Whiteshell Nuclear Research Establishment.

TABLE OF CONTENTS

PAGE

NOMENCLATURE

A.M.C.	Added mass coefficients.
Ac	Acceleration of the oscillating cylinder.
As	Acceleration of the shaker.
F_{AZi}	The Hydrodynamic Force of cylinder i in the Z-direction.
F_{AYi}	The Hydrodynamic Force of cylinder i in the Y-direction.
G_c.	(Smallest inter-cylinder gap)/(cylinder radius).
g	Gravitational acceleration.
R_i	The radius of cylinder i.
R_o	The radius of the enclosing channel.
$\frac{\partial^2 u_\ell}{\partial t^2}$ $(a_{Z\ell})$	Acceleration of cylinder ℓ in the Z-direction.
$\frac{\partial^2 v_\ell}{\partial t^2}$ $(a_{Y\ell})$	Acceleration of cylinder ℓ in the Y-direction.
$\varepsilon_{i\ell}$	Added mass coefficient of cylinder i in Z-direction due to the motion of cylinder ℓ in Z-direction.
$\xi_{i\ell}$	Added mass coefficient of cylinder i in Y-direction due to the motion of cylinder ℓ in Z-direction.
$e_{i\ell}$	Added mass coefficient of cylinder i in Z-direction due to the motion of cylinder ℓ in Y-direction.
$f_{i\ell}$	Added mass coefficient of cylinder i in Y-direction due to the motion of cylinder ℓ in Y-direction.
θ	The orientation of the pinhole on the pressure transducer bearing cylinder, where pressures were sensed.
π	= 3.141592....

ρ	Density of the fluid.
ϕ	Phase angle between the pressure and the acceleration of the oscillating cylinder signals.
$\Delta\phi$	Variation of the phase angle (ϕ) with respect to frequency changes.

CHAPTER 1

INTRODUCTION

For a rigid body immersed in an incompressible fluid, the effects of inviscid fluid forces acting on the body, arising from the instantaneous fluid motion which results from an acceleration of the body, may be interpreted as an "Added Mass". A more rigorous explanation of this phenomenon can be found in the textbook on hydrodynamics by H. Lamb (1932) and L.M. Milne-Thompson (1938). The concept of "Added Mass" was introduced by Pierre Louis Gabriel Dubuat (1779) from an observation on spherical pendulum bobs of lead, glass and wood oscillating in water. He noticed that a simple buoyancy correction for the submerged sphere was not sufficient; in addition, the fluid increased the effective mass of the sphere by approximately one-half the mass of the fluid that was displaced. Since then, the added mass due to motion of a body in a fluid has been the subject of many analytical and experimental investigations.

The nature of added mass is of particular interest in diverse problems, *e.g.* roll, pitch and vibration of ships; acceleration of submarines, ships and dirigibles; entrance of projectiles and seaplane floats into water; sediment movement and wave action; the vibration of plates and structures in fluids of non-negligible relative density, *etc.* Whenever a solid in contact with a heavy fluid accelerates, the added mass is a factor that should not be overlooked.

The major impetus of the present investigation is to provide information which would be useful in the design of heat exchanger tubing or nuclear reactor fuel elements, where the tube banks and fuel-element bundles are susceptible to excitation by the coolant flow. In analyzing the vibration response to these excitations, proper accounting of the added mass is an important consideration.

Generally, the added mass of a cylindrical rod is assumed to be equal to the mass of fluid displaced by the rod. This is true for a long rod submerged in an infinite fluid. Several experimental studies have been conducted to evaluate the added mass of a solitary cylinder oscillating in fluid contained within finite, as well as infinite, boundaries. The methods used in most of these studies were based either on the measurement of the natural frequencies of the oscillating objects in the fluid or on the inertia forces exerted on the moving body due to its own motion. Stelson and Mavis (1957) obtained the added mass for a sphere, cube and long circular cylinder through the mass-frequency relationship. Experimental results agreed with the analytical potential flow studies.

More recently, work has concentrated on underwater applications where the effect of oscillating flow is of importance. Hamann and Dalton (1971) measured the dynamic forces generated by the cylinder while oscillating sinusoidally in still water, wherein the added mass coefficients as well as the drag coefficients were calculated. Later, Sarpkaya (1975) determined experimentally the drag, added mass and lift coefficients based on the so-called Morison's Equations (Morison *et al.*, 1950), using the hydrodynamic forces measured on a fixed cylinder in a sinusoidally oscillating fluid. Both of Hamann and Dalton's and Sarpkaya's techniques involved displacement and velocity of the cylinder relative to the fluid of magnitudes large enough to allow separation and vortex formation. These effects are of interest in the vibration of cylindrical structures subjected to cross flow.

Recently, Chen, Wambsganss and Jendrzejczyk (1976) developed a "viscous" mathematical model for a vibrating rod surrounded by a fluid annulus. In this model, the resultant force per unit length of cylinder is decomposed into two components, the inertia component in phase with acceleration, and the damping component opposing the movement of the cylinder, 90° out of phase. The coefficients of these two components, namely the added mass and damping coefficients, are expressed in terms of constants obtained from the solution of the equation of motion for the fluid (Schlichting, 1960). Although both the coefficients are frequency-dependent, results indicate that the added mass coefficients are not so sensitive to frequency change, while the damping ones of course are. Tests were done by forcing a cantilever beam vibrating in viscous fluid, such as water, mineral oil and silicone oil, contained by a rigid cylindrical shell. By measuring the natural frequencies of the rod in air and in the fluid, the added mass and damping coefficients were then calculated using the equation for determining the natural frequency of a cantilever beam and bandwidth method, respectively. In this study, results for water were found to be in better agreement with analytical solutions than for mineral oil and silicone oil.

The foregoing gives a cross-section of the literature on the added mass of a single cylinder. For a cluster of cylinders, the added mass is affected by adjacent rods and the confining boundary. The composite effect of this fluid coupling may be expressed in terms of a matrix of added mass coefficients associated with the cylinders in the system. Numerical techniques for the calculation of the added mass matrix were first developed by S.S. Chen and, Levy and Wilkinson. S.S. Chen (1975b) calculated the added mass matrix of arrays of cylinders in unbounded fluid by means of classical ideal flow theory and studied their free vibration characteristics. Levy and Wilkinson (1975) evaluated the added masses of axisymmetric bodies in a containing vessel by means of fluid finite elements. Later, Chung and Chen (1976) extended Chen's theory to deal with clusters of cylinders in fluid confined by a circular container. At the same time, Suss, Pustejovsky and Paidoussis (1976) presented both a classical method and finite element techniques for determing the added mass matrix from a point of view distinctly different from that of Chung and Chen's (1976) theory. It is noted that the applicability of the classical method extends only to cases where the cylinders and container are cylindrical, whereas the finite element method can deal, in principle, with any geometry. (The classical method derived by Suss, Pustejovsky and Paidoussis (1976) is described in detail in Chapter 2). Recently, Yang and Moran (1979) developed a finite element technique to compute the added mass coefficient matrix as well as the damping coefficient matrix by solving the linearized Navier-Stokes and continuity equations, instead of using ideal potential flow theory. The coefficients obtained from this theory turn out to be functions of frequency. Comparison between the experimental data measured by Chen (1976) for one single cylinder vibrating in a viscous fluid enclosed by a rigid concentric cylindrical shell and the numerical results of this method shows good agreement. Nevertheless, in the case of two cylinders, the added mass coefficients were shown as a function of Re $(=\omega d^2/\nu)$. Since none of the added mass coefficients derived from the other theories mentioned above are frequency-dependent, it is not possible to compare this theory with the other ones.

As to experimental studies, a series of tests have been done at the Department of Mechanical Engineering of McGill University under the supervision of Professor M.P. Paidoussis. In the first test conducted by Issid (1977), three cylinders in equilateral form were immersed vertically in a water tank enclosed by a cylindrical Plexiglas shell. With one of the cylinders vibrating laterally, the inviscid hydrodynamic forces on the other cylinders induced by the displaced fluid, were measured by means of a force transducer. The added mass coefficients were then determined from the measured forces. Results of this test are far away from the theoretical values due to the fact that the force transducer was not properly positioned; also the method of attachment of the vibrating cylinder to the shaker was such that the assumption that the cylinder is moving as a rigid body was uncertain. In a second set of experiments, the vertical arrangement of the cylinders and cylindrical Plexiglas shell was changed to a horizontal configuration. One of the fixed cylinders was provided with a plastic collar with a 0.0794 cm (1/32 in.) diameter hole in it. An axial hole in the cylinder connects the pinhole in the collar to tubing, leading to a pressure transducer at one end of the cylinder. The collar was built in such a way that the pinhole may be rotated through 360 degrees with a stop at each 10-degree interval, which enables a measurement of the pressure distribution on this particular fixed cylinder. Integration of the pressure distribution gives the hydrodynamic forces, hence the added mass coefficients. Several unwanted effects were found during the test, such as significant extraneous pressure components induced by the vibration of the wall of cylindrical shell, air bubbles trapped in the axial pressure-sensing chamber, the oscillation of the fluid in the chamber, large components of noise and lack of repeatability in the pressure signals. Thus, the results obtained were inconclusive. Later, Pustejovsky (1978) presented a brief report of his study using the same experimental set up designed by Issid (1977) for his second set of tests, with a modification of the measuring system. The pressure transducer was placed inside the fixed cylinder near the pinhole of the collar. Consequently, the length of the axial hole (*i.e.*, the pressure-sensing chamber) was shorter; this reduced the amount of oscillating fluid in the chamber. His results showed that the dynamic pressure responded in a rather haphazard way and the measured pressure profiles exhibited irregular shapes.

During the same period, experiments on fluidelastic vibration of cantilevered tube bundles by Chen and Jendrzejczyk (1978) were reported. Studies include natural frequencies, mode shapes of coupled modes as well as tube responses of three different tube bundle geometries. Among the experimental results obtained, the measured natural frequencies were found to be in good agreement with the theoretical values, where the theoretical values are evaluated from the equation of motion using the theoretical added mass matrix (Chen, 1975b). This agreement implies that the added mass matrix obtained from Chen's analytical method is also reliable. However, the validation of the added mass matrix itself is not well proved, since the verification is done indirectly through the comparison of the natural frequencies of the system. Hence, a more fundamental measurement of the added mass matrix is still necessary to test the theoretical one more adequately.

Recently, Barbir and Pham (1979) used the same approach and the same experimental set up employed by Pustejovsky (1978) with the Plexiglas shell eliminated. Similar pressure response to frequency change was observed in their tests. Another interesting feature of their results was the presence of a phase lag between the pressure and acceleration of the oscillating signals, which is believed to be attributed to the effects of viscosity. However, these tests also were unfortunately inconclusive.

In the present work, the cylinders were immersed in fluid contained by a rectangular tank. Tests were carried out by oscillating one of the cylinders, with frequency ranging from 50 to 250 Hz, and measuring the dynamic pressure at points around the surface of, generally, another cylinder. Investigation was not restricted to three-cylinder systems; cases of a single cylinder and two-cylinder systems were also studied. Calculation of the terms of the added mass matrix is made by integrating the pressure distribution on the surface of the cylinder to obtain the inviscid hydrodynamic forces; the added mass coefficients are then related to the force components by the associated acceleration. The experimental set up used in this study was essentially a modified form of the one built by Barbir and Pham (1979). Several components of the set up were stiffened to improve the rigidity of the system. To measure the pressure, a more sensitive quartz pressure transducer was selected, with a sensitivity of 257.7 mv/psi, which produces clear signals even without the use of an amplifier. The arrangement of the pressure transducer in the fixed cylinder was modified by placing it normal to the axis of the cylinder. Such design reduces the space of the pressure-sensing chamber, thus the fluid oscillation and air bubble problems can be avoided. With the sensing-surface (diaphragm) of the pressure transducer normal to the surface of the cylinder, the transducer detects the pressure signals more directly.

In the tests, four distinct aspects of inter-cylinder coupling were studied. These are (i) pressure response at a specific angle on a cylinder as a function of frequency of the oscillating one, (ii) phase angles between pressure and acceleration signals, (iii) pressure distribution on either the oscillating cylinder or the fixed cylinders, (iv) the added mass coefficients for the system. Attention has been directed to measurement in the presence of small amplitude (2 g) transverse motion of the oscillating cylinder in nominally still fluid, so that perturbed fluid motion may be considered to be laminar and irrotational. Some tests were also conducted with three cylinders enclosed by an 11.43 cm (4.5 in.) radius shell; these tests were conducted in water, lubricating oil, as well as ethylene glycol. These provide valuable information concerning the effects of both density and viscosity of the fluids on the added mass coefficients. Finally, the pressure profiles and added mass coefficients are plotted and compared with theoretical values obtained from the analytical solution derived by Suss, Pustejovsky and Paidoussis (1976).

CHAPTER 2

THEORETICAL MODEL FOR THE ADDED MASS OF A CLUSTER OF VIBRATING CYLINDERS

2.1 DESCRIPTION OF THE SYSTEM

The system under consideration consists of a cluster of k uniform flexible vibrating cylinders contained in a rigid cylindrical channel. The cylinders are slender and are supported at both of their extremities. The axes of the cylinders at rest are all parallel to the axis of the channel, here referred to as the X-axis in Fig. 2.1. An incompressible fluid of zero nominal velocity is contained within the surrounding channel. The hydrodynamic field of such a system is three-dimensional, due to the fact that the hydrodynamic forces at each cross-section of the bundle will depend on both the local displacements and slopes (mode of deformation) of the individual elements. However, several simplifying assumptions are made to facilitate this mathematical modelling, *i.e.*,

(a) the fluid is irrotational,

(b) viscous effects can be neglected,

(c) local velocities of the cylinders are such that separation never occurs,

(d) the cylinder is sufficiently slender so that the potential flow field due to its motion could be considered to be identical to the two-dimensional field in each cross sectional plane that would result from the motion of an infinitely long cylinder of the same inclination and cross-sectional area, as shown by Lighthill (1960).

The method described here uses potential flow theory to determine (i) the velocity potential in the fluid due to arbitrary small motions of the cylinders, and (ii) the forces acting on each cylinder as a result of the motion of other cylinders in the system or the cylinder itself. Based on that, the so-called added mass matrix of an array of parallel, infinitely long rigid cylinders is then determined.

2.2 THE FLUID VELOCITY POTENTIAL

For an inviscid, incompressible and irrotational fluid, the velocity potential must satisfy Laplace's equation,

$$\nabla^2\phi = 0 . \tag{2.1}$$

In accordance with the slender-body approximation (assumption (d) of section 2.1), the problem is assumed to be effectively two-dimensional and the velocity potential analysis may be confined to a cross-sectional slice of the cylinder-fluid system as if the cylinders were infinitely long and vibrating as rigid bodies.

Referring to Fig. 2.2, a system of polar coordinates centered on the axis of each of the cylinders is defined such that (r_j, θ_j) is the position of any point in the plane as measured from the moving center of cylinder j. For the case of a cylinder with origin at the center of the boundary channel, the position of any point in the plane, as measured from this frame, is denoted by (r_o, θ_o).

In what follows we shall adopt the following notation:

(i) ϕ_j is the velocity potential due to the presence of cylinder j, expressed in terms of the coordinate system centered on cylinder j;

(ii) ϕ_j^i is the velocity potential due to the presence of cylinder j, expressed in terms of the coordinate system centered on cylinder i;

(iii) ϕ^i is the total velocity potential in terms of coordinates centered on cylinder i;

(iv) the subscript or superscript "o" refers to the outer channel and to coordinates at the centre of this channel.

The fluid velocity potential due to the presence of cylinder j in the system, denoted by $\phi_j(r_j, \theta_j)$, satisfies

$$\nabla^2 \phi_j = 0 \; . \tag{2.2}$$

In polar coordinates, equation (2.2) can be written as:

$$\frac{1}{r_j}\frac{\partial}{\partial r_j}\left(r_j\frac{\partial\phi_j}{\partial r_j}\right)+\frac{1}{r_j^2}\frac{\partial^2\phi_j}{\partial\theta_j^2}=0 \quad . \qquad (2.3)$$

By separation of variables, the solution of this equation gives:

$$\phi_j(r_j,\theta_j) = \sum_{n=1}^{\infty}\left\{A_{nj}r_j^n\cos n\theta_j + B_{nj}r_j^n\sin n\theta_j \right.$$

$$\left. + C_{nj}r_j^{-n}\cos n\theta_j + D_{nj}r_j^{-n}\sin n\theta_j\right\} \quad , \qquad (2.4)$$

where A_{nj}, B_{nj}, C_{nj} and D_{nj} are variable constants to be determined using the boundary conditions, as follows:

(i) the fluid velocity normal to the inner surface of the enclosing channel is zero;

(ii) the fluid velocity normal to the surface of each of the k cylinders is equal to the velocity of the cylinder in that direction.

These boundary conditions can be expressed mathematically as:

$$\text{(i)} \quad \left.\frac{\partial\phi_j^o}{\partial r_o}\right|_{r_o=R_o} = 0, \qquad j = 1,2,3.\ldots,k \quad , \qquad (2.5)$$

$$\text{(ii)} \quad \left.\frac{\partial\phi^i}{\partial r_i}\right|_{r_i=R_i} = \frac{\partial u_i}{\partial t}\cos\theta_i + \frac{\partial v_i}{\partial t}\sin\theta_i \quad , \tag{2.6}$$

for $i = 1,2,3.....,k$

where u_i and v_i are the displacements of the i^{th} cylinder in the Z and Y directions, respectively.

Because of the linearity of equation (2.1), the total potential at any point in the plane can be written as the sum of the individual velocity potentials due to the presence of each cylinder within the channel,

$$\phi = \sum_{j=1}^{k} \phi_j\ (r_j,\theta_j) \quad . \tag{2.7}$$

In order to apply the boundary condition (i) and (ii), it is necessary to express each ϕ_j in terms of coordinates centered on each of the other cylinders, that is, to be able to write $\phi_j(r_j,\theta_j)$ into $\phi_j(r_i,\theta_i)$, where $i,j = 0,1,2,...,k$.

This can be done by the use of the coordinate transformation

$$r_j e^{i\theta_j} = r_i e^{i\theta_i} - R_{ij} e^{i\psi_{ij}} \tag{2.8}$$

and using Taylor series expansions for

$$r_j^n e^{in\theta_j} = \left\{ r_i e^{i\theta_i} - R_{ij} e^{i\psi_{ij}} \right\}^n ,$$

with R_{ij} being the length of the line joining the center of cylinders i and j, and ψ_{ij} being the angle formed by line R_{ij} and positive Z-axis.

From these manipulations, the real and imaginary parts will yield expressions for $r_j^n \cos n\theta_j$ and $r_j^n \sin n\theta_j$, and similarly for $r_j^{-n} \cos n\theta_j$ and $r_j^{-n} \sin n\theta_j$.

By using the coordinate transformation, the potential due to the motion of cylinder j, with all other cylinders stationary, expressed in terms of the coordinate system centered on cylinder i, may then be written as:

$$\phi_j^i(r_i, \theta_i) = \sum_{n=1}^{\infty} \sum_{m=0}^{n} \frac{(-1)^{n-m} R_{ij}^{n-m} r_i^m n!}{m!(n-m)!} \left\{ A_{nj} \cos[n\theta_i + (n-m)\psi_{ij}] \right.$$

$$\left. + B_{nj} \sin[m\theta_i + (n-m)\psi_{ij}] \right\} + \sum_{n=1}^{\infty} \sum_{m=0}^{\infty} \frac{(-1)^n (n+m-1)! r_i^m}{m!(n-1)! R_{ij}^{n+m}}$$

$$\left\{ C_{nj} \cos[m\theta_i - (n+m)\psi_{ij}] + D_{nj} \sin[m\theta_i - (n+m)\psi_{ij}] \right\} \qquad (2.9)$$

which converges for $r_i < R_{ij}$, and

$$\phi_j^i(r_i,\theta_i) = \sum_{n=1}^{\infty}\sum_{m=0}^{n} \frac{(-1)^{n-m}R_{ij}^{n-m}r_i^m n!}{m!(n-m)!}\Big\{A_{nj}\cos[n\theta_i+(n-m)\psi_{ij}]$$

$$+ B_{nj}\sin[m\theta_i+(n-m)\psi_{ij}]\Big\} + \sum_{n=1}^{\infty}\sum_{m=n}^{\infty}\frac{(m-1)!R_{ij}^{m-n}}{(n-1)!(m-n)!r_i^m}$$

$$\Big\{C_{nj}\cos[m\theta_i-(m-n)\psi_{ij}] + D_{nj}\sin[m\theta_i-(m-n)\psi_{ij}]\Big\} \qquad (2.10)$$

converging for $R_{ij} < r_i$.

With ϕ^i denoted as the total velocity potential written in terms of coordinates centered on cylinder i, and ϕ_i being the potential due to the presence of cylinder i alone, we arrive at:

$$\phi^i = \sum_{j=1}^{k}\phi_j^i + \phi_i \; . \qquad (2.11)$$

Applying boundary conditions (i) and (ii) to equation (2.11), the constants A_{nj}, B_{nj}, C_{nj} and D_{nj} can be determined and turn out to be of the following forms:

$$A_{nj} = R_j^{1-n}\sum_{\ell=1}^{k}\left\{\alpha_{nj\ell}\frac{\partial u_\ell}{\partial t} + a_{nj\ell}\frac{\partial v_\ell}{\partial t}\right\} , \qquad (2.12)$$

$$B_{nj} = R_j^{1-n} \sum_{\ell=1}^{k} \left\{ \beta_{nj\ell} \frac{\partial u_\ell}{\partial t} + b_{nj\ell} \frac{\partial v_\ell}{\partial t} \right\} , \tag{2.13}$$

$$C_{nj} = R_j^{n+1} \sum_{\ell=1}^{k} \left\{ \gamma_{nj\ell} \frac{\partial u_\ell}{\partial t} + c_{nj\ell} \frac{\partial v_\ell}{\partial t} \right\} , \tag{2.14}$$

$$D_{nj} = R_j^{n+1} \sum_{\ell=1}^{k} \left\{ \delta_{nj\ell} \frac{\partial u_\ell}{\partial t} + d_{nj\ell} \frac{\partial v_\ell}{\partial t} \right\} , \tag{2.15}$$

where the unknowns $\alpha_{nj\ell}$ to $d_{nj\ell}$ are determined by the following twelve equations:

$$\sum_{j=1}^{k}{}^{*} \sum_{n=m}^{\infty} \frac{(-1)^{n-m} n! R_{ij}^{n+m} R_i^{m-1}}{(m-1)!(n-m)! R_j^{n-1}} \left\{ [\alpha_{nj\ell} \cos(n-m)\psi_{ij} \mp \beta_{nj\ell} \sin(n-m)\psi_{ij}] \right\}$$

$$+ \sum_{j=1}^{k}{}^{*} \sum_{n=1}^{\infty} \frac{(-1)^{n} (n+m-1)! R_i^{m-1} R_j^{n+1}}{(n-1)!(m-1)! R_{ij}^{n+m}} \left\{ [\gamma_{nj\ell} \cos(n+m)\psi_{ij} + \delta_{nj\ell} \sin(n+m)\psi_{ij}] \right\}$$

$$+ m\alpha_{mi\ell} - m\gamma_{mi\ell} = \delta_{1m}\, \delta_{i\ell} , \tag{2.16}$$

$$\sum_{j=1}^{k}{}^{*} \sum_{n=m}^{\infty} \frac{(-1)^{n-m} n! R_{ij}^{n-m} R_i^{m-1}}{(m-1)!(n-m)! R_j^{n-1}} \left\{ [a_{nj\ell} \cos(n-m)\psi_{ij} + b_{nj\ell} \sin(n-m)\psi_{ij}] \right\}$$

$$+ \sum_{n=1}^{k}{}^{*} \sum_{n=1}^{\infty} \frac{(-1)^{n}(n+m-1)! R_i^{m-1} R_j^{n+1}}{(n-1)!(m-1)! R_{ij}^{n+m}} \left\{ [c_{nj\ell} \cos(n+m)\psi_{ij} + d_{nj\ell} \sin(n+m)\psi_{ij}] \right\}$$

$$+ m a_{mi\ell} - m c_{mi\ell} = 0 \quad , \qquad (2.17)$$

$$\sum_{j=1}^{k}{}^{*} \sum_{n=m}^{\infty} \frac{(-1)^{n-m} n! R_{ij}^{n-m} R_i^{m-1}}{(m-1)!(n-m)! R_j^{n-1}} \left\{ [-\alpha_{nj\ell} \sin(n-m)\psi_{ij} + \beta_{nj\ell} \cos(n-m)\psi_{ij}] \right\}$$

$$+ \sum_{j=1}^{k}{}^{*} \sum_{n=1}^{\infty} \frac{(-1)^{n}(n+m-1)! R_i^{m-1} R_j^{n+1}}{(n-1)!(m-1)! R_{ij}^{n+m}} \left\{ [\gamma_{nj\ell} \sin(n+m)\psi_{ij} - \delta_{nj\ell} \cos(n+m)\psi_{ij}] \right\}$$

$$+ m\beta_{mi\ell} - m\delta_{mi\ell} = 0 \quad , \qquad (2.18)$$

$$\sum_{j=1}^{k}{}^{*} \sum_{n=m}^{\infty} \frac{(-1)^{n-m} n! R_{ij}^{n-m} R_i^{m-1}}{(m-1)!(n-m)! R_j^{n-1}} \left\{ [-a_{nj\ell} \sin(n-m)\psi_{ij} + b_{nj\ell} \cos(n-m)\psi_{ij}] \right\}$$

$$+ \sum_{j=1}^{k}{}^{*} \sum_{n=1}^{\infty} \frac{(-1)^{n}(n+m-1)! R_i^{m-1} R_j^{n+1}}{(n-1)!(m-1)! R_{ij}^{n+m}} \left\{ [c_{nj\ell} \sin(n+m)\psi_{ij} - d_{nj\ell} \cos(n+m)\psi_{ij}] \right\}$$

$$+ m b_{mi\ell} - m d_{mi\ell} = \delta_{1m}\, \delta_{i\ell} \quad , \qquad (2.19)$$

with m = 1,2,3,.... ; i,ℓ = 1,2,3,...., k;

$$\sum_{n=m}^{\infty} \frac{(-1)^{n-m} n! R_{oj}^{n-m} R_o^{m-1}}{(m-1)!(n-m)! R_j^{n-1}} \left\{ [\alpha_{nj\ell} \cos(n-m)\psi_{oj} + \beta_{nj\ell} \sin(n-m)\psi_{oj}] \right\}$$

$$- \sum_{n=1}^{m} \frac{m! R_{oj}^{m-n} R_j^{n+1}}{(n-1)!(m-n)! R_o^{m+1}} \left\{ [\gamma_{nj\ell} \cos(m-n)\psi_{oj} - \delta_{nj\ell} \sin(m-n)\psi_{oj}] \right\} = 0 \ , \tag{2.20}$$

$$\sum_{n=m}^{\infty} \frac{(-1)^{n-m} n! R_{oj}^{n-m} R_o^{m-1}}{(m-1)!(n-m)! R_j^{n-1}} \left\{ [a_{nj\ell} \cos(n-m)\psi_{oj} + b_{nj\ell} \sin(n-m)\psi_{oj}] \right\}$$

$$- \sum_{n=1}^{m} \frac{m! R_{oj}^{m-n} R_j^{n+1}}{(n-1)!(m-n)! R_o^{m+1}} \left\{ [c_{nj\ell} \cos(m-n)\psi_{oj} - d_{nj\ell} \sin(m-n)\psi_{oj}] \right\} = 0 \ , \tag{2.21}$$

$$\sum_{n=m}^{\infty} \frac{(-1)^{n-m} n! R_{oj}^{n-m} R_o^{m-1}}{(m-1)!(n-m)! R_j^{n-1}} \left\{ [\alpha_{nj\ell} \sin(n-m)\psi_{oj} - \beta_{nj\ell} \cos(n-m)\psi_{oj}] \right\}$$

$$+ \sum_{n=1}^{m} \frac{m! R_{oj}^{m-n} R_j^{n+1}}{(n-1)!(m-n)! R_o^{m+1}} \left\{ [\gamma_{nj\ell} \sin(m-n)\psi_{oj} + \delta_{nj\ell} \cos(m-n)\psi_{oj}] \right\} = 0 \ , \tag{2.22}$$

$$\sum_{n=m}^{\infty} \frac{(-1)^{n-m} n!\, R_{oj}^{n-m} R_o^{m-1}}{(m-1)!\,(n-m)!\, R_j^{n-1}} \left\{ [a_{nj\ell} \sin(n-m)\psi_{oj} - b_{nj\ell} \cos(n-m)\psi_{oj}] \right\}$$

$$+ \sum_{n=1}^{m} \frac{m!\, R_{oj}^{m-n} R_j^{n+1}}{(n-1)!\,(m-n)!\, R_o^{m+1}} \left\{ [c_{nj\ell} \sin(m-n)\psi_{oj} + d_{nj\ell} \cos(m-n)\psi_{oj}] \right\} = 0 \;. \tag{2.23}$$

with $m = 1,2,3,\ldots.$

$\ell = 1,2,3,\ldots., k$

$j = 1,2,3,\ldots., k \qquad j \neq q;$

for $j = q$,

$$\left(\frac{R_o}{R_q}\right)^{n-1} \alpha_{nq\ell} - \left(\frac{R_q}{R_o}\right)^{n+1} \gamma_{nq\ell} = 0 \;, \tag{2.24}$$

$$\left(\frac{R_o}{R_q}\right)^{n-1} a_{nq\ell} - \left(\frac{R_q}{R_o}\right)^{n+1} c_{nq\ell} = 0 \;, \tag{2.25}$$

$$-\left(\frac{R_o}{R_q}\right)^{n-1} \beta_{nq\ell} + \left(\frac{R_q}{R_o}\right)^{n+1} \delta_{nq\ell} = 0 \;, \tag{2.26}$$

$$-\left(\frac{R_o}{R_q}\right)^{n-1} b_{nq\ell} + \left(\frac{R_q}{R_o}\right)^{n+1} d_{nq\ell} = 0 \;. \tag{2.27}$$

with $n = 1,2,3,\ldots$ and $\ell = 1,2,3,\ldots., k$.

For equations (2.16) to (2.19), the starred summation excludes $j = i$. Also, it is noted that the δ's with two subscripts are Kronecker deltas.

The set of infinite equations (2.16) to (2.27) can be truncated to solve for a finite number of constants to give a desired accuracy. A computer program known as "COUPLING" has been developed by Suss (1977a) to handle these calculations. The manual for this program (Suss, 1977b) is available. A modified version of this computer program called "COUPRESS", which also gives the pressure distribution of each cylinder in the system has been developed and is listed in Appendix A.1.

2.3 THE INVISCID HYDRODYNAMIC FORCES

The resulting force due to the inviscid flow around the i^{th} cylinder can be decomposed into Z- and Y-components as

$$F_{AZi} = - \int_0^{2\pi} p^i \bigg|_{r_i=R_i} R_i \cos\theta_i d\theta_i \quad , \qquad (2.28)$$

$$F_{AZi} = - \int_0^{2\pi} p^i \bigg|_{r_i=R_i} R_i \sin\theta_i d\theta_i \quad , \qquad (2.29)$$

where p^i is the fluid pressure expressed in terms of coordinate system centered on cylinder i.

From Bernoulli's equation, we can write that

$$p^i\Big|_{r_i=R_i} = -\rho \frac{\partial \phi^i}{\partial t}\Big|_{r_i=R_i} . \qquad (2.30)$$

Making use of equation (2.11), and taking the required derivative to obtain p^i, then substituting into equation (2.28) and equation (2.29), the hydrodynamic forces become:

$$F_{AZi} = \rho \pi R_i^2 \sum_{\ell=1}^{k} \left\{ \varepsilon_{i\ell} \frac{\partial^2 u_\ell}{\partial t^2} + e_{i\ell} \frac{\partial^2 v_\ell}{\partial t^2} \right\} , \qquad (2.31)$$

$$F_{AZi} = \rho \pi R_i^2 \sum_{\ell=1}^{k} \left\{ \xi_{i\ell} \frac{\partial^2 u_\ell}{\partial t^2} + f_{i\ell} \frac{\partial^2 v_\ell}{\partial t^2} \right\} , \qquad (2.32)$$

for i = 1,2,3,...., k, where

$$\varepsilon_{i\ell} = \sum_{j=1}^{k}{}^{*} \sum_{n=1}^{\infty} \left\{ (-1)^n \left(\frac{R_{ij}}{R_j}\right)^{n-1} [\alpha_{nj\ell} \cos(n-1)\psi_{ij} + \beta_{nj\ell} \sin(n-1)\psi_{ij}] \right.$$

$$\left. + (-1)^n n \left(\frac{R_j}{R_{ij}}\right)^{n+1} [\gamma_{nj\ell} \cos(n+1)\psi_{ij} + \delta_{nj\ell} \sin(n+1)\psi_{ij}] \right\}$$

$$+ \alpha_{1i\ell} + \gamma_{1i\ell} , \qquad (2.33)$$

$$e_{i\ell} = \sum_{j=1}^{k}{}^{*} \sum_{n=1}^{\infty} \left\{ (-1)^n \left(\frac{R_{ij}}{R_j}\right)^{n-1} [a_{nj\ell} \cos(n-1)\psi_{ij} + b_{nj\ell} \sin(n-1)\psi_{ij}] \right.$$

$$\left. + (-1)^n n \left(\frac{R_j}{R_{ij}}\right)^{n+1} [c_{nj\ell} \cos(n+1)\psi_{ij} + d_{nj\ell} \sin(n+1)\psi_{ij}] \right\}$$

$$+ a_{1i\ell} + c_{1i\ell} , \tag{2.34}$$

$$\xi_{i\ell} = \sum_{j=1}^{k}{}^{*} \sum_{n=1}^{\infty} \left\{ (-1)^n \left(\frac{R_{ij}}{R_j}\right)^{n-1} [\beta_{nj\ell} \cos(n-1)\psi_{ij} - \alpha_{nj\ell} \sin(n-1)\psi_{ij}] \right.$$

$$\left. + (-1)^n n \left(\frac{R_j}{R_{ij}}\right)^{n+1} [-\delta_{nj\ell} \cos(n+1)\psi_{ij} + \gamma_{nj\ell} \sin(n+1)\psi_{ij}] \right\}$$

$$+ \beta_{1i\ell} + \delta_{1i\ell} , \tag{2.35}$$

$$f_{i\ell} = \sum_{j=1}^{k}{}^{*} \sum_{n=1}^{\infty} \left\{ (-1)^n \left(\frac{R_{ij}}{R_j}\right)^{n-1} [b_{nj\ell} \cos(n-1)\psi_{ij} - a_{nj\ell} \sin(n-1)\psi_{ij}] \right.$$

$$\left. + (-1)^n n \left(\frac{R_j}{R_{ij}}\right)^{n+1} [-d_{nj\ell} \cos(n+1)\psi_{ij} + c_{nj\ell} \sin(n+1)\psi_{ij}] \right\}$$

$$+ b_{1i\ell} + d_{1i\ell} . \tag{2.36}$$

2.4 THE ADDED MASS COEFFICIENTS

Comparing equation (2.16) with (2.33) when m = 1 and $2\gamma_{1i\ell}$ has been added to both sides, it can be seen that

$$\varepsilon_{i\ell} = \delta_{i\ell} + 2\gamma_{1i\ell} . \tag{2.37}$$

Similarly, from equation (2.17) with (2.34) when m = 1, we have

$$e_{i\ell} = 2c_{1i\ell} . \tag{2.38}$$

Also, from equation (2.18) and (2.19) with m = 1, we obtain

$$\xi_{i\ell} = 2\delta_{1i\ell} , \tag{2.39}$$

$$f_{i\ell} = \delta_{i\ell} + 2d_{1i\ell} , \tag{2.40}$$

where $\delta_{i\ell}$ is the Kronecker delta.

We may now re-write equations (2.31) and (2.32) in the final simple forms:

$$F_{AZi} = \rho \, \pi \, R_i^2 \sum_{\ell=1}^{k} \left\{ (\delta_{i\ell} + 2\gamma_{1i\ell}) \frac{\partial^2 u_\ell}{\partial t^2} + (2c_{1i\ell}) \frac{\partial^2 v_\ell}{\partial t^2} \right\} \tag{2.41}$$

$$F_{AZi} = \rho \pi R_i^2 \sum_{\ell=1}^{k} \left\{ (2\delta_{1i\ell}) \frac{\partial^2 u_\ell}{\partial t^2} + (\delta_{i\ell} + 2d_{1i\ell}) \frac{\partial^2 v_\ell}{\partial t^2} \right\} \tag{2.42}$$

The quantities $(\delta_{i\ell} + 2\gamma_{1i\ell})$ and $2c_{1i\ell}$, or $\varepsilon_{i\ell}$ and $e_{i\ell}$, are the non-dimensional added mass coefficients for cylinder i corresponding to the Z component of the force associated with the acceleration $(\partial^2 u_\ell/\partial t^2)$ and $(\partial^2 v_\ell/\partial t^2)$ in the Z- and Y-directions of the ℓ^{th} cylinder, respectively.

Similarly, $2\delta_{1i\ell}$ and $(\delta_{i\ell} + 2d_{1i\ell})$, or $\xi_{i\ell}$ and $f_{i\ell}$, are the non-dimensional added mass coefficients for cylinder i corresponding to the Y component of the force associated with the accelerations of the ℓ^{th} cylinder in Z- and Y-directions, respectively - to be found on p. 27.

These non-dimensional added mass coefficients, for convenience, can be expressed in matrix form as in equation (2.43).

An alternative algorithm for obtaining the added mass coefficient matrix of the same system has also been developed using the Finite Element Method. Details of this work can be found in a report by Suss, Pustejovsky* and Paidoussis (1976).

*A report concerning the generation of the mesh for the F.E. Method computer program written by M. Pustejovsky (1977) has also been listed as a reference.

$$
\begin{pmatrix}
\varepsilon_{11} & \cdot & \cdot & \cdot & \cdot & \varepsilon_{1k} & e_{11} & \cdot & \cdot & \cdot & \cdot & e_{1k} \\
\cdot & \cdot & \cdot & \cdot & \cdot & \cdot & \cdot & \cdot & \cdot & \cdot & \cdot & \cdot \\
\cdot & \cdot & \cdot & \cdot & \cdot & \cdot & \cdot & \cdot & \cdot & \cdot & \cdot & \cdot \\
\cdot & \cdot & \cdot & \cdot & \cdot & \cdot & \cdot & \cdot & \cdot & \cdot & \cdot & \cdot \\
\cdot & \cdot & \cdot & \cdot & \cdot & \cdot & \cdot & \cdot & \cdot & \cdot & \cdot & \cdot \\
\varepsilon_{k1} & \cdot & \cdot & \cdot & \cdot & \varepsilon_{kk} & e_{k1} & \cdot & \cdot & \cdot & \cdot & e_{kk} \\
\xi_{11} & \cdot & \cdot & \cdot & \cdot & \xi_{1k} & f_{11} & \cdot & \cdot & \cdot & \cdot & f_{1k} \\
\cdot & \cdot & \cdot & \cdot & \cdot & \cdot & \cdot & \cdot & \cdot & \cdot & \cdot & \cdot \\
\cdot & \cdot & \cdot & \cdot & \cdot & \cdot & \cdot & \cdot & \cdot & \cdot & \cdot & \cdot \\
\cdot & \cdot & \cdot & \cdot & \cdot & \cdot & \cdot & \cdot & \cdot & \cdot & \cdot & \cdot \\
\cdot & \cdot & \cdot & \cdot & \cdot & \cdot & \cdot & \cdot & \cdot & \cdot & \cdot & \cdot \\
\xi_{k1} & \cdot & \cdot & \cdot & \cdot & \xi_{kk} & f_{k1} & \cdot & \cdot & \cdot & \cdot & f_{kk}
\end{pmatrix} \tag{2.43}
$$

CHAPTER 3

EXPERIMENTAL EQUIPMENT

The experimental equipment used in this study was designed to have a cluster of up to three cylinders, immersed horizontally in a rectangular water tank, with one of the cylinders forced to oscillate vertically in harmonic motion. Part of the experimental system is instrumentation for measuring the pressure around the surface of any cylinder, acceleration of the oscillating cylinder, as well as the phase angle between the two signals. Such an experimental set up shown in picture 1 is composed mainly of the following five sub-units: (i) water tank, (ii) shaker with control system, (iii) three hollow cylinders, (iv) structural components for holding the cylinders, and (v) the associated instrumentation for measurements. These will be described in some detail below.

3.1 THE WATER TANK

The rectangular water tank (picture 2), made of 0.95 cm (3/8 in.) thick Plexiglas, has internal dimensions of 38.10 cm x 85.09 cm x 39.37 cm (15 in. x 33 1/2 in. x 15 1/2 in.) with two sheets of 1.26 cm (1/2 in.) thick Plexiglas as a removable cover. In order to stiffen the tank, three lines of aluminum belts and strips of Plexiglas have been added to the walls. The tank sits on a steel frame, with leveling screws at the four corners, giving it certain mobility in its positioning under the shaker. A valve is provided near the bottom of the tank for draining the liquid after a test.

3.2 SHAKER WITH CONTROL SYSTEM

The shaking system (picture 3) includes a shaker, an exciter control unit and a power amplifier. The shaker is a Brüel and Kjaer type 4801 electrodynamic vibration exciter. On it, a type 4812 exciter head is mounted. This head has a force rating of 444.82 N (100 lbf), a displacement limit of 12.7 cm (5 in.) and a resonance frequency at 7200 Hz. Using this head, the shaker is capable of performing simple harmonic oscillations at different amplitudes and frequencies up to 10 KHz with low cross distortion and low cross motion. The shaker, with its own support, rests on a four-legged inverted U-shaped steel frame with features leveling support screws and four wheels at the bottom allowing the shaker to move easily.

Equipment for controlling the shaker includes a B.&K. type 2707 power amplifier and a B.&K. type 1047 exciter controller. The exciter controller generates variable sinusoidal voltage signals to drive the vibration exciter through the power amplifier in the frequency range of 5 Hz to 10 KHz.

3.3 THE HOLLOW CYLINDERS

There is a maximum of three cylinders involved in these experiments. Each cylinder is made of aluminum with outside and inside diameters of 6.35 cm (2 1/2 in.) and 4.45 cm (1 3/4 in.), respectively. The two stationary cylinders are 52.1 cm (20 1/2 in.) in length, while the oscillating one is 6.35 cm (2 1/2 in.) shorter. To prevent water from going into these hollow cylinders, plugs made of either aluminum or teflon are provided for both ends.

A high sensitivity pressure transducer (described in 3.5 of this chapter) is placed inside the pressure measuring cylinder (picture 4) at a hole 8.89 cm (3 1/2 in.) from one of its ends. A cross-sectional view of the cylinders, at the position where the pressure transducer is set, and the lock nut used to keep the transducer stayed properly in the cylinder are shown in Fig. 4.1. Pressure is sensed through a 0.0635 cm (0.025 in.) diameter pinhole on the top surface of the lock nut to the chamber where the diaphragm of the pressure transducer received the signals. The pinhole has a depth of 0.254 cm (0.1 in.) to prevent the transducer from sensing those fluctuating velocity components not normal to the surface of the cylinder.

3.4 STRUCTURAL COMPONENTS FOR HOLDING THE CYLINDERS

For the system consisting of two or three cylinders, the stationary cylinders are supported at both ends. Each support has two pieces (pictures 5 and 6). The top one is a rectangular piece with two holes having a dimension good enough to provide a clearance of 1.27×10^{-2} cm (5×10^{-3} in.) for the cylinders to rotate. A steel ball-and-spring index mechanism built inside the inner surface of the hole, along with 40 index holes around the circular surface of the cylinder end-plug (picture 4), enable the cylinder to rotate through 360 degrees with a stop at every 9 degrees. The bottom pieces and the bottom aluminum plate have been designed in such a way that they allow the cylinders to have four different geometric arrangements (Fig. 4.5 and Fig. 4.6), as well as variations in cylinder gap. These supports are joined together and attached to the aluminum plate at the bottom of the water tank using socket head screws.

As to the oscillating cylinder, it is held horizontally by an aluminum tube of 3.81 cm (1 1/2 in.) outside diameter, 2.54 cm (1 in.) inside diameter and 25.4 cm (10 in.) long, mounted to the shaking table of the shaker by means of a square piece with four screws at the corners (picture 7). Two triangular aluminum fins have been added to increase the stiffness of this tube. The motion of the shaker is then transmitted through the tube to the cylinder attached to it, thereby creating a pressure field in the liquid medium in which this and the other cylinders are immersed.

In one single-cylinder test, the pressure measurements were taken around the surface of the oscillating cylinder itself. Hence, the rectangular piece (picture 8) which joins the tube and the oscillating cylinder was in this case especially made of two pieces held together by four 0.635 cm (1/4 in.) diameter socket head screws at the four corners. For rotating the cylinder, the holding piece has to be loosened by unscrewing the screws and relocked after the cylinder has been rotated through the desired angle. The bottom part of this holding piece also bears an index mechanism, same as the one in the supports for the stationary cylinders. However, there are only 36 index holes and are located on the circular surface of the cylinder (picture 4) instead of on the cylinder plug.

3.5 INSTRUMENTATION FOR MEASUREMENTS

The instruments used in the experiments and a circuit diagram of the measuring system are shown in picture 9 and Fig. 4.3, respectively.

The pressure field was measured by using a high sensitivity PCB quartz pressure transducer, Model 106B. This high-level-output transducer is designed to measure pressure perturbations in air or in liquid in severe environments, *e.g.* in a high vibration environment. A built-in seismic mass acting on another quartz crystal effectively cancels the spurious signal produced by the acceleration of the mass of the diaphragm and end piece acting upon the very sensitive crystals in the presence of axial vibration inputs. This design produces an extremely high level output signal with good resolution, relatively free from unwanted vibration effects. The main specifications of this transducer are as follows:

Sensitivity	257.7	mV/psi
Resolution	0.0001	psi (rms)
Resonance frequency	60	KHz
Maximum pressure	300	psi
Acceleration sensitivity	0.0012	psi/g.

Along with this transducer is a PCB 482A Power Supply, which provides a 22 Volt D.C. power source.

Two piezoelectric accelerometers are used in these experiments. One, with acceleration sensitivity equal to 74.8 mV/g, is mounted at the shaking table of the shaker and gives a signal to control the shaker through the control system. The other, having an acceleration sensitivity of 53.3 mV/g, is mounted inside the oscillating cylinder (with its mounting surface face down) to measure the acceleration of this cylinder in the vertical direction. A Brüel and Kjaer (B&K) Type 2805 Power Supply is utilized to provide a 28 Volt D.C. power source for the accelerometers. Signals coming out from the accelerometers are fed into a B&K Type 2625 vibration pick up preamplifier, which works as an impedance transformer.

In order to see the effect of the boundary on the measured pressure distributions, tests were also done with a circular outer channel. This was accomplished by inserting a cylindrical barrel (picture 10) into the central portion of the tank. This barrel was made of 22.86 cm (9 in.) diameter, 0.9525 cm (3/8 in.) thick aluminum cut into two pieces to make things easy for assembly. A hole on its top provides clearance for the tube carrying the oscillating cylinder to pass through. Four pieces of 1 in. thick Plexiglas were built to support the barrel, and also to keep it sitting securely in the tank, at the correct position. Two photographs exhibit the arrangement of this boundary channel in the water tank (pictures 11 and 12). During the experiments, the top cylinder is vibrating, while pressure readings are taken on the blue cylinder below.

CHAPTER 4

EXPERIMENTAL PROCEDURE AND DATA ANALYSIS

This chapter consists of two sections. The first one outlines the steps undertaken to complete an experiment, wherein the pressure distribution on cylinders in the system, the acceleration of the oscillating cylinder and the phase angles between pressure and acceleration signals were measured. The second describes the method used in this study for deriving the added mass coefficients from the measured data.

4.1 EXPERIMENTAL PROCEDURE

The procedure outlined here is the typical procedure for measuring the pressure profile on one of the stationary cylinders in a cluster of three cylinders; it proceeds as follows:

1. An accelerometer is placed inside the oscillating cylinder. This cylinder is then mounted to the shaker through the tube structure (see picture 7).

2. The stationary cylinder without pressure transducer is mounted to the cylinder support components which stand on the bottom aluminum plate of the water tank.

3. The tank is now filled with water.

4. The sensitive pressure transducer is placed into

the pressure-measuring cylinder before this cylinder is put into the tank.

5. The lock nut (Fig. 4.1) is then screwed to the top of the pressure-measuring chamber to keep the pressure transducer in position. This procedure is done while the cylinder is in water, to avoid air bubbles being trapped in the pressure-measuring chamber.

6. The cylinders are aligned in proper position by adjusting the leveling screws either on the support of the shaker or on the steel frame of the water tank and also by sliding the cylinder support components. Two level gages and two sets of aluminum pieces with three holes drilled out in the prescribed geometrical configuration (picture 8) are used to facilitate this job. The cylinder support components are then attached to the aluminum plate at the bottom of the water tank with socket head screws.

7. The top of the water tank is covered with two pieces of Plexiglas using five screws. Care is taken to ensure that no air bubbles are trapped.

8. The shaker control system and the HP Digital Signal Analyzer are set as follows:

(i) Exciter Control Type 1047

Compressor rate:	1 db/s per Hz
Max. compressor speed:	30 db/s.
Sweep control:	manual.
Output voltage:	maximum.
Mode switch:	acceleration.

Mode level:	100 g (max.)
Cross over switch:	"A" position.
Input:	Signal from accelerometer attached on the shaker through the Vibration Pick-up Preamplifier Type 2625.
Output:	to Power Amplifier Type 2707.

(ii) Power Amplifier Type 2707

Current range:	30 A (rms).
Head constant:	2 in./v.s. (v.s. = volt sec).
Displacement limit:	0.5 in.
Current limit:	18 A (rms).
Output impedance:	low.
Direct current output:	5.
Amplifier gain:	7.
Voltage range:	30 V (rms).
Phase:	0°.
Exciter interlock:	in.
Signal reference:	chassis.
Input:	signal from Exciter Control 1047
Output:	to the shaker.

(iii) Vibration Pick-Up Preamplifier Type 2625

Mode knob:	acceleration - $10 m/sec^2$.
Gain & channel selector:	0 to 20 db, x-channel.
Input:	x-channel.

(iv) HP Digital Signal Analyzer Type 5420A

Mode:	Transfer function.
Channel no. 1:	signal from the accelerometer inside the moving cylinder, through Vibration Pick-Up Preamplifier 2625.
Channel no. 2:	signal from the pressure transducer through Power Supply PCB 482A.

Coordinate board: phase.
Set up status: see Fig. 4.2.

9. An accelerometer is attached to the flat surface on the shaker head, which will provide a signal forcing the shaker to operate at the chosen constant magnitude of acceleration, even though the frequency is varied.

10. The wiring for the shaker control system, as well as the measuring system is connected as in Fig. 4.3.

11. The pressure readings and the acceleration amplitude of the oscillating cylinder are taken down, while the cylinder is oscillating. These readings are read ~~off~~ two high-resolution digital voltmeters. Also taken down are the phase angle, between pressure and acceleration signals, read off the Digital Signal Analyzer, by placing the cursor at the operating frequency.

12. By rotating the pressure measuring cylinder, thus changing the azimuthal orientation of the pinhole on the top of the lock-nut, the pressure and the rest of the readings described in step 11 above are taken at a location 9° away. The procedure is repeated until all the above readings are taken around the surface of the cylinder at 9° intervals.

13. The test is repeated for different frequencies while the amplitude of acceleration of the shaker is kept constant at 2 g.

Hence, for each configuration, if eight frequencies are chosen, a total number of 648 readings (pressure (320), phase angle (320), acceleration (8)) have to be taken down before the added mass coefficients can be calculated.

In addition, a study of the variation with frequency of the phase angle, between pressure and acceleration, was also done. The procedure is similar except that the "Repeat" button on the sweep control panel of the Exciter Control 1047 has to be at the "in" position, with sweep rate range at 1-10 Hz/sec and sweep rate at 1 Hz/sec. Also, the upper limit and lower limit knobs are set at the desired frequencies. When the shaker is in operation, the "Up" button is then pressed, and the oscillating frequency will sweep up; it will then sweep down when the frequency hits its upper limit value. This frequency sweep will keep going unless the "stop" button is pressed. For the phase response investigation, tests with different angles as well as acceleration amplitudes of 1.5, 2, 4.5 g have been carried out.

For the case of measuring the pressure profile on the oscillating cylinder itself, this cylinder is replaced by the pressure-transducer-bearing cylinder, and a similar procedure was then followed.

4.2 ANALYSIS OF THE EXPERIMENTAL DATA

This section describes the method for deriving the added mass coefficients from the experimental data. In each experiment, a pressure field about the measuring cylinder is measured. This pressure field, induced either by the oscillation of the measuring cylinder itself or by other cylinders in the system, together with the acceleration of the oscillating cylinder are then used to determine the added mass coefficients.

4.2.1 Calculation of the Acceleration

As previously discussed, the output of the accelerometer located in the oscillating cylinder is connected to a voltmeter. The peak magnitude of the acceleration of this cylinder can easily be calculated as follows:

$$\text{Accel. (g)} = \frac{\text{Accel. readings (mV)} \times \sqrt{2}}{\text{Accel. sensitivity (mV/g)}}$$

Here it should be noted that the digital voltmeter gives a root-mean-square value; this is why all the readings are multiplied by $\sqrt{2}$, as shown above, to get the peak values.

4.2.2 Calculation of the Pressure

As previously stated, the instrument used for measuring the pressure is a high sensitivity quartz pressure transducer, with a sensitivity of 257.7 (mV/psi).† Although the pressure is small in magnitude (0.1 ∿ 30.0 mV), the signals can be picked up clearly without using an amplifier. There is a phase difference between the pressure and acceleration signals. As a matter of convenience, we chose the pressure corresponding to peak acceleration to calculate the added mass coefficients. Thus, the true values of these pressure readings are associated with the component which is in phase with this peak acceleration, and are given by:

$$\text{Press. (psi)} = \frac{\text{Press. readings (mV)} \times \sqrt{2} \times \cos\phi}{\text{Sensitivity of Press. Transducer (mV/psi)}}$$

where ϕ is defined as the phase angle between the acceleration and pressure signals.

4.2.3 Calculation of the Hydrodynamic Forces

In each test, the pressures around the surface of the cylinder were taken at each interval of 9°. Thus, each experimental set provides 40 pressure readings. With these readings one can obtain the hydrodynamic forces from the following equations:

$$F_{AZi} = - R_i \int_0^{2\pi} P(\theta) \cos\theta \, d\theta \qquad (4.1)$$

†The pressure transducer was not calibrated by the author; the manufacturer's calibration was accepted.

$$F_{AYi} = - R_i \int_0^{2\pi} P(\theta)\ sin\theta\ d\theta \qquad (4.2)$$

where $P(\theta)$ is the pressure reading taken on cylinder i at the angle θ; R_i is the radius of cylinder i and $d\theta$ is the measurement interval (9°). (It is noted that in the case of a single cylinder, pressure readings were taken at 10° intervals, instead of 9°).

The integration of the above equations was done by using Simpson's Rule.

4.2.4 Calculation of the Added Mass Coefficients

Referring to Chapter 2, the force per unit length due to the inviscid flow field acting on cylinder i in Z and Y directions are:

$$F_{AZi} = \rho\ \pi\ R_i^2 \sum_{\ell=1}^{k} \left\{ \varepsilon_{i\ell} \frac{\partial^2 u_\ell}{\partial t^2} + e_{i\ell} \frac{\partial^2 v_\ell}{\partial t^2} \right\} , \qquad (4.3)$$

$$F_{AYi} = \rho\ \pi\ R_i^2 \sum_{\ell=1}^{k} \left\{ \xi_{i\ell} \frac{\partial^2 u_\ell}{\partial t^2} + f_{i\ell} \frac{\partial^2 v_\ell}{\partial t^2} \right\} , \qquad (4.4)$$

for i = 1,2,3....k, where $\varepsilon_{i\ell}$, $e_{i\ell}$, $\xi_{i\ell}$ and $f_{i\ell}$ are the non-dimensional added mass coefficients and $\partial^2 u_\ell/\partial t^2$, $\partial^2 v_\ell/\partial t^2$ are the accelerations of ℓ^{th} cylinder in Z and Y directions, respectively.

Considering a system of two cylinders (Fig. 4.2a) as an example, if the oscillating cylinder is accelerated harmonically in the Z-direction, the acceleration in the Y-direction is zero. Equations (4.3) and (4.4) then become:

$$F_{AZi} = \rho \pi R_i^2 \left(\varepsilon_{i\ell} \frac{\partial^2 u_\ell}{\partial t^2} \right) , \tag{4.5}$$

$$F_{AYi} = \rho \pi R_i^2 \left(\xi_{i\ell} \frac{\partial^2 u_\ell}{\partial t^2} \right) . \tag{4.6}$$

Thus, the added mass coefficients in the Z-direction are:

$$\varepsilon_{i\ell} = \frac{F_{AZi}}{\rho \pi R_i^2 (\partial^2 u_\ell / \partial t^2)} , \tag{4.7}$$

$$\xi_{i\ell} = \frac{F_{AYi}}{\rho \pi R_i^2 (\partial^2 u_\ell / \partial t^2)} . \tag{4.8}$$

Similarly, the added mass coefficients in the Y-direction are given by:

$$e_{i\ell} = \frac{F_{AZi}}{\rho \pi R_i^2 (\partial^2 v_\ell / \partial t^2)} , \tag{4.9}$$

$$f_{i\ell} = \frac{F_{AYi}}{\rho \ \pi \ R_i^2 \ (\partial^2 v_\ell / \partial t^2)} \quad . \tag{4.10}$$

A computer program called "EXPAMC" was written to handle the calculation for the added mass coefficients from the experimental data as described above. A listing of this program and output can be found in Appendices A.4 and C.4, respectively.

4.2.5 Calculation of the Effective Radius of the Boundary Channel

In Suss' analytical solution (and in the "COUPRESS" program also), the added mass coefficients are calculated for a group of cylinders oscillating in a circular boundary channel. Since most of the experiments were conducted in a rectangular water tank, an approximation for the effective radius of the outer channel is necessary. This is done by setting the lengths of solid walls of the cross section of the water tank equal to the circumference of the circular channel. Such an approximation is illustrated for the configuration shown below as an example.

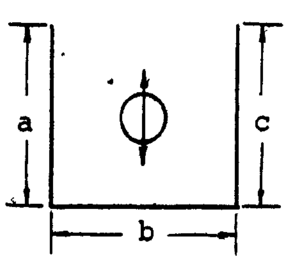

Sketch 4.2.1. Cross-sectional view of the tank.

$$a + b + c = 2 \pi R_o \quad , \tag{4.11}$$

where R_o is the effective radius of the outer channel;

hence,

$$R_o = \frac{a + b + c}{2\pi} \quad . \tag{4.12}$$

This is, of course, approximate. However, as will be shown later the value of R_o (because $R_o >> R_i$) has little influence on the calculated added mass coefficients.

CHAPTER 5

THEORETICAL RESULTS

In this experimental investigation, two major sets of the experimental data are employed to compare with theory. These are the pressure distribution on the surface of cylinders in the system and the added mass coefficients. Theoretical results used for comparison are obtained from Suss' (1976) analytical solution. These are presented and discussed in this chapter.

5.1 THEORETICAL PRESSURE PROFILES

Theoretical pressure profiles are calculated using the computer program "COUPRESS", which is a modified version of the program "COUPLING" (Suss, 1977a). "COUPRESS" gives us the pressure distribution on any cylinder in the system, in addition to the added mass coefficients. The algorithm used in the program is described in Appendix B. It should be noted that the pressure values, obtained from the program output (an example is shown in Appendix C.1) are normalized by the product of the acceleration of the oscillating cylinder and the density of fluid.

A typical set of pressure profiles for the case of three cylinders is shown in Figs. 5.1 to 5.5. In order to make it easy to understand, these profiles are plotted 180° out of phase (by changing the signs of the pressure values) with respect to the outputs obtained from "COUPRESS". That means these profiles correspond to the peak acceleration of the moving cylinder, which is in the direction shown with a long arrow; (this, it should be noted, is opposite to the output, as given by "COUPRESS"). The inner (small) arrow indicates the cylinder on which the pressure profile was taken. Also, for certain profiles, such as the two in Fig. 5.8 plotted in red, it is difficult to be able to perceive when they are plotted with exact values from the program output using conventional polar-coordinates. Therefore, a dummy value was added to make the suction part show explicitly in a special polar-coordinate with a negative value portion in the origin. These are now plotted in green.

Examining these pressure profiles, one will notice that there always is a suction zone at the back of the moving cylinder when it moves forward, as shown in Figs. 5.1a, 5.2b and 5.5a. These figures also exhibit a "stronger coupling" towards the inner region of the cylinder system, manifested by a somewhat larger pressure at the inner region. As to the coupled pressure profiles on the stationary cylinders, different profiles are obtained for different locations. For the stationary cylinder which stood in the front of the moving cylinder. The pressure distribution yields a positive reading at any orientation. However, negative pressure (or suction) appears on the back surface of the pressure measuring cylinder when it's not located directly in front (with respect to the direction of the oscillation) of the shaking cylinder. These effects can be seen in Figs. 5.3a, 5.2a and 5.5b.

In order to study the effect of the outer boundary, four distinct pressure profiles with the radius of the enclosing channel (R_o) equal to 11.43 cm (4.5 in.), 23.368 cm (9.2 in.), and 2.54×10^4 cm (1×10^4 in.) are plotted in black, red and blue, respectively, as shown in Figs. 5.6 and 5.7. Evidently, the pressure profiles for R_o equal to 23.368 cm (9.2 in.) and 2.54×10^4 cm (1×10^4 in.) are similar. This implies that the boundary effect of an enclosing channel with the former radius for such a system, essentially approximates a channel infinitely far away, *i.e.*, the case of unconfined fluid. Moreover, it seems that the existence of the enclosing channel with a smaller radius enlarges the pressure profiles; this effect is more pronounced on the stationary cylinders than on the "self-coupled" profiles relating to the moving cylinder - *cf.* Figs. 5.6b to 5.6a.

5.2 THE ADDED MASS COEFFICIENTS

For the purpose of comparison to experiments, the theoretical added mass coefficient matrix is calculated making use of the computer program "COUPRESS". A listing of the program as well as output samples can be found in Appendices A and C, respectively. The results are shown in Tables 5.1-5.3, for one, two and three cylinders, respectively. For simplicity, only the terms used to compare with experimental data in the added mass coefficient matrix are shown in the tables.

<u>Table 5.1</u>: Added mass coefficients (A.M.C.) for one vibrating cylinder system. R = radius of the vibrating cylinder; R_o = radius of enclosing channel.

R_o (in.)	R_o/R	A.M.C.	Configuration
6.2	4.96	f_{11} = -1.0847	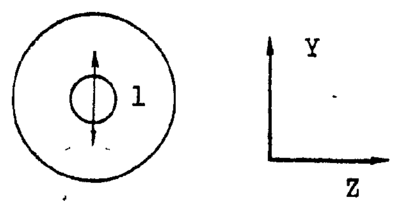
6.8	5.44	f_{11} = -1.0700	

Some of the added mass coefficients in these tables may have a different sign when compared with the experimental results. The reason is that the orientation of the configuration is different for the experiment, as compared with the one in theory (*e.g.* the cylinder numbers change and the orientation of the

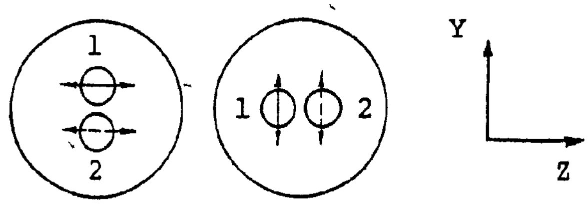

Sketch 5.2.1. Cylinder 1 vibrates in the direction shown by the solid arrows, whereas the direction of coupling is shown by the dashed arrows.

<u>Table 5.2</u>: Added mass coefficients (A.M.C.) for the two-cylinder system. ↔: Vibrating cylinder; ↖ : Fixed cylinder on which pressure measurements were made; R = radius of the cylinders; R_o = radius of the enclosing channel; G_c = cylinder minimum gap/R.

G_c	G_c/R	A.M.C.	Configuration
0.375	0.3	$\varepsilon_{21} = 0.39211$	
1.0	0.8	$\varepsilon_{21} = 0.23573$	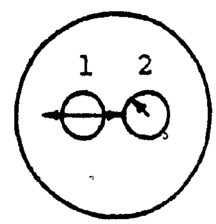
2.0	1.6	$\varepsilon_{21} = 0.12735$	
2.5	2.0	$\varepsilon_{21} = 0.09735$	$R_o = 9.2"$
0.375	0.3	$f_{21} = -0.47847$	$R_o/R = 7.36$ 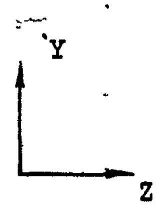
1.0	0.8	$f_{21} = -0.31205$	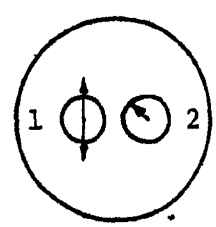
2.0	1.6	$f_{21} = -0.19742$	
2.5	2.0	$f_{21} = -0.16516$	

<u>Table 5.3</u>: Added mass coefficients (A.M.C.) for the three-cylinder system. ↔: Vibrating cylinder; ↖ : Fixed cylinder on which pressure measurements were made: R = radius of the cylinders; R_o = radius of enclosing channel; G_c = cylinder minimum gap/radius.

R_o (in.)	R_o/R	A.M.C.	Configuration
4.5	3.60	$\varepsilon_{31} = -0.37567$	
		$\xi_{31} = -0.43313$	
6.8	5.44	$\varepsilon_{31} = -0.23785$	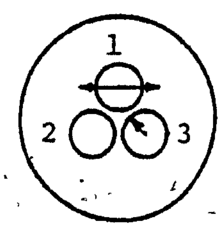
		$\xi_{31} = -0.35902$	
9.2	7.36	$\varepsilon_{31} = -0.20011$	
		$\xi_{31} = -0.33887$	$G_c = \frac{0.375}{1.25}$ 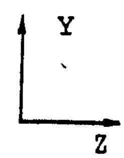
4.5	3.60	$e_{31} = -0.52507$	$= 0.3$
		$f_{31} = 0.17755$	
6.8	5.44	$e_{31} = -0.52235$	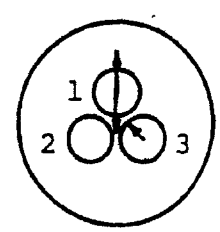
		$f_{31} = 0.27101$	
9.2	7.36	$e_{31} = -0.52429$	
		$f_{31} = 0.29866$	

axes may be different for experimental convenience). Taking the figures shown as an example, ε_{21} of the left configuration and f_{21} of the right configuration are identical, but they are of opposite sign. It should also be mentioned that the added mass coefficients in the printouts of the "COUPRESS" program are arranged in matrix form as:

$$\begin{bmatrix} \varepsilon_{00} & \cdot & \cdot & \cdot & \cdot & \varepsilon_{0k} & e_{00} & \cdot & \cdot & \cdot & \cdot & e_{0k} \\ \cdot & \varepsilon_{11} & \cdot & \cdot & \cdot & \cdot & \cdot & e_{11} & \cdot & \cdot & \cdot & \cdot \\ \cdot & \cdot & \varepsilon_{22} & \cdot & \cdot & \cdot & \cdot & \cdot & e_{22} & \cdot & \cdot & \cdot \\ \cdot & \cdot & \cdot & \cdot & \cdot & \cdot & \cdot & \cdot & \cdot & \cdot & \cdot & \cdot \\ \cdot & \cdot & \cdot & \cdot & \cdot & \cdot & \cdot & \cdot & \cdot & \cdot & \cdot & \cdot \\ \varepsilon_{k0} & \cdot & \cdot & \cdot & \cdot & \varepsilon_{kk} & e_{k0} & \cdot & \cdot & \cdot & \cdot & e_{kk} \\ \xi_{00} & \cdot & \cdot & \cdot & \cdot & \xi_{0k} & f_{00} & \cdot & \cdot & \cdot & \cdot & f_{0k} \\ \cdot & \xi_{11} & \cdot & \cdot & \cdot & \cdot & \cdot & f_{11} & \cdot & \cdot & \cdot & \cdot \\ \cdot & \cdot & \xi_{22} & \cdot & \cdot & \cdot & \cdot & \cdot & f_{22} & \cdot & \cdot & \cdot \\ \cdot & \cdot & \cdot & \cdot & \cdot & \cdot & \cdot & \cdot & \cdot & \cdot & \cdot & \cdot \\ \cdot & \cdot & \cdot & \cdot & \cdot & \cdot & \cdot & \cdot & \cdot & \cdot & \cdot & \cdot \\ \xi_{k0} & \cdot & \cdot & \cdot & \cdot & \xi_{kk} & f_{k0} & \cdot & \cdot & \cdot & \cdot & f_{kk} \end{bmatrix}$$

where the elements subscripted with 0 are the added mass coefficients for the enclosing channel, which are of no interest to us in this thesis.

By making use of the "COUPRESS", it was found that the existence of the enclosing channel, reasonably close to the cylinders, increases the coupling effect in one direction and decreases it in the other direction. Considering the two-cylinder cases as an example, the "COUPRESS" output, shown in Appendix C.2 indicates that closeness of the enclosing channel causes coupling in the Y direction to increase while coupling in the Z direction to decrease, as compared to the output in Appendix C.3.

Since the theoretical added mass coefficients used for comparison are obtained from Suss' analytical solution, it is of particular importance that one should check the reliability of this theory - further to the checks already undertaken by Paidoussis *et al.* (1977), who compared this theory to that of Chung and Chen (1977). There are two theoretical models available for doing this job, a new "viscous" model by Chen (1976) for the case of one single cylinder, and another by Mazur (1970) for the two-cylinder case. A brief description of the final results of these theories are outlined in what follows.

S.S. Chen's Theory

In this theory, Chen defines the added mass coefficient for an infinitely long cylinder oscillating in viscous fluid confined by a cylindrical annulus as:

$$C_M = \text{Re}\ (H);\tag{5.1}$$

H is given by:

$$H = \frac{[\alpha^2(1+\gamma^2)-8\gamma]\,sinh(\beta-\gamma)+2\alpha(2-\gamma+\gamma^2)\,cosh\,(\beta-\alpha)-2\gamma^2\sqrt{\alpha\beta}\ -\ 2\alpha\sqrt{\alpha/\beta}}{\alpha^2(1-\alpha^2)\,sinh\,(\beta-\alpha)-2\alpha\gamma(1+\gamma)\,cosh\,(\beta-\alpha)+2\gamma^2\sqrt{\alpha\beta}\ +\ 2\alpha\sqrt{\alpha/\beta}}^{\dagger}\tag{5.2}$$

provided α and β are large, where

$$\alpha = kr\ ,\tag{5.3}$$

$$\beta = kR_o\ ,\tag{5.4}$$

$$k = \sqrt{i\omega/\nu}\ ;\tag{5.5}$$

in the above, Re(H) represents the real part of H, ω is the frequency of oscillation, ν is the kinematic viscosity of the fluid, r and R_o are the radii of the oscillating cylinder and the confining outer cylinder. A computer program written to handle these calculations is listed in Appendix A.2. It is noted that the added mass coefficient, obtained from Chen's viscous theory, is a function of frequency, while the one from Suss' is frequency independent. However, the effect of frequency is not significant, as can be seen in the following table.

---

† As pointed out by one of the Examiners, the last terms on both numerator and denominator should be $2\alpha\gamma\sqrt{\gamma}$ [Errata, J.Appl.Mech., 1976, 98, p.700].

Table 5.2.1: Comparison of the Added Mass Coefficients obtained from Chen's theory to the ones from Suss' theory.

Frequency (Hz)	R_o = 6.2 in. (R_o/R = 4.96)		R_o = 9.2 in. (R_o/R = 7.36)	
	f_{11} (Chen's)	discrepancy	f_{11} (Chen's)	discrepancy
50	-1.090200	0.50%	-1.042802	0.50%
70	-1.089355	0.43%	-1.041999	0.42%
80	-1.089057	0.40%	-1.041716	0.39%
90	-1.088810	0.38%	-1.041480	0.37%
100	-1.088601	0.36%	-1.041282	0.35%
110	-1.088420	0.34%	-1.041112	0.34%
130	-1.088126	0.31%	-1.040832	0.31%
140	-1.088003	0.30%	-1.040714	0.30%
150	-1.087893	0.29%	-1.040610	0.29%
160	-1.087791	0.28%	-1.040514	0.28%
170	-1.087702	0.27%	-1.040427	0.27%
180	-1.087618	0.27%	-1.040349	0.26%
190	-1.087540	0.26%	-1.040276	0.26%
200	-1.087469	0.25%	-1.040209	0.25%

The percentage discrepancy in the above table is defined as,

$$\text{Discrepancy (\%)} = \frac{\text{Chen's A.M.C.} - \text{Suss' A.M.C.}}{\text{Suss' A.M.C.}} \times 100 \tag{5.6}$$

with the Added Mass Coefficients from Suss' theory as follows:

for $R_o = 6.2$ in. $(R_o/R = 4.96)$, $f_{11} = -1.08474$.

for $R_o = 9.2$ in. $(R_o/R = 7.36)$, $f_{11} = -1.03762$

Agreement for the coefficients between the two theories is excellent (less than 1%). The discrepancy becomes smaller as frequency increases. In other words, variation of the coefficients can be neglected when the oscillating frequency is high. This is consistent with the fact that viscous effects can be expected to be most important at low Reynolds numbers - *i.e.* for a given amplitutde, the rms velocity of the cylinder is lower, when the frequency is lower. Comparisons between Chen's theory and the experimental results have also been made and shown in Tables 1 to 3 (pp. 108-110).

Mazur's Theory

This theory is easily found by referring to Chen's paper (1975a), in which Mazur's theory is applied to the study of the dynamic response of two parallel circular cylinders in an unconfined fluid. Mazur obtained the hydrodynamic forces based on a two-dimensional theory - assuming that the three-dimensional effects are very small for large wave-length motions, as discussed by Chen (1974). Thus, the theory is based on the same assumptions as Suss' or Chen's, but the result obtained is in a neat closed form - at least only for this case of two cylinders. The hydrodynamic forces are expressed as follows:

(a) for in-plane motion (*i.e.*, in the plane of the cylinder long axes),

$$F_1 = -M_1\mu_1 \frac{\partial^2 u_1}{\partial t^2} + M_1\mu_3 \left(\frac{R_2}{R}\right)^2 \frac{\partial^2 u_2}{\partial t^2} , \tag{5.7}$$

$$F_2 = -M_2\mu_2 \frac{\partial^2 u_2}{\partial t^2} + M_2\mu_3 \left(\frac{R_1}{R}\right)^2 \frac{\partial^2 u_1}{\partial t^2} . \tag{5.8}$$

(b) for out-of-plane motion,

$$F_1 = -M_1\mu_1 \frac{\partial^2 u_1}{\partial t^2} - M_1\mu_3 \left(\frac{R_2}{R}\right)^2 \frac{\partial^2 u_2}{\partial t^2} , \tag{5.9}$$

$$F_2 = -M_2\mu_2 \frac{\partial^2 u_2}{\partial t^2} - M_2\mu_3 \left(\frac{R_1}{R}\right)^2 \frac{\partial^2 u_1}{\partial t^2} , \tag{5.10}$$

where F_1 and F_2 are the hydrodynamic forces on cylinder 1 and 2, respectively. R here is the center-to-center distance between the two cylinders, M_1 is the displaced mass of fluid by cylinder 1 with radius R_1 while M_2 is the displaced mass of fluid by cylinder 2 with radius R_2. The μ's in equations

(5.7)-(5.9) are given by:

$$\mu_1 = 1 + \frac{R^4-2R^2(R_1{}^2+R_2{}^2)+(R_2{}^2-R_1{}^2)^2}{R^2R_1{}^2}\left\{\sum_{k=1}^{\infty} k\,\frac{\exp[-k(h+h_1)]}{\sinh\,(kh)}\right\}, \tag{5.11}$$

$$\mu_2 = 1 + \frac{R^4-2R^2(R_1{}^2+R_2{}^2)+(R_2{}^2-R_1{}^2)^2}{R^2R_2{}^2}\left\{\sum_{k=1}^{\infty} k\,\frac{\exp[-k(h+h_2)]}{\sinh\,(kh)}\right\}, \tag{5.12}$$

$$\mu_3 = 1 + \frac{R^4-2R^2(R_1{}^2+R_2{}^2)+(R_2{}^2-R_1{}^2)}{R_1{}^2R_2{}^2}\left\{\sum_{k=1}^{\infty} k^{\dagger}\,\exp(-2kh)\coth(kh)\right\} \tag{5.13}$$

with,

$$h = \ln\left\{\frac{R^2-R_1{}^2-R_2{}^2}{2R_1R_2} + \left[\left(\frac{R^2-R_1{}^2-R_2{}^2}{2R_1R_2}\right)^2 - 1\right]^{1/2}\right\}, \tag{5.14}$$

$$h_1 = 2\ln\left\{\frac{R^2+R_1{}^2-R_2{}^2}{2RR_1} + \left[\left(\frac{R^2+R_1{}^2-R_2{}^2}{2RR_1}\right)^2 - 1\right]^{1/2}\right\}, \tag{5.15}$$

$$h_2 = 2\ln\left\{\frac{R^2-R_1{}^2-R_2{}^2}{2RR_2} + \left[\left(\frac{R^2-R_1{}^2+R_2{}^2}{2RR_2}\right)^2 - 1\right]^{1/2}\right\}. \tag{5.16}$$

Now, recalling equations (2.31) and (2.32) of Chapter 2, we have:

---

† A printing error was found in S.S. Chen's paper, it should be k instead of h.

$$F_{AZi} = M_i \sum_{\ell=1}^{k} \left\{ \varepsilon_{i\ell} \frac{\partial^2 u_\ell}{\partial t^2} + e_{i\ell} \frac{\partial^2 v_\ell}{\partial t^2} \right\} , \tag{5.17}$$

$$F_{AYi} = M_i \sum_{\ell=1}^{k} \left\{ \xi_{i\ell} \frac{\partial^2 u_\ell}{\partial t^2} + f_{i\ell} \frac{\partial^2 v_\ell}{\partial t^2} \right\} . \tag{5.18}$$

For so-called "in-plane" motion, with coordinates shown in the figure on the R.H.S., the acceleration in the Z-direction is zero, *i.e.*, $\partial^2 u_\ell/\partial t^2 = 0$, and equation (5.17) becomes:

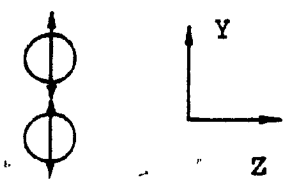

$$F_{AYi} = M_1 f_{11} \left(\frac{\partial^2 v_1}{\partial t^2} \right) + M_2 f_{12} \left(\frac{\partial^2 v_2}{\partial t^2} \right) , \tag{5.19}$$

Similarly, for out-of-plane motion, $\partial^2 v_\ell/\partial t^2 = 0$, and equation (5.17) becomes:

$$F_{AZi} = M_1 \varepsilon_{11} \left(\frac{\partial^2 u_1}{\partial t^2} \right) + M_2 \varepsilon_{12} \left(\frac{\partial^2 u_2}{\partial t^2} \right) . \tag{5.20}$$

Now, comparing equation (5.7) to (5.19) and equation (5.9) to (5.20), one may find that the non-dimensional added mass coefficients between the two theories can be correlated as:

$$\varepsilon_{11} = -\mu_1 , \tag{5.21}$$

$$\varepsilon_{12} = -\frac{M_1}{M_2}\,\mu_3\left(\frac{R_2}{R}\right)^2 \quad , \qquad (5.22)$$

$$f_{11} = -\mu_1 \quad , \qquad (5.23)$$

$$f_{12} = \frac{M_1}{M_2}\,\mu_3\left(\frac{R_2}{R}\right)^2 \quad , \qquad (5.24)$$

where once again, it is noted that Mazur's notation is used on the R.H.S. of the equations (in our case, R is defined as R_{12} and so on).

If the acceleration as well as the radius of the two cylinders are the same, there will be no difficulty to prove that $F_1 = F_2$; also μ_1 and μ_2 are then identical. Calculations of ε_{11} and ε_{12} are handled by using a Hewlett-Packard digital computer program. A listing of this program is given in Appendix A.3. One should be reminded here that the system which Suss considered is a cluster of cylinders oscillating in fluid with a confined boundary. In order to be able to compare with Mazur's results, the coefficients are calculated using "COUPRESS" with the assumption that the radius of the enclosing channel is essentially infinite, accomplished by employing a value 8,000 times the radius of the cylinders (10,000 in. to 1.25 in.). Results obtained from Mazur's theory for different cylinder center-to-center distances are tabulated in Table 5.2.2 below.

Table 5.2.2: Added Mass Coefficients for the two-cylinder system obtained using Mazur's theory.

Cylinder center-to center distance (in.)	No. of terms for solving the equation	A.M.C.
2.875	K = 8	$\varepsilon_{11} = -1.1218$ $\varepsilon_{12} = -0.4174$
3.5	K = 5	$\varepsilon_{11} = -1.0441$ $\varepsilon_{12} = -0.2628$
4.5	K = 4	$\varepsilon_{11} = -1.0141$ $\varepsilon_{12} = -0.1556$
5.0	K = 4	$\varepsilon_{11} = -1.0089$ $\varepsilon_{12} = -0.1256$

The added mass coefficients calculated by "COUPRESS" turn out to be exactly the values obtained from Mazur's solution (to four significant digits). According to this, it is reasonable to say that Suss' theoretical model is reliable for the two-cylinder cases, at least in the case of unconfined fluid. As there is nothing special between the two, three or k cylinders, it can be said that Suss' theory stands up well, when compared to the others.

CHAPTER 6

EXPERIMENTAL RESULTS

In this chapter, three sets of experimental results, classified according to the number of the cylinders with configurations shown in Figs. 4.4 to 4.6, are presented. Through all the cases, the moving cylinder was oscillating vertically at a frequency ranging from 70 to 250 Hz (displacement ranging from 2.96×10^{-3} R to 2.08×10^{-4} R; the radius of the cylinders (R) is 3.175 cm (1.25 in.)), with the magnitude of acceleration of the shaker (defined as As) kept constant at 2 g. Perfect sinusoidal signals were obtained for both the pressure signals measured on the stationary cylinder and the acceleration of the moving cylinder (defined as Ac). In addition to the added mass coefficients, several other aspects are explored, such as the pressure distribution around the surface of the stationary cylinder, the phase angle (defined as ϕ) between the pressure and acceleration (Ac) signals, and the pressure and phase angle response to frequency change.

6.1 ONE CYLINDER

For this test, besides the accelerometer, a pressure transducer was also placed inside the oscillating cylinder to measure the pressure field induced by its own motion. The experiments have been performed with three different configurations (Figs. 4.4a to 4.4c). The moving cylinder was oscillated at a frequency varied from 50 to 200 Hz, where in the readings of pressure, acceleration, as well as the phase angle between them, were taken down at each 10 Hz interval - except at 60 and 120 Hz at which resonances existed (the former mechanical and the latter probably electrical). The pressure transducer used in this experiment is a highly sensitive quartz pressure transducer having a sensitivity of 257.7 mv/psi and acceleration sensitivity of 0.00121 psi/g, as stated previously. Since the transducer was mounted on the moving cylinder, the pressure component due to the acceleration of the transducer itself must be subtracted when we calculate the pressure values. These small acceleration-induced pressure components were obtained by oscillating the cylinder in water with the pinhole on the top surface of the lock-nut sealed, when no water was in the pressure-sensing chamber (see Fig. 4.1). With the cylinder oscillating with an acceleration magnitude of 2 g, the magnitude of these small components was found to vary from 0.0 up to 0.005 psi, depending on the orientation (θ) of the pinhole (where pressure signals were sensed) while the "true" pressure readings - with the pinhole uncovered - vary from 0.0 to 0.15 psi. Here it is noted that the acceleration compensating feature of this transducer is adequate, only as long as the pressure measured is relatively high. For our case, where very small pressure signals are involved, the added correction described above (for each θ) is necessary.

As it can be seen from Suss' theory, the added mass coefficients should only be geometry-dependent. In other words, the pressure should not be affected by a change of the oscillating frequency. However, the pressure curves plotted against frequency (Figs. 6.1 to 6.3), show a high and low peak appearing at 110 and 130 Hz, respectively. The curves are not straight as expected, but go up and down as frequency changes.

Another, initially unexpected observation, is that a phase angle (ϕ) exists between the pressure and acceleration signals. The variation of this phase angle with frequency is small (within 30°). On the top half surface of the moving cylinder, ϕ varies between 3° and 10°, whereas the bottom half has a variation of 170° to 180°. However, for the region near $\theta = 90°$ and $\theta = 270°$, the variations of ϕ are twice as large. Such typical distribution of the phase angles around the cylinder is shown in Fig. 6.4. These phase variations are thought to be related to viscous effects; theoretically, according to inviscid theory, the upper surface of the cylinder pressures should be in-phase and the lower surface ones 180° out-of-phase with acceleration.

The pressure distributions around the surface of the moving cylinder for the arrangements of Figs. 4.4a to 4.4c, at different frequencies, have been plotted in Figs. 6.5 to 6.7. These pressure profiles were taken at the moment that the moving cylinder reached its peak acceleration. As was mentioned earlier, the phase angles, ϕ, at the bottom half surface have a value about 180°, which give the pressure readings at this half portion of the profile negative values when they are multiplied by $\cos\phi$ (see the calculation of pressure in Section 4.2.2). This implies a suction occurs at the bottom of the cylinder when it moves up, which is physically reasonable. At the position where the cylinder reaches its peak acceleration, the negative part (suction) of the pressure profile is almost equal to the positive one.

For 30 and 40 Hz oscillation, the profiles are not symmetric as shown in Fig. 6.5, both in size and in direction. The situation improves as frequency goes above the resonance frequency zone (about 60 Hz). Theoretical prediction of the pressure profiles is in good agreement with experimental results for all the three cases (Figs. 4.4a to 4.4c).

A comparison of the experimental added mass coefficients f_{11} for the configurations in Fig. 4.4 to the theoretical results obtained from the computer program "COUPRESS" are shown in Fig. 6.8. Agreement for all the cases is excellent, with an average discrepancy* within 5%. These results indicate that the water tank is large enough to avoid

---

*

$$\text{Ave. discrepancy} = \frac{\text{Suss' A.M.C.} - (\text{Exp. A.M.C.})\ \text{ave.}}{\text{Suss' A.M.C.}} \times 100\%.$$

any significant side effect to the measurements due to the existence of a free surface; (as shown in Figs. 4.4a to 4.4c one-cylinder tests were conducted with the tank not covered). Also, the approximation of a rectangular tank by an equivalent circular channel is evidently acceptable.

It should be noted that the signs for the added mass coefficients used in all the coefficient plots in this thesis correspond to theoretical values obtained from "COUPRESS", and are not necessarily those obtained from the experiments ("raw" values) as already explained in Section 5.2.

6.2 TWO CYLINDERS

To study the coupling effect induced by the moving cylinder, we start with a simple system of two cylinders. The experiments were carried out with the six distinct configurations shown in Fig. 4.5. For each configuration, six to eight different oscillating frequencies were chosen. The moving cylinder oscillated vertically while the pressure measurements were taken on the stationary cylinder.

The tests were first conducted for the geometries of Figs. 4.5a, 4.5d, 4.5e and 4.5f. The variation of pressure with frequency behaves somewhat similarly to the case of one cylinder, *i.e.* the curves are not straight as expected, as shown in Fig. 6.9. Moreover, the acceleration of the moving cylinder (Ac) does not remain constant with frequency, but we obtain a zig-zag curve instead. This unusual phenomenon urges one to question the stiffness of the experimental setup, in particular the tube which carries the oscillating cylinder. As described in Chapter 3, this aluminum tube has a length of 25.4 cm (10 in.) with outside and inside diameters of 3.81 cm (1.5 in.) and 2.54 cm (1 in.), respectively. It seems too heavy for such a small tube to carry a 4.55 kg (10.0 lbs) load (the oscillating cylinder) and to oscillate it at an acceleration of 2 g with frequency up to 200 Hz.

To eliminate this weakness, two aluminum fins were added to stiffen the tube. Also, a certain amount of material was removed from the inner surface of the oscillating cylinder. As a result, its thickness is now reduced to 0.635 cm (0.25 in.) and its weight reduced proportionally. Moreover, to ensure that the pressure transducer mounted in the moving cylinder does not sense fluctuating velocity components tangential to the cylinder, *i.e.* anything other than the pressure normal to the surface of the cylinder, the depth of the pinhole in the lock nut (see Fig. 4.1) was increased to 0.38 cm (0.15 in.) for the original 0.254 cm (0.1 in.), which is six times the diameter of the hole. At the same time, some additional steel bars were welded to the supporting structure of the shaker. Remarkable improvements were seen in Figs. 6.10 and 6.11, as compared with Fig. 6.9. On the other hand, a significant resonance occurs to the shaking system at a frequency near 85 Hz. Hence, the frequency range chosen for measuring the pressure was now changed to cover 100 to 250 Hz.

An investigation focused on the behavior of the phase angle (denoted by ϕ) *versus* frequency with θ as parameter; it is recalled that ϕ is the phase lag between pressure and acceleration (Ac) signals. During the test, the shaking control was set in the "auto frequency sweep mode", with a frequency range of 100 to 300 Hz. Under this control, the moving cylinder is oscillated with a change of 1 Hz/sec in frequency. The response of ϕ was taken down from the transfer function using a HP 4520A Digital Signal Analyzer. Two configurations were studied. For the arrangement of Fig. 4.5a, values of ϕ plotted against frequency at different θ are shown in Figs. 6.12 to 6.15. It was found that at the measuring point where the pressure signal is strong (*e.g.* $\theta = 0°$), the phase angle between pressure and Ac is small and sensibly constant with frequency (within 5°), while at the less sensitive region such as $\theta = 45°$ and 315°, ϕ varies between 0° and -20°; it then increases to between 90° and -20° at $\theta = 135°$ and 225°, and reaches its maximum at $\theta = 180°$, where the variation of ϕ *versus* frequency ($\Delta\phi$) is between 165° and -10° for frequency changes from 100 to 300 Hz (Fig. 6.15a). It should be noted that for all the cases, ϕ curves are stable and repeatable. Also examined was the response of ϕ to changes in Ac. Large changes in the ϕ-*versus*-frequency curves with varying Ac were obtained only at the bottom half surface of the stationary cylinder, as is illustrated by two typical plots shown in Figs. 6.16 and 6.17.

For the configuration of Fig. 4.5b, the strong coupling region (*i.e.*, the region of strong pressure readings) was found for θ between 0° and 180°; at this sensitive region, the ϕ curves shown in Figs. 6.18 to 6.21 have smaller fluctuations with frequency than those at the rest of the circumference. However, there is an exception at $\theta = 90°$ (Fig. 19a), where the pressure sensed by the pressure transducer is the one normal to the direction of the acceleration of the oscillating cylinder. At this particular measuring point, $\Delta\phi$ seems to violate the previously mentioned variation trend, *i.e.* the weak signal region always yields larger $\Delta\phi$. The influence of Ac on the ϕ-*versus*-frequency, shown in Figs. 6.22 and 6.23 is similar but smaller than that of Figs. 6.16 and 6.17 due to the fact that coupling effect is weaker for this configuration. Consistent results were obtained for the same configuration with cylinder gap increased.

Pressure profiles for the various two-cylinder configurations are displayed in Figs. 6.24 to 6.28. The black curves represent the theoretical pressure profiles obtained from the computer program "COUPRESS" after multiplying by the values of the density of fluid and the acceleration of the moving cylinder at the corresponding frequency, whereas the red ones are the experimental results. Of all the four profiles in Figs. 6.24 and 6.25, two are not symmetric; they also exhibit a small concavity at the bottom left. The other two profiles are in agreement, in terms of shape, with the theoretical data. In certain frequencies, the concavity of the pressure profile becomes larger. A possible explanation for the asymmetric profiles is that when the moving cylinder is oscillating at a frequency which happens to be one of the resonance frequencies of any part of the system, the neglected side (horizontal) motion of the moving cylinder becomes enlarged; hence, an asymmetric pressure distribution was obtained. It is very encouraging to see a consistency in pattern between the experimental and theoretical pressure profiles for all the two-cylinder cases. The change in shape predicted by theory when the cylinder gap increases, as well as the concavity (which exists only for small cylinder gaps) at $\theta = 45°$, are well reproduced by the experimental pressure profiles. No improvement was found after the experimental setup was modified, as can be seen in Figs 6.25a and 6.25b and also Figs. 6.27a and 6.27b. In general, better agreement between theoretical and experimental profiles is obtained for configurations with larger inter-cylinder gaps.

The graphs in Figs. 6.29 to 6.32 are the added mass coefficients plotted against frequency for all two-cylinder cases. In these figures, the moving cylinder oscillated in the direction shown by the solid arrow, while the dashed-line arrow indicates the direction of the calculated force on the stationary cylinder and hence of the added mass coefficient. [This also applies to the three-cylinder cases to be discussed later]. In examining these results, it should be pointed out that the experimental added mass coefficients are always larger than the theoretical ones for the in-line configurations (*e.g.* Figs. 4.5a and 4.5c) and smaller for the side-by-side configurations (*e.g.* Figs. 4.5b and 4.5d). Moreover, coupling as "measured" by the experimental coefficients for the in-line configurations is larger than coupling for the side-by-side configurations, while the theoretical values exhibit the reverse tendency. Also, configurations of larger inter-cylinder gaps seem to be in better agreement with theory than smaller ones. The modification of the experimental setup discussed earlier in this section does show an improvement of agreement between theory and experiment for the configuration of Fig. 4.5a, as shown in Fig. 6.29; however, it turns out to make agreement worse for the configuration of Fig. 4.5c, as shown in Fig. 6.31. Thus, despite the fact that the pressure-*versus*-frequency curves were improved by the modification, the added mass coefficients derived from the pressure distributions are not necessarily closer to the theoretical results; in any case, the same added mass coefficient can be obtained from many possible pressure distributions.

6.3 THREE CYLINDERS

In order to proceed further in this study of hydrodynamic coupling forces, a system of three cylinders was considered next. Tests were first conducted with two different cylinder arrangements and a free surface on the top, as shown in Figs. 4.6a and 4.6b. The shaking system was arranged in such a way that it gives the moving cylinder a vertical motion (shown in the figure by the long arrow) with a constant acceleration of 2 g magnitude. The inner arrow indicates the cylinder where pressure measurements were taken. It is recalled that the cylinders used in all the experiments discussed in this thesis have the same radius of 3.175 cm (1.25 in.). Since the cylinder system is symmetrical (in the sense that the geometry is that of an equilateral triangle), the coupling effect on either of the stationary cylinders due to the oscillation of the moving cylinder should be the same. Therefore, only one of the stationary cylinders was chosen on which to take the pressure measurements.

Later, tests were done with the same cylinder geometries as above, except that a Plexiglas cover was put on the water surface. In addition to these, cases of three cylinders enclosed by a circular channel were also investigated. The geometrical configurations for these latter cases are illustrated in Figs. 4.6c to 4.6f.

Figures 6.33 to 6.42 show the pressure at different θ plotted against frequency for different configurations. Those shown in Figs. 6.33 and 6.34 were taken from the tests before the modification of the experimental setup. A resonance frequency zone occurs at 100 to 150 Hz, where the acceleration of the moving cylinder does not correspond to that of the shaker. Hence, the pressure behaves in a peculiar way. Pressure taken at positions where the signal is strong (*e.g.* θ = 0° to 108°), increases gradually with frequency, while at weak signal regions (*e.g.* θ = 243° to 270°), the pressure tends to decrease with increasing frequency. The situation improved after the modification of the experimental setup, especially, for Ac as plotted in Figs. 6.35 and 6.36. Unfortunately, no similar improvement in the pressure curves could be observed, contrary to expectation. For the case of the cylinder geometry of Fig. 4.6d, a fairly straight line for the variation of pressure with respect to frequency change is obtained, as shown in Fig. 6.36; on the other hand, the corresponding curves (Fig. 6.35) for the arrangement of Fig. 4.6c do not. This implies the aforementioned resonance in the system is not the only cause that gives rise to the strange behavior of pressure as a function of frequency, but that cylinder geometry is also an important factor.

For the cases of three cylinders arranged in the center of an 11.43 cm (4.5 in.) radius circular channel, two additional fluids other than water were used to extract more information concerning the effects of density and viscosity on the added mass coefficients. The properties of these fluids, as well as of water for comparison, are given in the following table. The viscosity units of C.S. stand for centistokes.

Liquid	Specific Gravity at 15.6°C (60°F)	Viscosity at 40°C (104°F)
Ethylene glycol	1.115	20 C.S.
Water	1.0	1.0 C.S.
Lubricating oil (ESSO (NUTO,A-10))	0.860	10 C.S.

In Figs. 6.37 to 6.39, we can see a sharp drop of the acceleration of the moving cylinder (Ac) at 270 Hz for the tests with water and ethylene glycol, but for oil, it shifts 10 Hz higher. The drop in acceleration is assumed to be the result of antiresonance, and the shift in frequency to be a combined effect of the density and viscosity of the fluids, where viscosity limits this sharp drop while density exaggerates it. Moreover, it shows that fluid with lighter viscosity gives the Ac curve a steeper slope.

Another interesting feature to point out is that, after a sharp drop, Ac goes up again as frequency increases. However, the three different fluids give three different kinds of response.

As to pressure measurements, the biggest signals are obtained at $\theta = 54°$, while at $\theta = 243°$, the readings are the smallest. The effect on pressure of density changes is as expected: the higher the density is, the larger are the signals. Also the variation of pressure *versus* frequency is smoother† for oil than for water or glycol.

For Figs. 6.40 to 6.42, which are for a different arrangement of moving and measuring cylinders, we notice that both pressure and Ac curves are not as smooth as those in Figs. 6.37 to 6.39. Several peaks appear between 100 and 200 Hz; a similar drop in Ac (antiresonance trough) occurs at 270 and 280 Hz. Nevertheless, oil exhibits "better", *i.e.* smoother behavior. With this configuration, the maximum pressure readings were found at $\theta = 108°$ and the minimum at $\theta = 270°$. No remarkable distinctions of the pressure curves can be seen that could be attributed to the effect of density or viscosity of the fluids. According to these results, one may say that fluids with lighter density and higher viscosity give better performance, eventually leading to a closer agreement with theory,† as will be shown later in this section.

A significant difference in performance of both the

†These results are contrary to expectation and cannot be explained.

pressure and Ac *versus* frequency was observed when comparing Figs. 6.35 and 6.36 to Figs. 6.37 and 6.40, respectively. Pressure and Ac curves have higher slopes with frequency for clusters in a circular channel than in a rectangular boundary, and are also smoother especially for the latter case. Ac has a big jump after a minor drop at about 270 Hz for the rectangular boundary system rather than a tremendous drop observed only for the circular channel system.

It is difficult to suggest the true reasons for the unexpected behavior of the pressure, as well as Ac, with respect to frequency change. However, results reveal that cylinder geometry and the boundary effect play important roles in this strange performance.

The cases of three cylinders in the rectangular tank with a cover on the top and in a circular channel were chosen to study the variation of phase angle (defined as $\Delta\phi$) *versus* frequency. Results in Figs. 6.43 and 6.44 show that large $\Delta\phi$ only existed at the region of the cylinders where the pressure signals are weak. With a circular boundary channel, the behavior of ϕ remains more or less the same as for the rectangular channel. The increase of viscosity of fluid seems to have a damping effect on the fluctuation of ϕ *versus* frequency, which seems reasonable, as may be seen from Figs. 6.45 to 6.50. Although no significant effect is found due to the difference in boundary, the pattern of ϕ curves in Fig. 6.48

is rather different when compared with Fig. 6.44. Also $\Delta\phi$ seems larger for the arrangements enclosed by the circular channel.

A few additional tests were made to observe the effect of changes in acceleration on the phase angle between pressure and acceleration. Three plots shown in Fig. 6.51 illustrate that the difference in acceleration has no effect on ϕ for the arrangement of Fig. 4.6e, at the azimuthal region where coupling (*i.e.* the pressure signal) is strong. Outside this region, there is a small effect on ϕ as Ac is changed. As for the arrangement of Fig. 4.6f, even at the pressure sensitive region, two distinct but similar ϕ curves are obtained - shown at the bottom graph of Fig. 6.51.

The pressure distributions, on the surface of the stationary cylinders are considered next. Some typical examples taken at chosen frequencies were plotted. From Figs. 6.52 to 6.55 it is clear that, as long as the cylinder geometry remains the same, pressure profiles of similar pattern are obtained despite the difference in channel boundary, as well as with smaller acceleration levels (*e.g.* 1.5 g). At high frequency, there always is a small concavity at $\theta \simeq 270°$. Theory (plotted in black) gives the same shape; however, the concavity is faint and occurs about 30° higher ($\theta \simeq 300°$), as compared with experimental results. Furthermore, the theoretical maximum values of pressure were predicted to occur at $\theta = 45°$, rather than 54° as observed in the experiments. No improvement can be seen from the tests done after the experimental setup was modified. (It is recalled that in this modification, the tube was stiffened, the lock nut was modified, the weight of the moving cylinder was reduced and the shaker supporting structure was welded with additional steel bars to increase its stiffness).

Also of interest are the pressure profiles of Figs. 6.56 to 6.58. A suction takes place between $\theta = 135°$ to 270°, except in the case with free surfaces on the top; this is believed to be the effect of the free surface. Another important fact to be noted is that the experimental pressure profiles are always smaller than those predicted by theory.

No extraordinary difference can be found between pressure profiles obtained from a cluster in a circular channel or a rectangular boundary. Notwithstanding, a smaller boundary does give a little influence on the shape of the profiles. By examining Figs. 6.59 to 6.61, one may see that the part of profile at θ about 180° to 270° is flatter than it is in Figs. 6.52 to 6.55. Also, the profiles in Figs. 6.62 to 6.64 are more "slender" than those in Figs. 6.56 to 6.58 in Z-direction. Furthermore, pressure readings do increase as a result of a smaller boundary, which agrees with theory.

The added mass coefficients derived from pressure profiles for all three-cylinder cases are plotted and shown in Figs. 6.65 to 6.78, where the values of the theoretical added mass coefficients is represented by a dashed straight line since it is frequency independent. Results in Figs. 6.65 to 6.67 show that, at high frequency (above 150 Hz), the coefficient e_{31} is always greater than the theoretical value, while f_{31} is less than the theoretical one. This is also true for test results obtained after the experimental setup was modified. Nevertheless, the modification does give better agreement with theory, as may be seen by comparing Figs. 6.68 to 6.67. Tests using two different levels of acceleration (*i.e.* Ac = 1.5 and 2.0 g) yielded similar results, as shown in Figs. 6.65 and 6.66; that means the added mass coefficients varied in a similar way as frequency changed. No significant difference can be seen from results in Figs. 6.66 and 6.67 (showing the effect of having the tank covered or uncovered); in fact, the existence of a free surface does not create any unwanted side effects, but paradoxically gives results in slightly better agreement with theory, as compared to those with a cover on top, especially at high frequencies. The added mass coefficients e_{31} and f_{31} for these two configurations (*i.e.* Figs. 4.6a and 4.6c) yield an average discrepancy of 15%.

Another study of the effect of free surface for three cylinder cases was done by measuring the pressure distribution on both the stationary cylinders for the configuration shown, along with results, in Figs. 6.69 and 6.70.

Similar variations of the added mass coefficients with frequency change were obtained; ξ_{31} is in better agreement with theoretical values than ε_{31}, with an average discrepancy of 20% for the first and 50% for the latter. Keeping the same cylinder geometry, but putting a cover on top of the water surface, ξ_{31} improves to an average discrepancy of 14%, and ε_{31} to 15%, as shown in Figs. 6.71 and 6.72. It is finally noticed that tests done after the modification of the experimental setup produce a notable agreement with the theoretical values for ξ_{31} at frequencies above 150 Hz.

Results in Figs. 6.73 to 6.78 reveal that the added mass coefficient e_{31} decreases as frequency increases and f_{31} is always greater than the theoretical value, but both ε_{31} and ξ_{31} are smaller than the theoretical values at all frequencies. As far as the effects of density and viscosity on the added mass coefficients are concerned, no particular remarks can be made; however, results obtained from mineral oil agree better with theoretical predictions than those in water and ethylene glycol.

CHAPTER 7

DISCUSSION

The test results presented in the previous chapters will be discussed under the following four headings: (i) Measurements of the pressure *versus* frequency; (ii) Phase angle between pressure and acceleration; (iii) Pressure distributions; and (iv) The added mass coefficients.

7.1 MEASUREMENTS OF THE PRESSURE *versus* FREQUENCY

Measurement of the structural natural frequencies was made in order to study the response of the experimental setup and its likely effect on the pressure measurements. An accelerometer was attached to each component of interest of the experimental setup. When the shaker was shaking, a signal was picked up and fed to the Hewlett Packard 5420A Digital Signal Analyzer, where the power spectral density of the vibration was obtained. The output was displayed in the form of a spectral plot of magnitude *versus* frequency on the screen. A hard copy could be obtained by using the HP plotter interfaced to the system. As shown in Figs. 7.1 to 7.6, several peaks appear in the frequency range of 0 to 400 Hz for each component, which happened to be the working frequency zone of the experimental study of the added mass coefficients. Further, different natural frequencies were obtained for the same component in different directions as illustrated in Figs. 7.1 and 7.2. Due to the many natural frequencies which occurred in the testing frequency range and the complexity of the experimental setup, a small excitation will induce a significant resonance to the system, exhibited for example in Figs. 7.2 to 7.6. It is difficult to claim that the resonances and the complexity of the system are the major causes for the haphazard observed variations of pressure *versus* frequency. However, it cannot be denied that they will have some effect on the pressure readings.

It should be noted that the measurement of natural frequency of the experimental setup described above was done before the modification. As the tube was stiffened, the thickness of the hollow oscillating cylinder was reduced, and the support of the shaker was stiffened, certain improvements on the response of pressure to frequency were obtained as shown in Figs. 6.10 and 6.11 for two-cylinder cases and Fig. 6.36 for three-cylinder cases, except for Fig. 6.35.

On the other hand, comparing Fig. 6.35 to 6.36, obtained with the same rectangular boundary but with different cylinder geometry, the pressure curves of the latter show better behaviour with respect to frequency changes than the first. Also, comparing Fig. 6.36 to 6.40 with the same cylinder goemetry but different boundary, the pressure curves are different.

These observations imply that it is not only the cylinder geometry, but also the boundary proximity and shape that affect the pressure response to frequency change. In addition, the density of the fluid seems to play a role in this peculiar performance. Oil with lighter density yields better results than water and ethylene glycol as can be seen in Figs. 6.37 to 6.42.

In the tests, pressure readings were taken around the surface of the pressure-measuring cylinder; hence, the pressure-transducer bearing cylinder has to be rotated through 360° with a stop at each 9° interval. Such rotation was done by reaching the cylinder at the opposite end from where pressure was measured, and rotating it manually. It is interesting to find that no change in the fluctuating pressure can be sensed while the cylinder is being rotated and the hand is immersed in the tank, except at low frequency (below 70 Hz for example). Even then, only a maximum variation of 5% was found.

7.2 PHASE ANGLE (ϕ) BETWEEN PRESSURE AND ACCELERATION

In the experiments, there was a phase difference between the pressure signal and the acceleration signal of the moving cylinder. The value of ϕ varies with the change of the orientation of the measuring point as well as frequency. Results of the phase angle *versus* frequency study suggest the possibility of wake formation on the surface of the stationary cylinders in the area facing the enclosing channel, rather than the moving cylinder (*e.g.* the area at θ = 135°-225° for the cylinder geometry shown in Fig. 4.5a). In this region the fluctuation of ϕ with frequency is significant. To test this possibility, an experiment was conducted with liquid dye to monitor the motion of fluid on the stationary cylinder. In order to simplify the test, we considered the case of two-cylinders in the configuration of Fig. 4.5a. The instrument arrangement is shown on the right-hand side. The pressure transducer bushing shown in Fig. 4.1 was replaced by a bushing with a tube through with the dye was injected. The pressure of the injection was adjusted by leveling the bottle. During the test, the dye came out of the pressure sensing hole with a pressure as close to the pressure on the surface of the cylinder as possible.

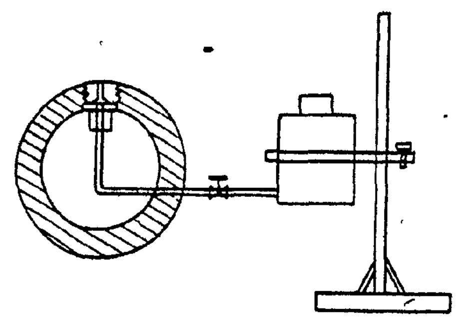

Cross-section view of the stationary cylinder with dye injection instrumentation.

The figure on the left-hand side of the following page shows the trace of the dye injected through the pressure sensing hole on the stationary cylinder while the top cylinder is not shaking. As the top cylinder starts oscillating up and down, the dye tends to flow up a little, while previously it fell down by gravity. Since the dye was dissolved into a solution with a density almost equivalent to water at the same temperature, the plunging of the dye under gravity was very slow.

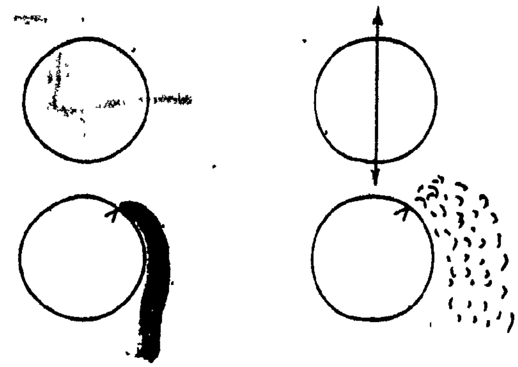

Both cylinders are stationary   Top cylinder is oscillating

For a dye injected at the bottom position, or the so-described as pressure-insensitive region, the trace of the dye did go up, and then sank down as it moved away from the motion affected region. The results indicate a suction exists, which tends to draw the fluid particles upward. However, such a force is weak and the affected region is small. Thus, as soon as the fluid particles move away from that region, the dye sinks again as a result of gravity. A possible explanation of this upward suction is that, because of the resistance of the stationary cylinder below and the absence of a similar cylinder above, the net force on the fluid in the downward direction (when the top cylinder goes down) is less than that in the upward direction (when the top cylinder goes up).

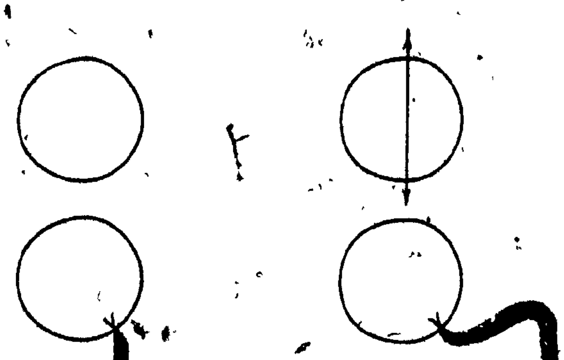

Both cylinders are stationary   Top cylinder is oscillating

Hence, for each cycle, a net force upward is produced.

Another interesting part of the test was to rotate the stationary cylinder slowly while the dye was coming out of the pinhole and the top cylinder was oscillating. The trace remained at the same place about one to two minutes before it disappeared. No remarkable difference can be seen for this test as the oscillating frequency changes from 100 to 250 Hz, and also, as the amplitude of the acceleration of shaker (As) varies from 1.5 g to 4.5 g.

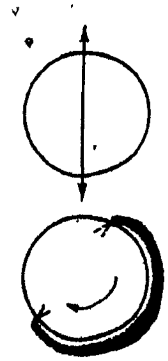

The dye kept coming out while the cylinder was rotating.

For the test of the side-by-side configuration of Fig. 4.5b, since the coupling is weak for this configuration, no obvious pattern can be seen. Never-the less, as the amplitude of acceleration of the shaker increases to 4.5 g, a wake-form of fluid pattern occurred. It is noted that in all the

Both cylinders are stationary.

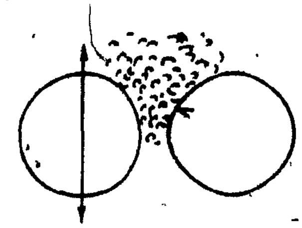

The left side cylinder is oscillating, while the dye comes out from the pinhole of the right side cylinder.

pressure measuring experiments, the maximum amplitude of acceleration is no more than 3 g (displacement of the oscillating cylinder ranging from 2.6×10^{-4} to 3.7×10^{-3} in.), hence no true wake formation is likely to have happened.

Results of these flow-pattern tests show that the theoretical assumption of no separation is upheld, at least for the stationary cylinder when the acceleration of the vibrating one is small; evidently, the hypothesis of wake formation at the so-called pressure-insensitive region (the area facing the enclosing channel) of the stationary cylinder is not true.

In principle, the phase angle (ϕ) is considered as the time lag between two signals (in our case, pressure and acceleration). However, the cylinder distance in our tests is too small, compared to the speed of sound in water (≈ 1500 m/sec), to be able to provide a significant value of ϕ. Besides, it was found that ϕ is sensitive to frequency changes. Therefore, instead of claiming that time lag is the cause of the occurrence of ϕ, one would rather suspect that it is mainly due to the viscous effects. Apart from these comments, it appears that the values of ϕ also depend on boundary condition and cylinder geometry. This may be seen by comparing Fig. 6.48 to 6.44: in Fig. 6.48, variations in ϕ of over 360° appeared at $\theta = 270°$ and 315°; in Fig. 6.44, on the other hand, variations in ϕ of over 360° occurred at $\theta = 225°$ and 270°.

Similar effect of the cylinder geometry can be seen by comparing Fig. 6.48 to Fig. 6.45, in which the variation of ϕ is much less for the latter at any θ.

As to the distributions of ϕ around the surface of the cylinders, measurements on the oscillating cylinder (*e.g.* Fig. 6.4) agree well with the ones predicted by the inviscid theory: *i.e.*, the upper surface of the cylinder pressures are in-phase and lower surface ones 180° out-of-phase with acceleration (see Fig. 6.4). However, the distribution measured on the stationary cylinder, shown in Fig. 7.7 as an example, does not give the pattern expected, but an attenuated form.

7.3 PRESSURE DISTRIBUTIONS

It should be recalled here that the pressure profiles shown in the last chapter correspond to peak acceleration of the moving cylinder at certain frequencies. During the tests, both the pressure and acceleration readings were taken at their peak values. In order to obtain the pressure corresponding to peak acceleration, these pressure readings were then multiplied by the cosine of the phase angle (ϕ) between the two signals. Since the values of ϕ vary tremendously around the circumference, the values of pressure will be affected. Fortunately, it is noted that in the region where the variations of ϕ with frequency are large occur where the pressure signals are weak. Hence, on the whole, the effect of ϕ on the overall pressure profile is not that serious a matter as was initially thought; this may be considered to be supported by the fact that the pressure profiles obtained from all the experiments agree well with theoretical predictions. Also, it should be mentioned that the consistency in shape of the profiles between theory and experiment, indicates that Suss' theory works even for a cluster with such small intercylinder gaps as 0.95 cm (0.375 in.), which is about one-seventh of the diameter of the cylinders that were used in all the experiments.

As to the response of pressure profile to the acceleration of the moving cylinder (Ac), results show that a large Ac produces a bigger pressure profile as expected; this can be seen through all the configurations, especially for two and three-cylinder cases. In other words, the pressure increases as Ac increases. Such a response of the pressure to Ac change is shown in Fig. 7.8.

7.4 THE ADDED MASS COEFFICIENTS

Experimental added mass coefficients derived from pressure profiles for different configurations were plotted against frequency and compared with theoretical values. In Suss' theory, the added mass coefficients should only be geometry-dependent, and should not be affected by the change in the frequency of oscillation. However, experimental results show that these coefficients are highly sensitive to frequency and that they change in a haphazard way, in particular for clusters of two-cylinders and three-cylinders.

A "viscous" theoretical model for one oscillating cylinder in a confined fluid by Chen (1976) shows that the added mass coefficients are almost frequency-independent; they decrease smoothly and very slightly as frequency increases. Results obtained from this theory for one cylinder yield differences within 1% for the added mass coefficients at 50 Hz and 200 Hz with $R_o/R = 4.96$ and much less than 1% for $R_o/R = 7.36$, where R_o and R are defined as the radii of the enclosing channel and of the cylinder, respectively.

Inspite of the frequency effects shown in the experiments, results for one oscillating cylinder are in good agreement (with 5% off) with theoretical prediction. Hence, discussion will be focused on the cases of two- and three-cylinder systems.

With the in-line two-cylinder configuration shown in Fig. 4.5a, one should expect a symmetric pressure profile (with respect to Y axis); yet, experimental data show non-symmetric profiles at some frequencies. As a result, a coupling component in the Z-direction was found which does not exist in theory. The cause or causes of this fact are unknown; however, they may be attributed to side motion of the oscillating cylinder created by the dynamic unbalance of the cylinder (if any, since this cylinder with tube structure (see picture 7) was balanced statically), as well as to small-amplitude resonance of some component of the vibrating system or the water tank and the shaker support system. An attempt to prove mathematically the existence of such an effect was conducted by making use of equations (2.31) and (2.32). Considering the three-cylinder case of Fig. 4.5d as an example with the pressure profiles taken on the stationary cylinder (in our case, it is cylinder 3), the two equations for the forces on this cylinder are:

$$F_{AZ3} = \rho \pi R_3^2[\varepsilon_{31}a_{Z1} + e_{31}a_{Y1}] \quad , \tag{7.1}$$

$$F_{AY3} = \rho \pi R_3^2[\xi_{31}a_{Z1} + f_{31}a_{Y1}] \quad . \tag{7.2}$$

where F_{AZ3} and F_{AY3} are the hydrodynamic forces exerted on cylinder 3 in Z- and Y-directions, respectively.

The method used in this simulation assumes a small side-ways acceleration ($a_Z = 0.05\ a_Y$) occurred while cylinder 1 oscillated in Y-direction; then with the experimental hydrodynamic forces F_{AZ} and F_{AY} (computed from the measured pressure profile) and the theoretical ε_{31} and ξ_{31}, the coefficients e_{31} and f_{31} can be obtained by equation (6.1) and equation (6.2). These are stated mathematically as follows:

Equations (7.1) and (7.2) are written as:

$$(F_{AZ3})_{exp.} = \rho \pi R_3^2 [0.05\ z_{Y1} (\varepsilon_{31})_{theor.} + a_{Y1} e_{31}] , \quad (7.3)$$

$$(F_{AY3})_{exp.} = \rho \pi R_3^2 [0.05\ a_{Y1} (\xi_{31})_{theor.} + a_{Y1} f_{31}] , \quad (7.4)$$

or

$$e_{31} = \frac{(F_{AZ3})_{exp.}}{\rho \pi R_3^2 a_{Y1}} - 0.05\ (\varepsilon_{31})_{theor.} \quad (7.5)$$

$$f_{31} = \frac{(F_{AY3})_{exp.}}{\rho \pi R_3^2 a_{Y1}} - 0.05\ (\xi_{31})_{theor.} \quad (7.6)$$

The main point of this method is assuming the experimental F_{AZ} and F_{AY} are the hydrodynamic forces as a result of both the acceleration a_Z and a_Y of the moving cylinder 1 instead of a_Y alone. If e_{31} and f_{31} obtained from this calculation agree better with theoretical values than the purely experimental e_{31} and f_{31} compared with the theoretical ones, the existence of the side motion effect of the moving cylinder is then proved. Unfortunately, no constant relation between these modified experimental added mass coefficients and the theoretical data can be seen from the results of this calculation. At some frequencies, these modified e_{31} and f_{31} improved, but become worse at others. (The resultant changes are of the order of 10%).

Thus, it is difficult to claim validation of this effect.

Although the experimental added mass coefficients for the two- and three-cylinder cases are not in good agreement with theoretical values, it is interesting to observe the dynamic response of the system for such experimental results and compare it to the theoretical one. A study was carried out by using results obtained from the cases of three-cylinders. The frequencies of the system were computed based on solving the equation of motion of the cylinder system considered. A computer program called "Solution" written by Suss (1977a) was employed for these computations. In this program, the added mass coefficient matrix (as mentioned in Chapter 2) is one of the required inputs to calculate the eigenvalues (A user's guide for this program has been presented by Suss (1977b)). For a three-cylinder system, the added mass coefficient matrix consists of 36 elements. Because of the symmetric nature of the system, some of the elements in the matrix are identical. Making use of this, sixteen elements in this theoretical added mass coefficient matrix obtained from "COUPRESS" were replaced by experimental values inspite of the fact that only four experimental coefficients, namely ε_{31}, ξ_{31}, e_{31} and f_{31} are available for each system. With this so-called semi-experimental added mass coefficient matrix as input and using three comparison functions, the eigenvalues (which are the frequency ω multiplied by $-i$ ($i = \sqrt{-1}$) of the system were calculated. A comparison of these results for the circular enclosing channel case, with the theoretical eigenvalues obtained by using the theoretical added mass coefficient matrix as "Solution"'s input, is shown in Table 7.1. (p. 95).

Remarkable agreement was found regardless of the discrepancy between the theoretical and experimental added mass coefficients. Another set of frequencies obtained by using the maximum values of the experimental added mass coefficients (among those obtained at different oscillating frequencies) for the so-called semi-experimental added mass coefficient matrix was compared with theoretical data. Agreement is also quite reasonable (± 6.5%) as shown in Table 4 (p. 111). For the same system but different boundary radii (*e.g.* R_o = 17.27 cm (6.8 in.) and R_o = 23.37 cm (9.2 in.)), results are also tabulated in Tables 5 to 7 (pp. 112-114). An important fact revealed by this analysis is that, even if half of the off-diagonal elements in the theoretical added mass coefficient matrix were replaced by the experimental values, of which several have a discrepancy as large as 67%, the frequencies obtained from such a system are still within reasonable range.

Here let us recall the work by Jendrzejczyk and Chen (1978) in an experimental study on fluidelastic vibration of cantilevered tube bundles. However, the method in that case is reversed. Theoretical added mass coefficient matrix

Table 7.1: The natural frequencies of three-cylinder cases with circular enclosing channel (R_o = 11.43 cm (4.5 in.)).

$$\text{Discrepancy (\%)} = \frac{\text{Theor. Freq. - Semi-exp. Freq.}}{\text{Theor. Freq.}} \times 100$$

	Theoretical Frequencies	Semi-exp. frequencies (using ave. A.M.C.)*	Discrepancy (%)
1st mode group	18.335601	17.857170	2.61
	19.128095	19.149628	-0.11
	19.128104	19.676233	-2.87
	22.473622	22.418528	0.25
	22.473626	23.287012	-3.62
	24.227658	23.410995	3.37
2nd mode group	50.542748	49.223936	2.61
	52.727286	52.786638	-0.11
	52.727309	54.238247	-2.87
	61.949351	61.797483	0.25
	61.949363	64.191490	-3.62
	66.784415	64.533254	3.37
3rd mode group	99.083970	96.498572	2.61
	103.366536	103.482891	-0.11
	103.366584	106.328625	-2.87
	121.445468	121.147745	0.25
	121.445491	125.840957	-3.62
	130.924123	126.510949	3.37

*The average values of the added mass coefficients obtained from different frequencies.

(Chung and Chen, 1977*) was used to calculate the theoretical values of the natural frequencies of the tube bundles through the equation of motion, and these natural frequencies are then compared with the measured natural frequencies from the tests. Excellent agreement was obtained. Thus, the comparison of theoretical and experimental added mass coefficients - and concluding that they are in good agreement - through comparison of the corresponding natural frequencies, is seen to be weak, in the sense that very large discrepancies in the added mass coefficients can be masked by agreement of frequencies. With respect to our own foregoing analysis, it may also be said that the diagonal elements, which were taken from theory in all cases, are dominant in determining the natural frequencies correctly.

*Chung and Chen (1977)'s theory is equivalent to the one derived by S. Suss (1977a).

CHAPTER 8

CONCLUSION

This thesis describes an experimental derivation of some of the added mass coefficients for a cluster of cylinders vibrating in still fluid contained by a rigid rectangular tank. The added mass coefficients were evaluated through measurements of the pressure distributions on the circular surfaces of the cylinders in the system. Studies also include the cases of three cylinders immersed in fluid enclosed by an 11.43 cm (4.5 in.) radius shell. In order to obtain extra information concerning the effect of viscosity and density of fluid to the values of added mass coefficients, the tests were conducted in three different fluids, *i.e.*, water, lubricating oil and ethylene glycol.

Unlike previous work by Pustejovsky (1978) and Barbir and Pham (1979), the pressure measuring system was designed to detect the pressure signals more directly and it was possible to eliminate the difficulties associated with flow oscillation and air bubbles trapped in the pressure sensing chamber. Also, by employing a highly sensitive pressure transducer and cylinders with larger radius, clear and perfect sinusoidal pressure and acceleration signals were obtained. Furthermore, a better understanding of the behaviour of the phase lag between pressure and acceleration signals was attained with the help of a Hewlett-Packard 5420A Digital Signal Analyzer.

Among three sets of experimental results distinguished by the number of cylinders, remarkably good agreement between experiment and theory was attained only for the cases of one single cylinder. Despite the fact that results for the studies of two - and three-cylinder systems are somewhat inconclusive, certain valuable information related to the characteristics of the cylinders vibrating in liquid were obtained.

As shown in the experiments, pressure signals are very sensitive to frequency change and response in a haphazard manner, which is believed to be attributed to the flexibility of the system. Hence an attempt to stiffen several components of the experimental setup has been done. Reasonable improvements were observed, the values of pressure increase linearly with respect to frequency, and with the magnitude of acceleration of the oscillating cylinder. However, there are a few exceptions, especially in the case of three cylinders enclosed by a circular shell. For the tests with different fluids, lubricating oil exhibits better pressure response to frequency as compared with water and ethylene glycol, suggesting viscosity and density of fluid are important factors, in addition to cylinder geometry.

The phase angle (ϕ) distributions on the circular surface of the pressure measuring cylinder, are quite reasonable for one single cylinder at three distinct configurations. The top half surface has a value $\phi \simeq 0°$, while the bottom half $\phi \simeq 180°$. In the cases of two and three cylinders, the values of ϕ at points on the pressure measuring cylinder depend on the cylinder geometry as well as on the boundary (*i.e.*, either rectangular or circular boundary). Studies of the response of phase angle to frequency show that large variations with frequency of the value of ϕ occur at the surface region where the pressure signals are weak and are smaller at the points where the pressure signals are strong. This would imply a wake formation at the so-called pressure-insensitive region. However, a flow visualization study for the vibration-induced flow for the cases of two cylinders has been done. No wakes can be seen until the magnitude of acceleration of the oscillating cylinder increases to 4.5 g. Hence, evidently, the assumption of wake formation at the pressure-insensitive region is unlikely for the present studies, where the acceleration for all the tests is no greater than 3 g. In general, the phase angle is the time lag between two signals (in our case, the time lag between pressure and acceleration signals). Nevertheless, it is noted that (i) the distributions of phase angle are different for different cylinder geometries, (ii) variations of ϕ with frequency of over 360° occurred only in the three-cylinder cases with cylinder arrangements such as those shown in Figs. 4.6d and 4.6f (for frequency changes from 100 to 250 Hz), and (iii) the damping effect of lubricating oil on ϕ is considerable. All these indicate that phase angle is not a matter of time lag only, but that it is also affected by the arrangement of the cylinders in the system, the boundary conditions, the viscosity of the fluid and perhaps by the structural response of the remainder of the system, through resonances within the frequency range tested.

The most successful part of the experimental study is the measurement of the pressure distributions on the surface of the cylinders and in particular for the single-cylinder case where excellent agreement between experimental and theoretical prediction was attained. The presence of a free surface for some cases does not produce any significant effect to the pressure profiles (as seen in the pressure distribution plots). Moreover, the pressure field patterns follow the predictions of Suss' theory as cylinder geometry changes, and the magnitude of the pressure signals measured do increase as containment becomes tighter.

As far as the added mass coefficients are concerned, experimental results obtained from all the single cylinder cases agree well with theoretical values computed by using Suss' classical method. This is as expected, since measured pressure profiles demonstrate both qualitative and quantitative similarities to the theoretical ones. For the system consisting of two or three cylinders, agreement with theoretical results is somewhat inadequate. The average discrepancy ranges from ±6% to ±67%. Notwithstanding this, some positive conclusions can be drawn. Results for configurations shown in Figs. 4.5a, 4.6a and 4.6c are always greater than theoretical values and smaller for configurations such as those of Figs. 4.5b, 4.6b and 4.6f. Increasing the stiffness of experimental setup did exhibit certain positive improvement in the agreement between theory and experiment. Nevertheless, results become worse as the enclosed boundary of the cylinders decreases, although this may be due to having additional structural elements which could respond to the fluid excitation. On the other hand, tests conducted in lubricating oil gave better performance insofar as pressure and phase angle are concerned and, consequently, yield better agreement with theory as compared with those of water and ethylene glycol.

By reviewing all the experimental results presented in Chapter 6, several general remarks can be made, as follows.

1. In the analysis, the fluid field is considered to be two-dimensional; that is, the axial motion of the fluid is neglected. This is justified in our case, since only the length and the diameter are of the same order of magnitude that three-dimensional effects of the flow should be considered as shown by S.S. Chen (1974).

2. It is found that the pressure distribution and, acceleration of the moving cylinder, phase angles as well as pressure distributions on the pressure-measuring cylinders, are sensitive to frequency changes, and consequently, so are the values of the added mass coefficients. In this respect, cylinder geometry, enclosing boundary of the cylinders, properties (*i.e.* viscosity and density) of the fluids and the structural response of the experimental setup are the likely factors giving rise to these variations with frequency.

3. Although no positive conclusions can be drawn from the flow visualization tests, the results indicate that separation is unlikely to have occurred in these tests, where the magnitude of acceleration of the oscillating cylinder was always less than 4.5 g.

4. The method used in this study to derive the added mass coefficients from the experimental data is not straightforward. The measured pressure profile, a result of the pressure readings taken at points around the surface of the considered cylinder and the corresponding phase angles, are integrated to obtain the inviscid hydrodynamic forces. The added mass coefficients are then calculated from these force components with the associated acceleration of the oscillating cylinder. By this method, 40 pressure readings and 40 phase angle readings are required to derive one single added mass coefficient. If the instrument error of each reading is 1%, it would not be

surprising to obtain the added mass coefficients far away from the theoretical values due to the accumulation of instrumentation errors.

5. Since the pressure, acceleration, phase angles and pressure distributions are sensitive to frequency changes, one would expect that the added mass coefficients should also be frequency dependent. However, at least for one cylinder, the theoretically predicted change in our experimental range of frequencies is small. This implies that the mathematical models developed by Chen (1976) and Yang and Moran (1979) should yield only slightly more reliable results than those derived from potential flow theory.

Apart from the results discussed in the last two chapters, an additional experiment was done while this thesis was being written for the two-cylinder system with the configuration of Fig. 4.5c. The pressures were taken on the oscillating cylinder instead of the stationary cylinder as done previously. Good agreement with theory is obtained in both the distribution of phase angles and the pressure profiles; the experimental added mass coefficients show an average discrepancy of 5% as compared with theory. This suggests that Suss' theory is able to predict the diagonal terms in the added mass coefficient matrix better than the off-diagonal ones.

In general, results exhibit consistency, and relative success in correlation between the experimental and theoretical derivation of the added mass coefficients. However, better performance can be expected if certain components of the present experimental setup were replaced. These include a strongly built stainless steel water tank, a permanently ground-mounted support for the shaker, a light but rigid oscillating cylinder, and an improved supporting tube and components for the oscillating cylinder which could hold it tightly without giving any disturbance to the pressure field exerted on the fixed cylinders; yet allow the oscillating cylinder to be rotated for measuring the self-coupled pressure field in the cases of cylinder clusters with small cylinder center-to-center distances.

In a future study, a new technique should be developed to evaluate the added mass coefficients more directly, by measuring the hydrodynamic forces instead of the pressure distributions on the cylinders. This could eliminate problems such as discrepancies due to integration errors, accumulation of the instrumentation errors, *etc.*.

REFERENCES

BARBIR, K.E. & PHAM, T.T., 1979
Mech. Lab. Report, Dept. of Mechanical Engineering, McGill University, Montreal, Quebec, Canada.

CHEN, S.S., 1974
Dynamics of a Rod-Shell System Conveying Fluid
Nuclear Engineering and Design, Vol. 30, pp. 223-233.

CHEN, S.S., 1975a
Dynamic Response of Two Parallel Circular Cylinders in a Liquid
Journal of Pressure Vessel Technology, Trans. ASME, Vol. 97, pp. 78-83.

CHEN, S.S., 1975b
Vibrations of a Row of Circular Cylinders in a Liquid
Journal of Engineering for Industry, Trans. ASME, Vol. 97, pp. 1212-1218.

CHEN, S.S., WAMBSGANSS, M.W. & JENDRZEJCZYK, J.A., 1976
Added Mass and Damping of a Vibrating Rod in Confined Viscous Fluids
Journal of Applied Mechanics, Vol. 43, pp. 325-329.

CHEN, S.S. & JENDRZEJCZYK, J.A., 1978
Experiments on Fluidelastic Vibration of Cantilevered Tube Bundles
Journal of Mechanical Design, Trans. ASME, Vol. 100, pp. 540-548.

CHUNG, H. & CHEN, S.S., 1977
Vibration of a Group of Circular Cylinders in Confined Fluid
Journal of Applied Mechanics, Vol. 44, pp. 213-217.

DUBUAT, P.-L.G., 1786
Principes d'Hydraulique
Paris, 2nd Ed., Vol. 2, pp. 226-259.

HAMANN, F.H. & DALTON, C., 1971
The Forces on a Cylinder Oscillating Sinusoidally in Water
Journal of Engineering for Industry, Trans. ASME, Vol. 93, pp. 1197-1202.

ISSID, P.B., 1977
Experiment to Derive the Virtual Mass Matrix for Three Rods in Water Surrounded by an Outer Rigid Cylinder
Internal Report, Dept. of Mech. Engineering, McGill University, Montreal, Quebec, Canada.

LAMB, H., 1932
Hydrodynamics
Cambridge University Press, London, 6th Ed., pp. 160-174.

LEVY, S. & WILKINSON, J.P.D., 1975
Calculation of Added Water Mass Effects for Reactor System Components
General Electric Company Corporate Research and Development Report 75CRD095.

LIGHTHILL, M.J., 1960
Note on the Swimming of Slender Fish
Journal of Fluid Mechanics, Vol. 9, pp. 305-317.

MAZUR, V.Y., 1970
Motion of Two Circular Cylinders in an Ideal Fluid
Izvestiya Akademic Nauk SSSR, Mekhanika Zhiakostii Gaza, Vol. 6, pp. 80-84.

MILNE-THOMPSON, L.M., 1938
Theoretical Hydrodynamics
The Macmillan Co., New York, 2nd Ed., pp. 228-229.

MORISON, J.R., *et al.*, 1950
The Forces Exerted by Surface Waves on Piles
Petroleum Trans., Vol. 189, pp. 149-159.

PAIDOUSSIS, M.P., SUSS, S. & PUSTEJOVSKY, M.A., 1977
Free Vibration of Clusters of Cylinders in Liquid-Filled Channels
Journal of Sound and Vibration, Vol. 55, pp. 443-459.

PUSTEJOVSKY, M.A., 1977
Automatic Mesh Generation for Two-Dimensional Finite Element Analysis
M.E.R.L. Report No. 77-1, Dept. of Mech. Engineering, McGill University, Montreal, Quebec, Canada.

PUSTEJOVSKY, M.A., 1978
Experimental Derivation of the Virtual Mass Matrix for a Cluster of Cylinders Contained in Still Fluid
Interim Report, Dept. of Mech. Engineering, McGill University, Montreal, Quebec, Canada.

SARPKAYA, T., 1975
Forces on Cylinders and Spheres in a Sinusoidally Oscillating Fluid
Journal of Applied Mechanics, Vol. 42, pp. 32-37.

SCHLICHTING, H., 1960
Boundary Layer Theory
4th Ed., McGraw-Hill, New York.

STELSON, T.E. & MAVIS, F.T., 1975
Virtural Mass and Acceleration in Fluids
Trans. ASCE, Vol. 122, pp. 518-525.

SUSS, S., PUSTEJOVSKY, M.A. & PAIDOUSSIS, M.P., 1976
The Virtual Mass Matrix of a Cluster of Cylinders in Liquid Contained by a Rigid Outer Cylinder
M.E.R.L. Report No. 76-1, Dept. of Mech. Engineering, McGill University, Montreal, Quebec, Canada.

SUSS, S., 1977a
Dynamics of Clusters of Flexible Cylinders in Bounded Axial Fluid Flow
Master's Thesis, Dept. of Mech. Engineering, McGill University, Montreal, Quebec, Canada.

SUSS, S., 1977b
User's Guide to the Computer Programs Used for Obtaining the Dynamics of Clusters of Flexible Cylinders in Bounded Axial Flow
M.E.R.L. Memo 77-2, Dept. of Mech. Engineering, McGill University, Montreal, Quebec, Canada.

YANG, C.L. & MORAN, T.J., 1979
Finite Element Solution of Added Mass and Damping of Oscillation Rods in Viscous Fluids
Journal of Applied Mechanics, Vol. 46, pp. 519-523.

TABLES

Table 1: Comparison of S.S. Chen's results with R_o = 15.75 cm (6.2 in.) and experimental results with single-cylinder configuration shown in Fig. 4.4a.

$$\text{Discrepancy (\%)} = \frac{\text{Exp. A.M.C.} - \text{S.S. Chen's A.M.C.}}{\text{S.S. Chen's A.M.C.}} \times 100$$

Frequency (Hz)	Added Mass Coefficient (f_{11})		Discrepancy (%)
	Experimental	S.S. Chen's	
50	-1.024762	-1.090200	-6.00
70	-1.107135	-1.089355	1.63
80	-1.013844	-1.089057	-6.91
90	-1.107848	-1.088810	1.75
100	-1.079440	-1.088601	-0.84
110	-1.046105	-1.088420	-3.89
140	-1.107206	-1.088003	1.76
150	-1.071773	-1.087893	-1.48
160	-1.089622	-1.087791	0.17
170	-1.098203	-1.087702	0.97
180	-1.110977	-1.087618	2.15
190	-1.107218	-1.087540	1.81
200	-1.113121	-1.087469	2.36

Table 2: Comparison of S.S. Chen's results with R_o = 17.27 cm (6.8 in.) and experimental results with single-cylinder configuration shown in Fig. 4.4b.

$$\text{Discrepancy (\%)} = \frac{\text{Exp. A.M.C.} - \text{S.S. Chen's A.M.C.}}{\text{S.S. Chen's A.M.C.}} \times 100$$

Frequency (Hz)	Added Mass Coefficient (f_{11})		Discrepancy (%)
	Experimental	S.S. Chen's	
50	-1.072021	-1.075317	-0.31
70	-1.090671	-1.074486	1.51
80	-1.141970	-1.074192	6.31
90	-1.095527	-1.073950	2.01
100	-1.090163	-1.073744	1.53
110	-1.081437	-1.073567	0.73
140	-1.135948	-1.073155	5.85
150	-1.117563	-1.073048	4.15
160	-1.105882	-1.072948	3.06
170	-1.106183	-1.072859	3.11
180	-1.104795	-1.072776	2.98
190	-1.101491	-1.072701	2.68
200	-1.096601	-1.072630	2.23

Table 3: Comparison of S.S. Chen's results with $R_o = 17.27$ cm (6.8 in.) and experimental results with single-cylinder configuration shown in Fig. 4.4c.

$$\text{Discrepancy (\%)} = \frac{\text{Exp. A.M.C.} - \text{S.S. Chen's A.M.C.}}{\text{S.S. Chen's A.M.C.}} \times 100$$

Frequency (Hz)	Added Mass Coefficient (f_{11})		Discrepancy (%)
	Experimental	S.S. Chen's	
50	-1.158337	-1.075317	7.72
70	-1.146795	-1.074486	6.73
80	-1.137051	-1.074192	5.85
90	-1.135966	-1.073952	5.77
100	-1.140692	-1.073744	6.24
110	-1.110469	-1.073567	3.44
140	-1.101587	-1.073155	2.65
150	-1.105204	-1.073048	3.00
160	-1.091693	-1.072948	1.75
170	-1.103530	-1.072859	2.86
180	-1.108376	-1.072776	3.32
190	-1.112181	-1.072701	3.68
200	-1.114672	-1.072630	3.92

Table 4: Natural frequencies of the three-cylinder system with R_o = 11.43 cm (4.5 in.).

$$\text{Discrepancy (\%)} = \frac{\text{Theor. Freq.} - \text{Semi-exp. Freq.}}{\text{Theor. Freq.}} \times 100$$

	Theoretical Frequencies	Semi-exp. frequencies (using max. A.M.C.)	Discrepancy (%)
1st mode group	18.335601	17.163750	6.39
	19.128095	19.152209	-0.13
	19.128104	19.313515	-0.97
	22.473622	22.435269	0.17
	22.473626	23.910804	-6.39
	24.227688	25.263518	-4.28
2nd mode group	50.542748	47.312496	6.39
	52.727286	52.793757	-0.13
	52.727310	53.238402	-0.97
	61.949351	61.843631	0.17
	61.949363	65.910996	-6.39
	66.784415	69.539801	-4.28
3rd mode group	99.083970	92.751386	6.39
	103.366536	102.496846	-0.13
	103.366584	104.368528	-0.97
	121.445468	121.238213	0.17
	121.445491	129.211873	-6.39
	130.924123	136.521820	-4.28

Table 5: Natural frequencies of the three-cylinder system with $R_o = 17.27$ cm (6.8 in.).

$$\text{Discrepancy (\%)} = \frac{\text{Theor. Freq.} - \text{Semi-exp. Freq.}}{\text{Theor. Freq.}} \times 100$$

	Theoretical Frequencies	Semi-exp. frequencies (using ave. A.M.C.)	Discrepancy (%)
1st mode group	18.416629	18.795823	-2.06
	20.151764	19.495744	3.26
	20.151786	20.120321	0.16
	23.010816	22.368302	2.79
	23.010854	22.996501	0.06
	24.306414	25.634739	-5.46
2nd mode group	50.766102	51.811367	-2.06
	55.549066	53.740722	3.26
	55.549127	55.462391	0.16
	63.430146	61.659032	2.79
	63.430251	63.390687	0.06
	67.001509	70.663083	-5.47
3rd mode group	99.521834	101.570970	-2.06
	108.898353	105.353277	3.26
	108.898472	108.728435	0.16
	124.348417	120.876327	2.79
	124.348624	124.271061	0.06
	131.349715	138.527861	-5.47

Table 6: Natural frequencies of the three-cylinder system with R_o = 23.37 cm (9.2 in.)

$$\text{Discrepancy (\%)} = \frac{\text{Theor. Freq.} - \text{Semi-exp. Freq.}}{\text{Theor. Freq.}} \times 100$$

	Theoretical Frequencies	Semi-exp. frequencies (using ave. A.M.C.)	Discrepancy (%)
1st mode group	18.42195	18.32526	0.53
	20.38719	20.38066	0.03
	20.38720	20.63316	-1.21
	23.15300	23.14015	0.06
	23.15305	23.35880	-0.89
	24.31157	23.92620	1.59
2nd mode group	50.78077	50.51423	0.53
	56.19802	56.18002	0.03
	56.19807	56.87604	-1.21
	63.82210	63.78665	0.06
	63.82221	64.38934	-0.89
	67.01573	65.95344	1.59
3rd mode group	99.55059	99.02807	0.53
	110.17056	110.13528	0.03
	110.17065	111.49976	-1.21
	125.11679	125.04730	0.06
	125.11702	126.22883	-0.89
	131.37760	129.29509	1.59

Table 7: Natural frequencies of the three-cylinder system with R_o = 23.37 cm (9.2 in.).

$$\text{Discrepancy (\%)} = \frac{\text{Theor. Freq. - Semi-exp. Freq.}}{\text{Theor. Freq.}} \times 100$$

	Theoretical Frequencies	Semi-exp. frequencies (using max. A.M.C.)	Discrepancy (%)
1st mode group	18.42195	18.99535	-3.11
	20.38719	19.05209	6.55
	20.38720	20.37953	0.04
	23.15300	22.05758	4.73
	23.15305	23.14781	0.02
	24.31157	23.92620	-12.98
2nd mode group	50.78077	52.36137	-3.11
	56.19802	52.51779	6.55
	56.19807	56.17692	0.04
	63.82210	60.80252	4.73
	63.82221	63.80776	0.02
	67.01573	75.71199	-12.98
3rd mode group	99.55059	102.64920	-3.11
	110.17056	102.95584	6.55
	110.17065	110.12921	0.04
	125.11679	119.19722	4.73
	125.11702	125.08870	0.02
	131.37760	148.42573	-12.98

FIGURES

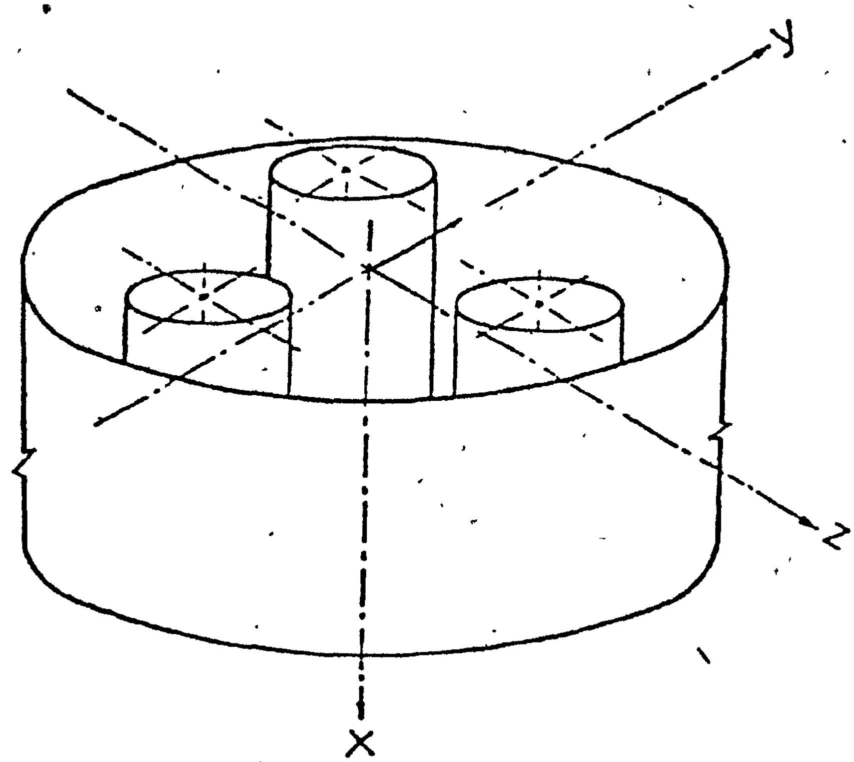

Fig. 2.1: Schematic diagram of the system under consideration.

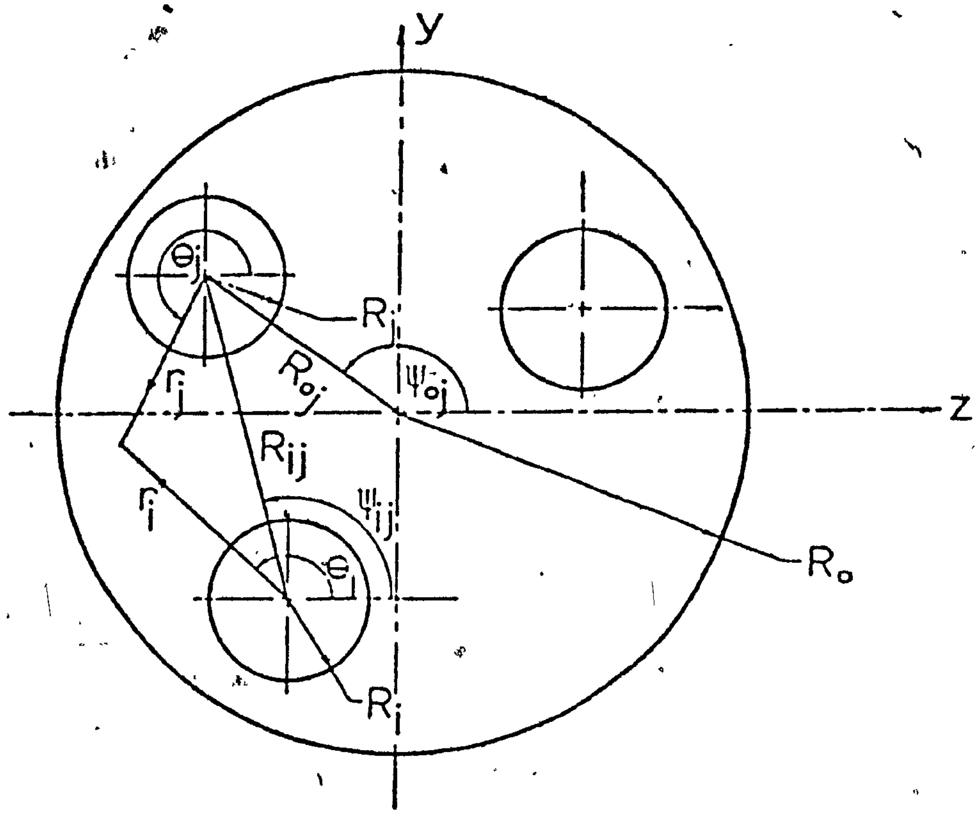

Fig. 2.2: Definition of the coordinate systems and symbols used for determination of the fluid velocity potential.

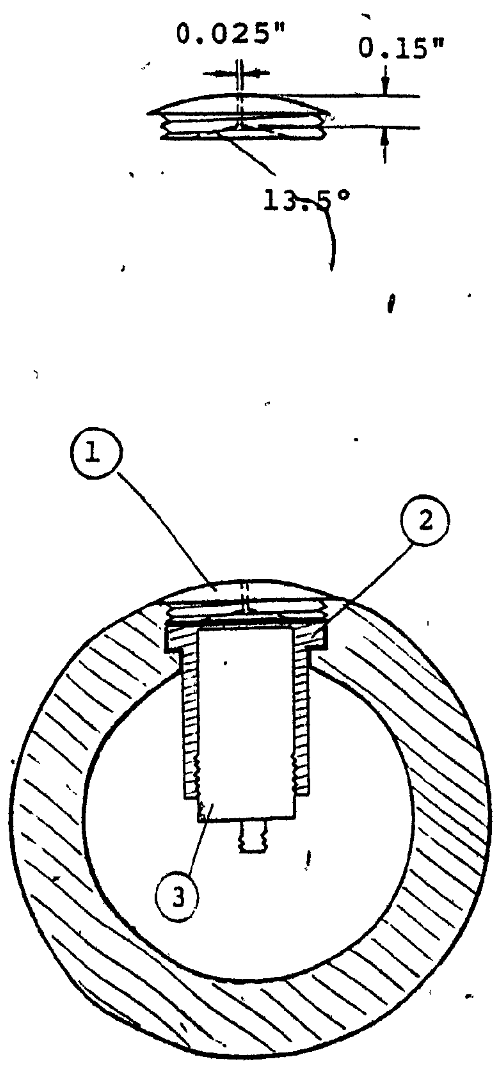

Lock nut detail

1. Lock nut.
2. Bushing for the pressure transducer.
3. Pressure transducer.

$$\frac{\text{Depth of the hole}}{\text{Diameter of the hole}} = \frac{0.15''}{0.025''}$$

$$= 6$$

Fig. 4.1: Cross-sectional view of the cylinder with pressure transducer.

SETUP STATE

MEASUREMENT : TRANSFER FUNCTION

AVERAGE : 1000 , STABLE

SIGNAL : SINUSOIDAL

TRIGGER : FREE RUN , CHNL 1

CENT FREQ : 0.0 HZ

BANDWIDTH : 400.000 HZ

TIME LENGTH : 640.000 mS

ΔF : 1.56250 HZ   ΔT : 625.000 µS

ADC CHNL	RANGE	AC/DC	DELAY	CAL (C1/C2)
* 1	10 V	AC	0.0 S	1.00000
* 2	10 V	AC	0.0 S	1.00000

Fig. 4.2: Setup state of the Digital Signal Analyzer for the phase angle measurements.

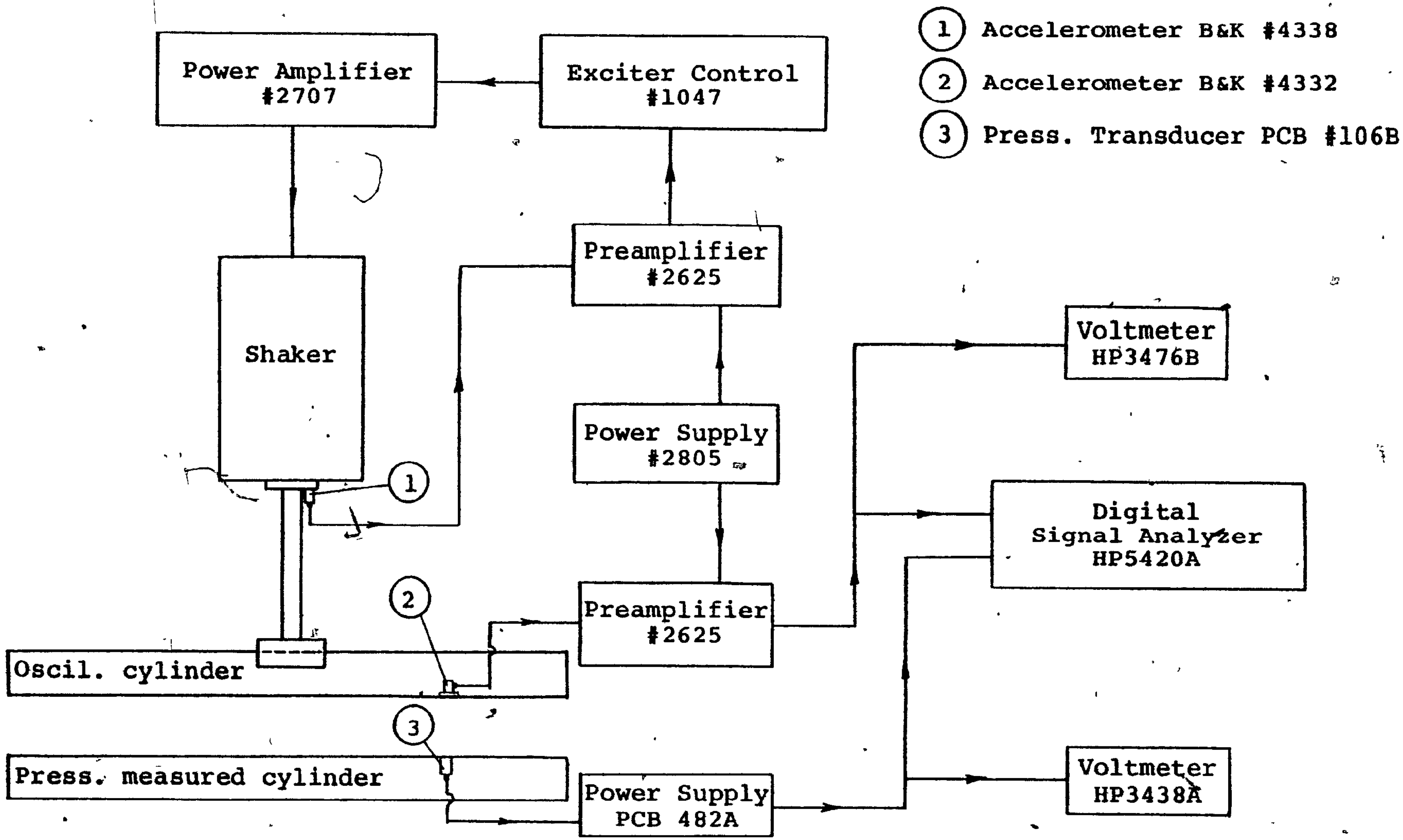

Fig. 4.3: Flow diagram of the experiment setup.

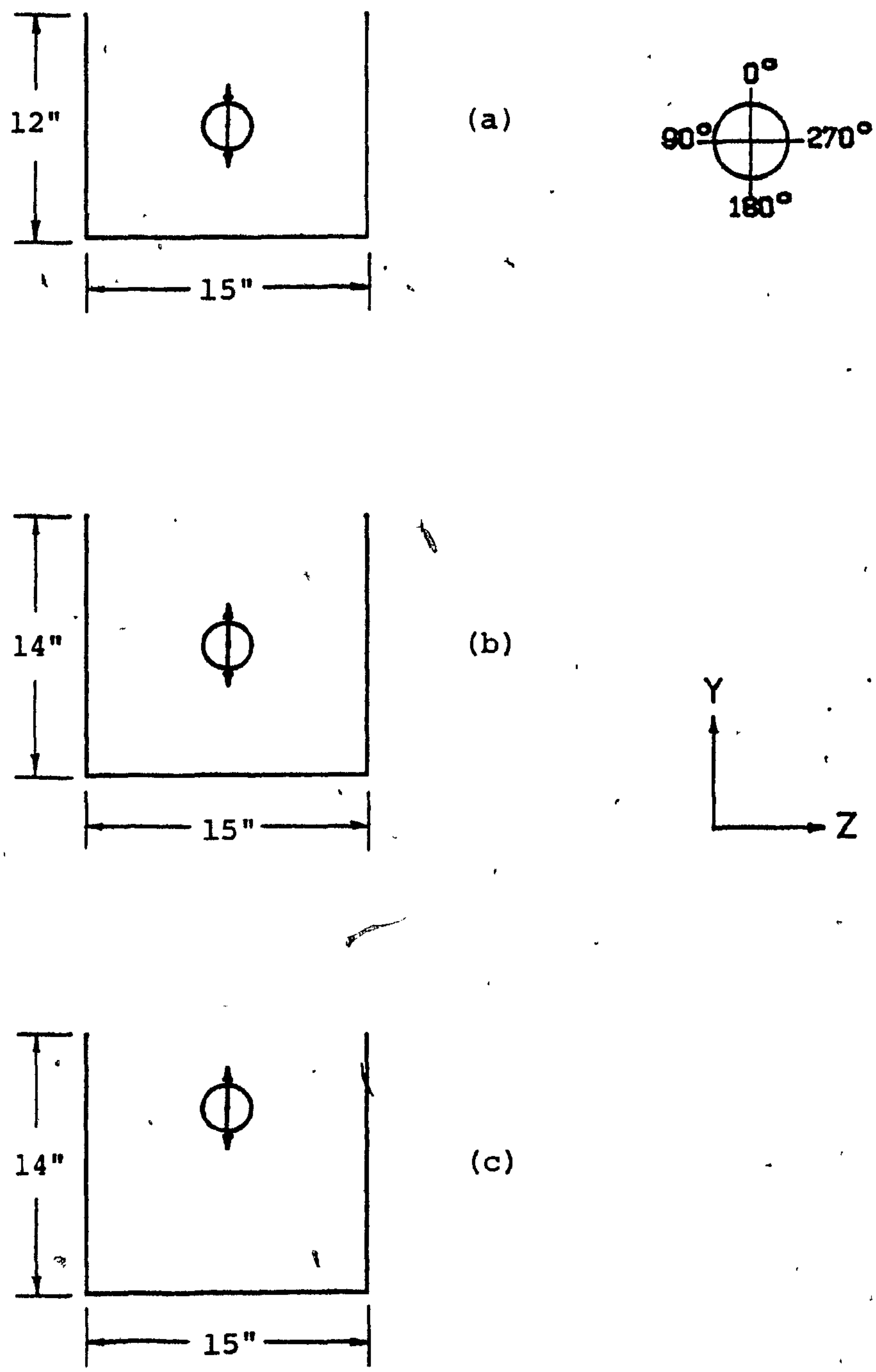

Fig. 4.4: Configurations of a single cylinder in the rectangular tank. The cylinder is centrally located in the Z-direction and is 15.24 cm (6 in.) 17.78 cm (7 in.) and 22.86 cm (9 in.) above the bottom of the tank for (a), (b) and (c), respectively. (Scale 1:10).

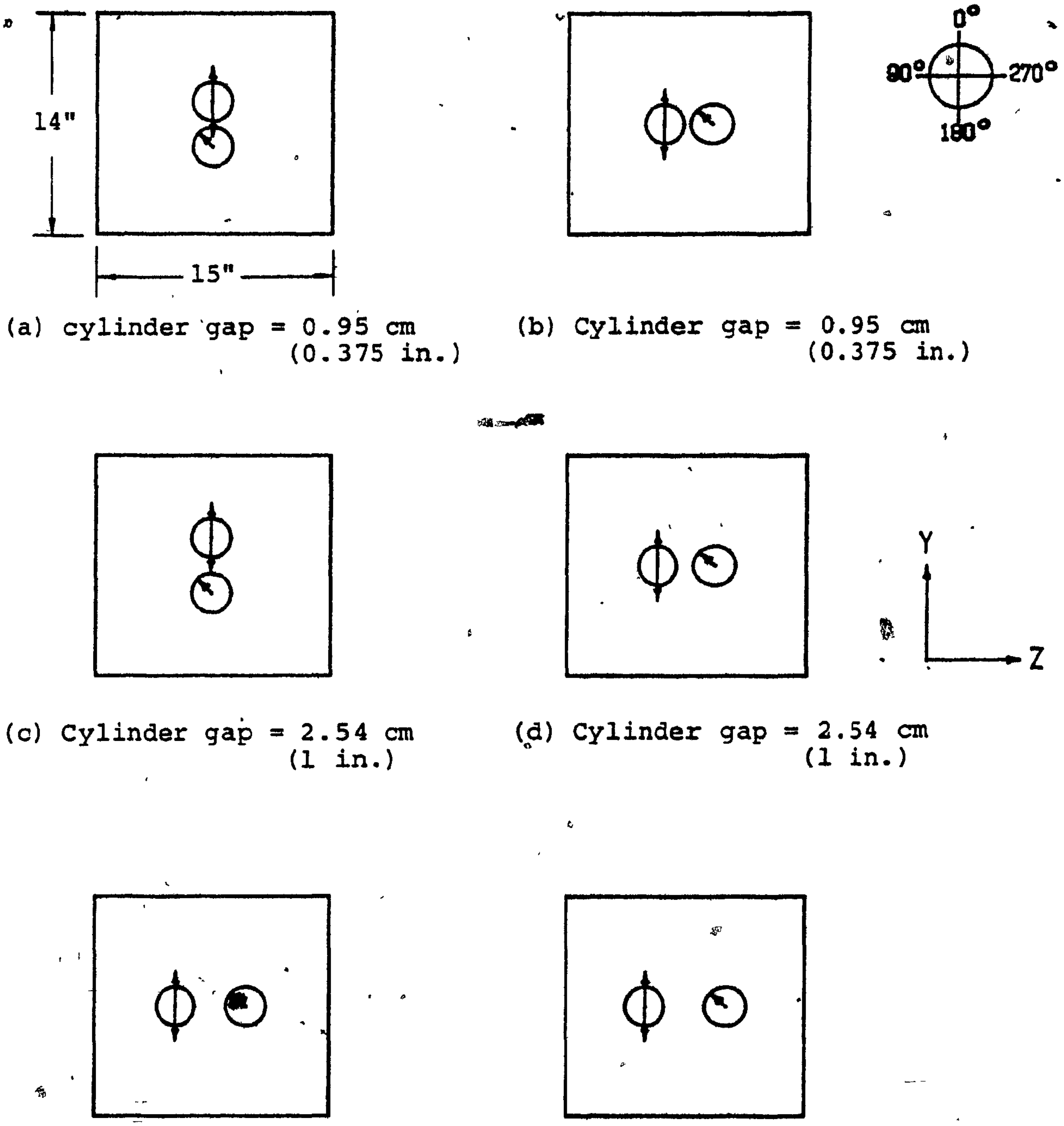

(a) cylinder gap = 0.95 cm (0.375 in.)

(b) Cylinder gap = 0.95 cm (0.375 in.)

(c) Cylinder gap = 2.54 cm (1 in.)

(d) Cylinder gap = 2.54 cm (1 in.)

(e) Cylinder gap = 5.08 cm (2 in.)

(f) Cylinder gap = 6.35 cm (2.5 in.)

Fig. 4.5: Configurations for the two-cylinder clusters considered. The moving cylinder is oscillating in the direction shown by the long arrow, while the cylinder with the inner arrow is the stationary one on which pressure readings were taken. (Scale 1:10).

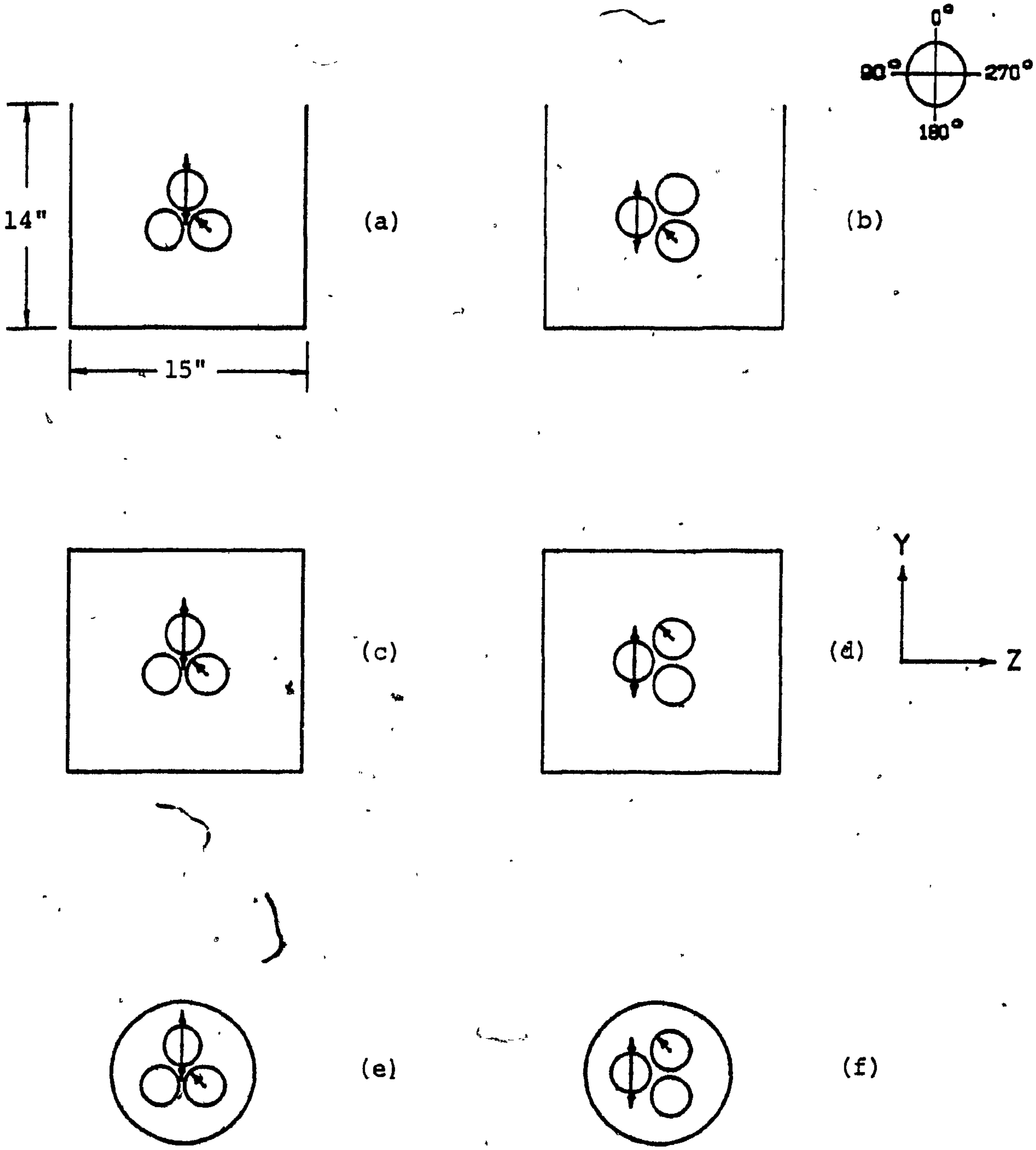

Fig. 4.6: The various configurations for the three-cylinder clusters tested. The cylinders are arranged in equilateral form with a constant inter-cylinder gap of 0.95 cm (0.375 in.). For (e) and (f), the radius of the outer channel is 11.43 cm (4.5 in.). (Scale 1:10).

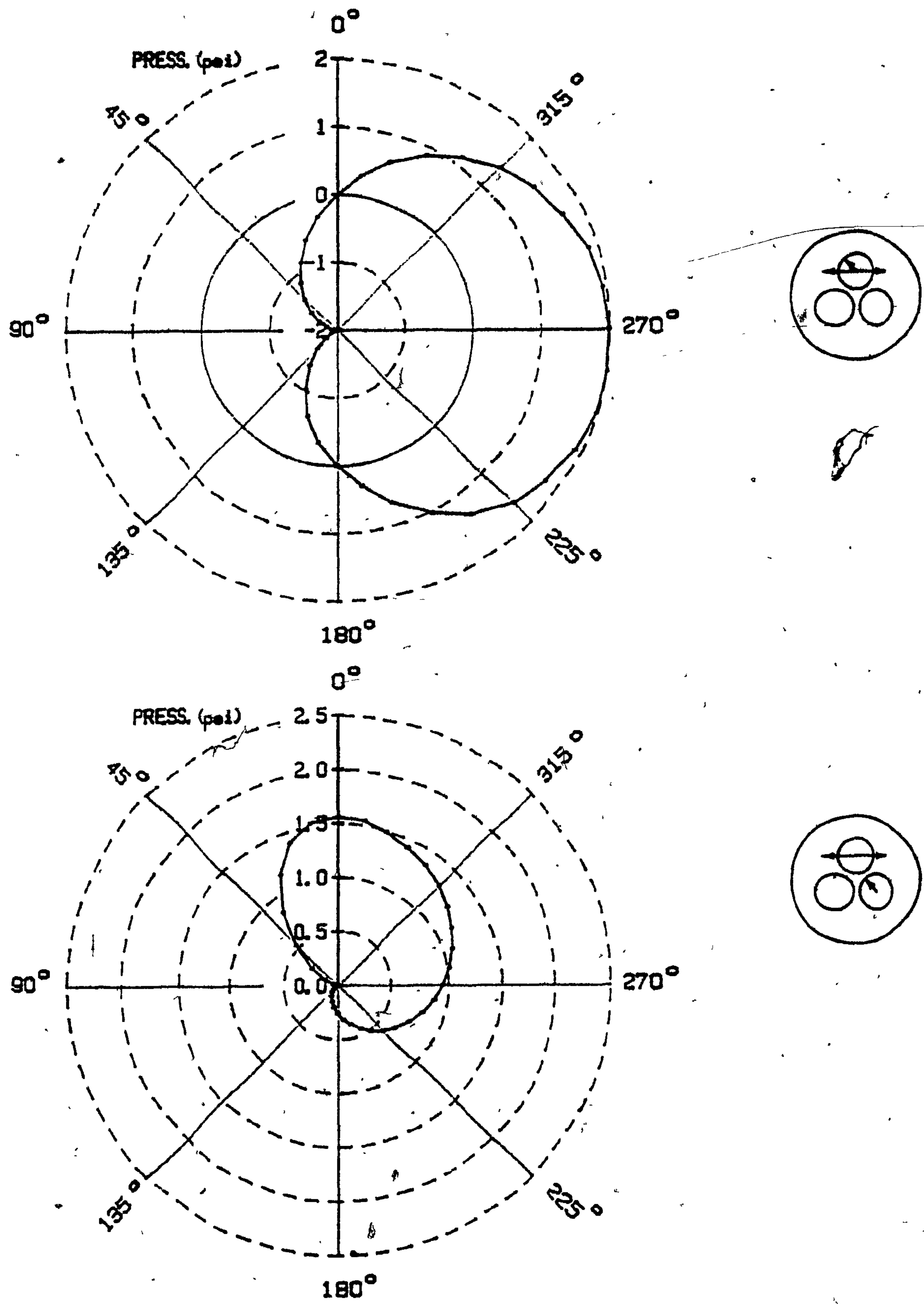

Fig. 5.1: Theoretical pressure profiles of the cylinder (with inner arrow) taken at peak acceleration of the oscillating cylinder (with longer arrow).

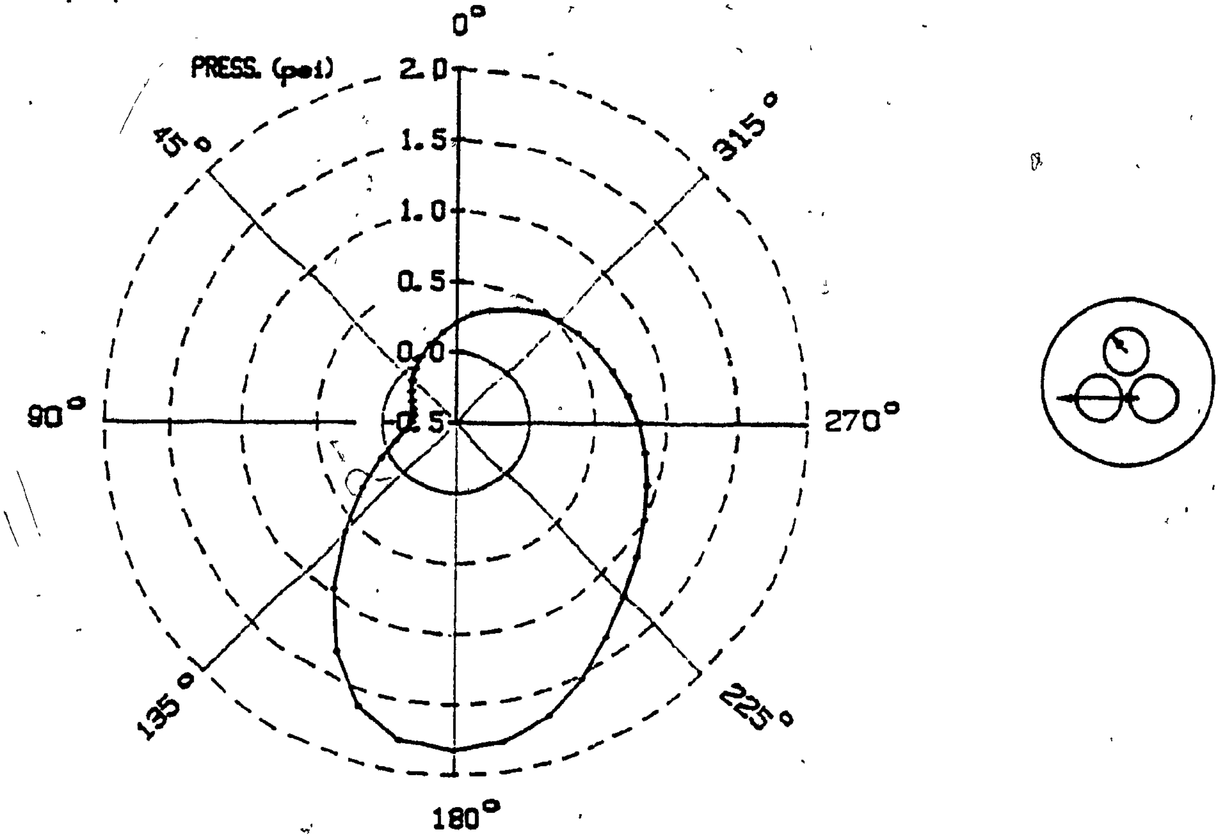

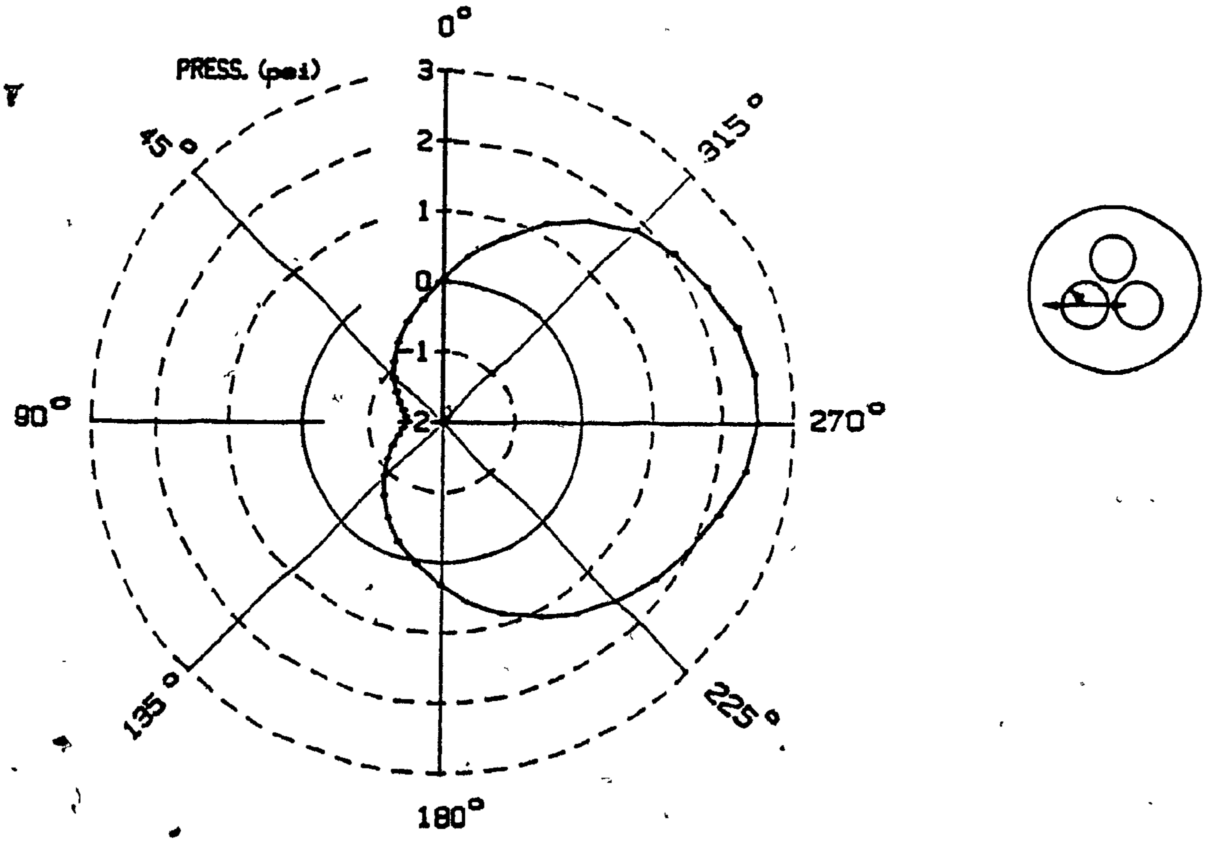

Fig. 5.2: Theoretical pressure profiles of the cylinder (with inner arrow) taken at peak acceleration of the oscillating cylinder (with longer arrow).

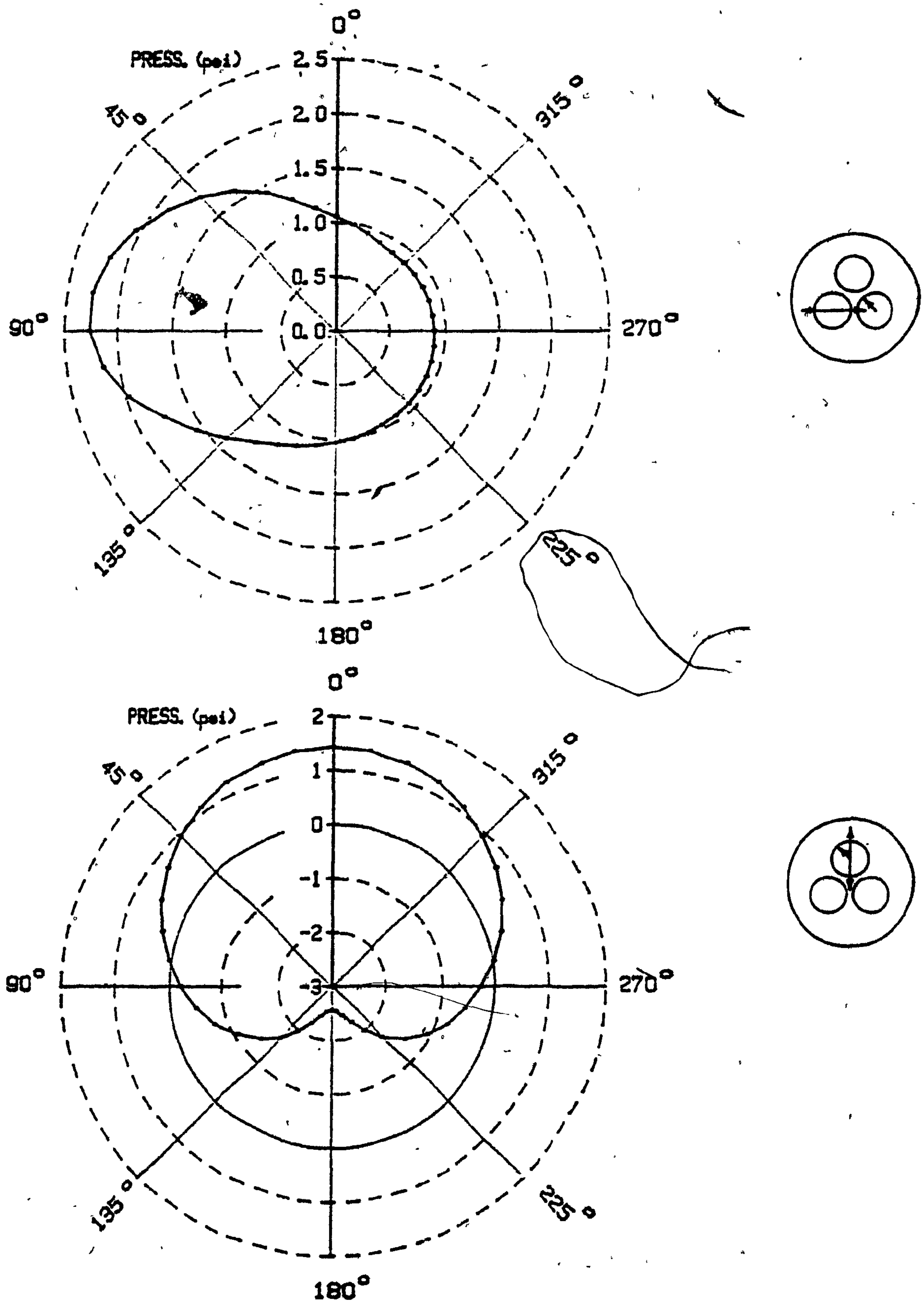

Fig. 5.3: Theoretical pressure profiles of the cylinder (with inner arrow) taken at peak acceleration of the oscillating cylinder (with longer arrow).

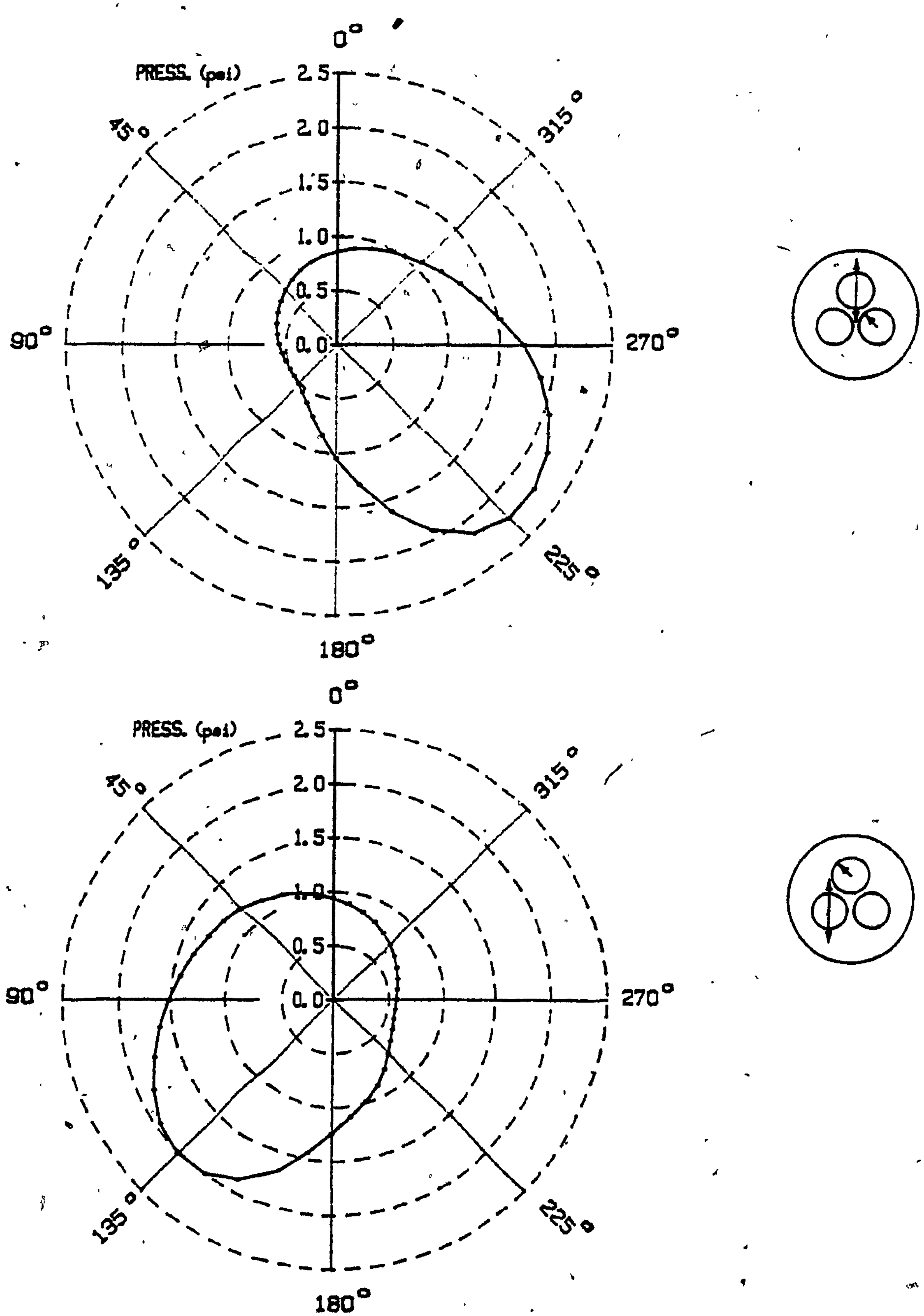

Fig. 5.4: Theoretical pressure profiles of the cylinder (with inner arrow) taken at peak acceleration of the oscillating cylinder (with longer arrow).

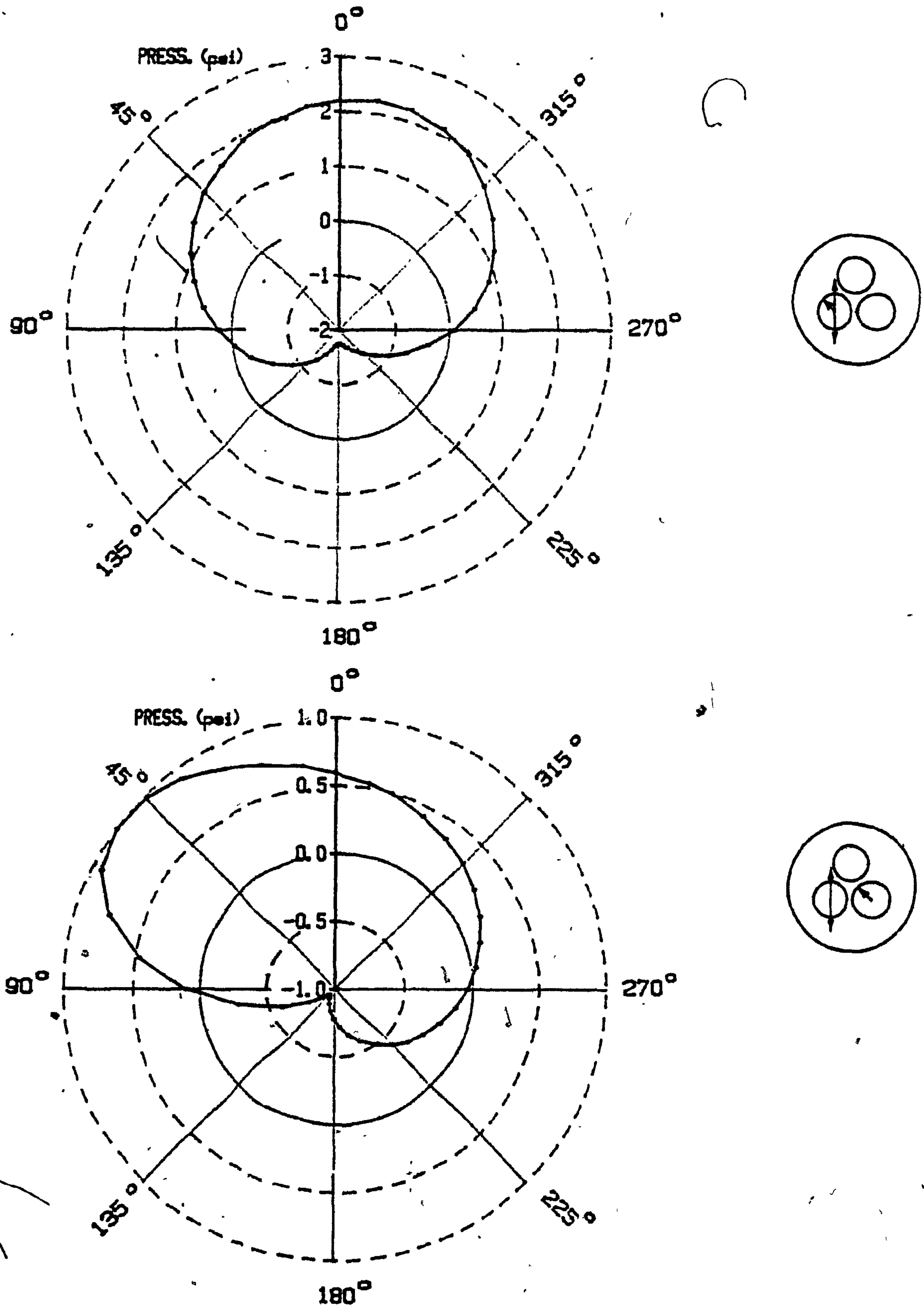

Fig. 5.5: Theoretical pressure profiles of the cylinder (with inner arrow) taken at peak acceleration of the oscillating cylinder (with longer arrow).

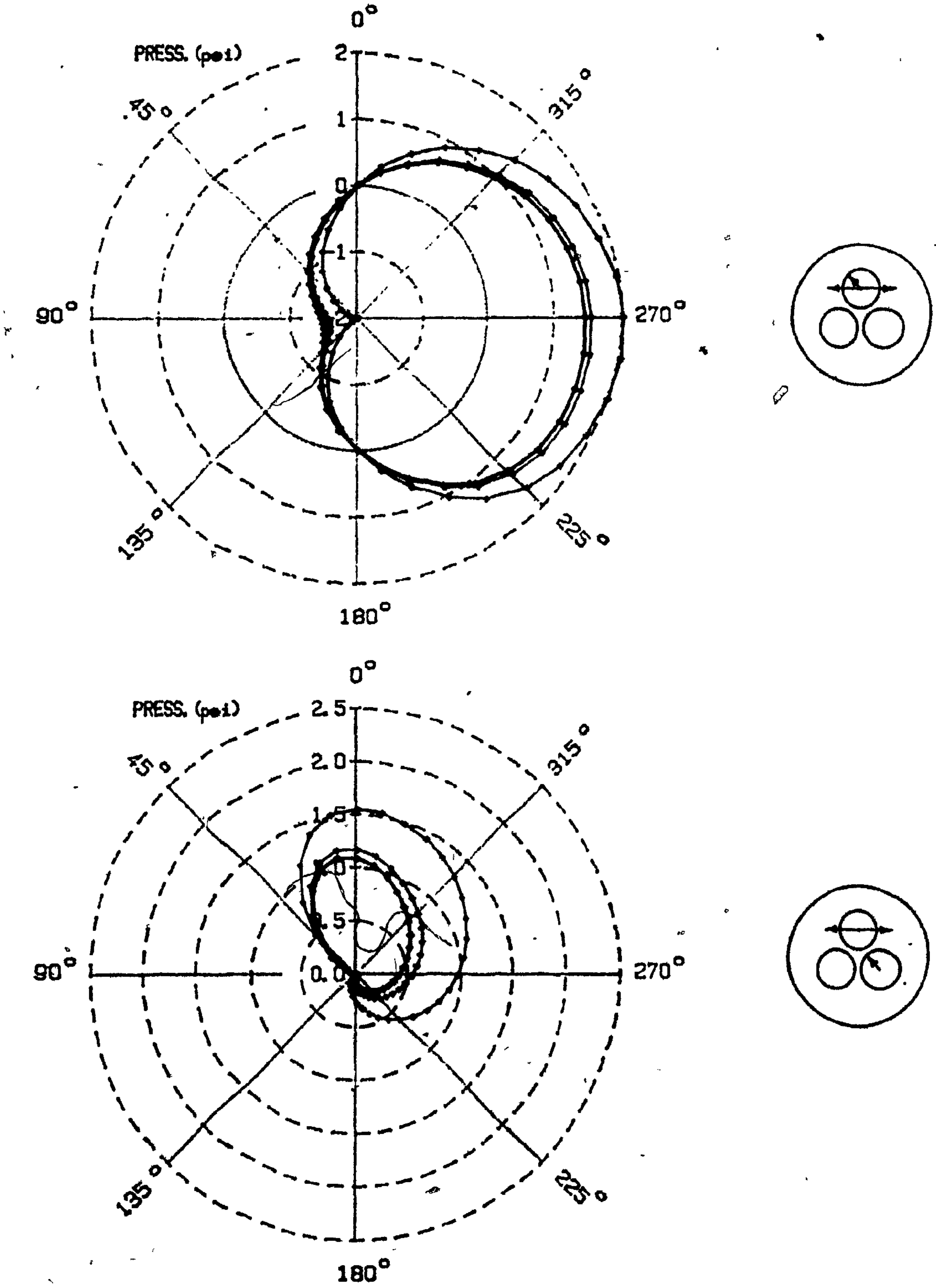

<u>Fig. 5.6</u>: Theoretical pressure profiles of the cylinder (with inner arrow) for R_o (radius of the outer shell) = 11.43 cm (4.5 in.), 23.37 cm (9.2 in.) and 25,400 cm (10,000 in.) using black, red and blue colours, respectively.

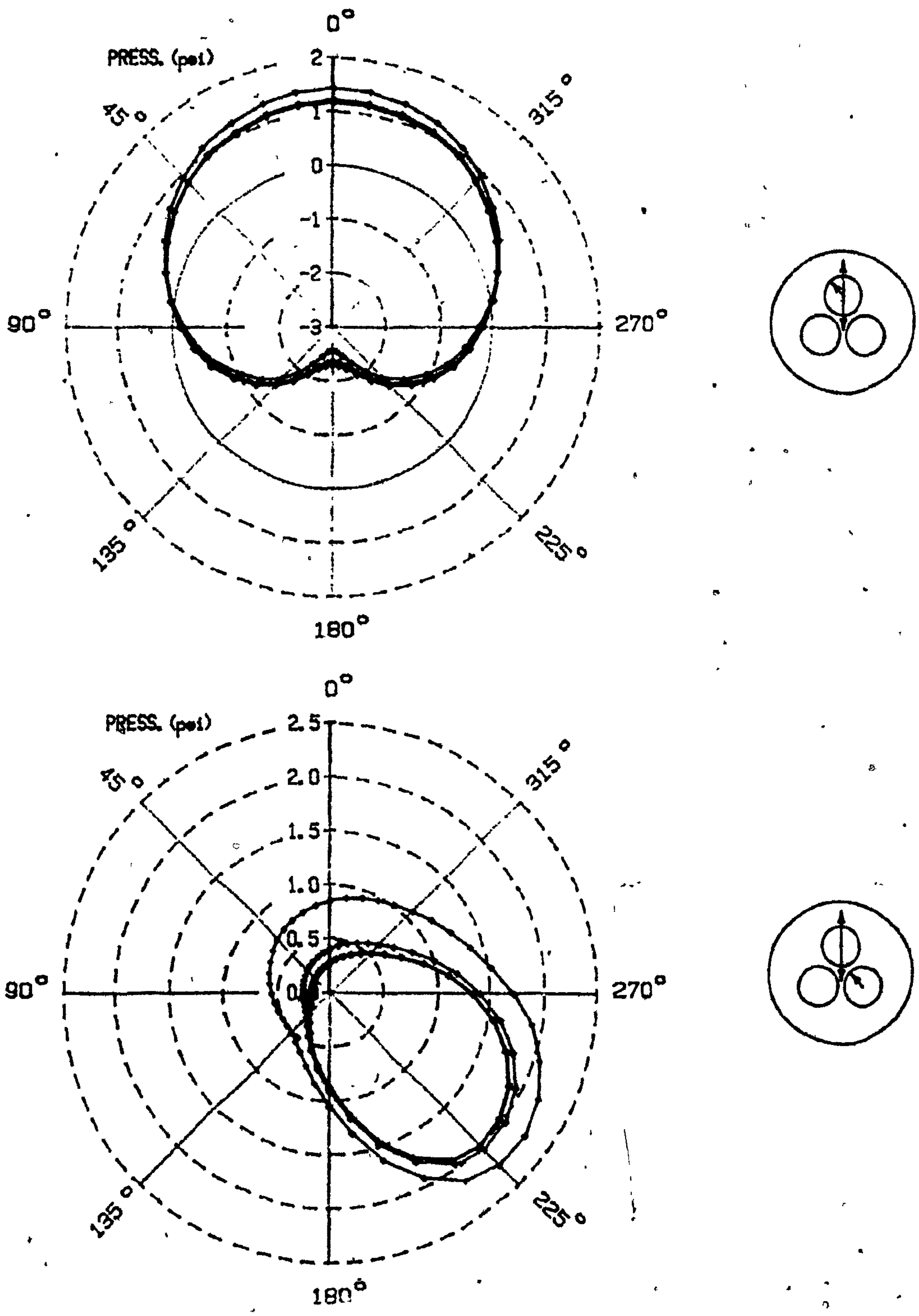

Fig. 5.7: Theoretical pressure profiles of the cylinder with inner arrow) for R_o(radius of the outer shell) = 11.43 cm (4.5 in.), 23.37 cm (9.2 in.) and 25,400 cm (10,000 in.) using black, red and blue colours, respectively.

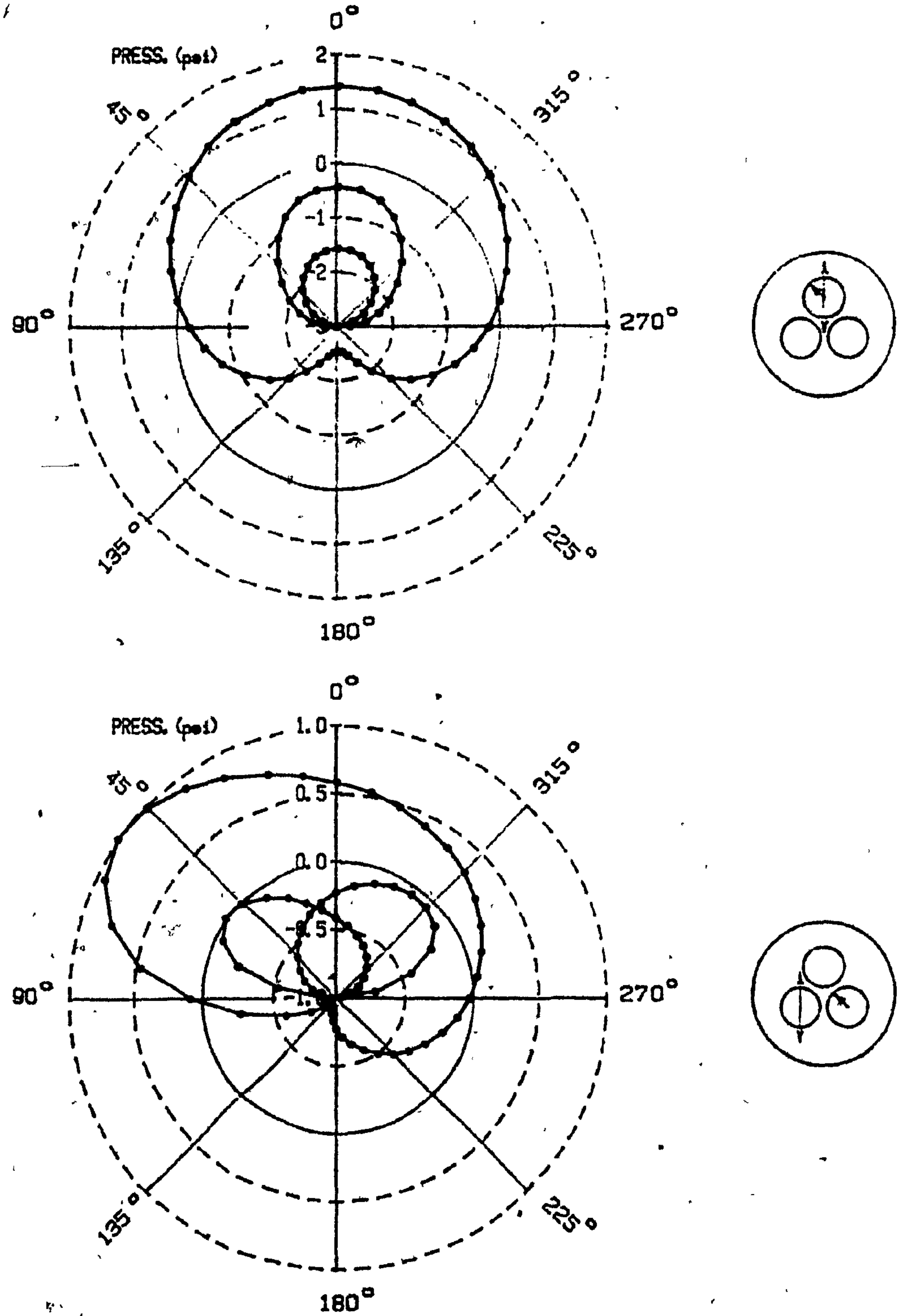

Fig. 5.8: Examples of pressure profiles plotted in two different polar coordinates.

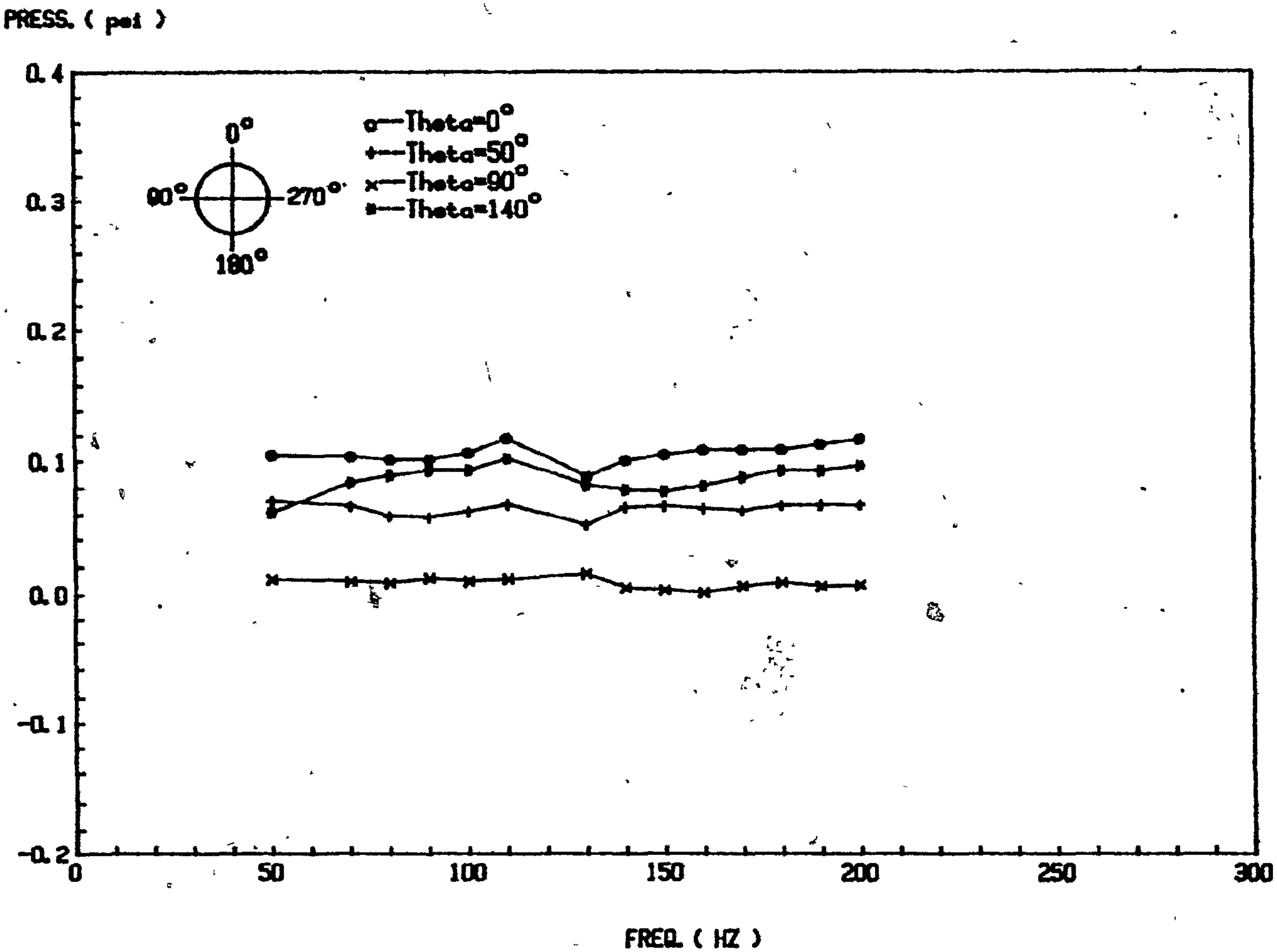

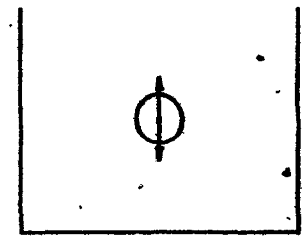

(Configuration of
Fig. 4.4a)

<u>Fig. 6.1</u>: Pressure *versus* frequency curves measured at θ = 0°, 50°, 90° and 140° for the configuration shown.

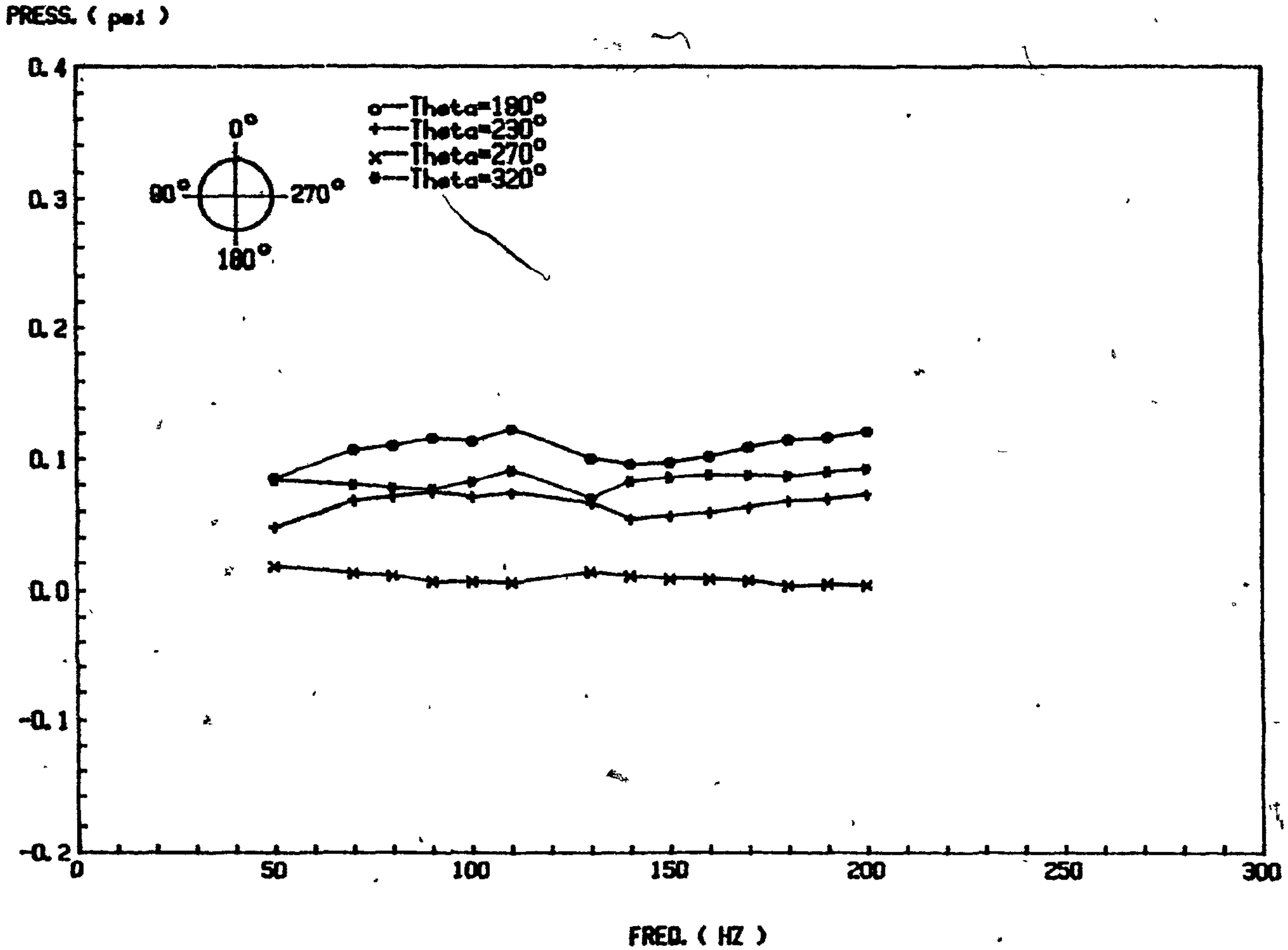

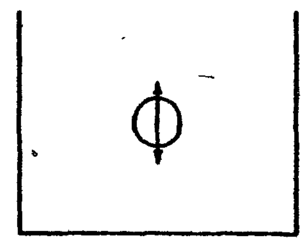

(Configuration of Fig. 4.4a)

<u>Fig. 6.2</u>: Pressure *versus* frequency curves measured at θ = 180°, 230°, 270° and 320° for the configuration shown.

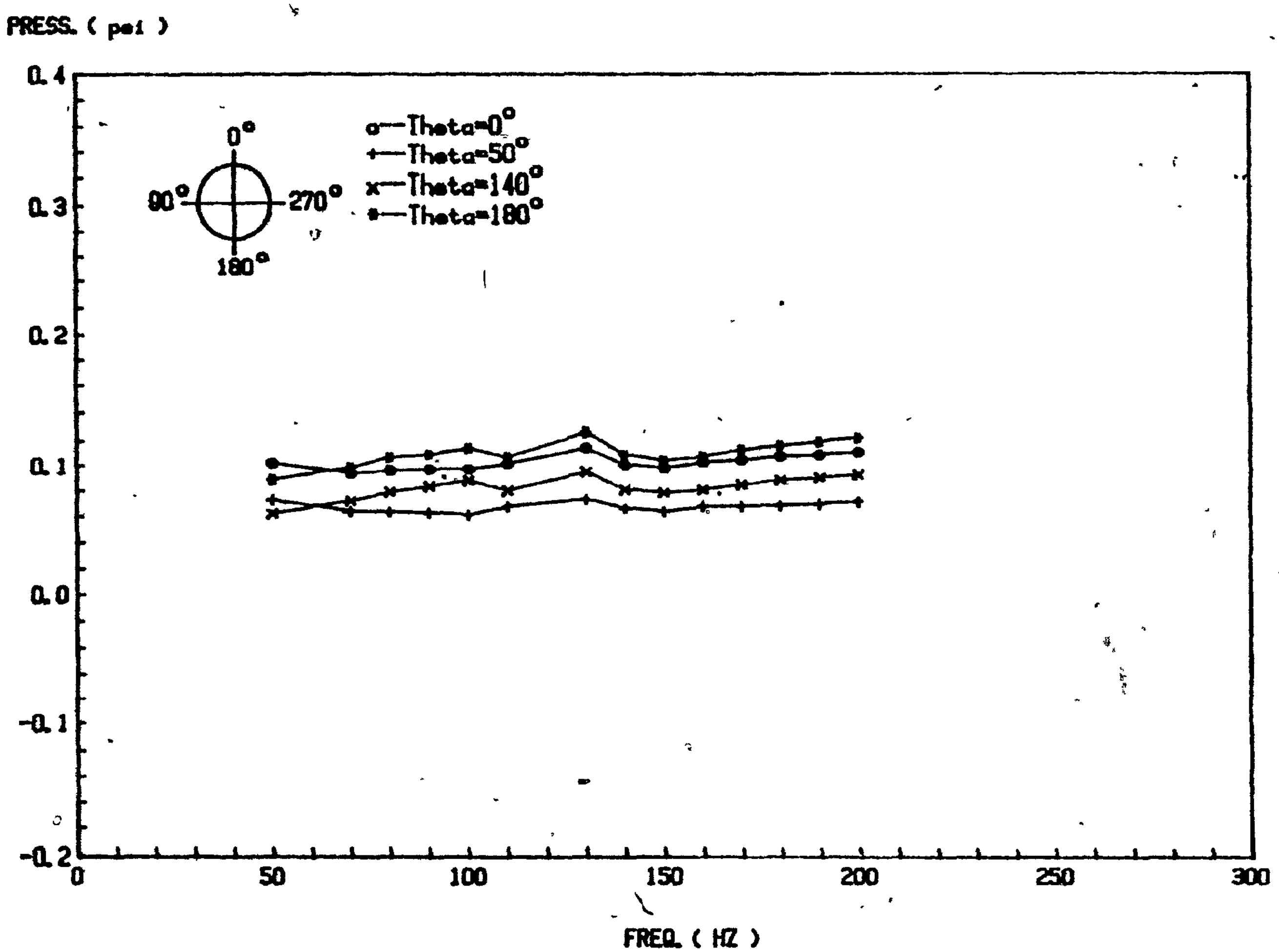

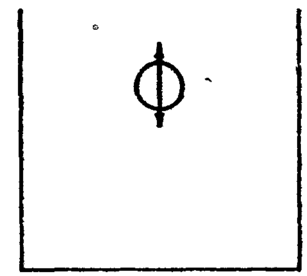

(Configuration of Fig. 4.4c)

Fig. 6.3: Pressure *versus* frequency curves measured at various θ for the configuration shown.

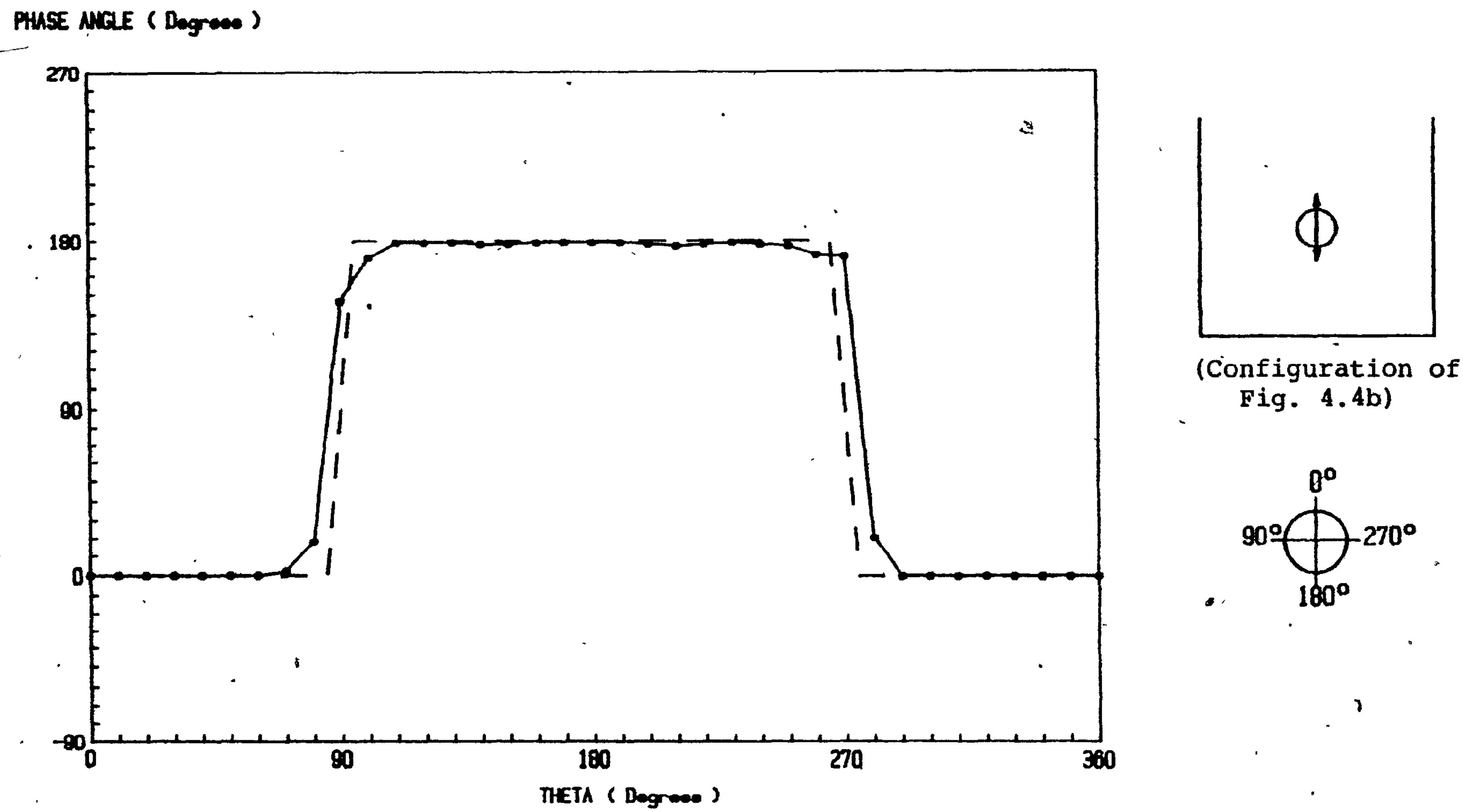

<u>Fig. 6.4</u>: The experimental distribution of phase angles around the surface of the oscillating cylinder (oscillating frequency = 180 Hz) is shown by a solid line, whereas the dashed line represents the distribution predicted by the Inviscid Theory.

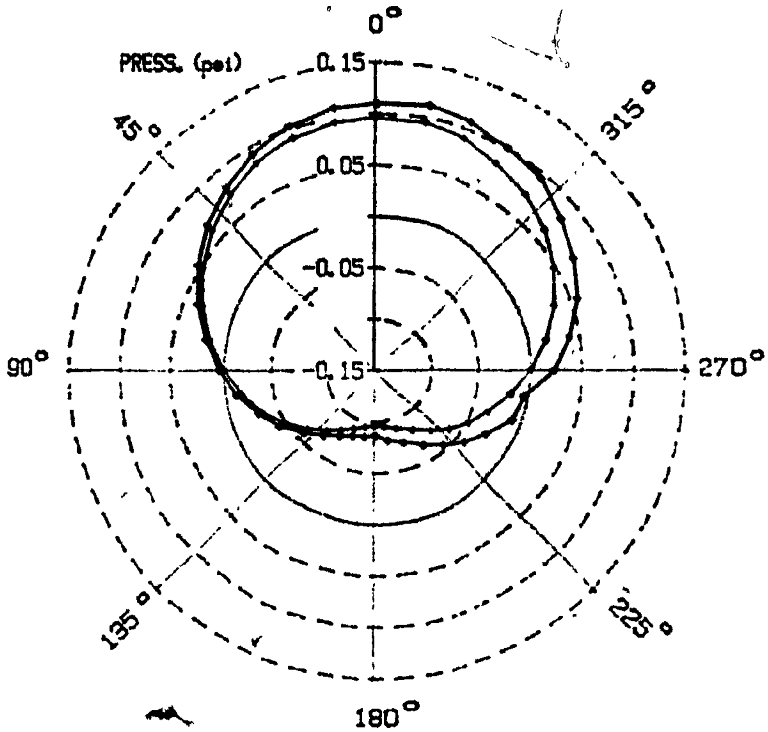

(a)

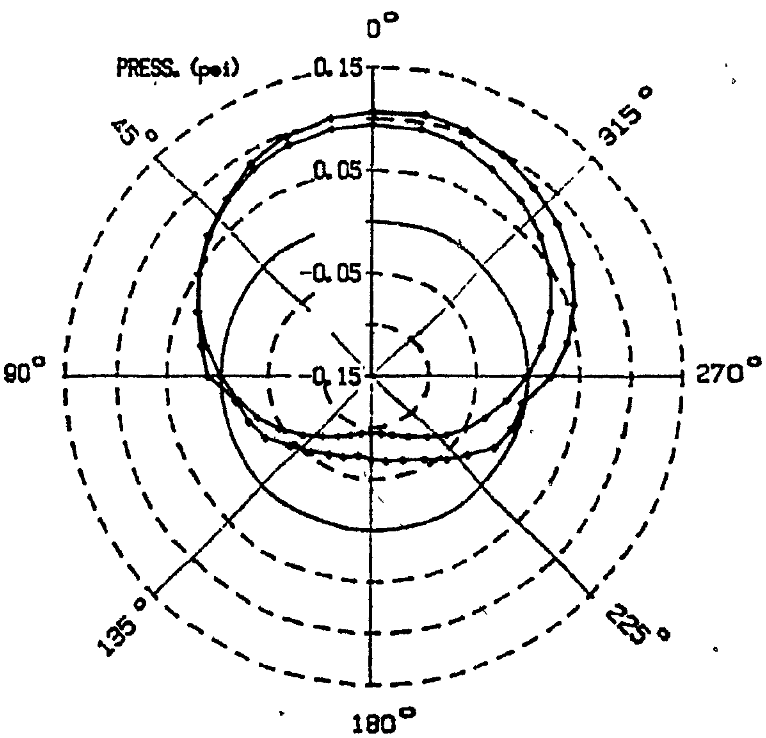

(b)

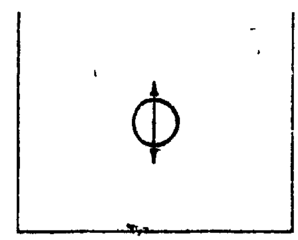

(Configuration of Fig. 4.4a)

Fig. 6.5: Experimental pressure profiles (red) of a single cylinder oscillated at different frequencies and accelerations. (a) Freq. = 30 Hz, Ac = 1.96 g; (b) Freq. = 40 Hz, Ac = 1.94 g. Theoretical profiles (black) were added for comparison.

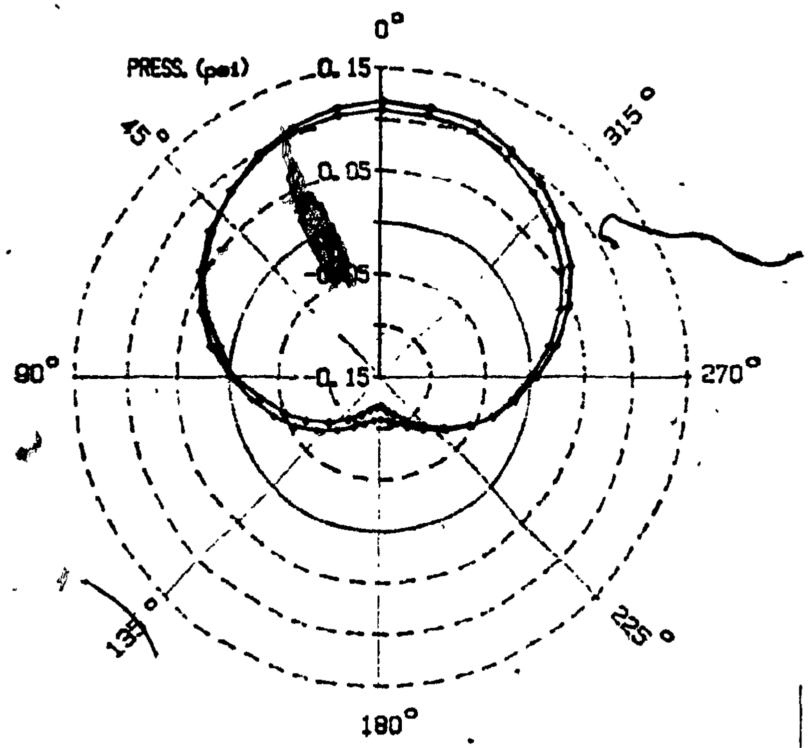

(a)

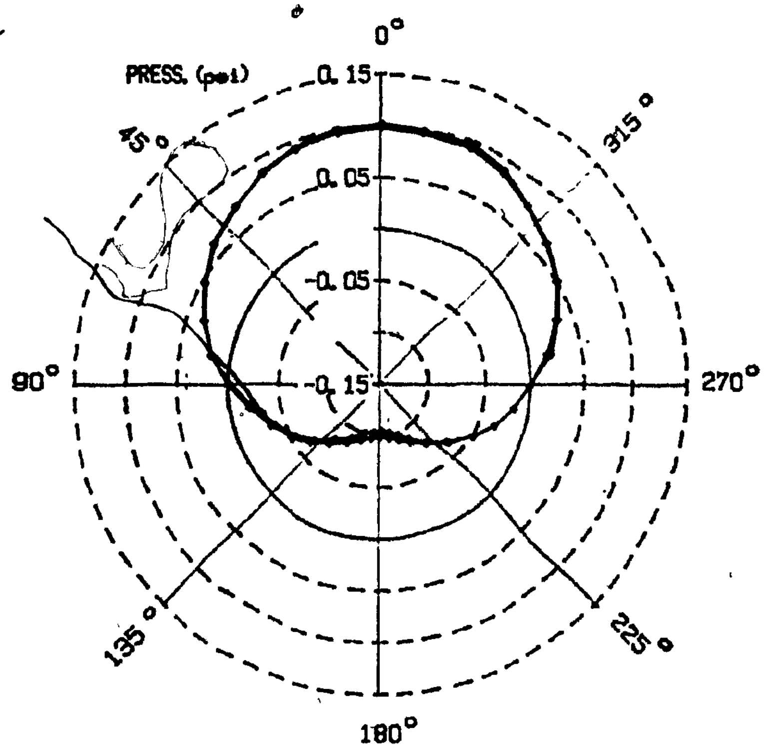

(b)

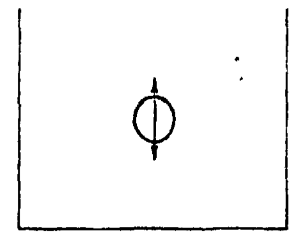

(Configuration of Fig. 4.4a)

Fig. 6.6: Experimental pressure profiles (red) of a single cylinder oscillated at different frequencies and accelerations. (a) Freq. = 200 Hz, Ac = 2.22 g; (b) Freq. = 70 Hz, Ac = 2.02 g. Theoretical profiles (black) were added for comparison.

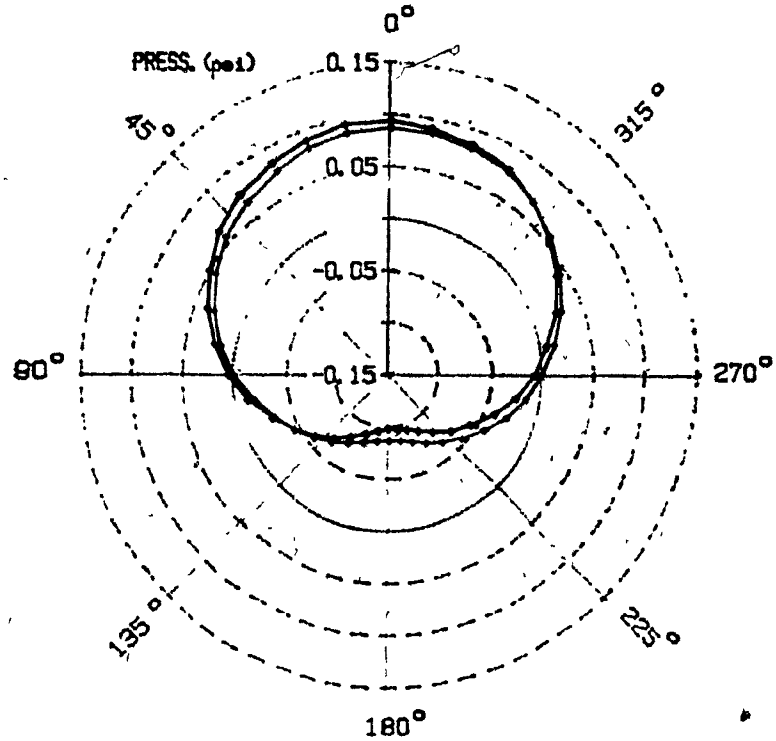

(a)

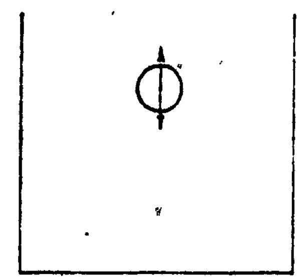

(Configuration of
Fig. 4.4c)

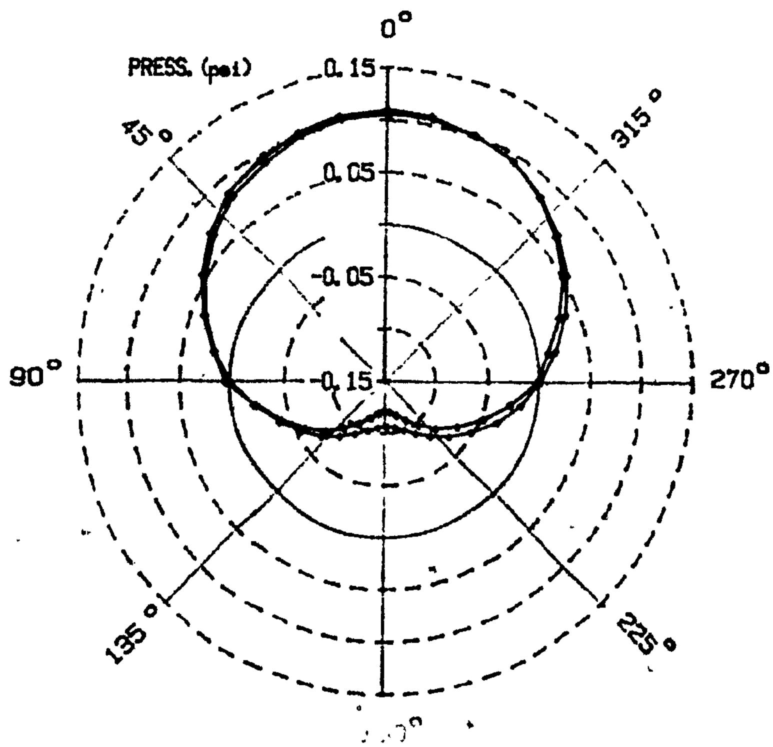

(b)

Fig. 6.7: Experimental pressure profiles (red) of a single cylinder oscillated at different frequencies and accelerations. (a) Freq. = 70 Hz, Ac = 1.80 g; (b) Freq. = 200 Hz, Ac = 2.22 g. Theoretical profiles (black) were added for comparison.

(a)

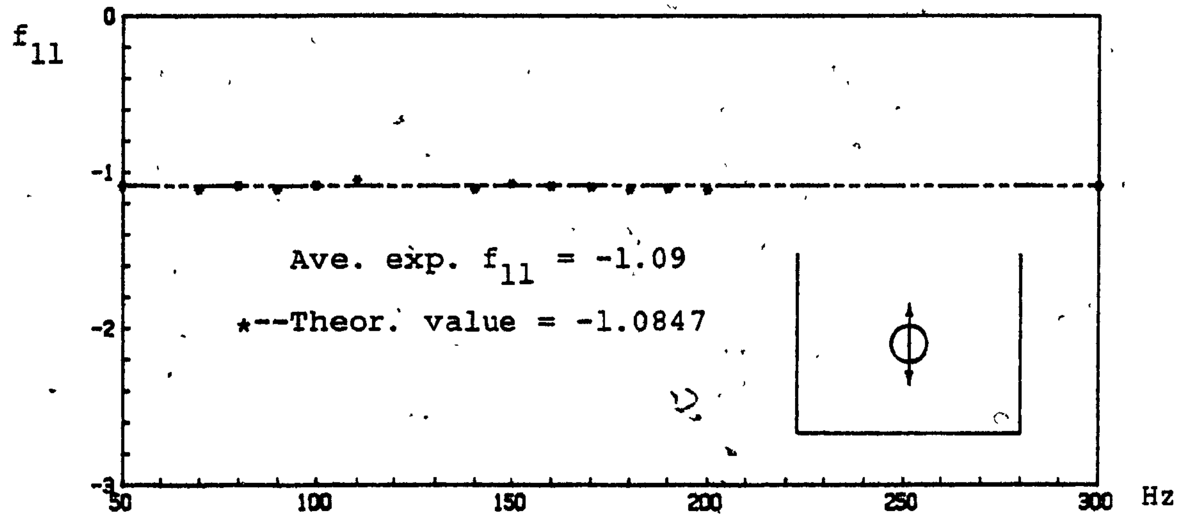

(b)

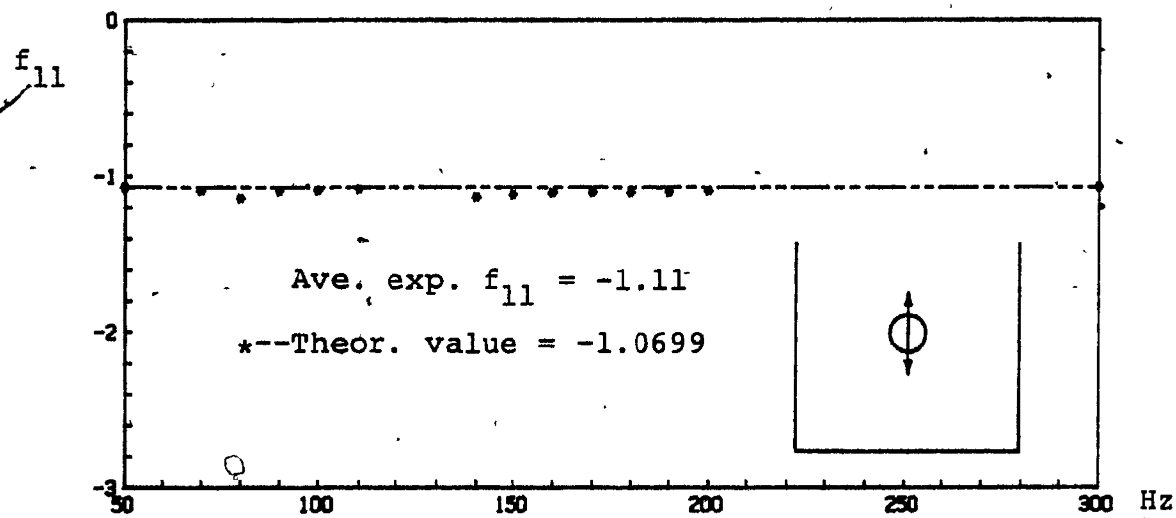

(c)

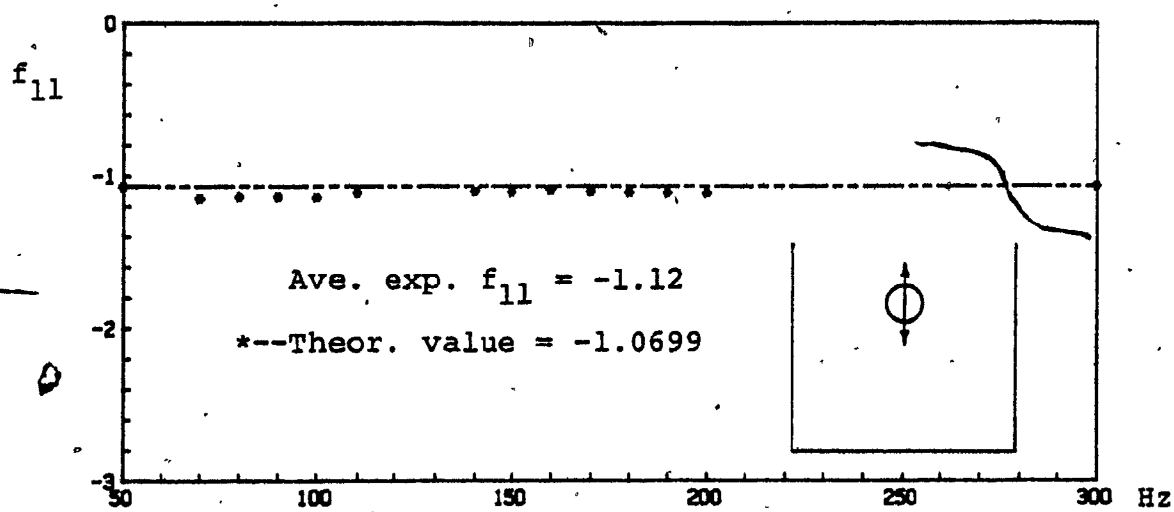

Fig. 6.8: Experimental added mass coefficients, f_{11}, *versus* frequency diagrams. (a) Average discrepancy = 0.8%, (b) Average discrepancy = 3.3%, (c) Average discrepancy = 4.4%.

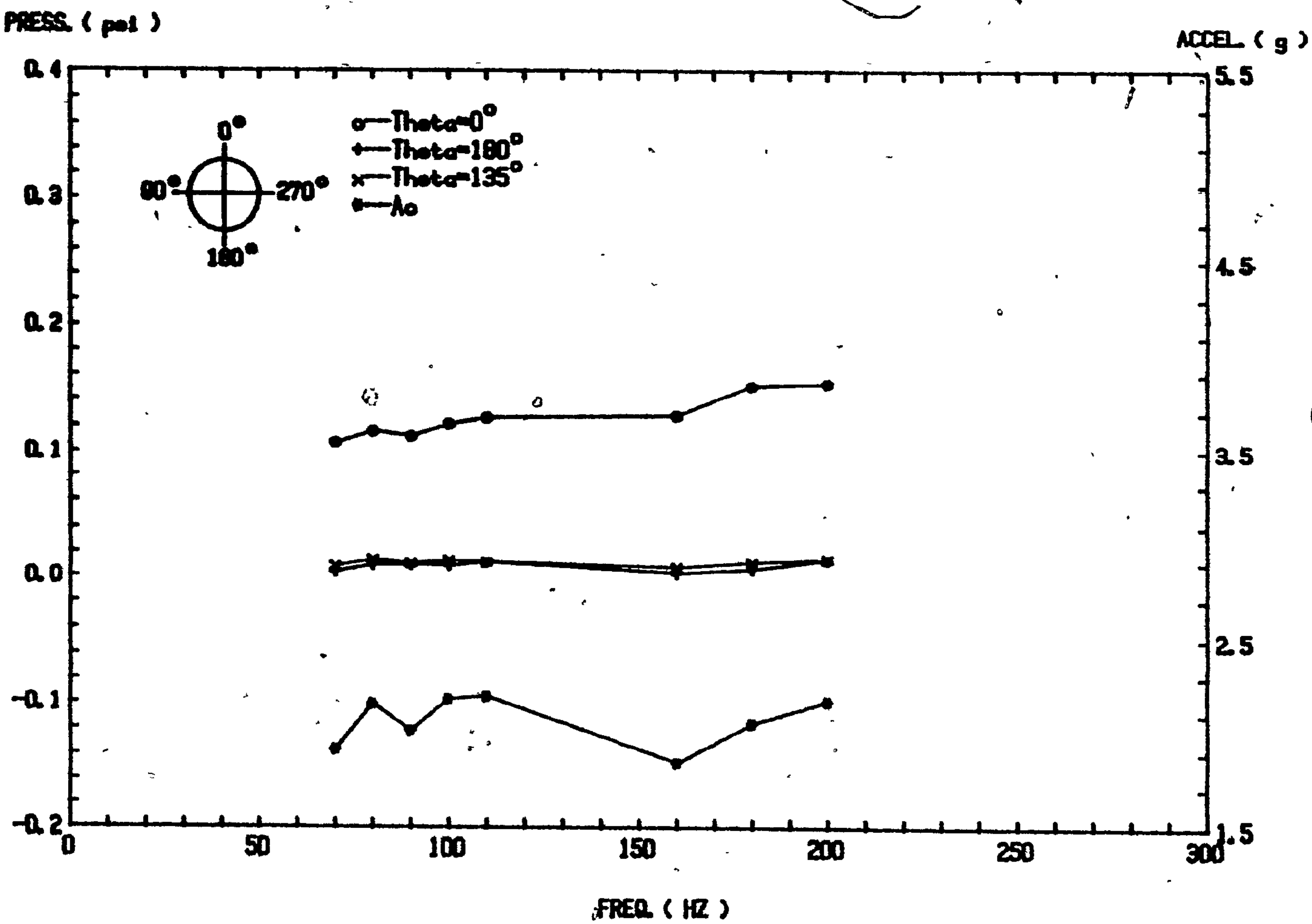

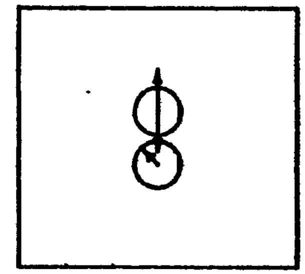

(Configuration of
Fig. 4.5a)

Fig. 6.9: Pressure *versus* frequency curves measured on the stationary cylinder (with small inner arrow) for various θ.

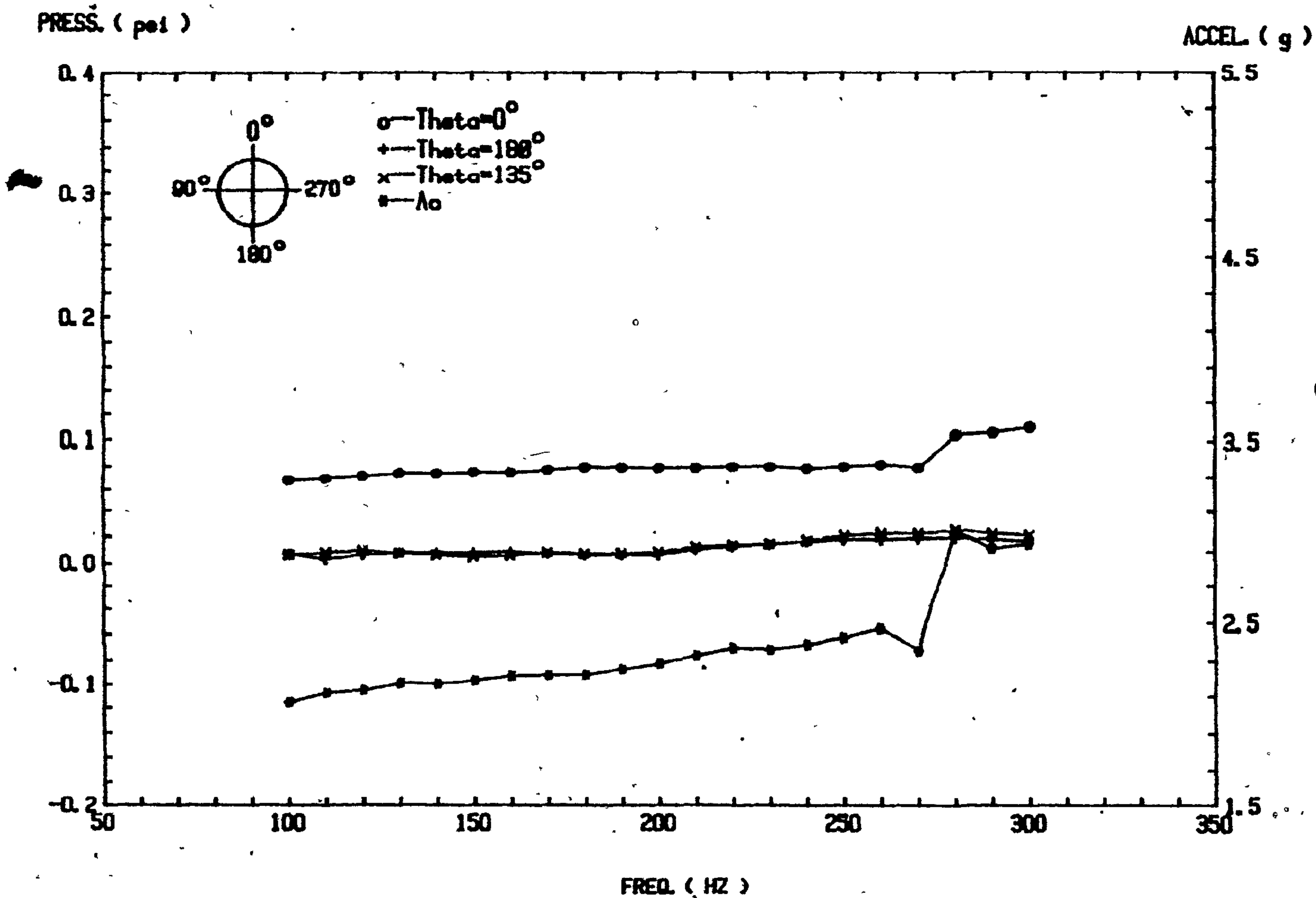

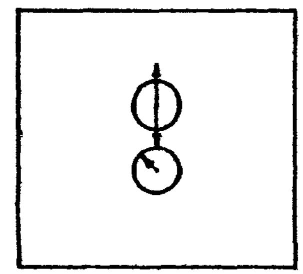

(Configuration of Fig. 4.5c)

Fig. 6.10: Pressure *versus* frequency curves measured on the stationary cylinder (with small inner arrow) for various θ. The test was done after the experimental setup was modified, as described in Section 6.2.

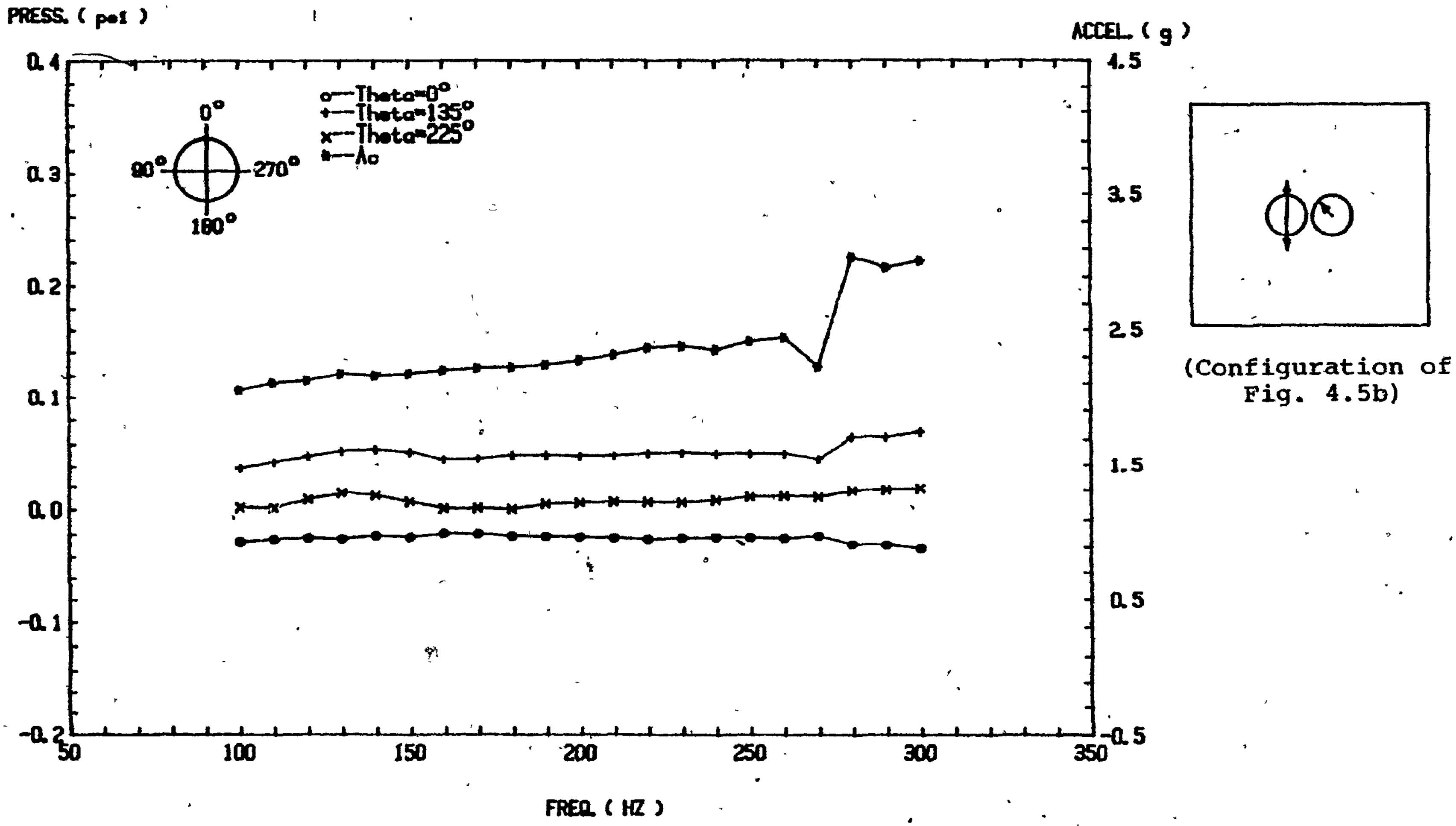

Fig. 6.11: Pressure *versus* frequency curves measured on the stationary cylinder (with small inner arrow) for various θ. The test was done after the experimental setup was modified, as described in Section 6.2.

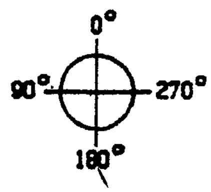

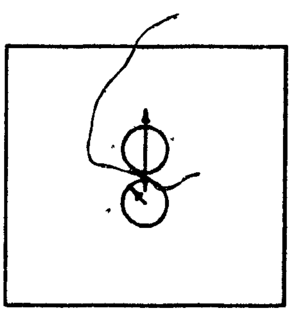

(Configuration of Fig. 4.5a)

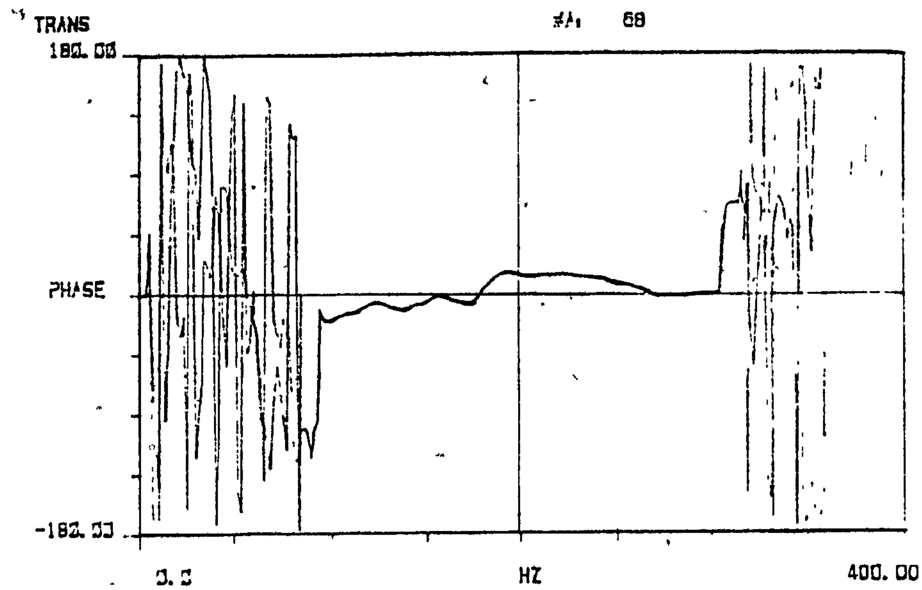

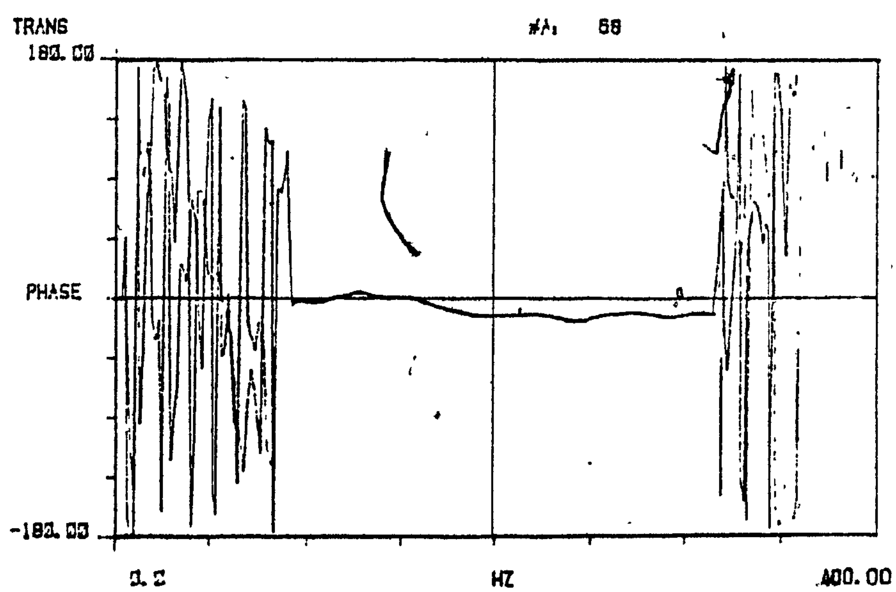

Fig. 6.12: Phase angle *versus* frequency diagrams measured at $\theta = 90°$ and $270°$ for the top and bottom figures, respectively. (Note that the curves are only valid from 100 to 300 Hz).

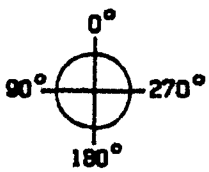

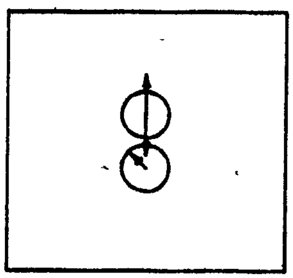

(Configuration of
Fig. 4.5a)

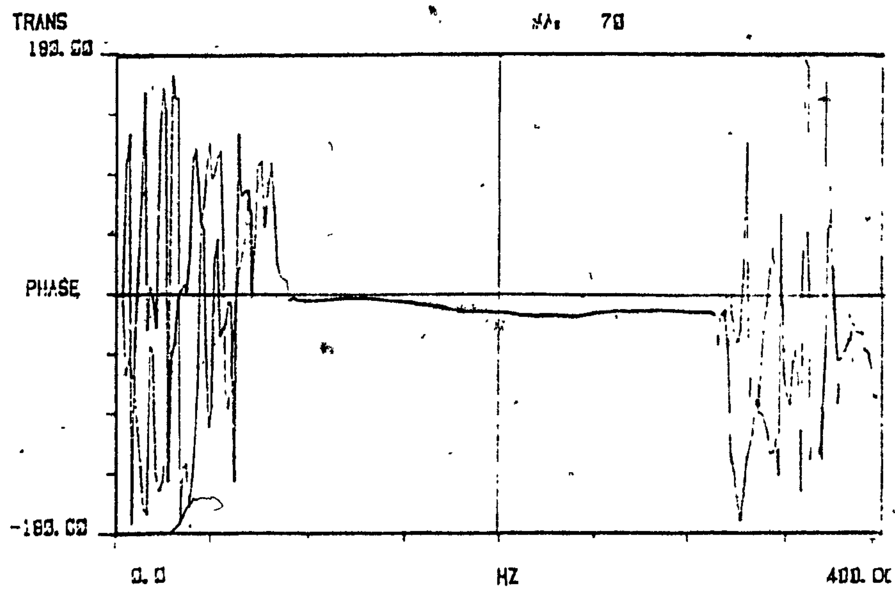

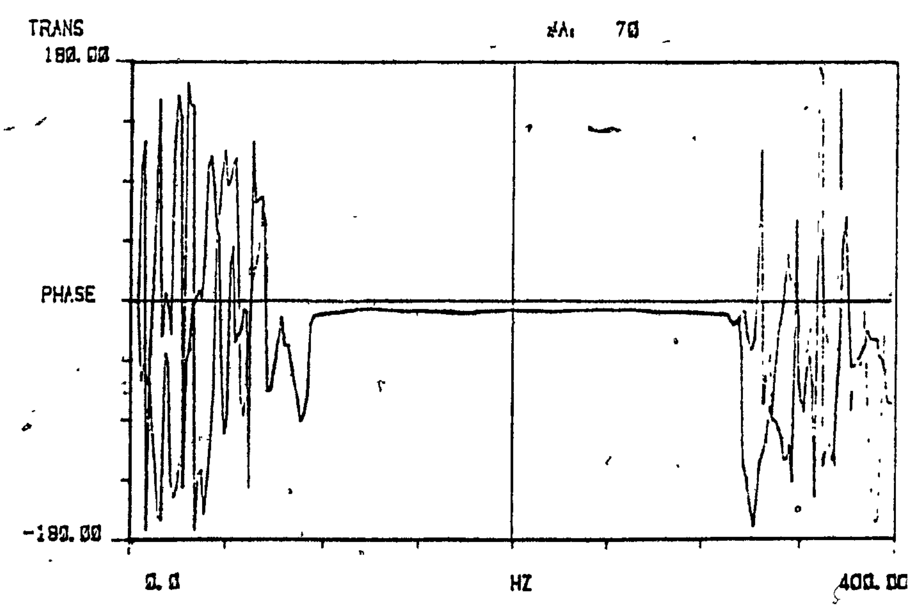

Fig. 6.13: Phase angle *versus* frequency diagrams measured at $\theta = 315°$ and $45°$ for the top and bottom figures, respectively. (Note that the curves are only valid from 100 to 300 Hz).

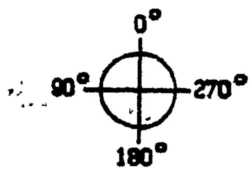

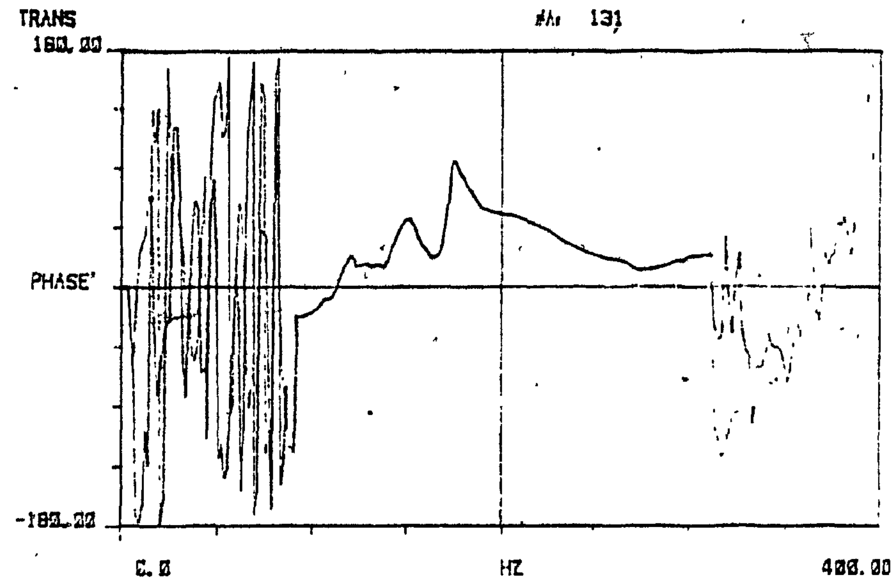

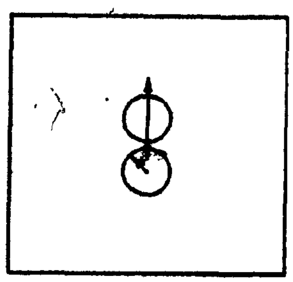

(Configuration of
Fig. 4.5a)

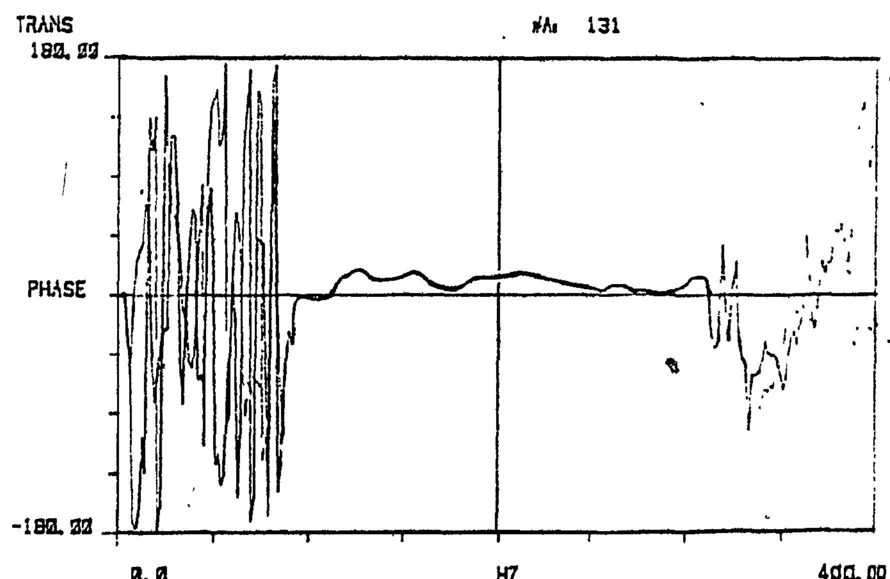

<u>Fig. 6.14:</u> Phase angle *versus* frequency diagrams measured at $\theta = 135°$ and $225°$ for the top and bottom figures, respectively. (Note that the curves are only valid from 100 to 300 Hz).

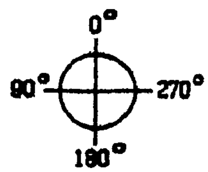

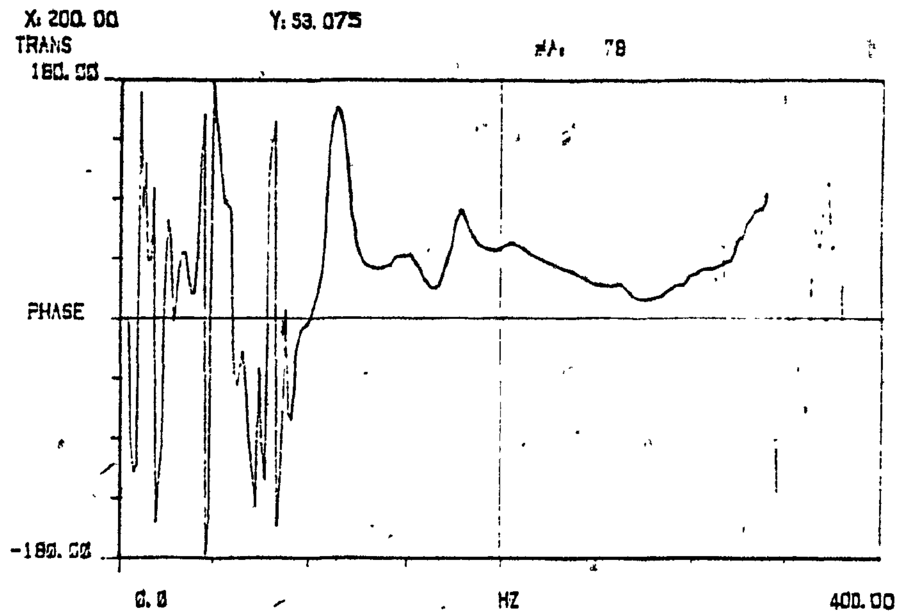

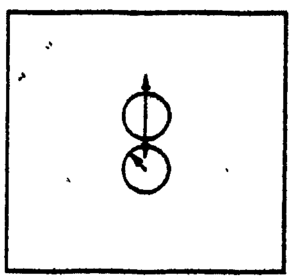

(Configuration of
Fig. 4.5a)

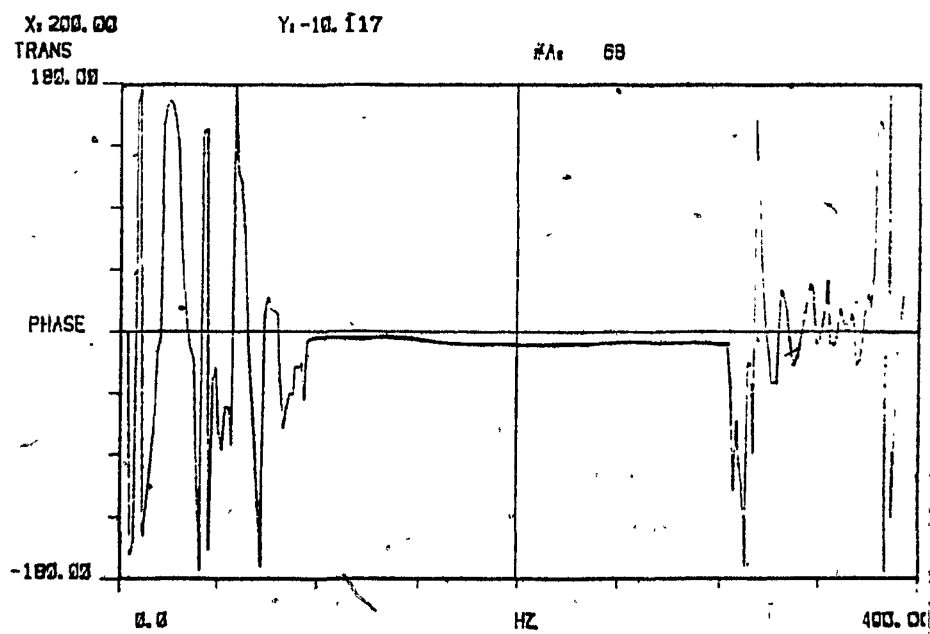

<u>Fig. 6.15:</u> Phase angle *versus* frequency diagrams measured at $\theta = 180°$ and $0°$ for the top and bottom figures, respectively. (Note that the curves are only valid from 100 to 300 Hz).

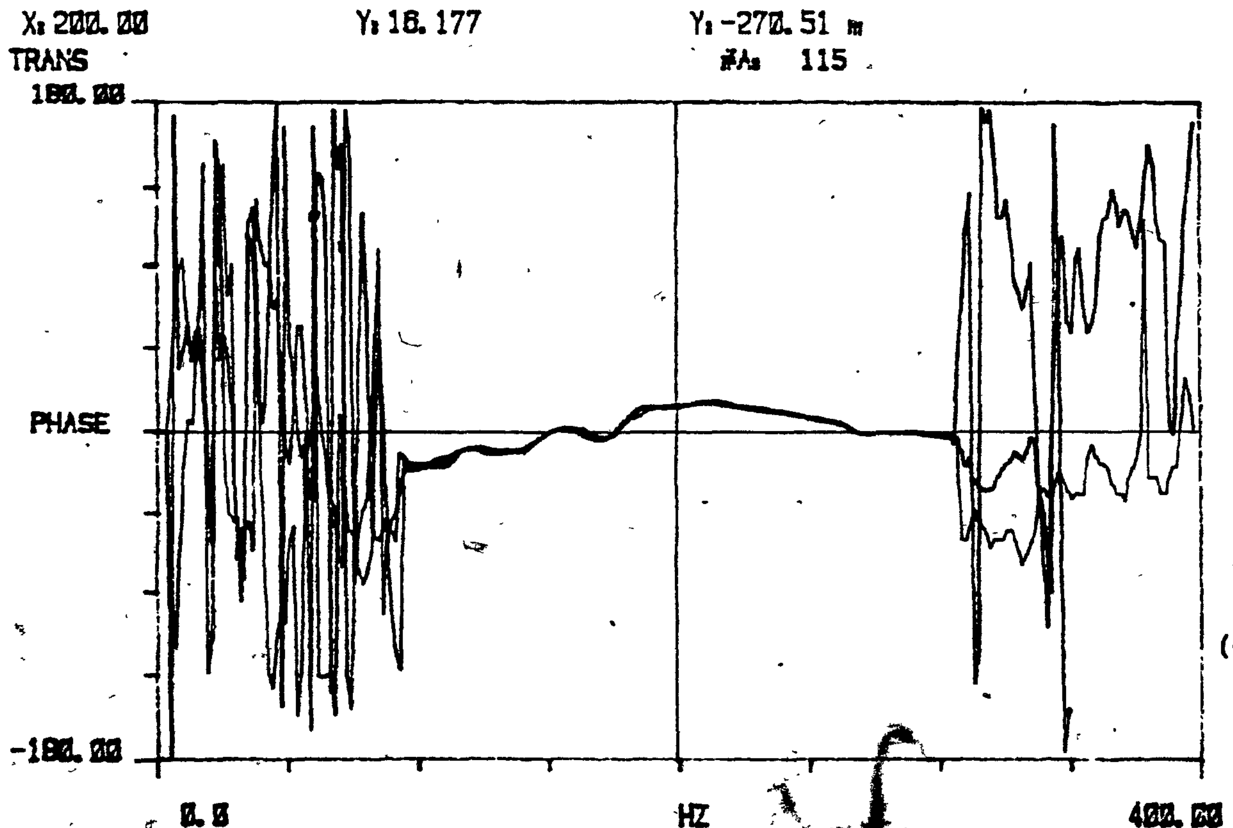

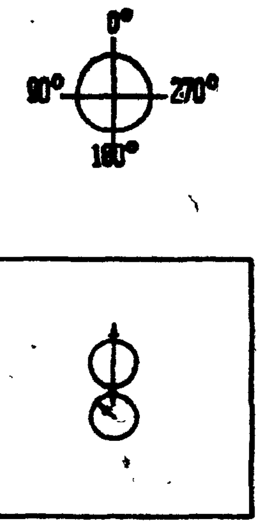

(Configuration of Fig. 4.5a)

Fig. 6.16: Phase angle *versus* frequency diagram, with blue, green and red curves measured at $\theta = 0°$ for Ac = 1.5, 2.0 and 4.5 g, respectively. (Note that the curves are only valid from 100 to 300 Hz).

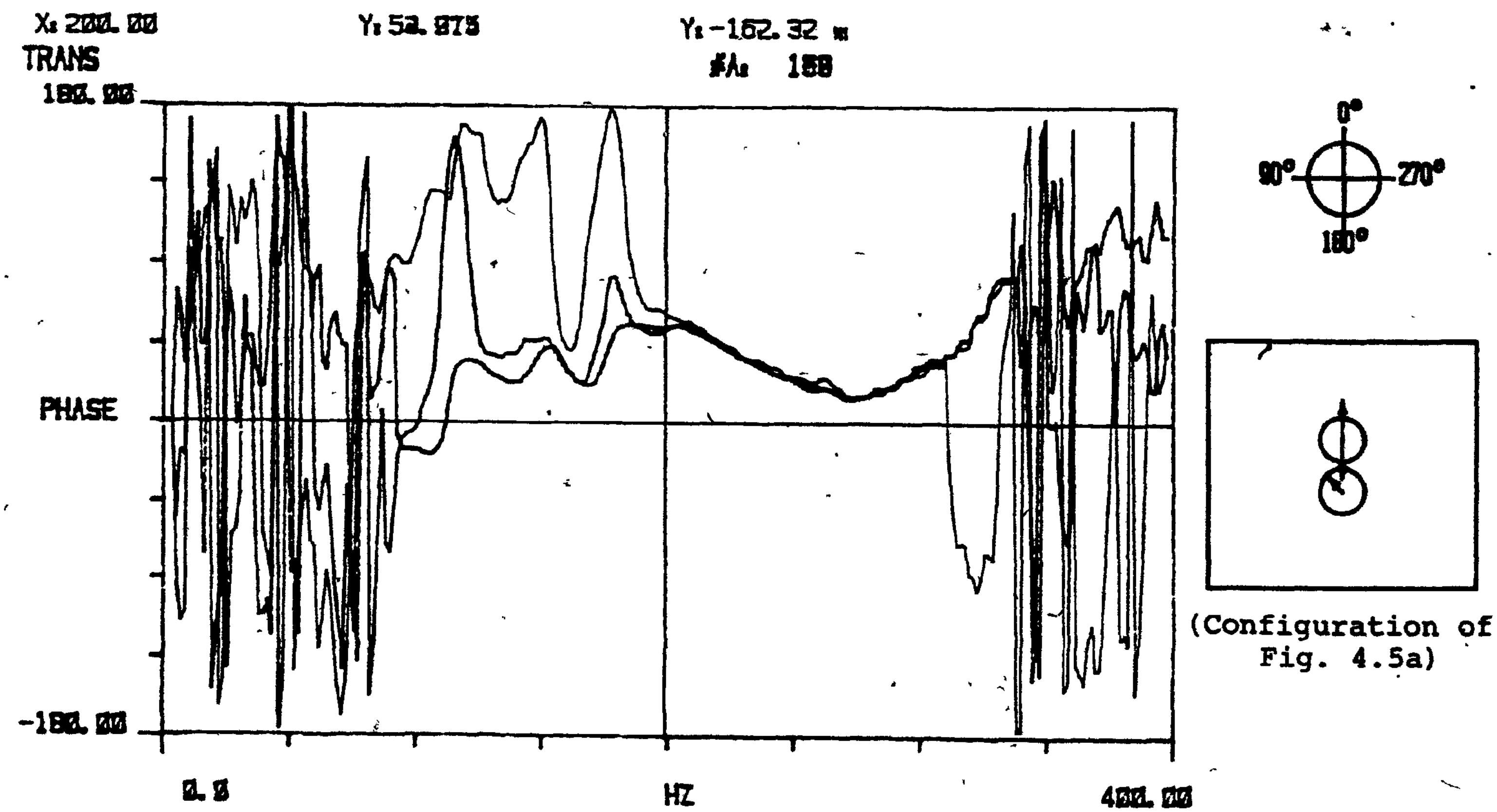

Fig. 6.17: Phase angle *versus* frequency diagram, with blue, green and red curves measured at θ = 180° for Ac = 1.5, 2.0 and 4.5 g, respectively. (Note that the curves are only valid from 100 to 300 Hz).

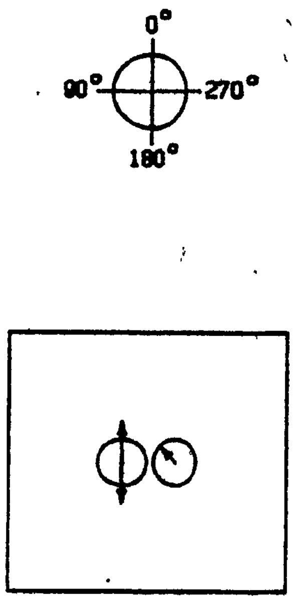

(Configuration of
Fig. 4.5b)

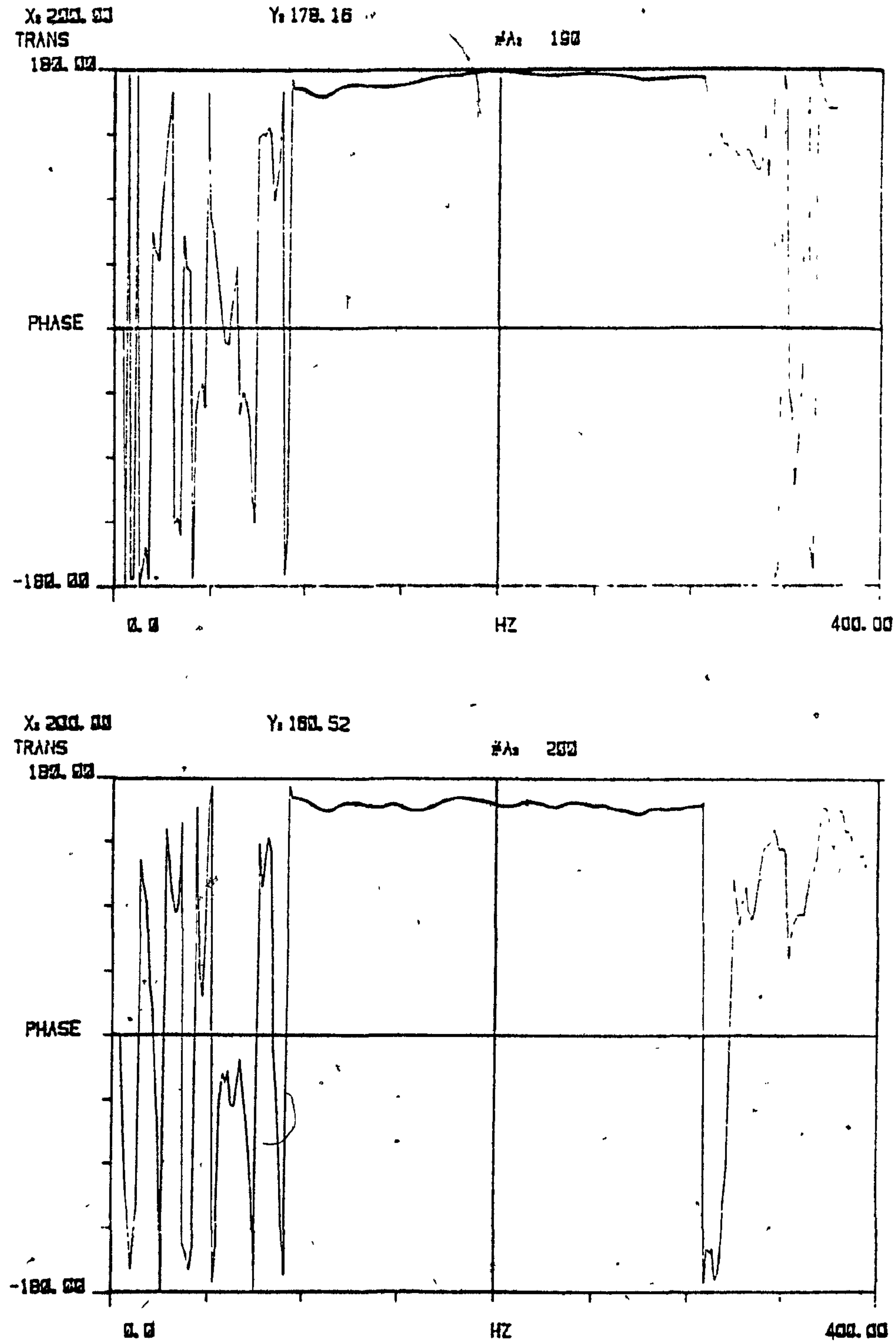

Fig. 6.18: Phase angle *versus* frequency diagrams measured at $\theta = 45°$ and $0°$ for the top and bottom figures, respectively. (Note that these curves are valid only from 100 to 300 Hz).

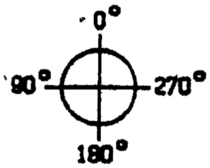

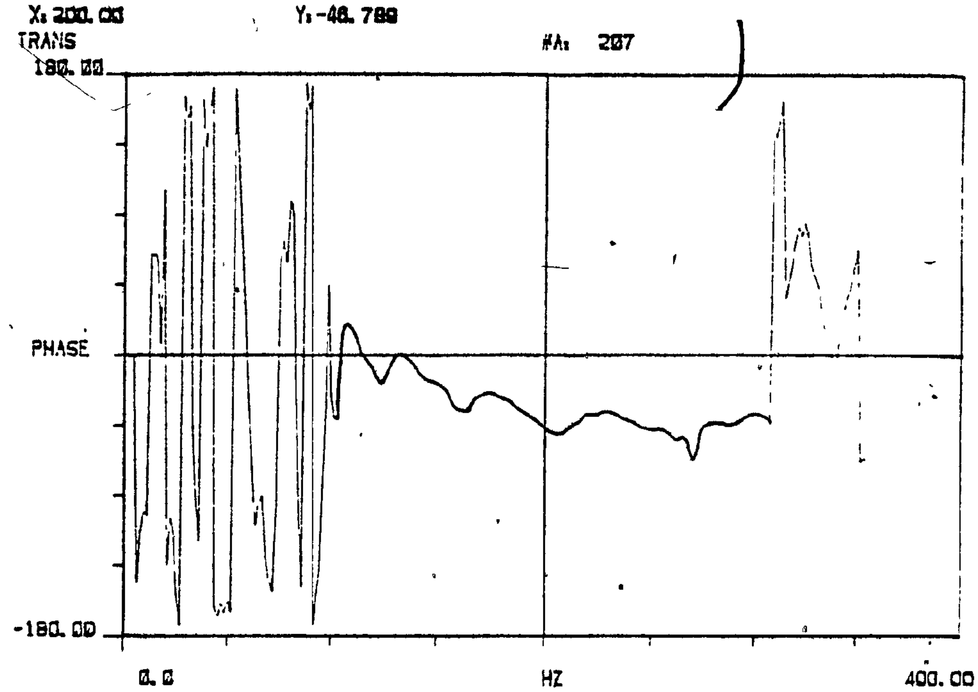

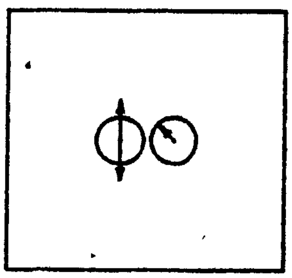

(Configuration of
Fig. 4.5b)

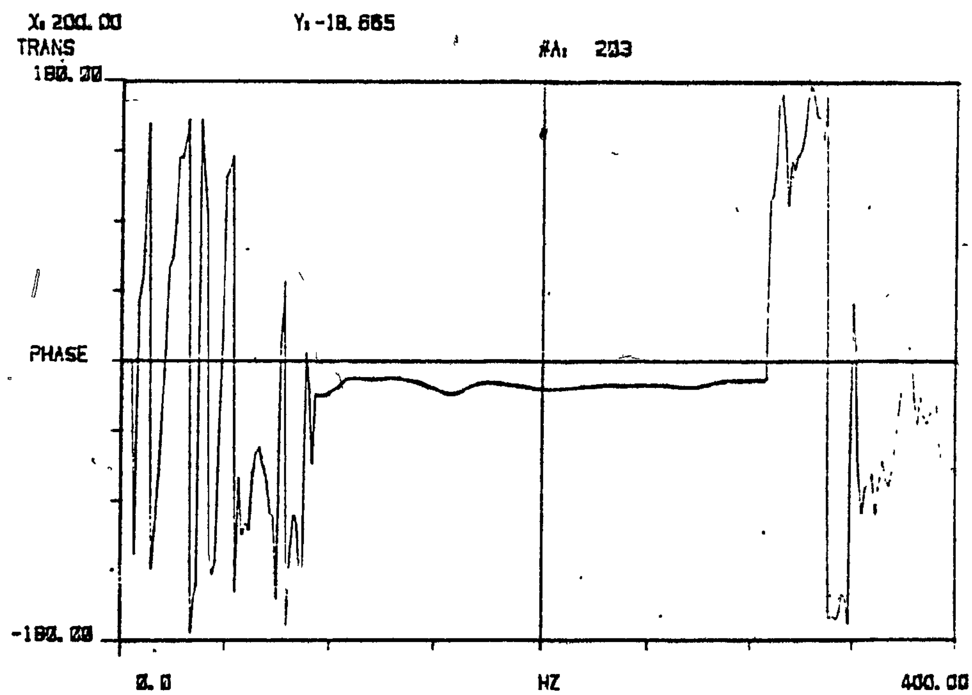

Fig. 6.19: Phase angle *versus* frequency diagrams measured at θ = 90° and 135° for the top and bottom figures, respectively. (Note that these curves are valid only from 100 to 300 Hz).

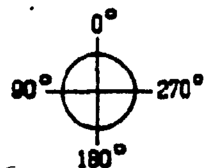

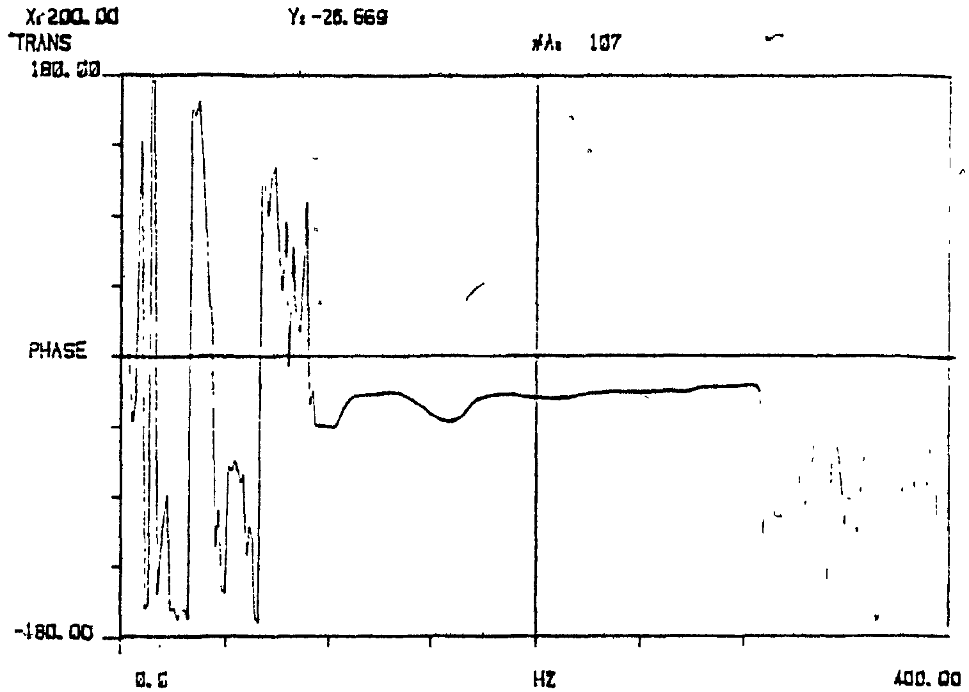

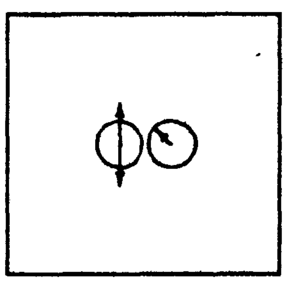

(Configuration of Fig. 4.5b)

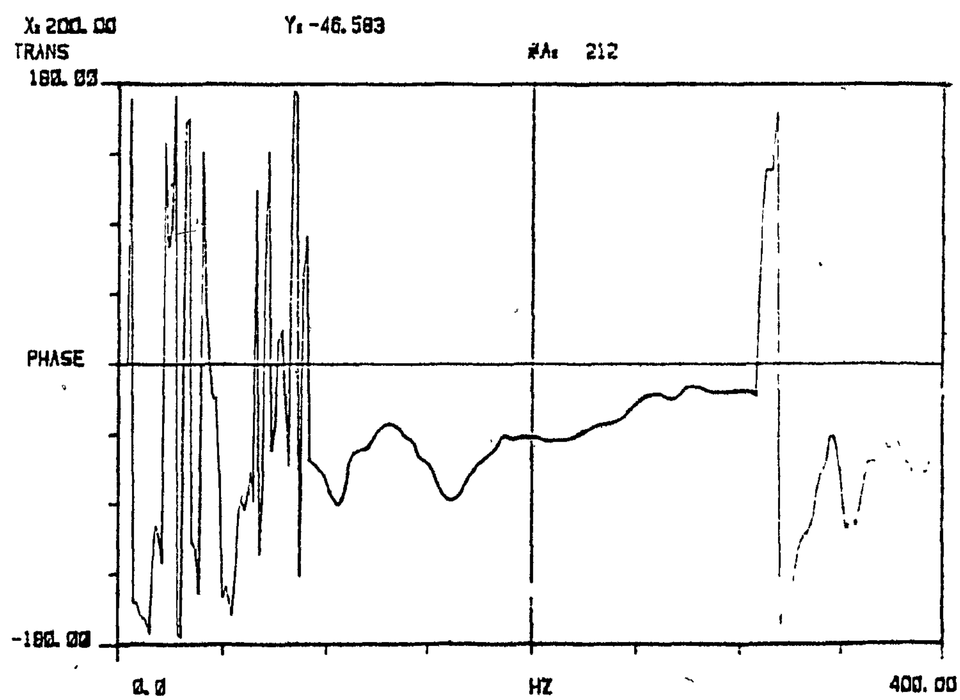

Fig. 6.20: Phase angle *versus* frequency diagrams measured at $\theta = 180°$ and $225°$ for the top and bottom figures, respectively. (Note that these curves are valid only from 100 to 300 Hz).

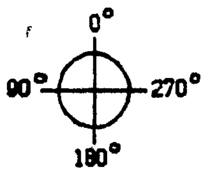

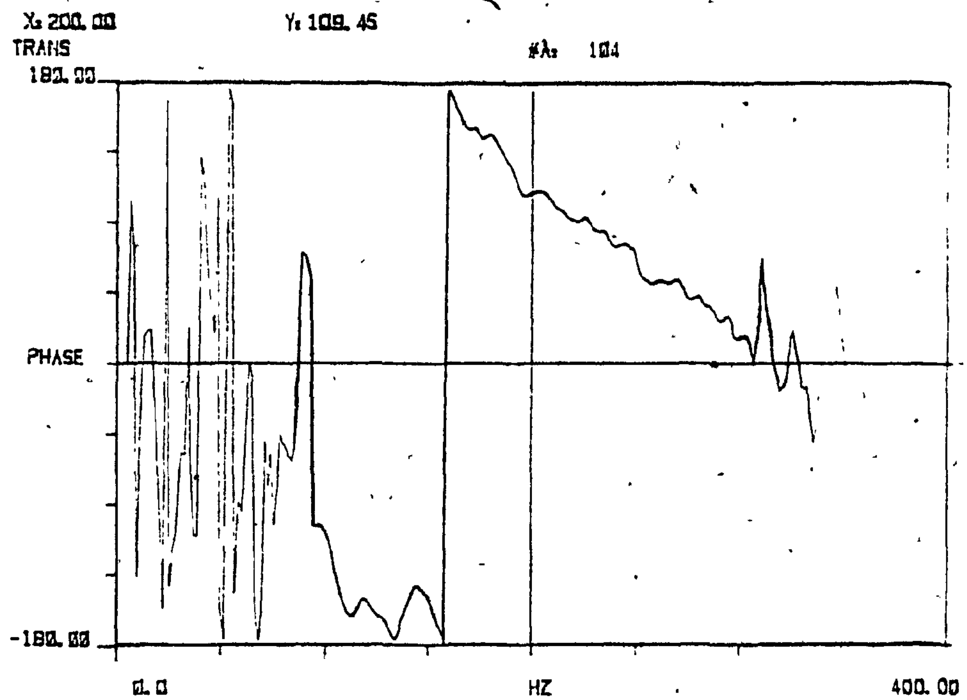

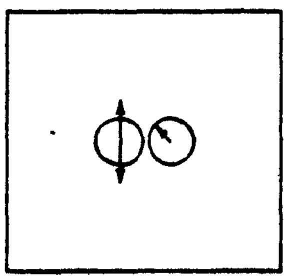

(Configuration of
Fig. 4.5b)

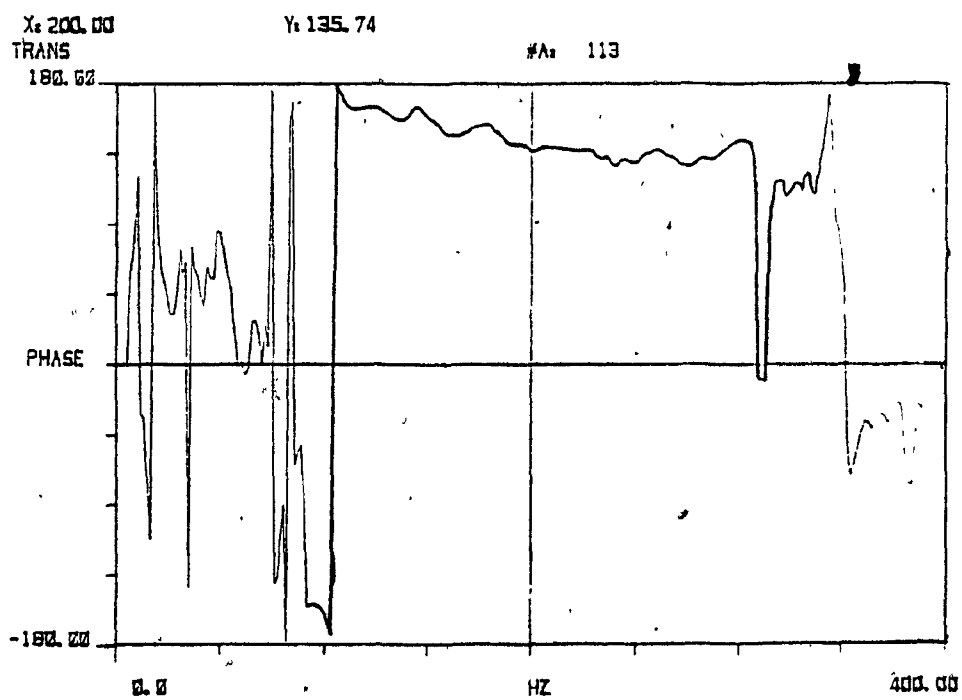

Fig. 6.21: Phase angle *versus* frequency diagrams measured at $\theta = 270°$ and $315°$ for the top and bottom figures, respectively. (Note that these curves are valid only from 100 to 300 Hz).

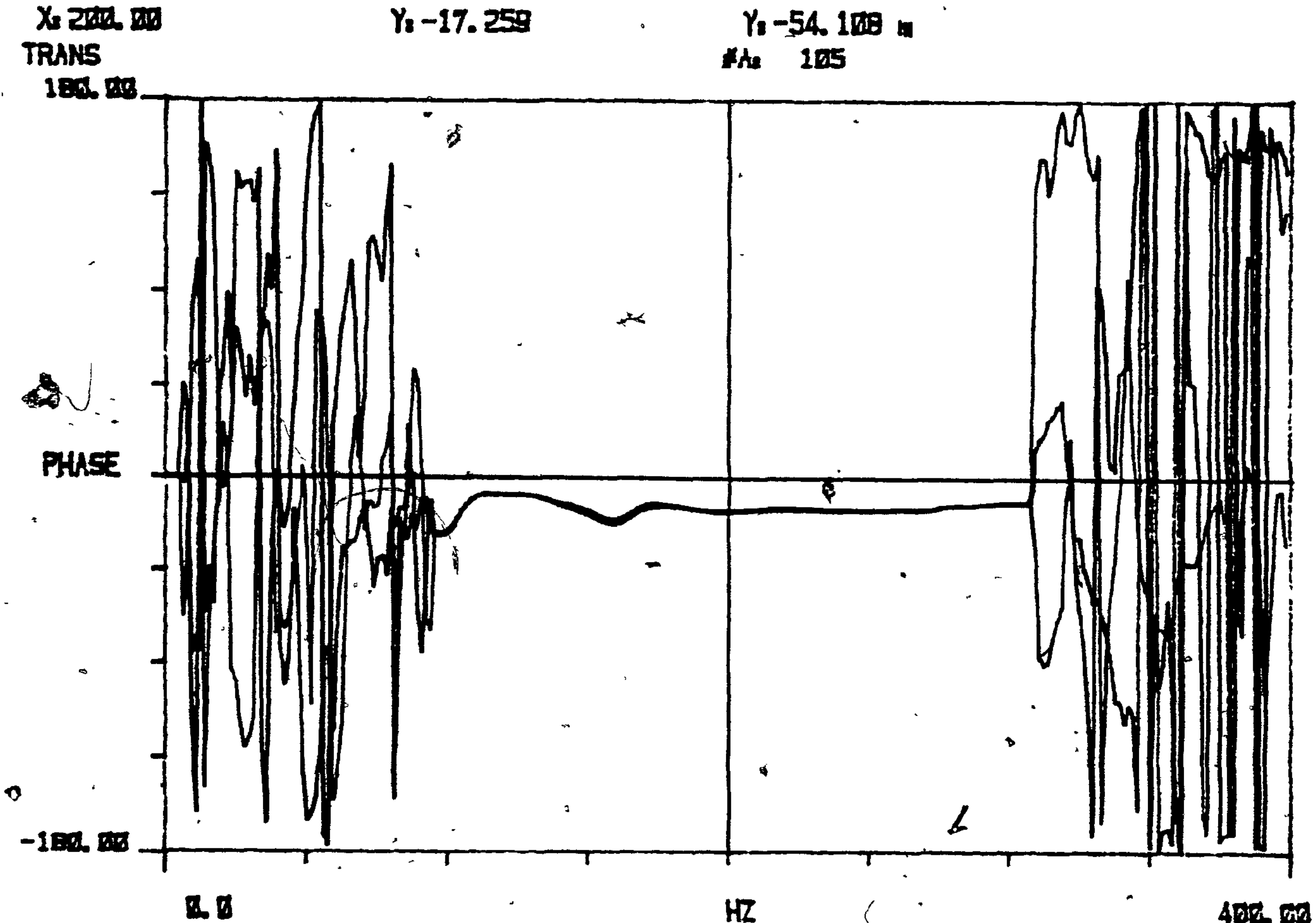

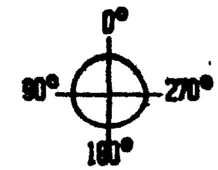

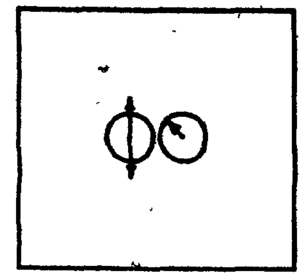

(Configuration of Fig. 4.5b)

<u>Fig. 6.22</u>: Phase angle *versus* frequency diagram with red, green and blue curves measured at $\theta = 135°$ for Ac = 1.5, 2.0 and 4.5 g, respectively. (Note that these curves are valid only from 100 to 300 Hz).

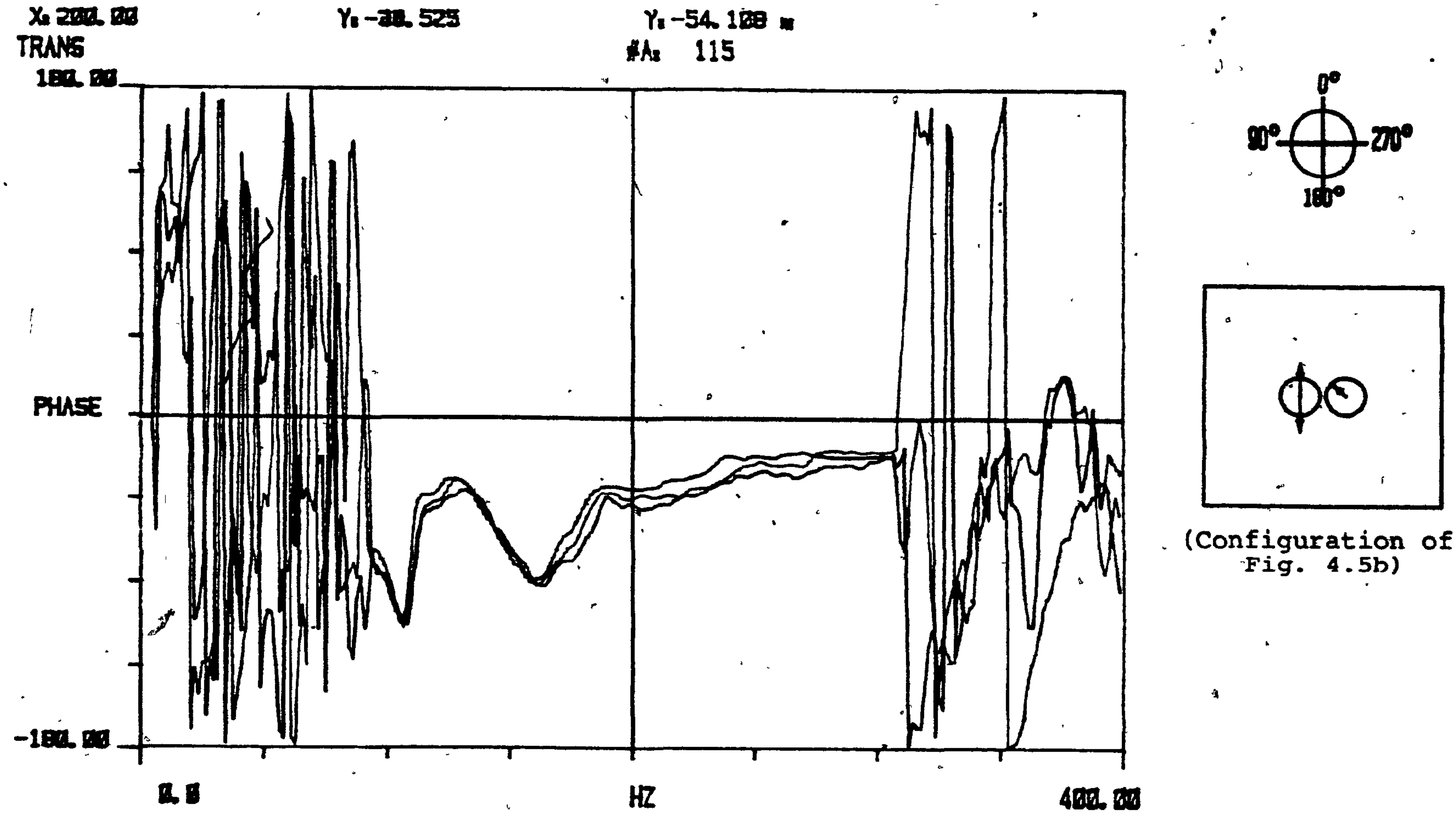

<u>Fig. 6.23</u>: Phase angle *versus* frequency diagram with red, green and blue curves measured at $\theta = 315°$ for Ac = 1.5, 2.0 and 4.5 g, respectively. (Note that these curves are valid only from 100 to 300 Hz).

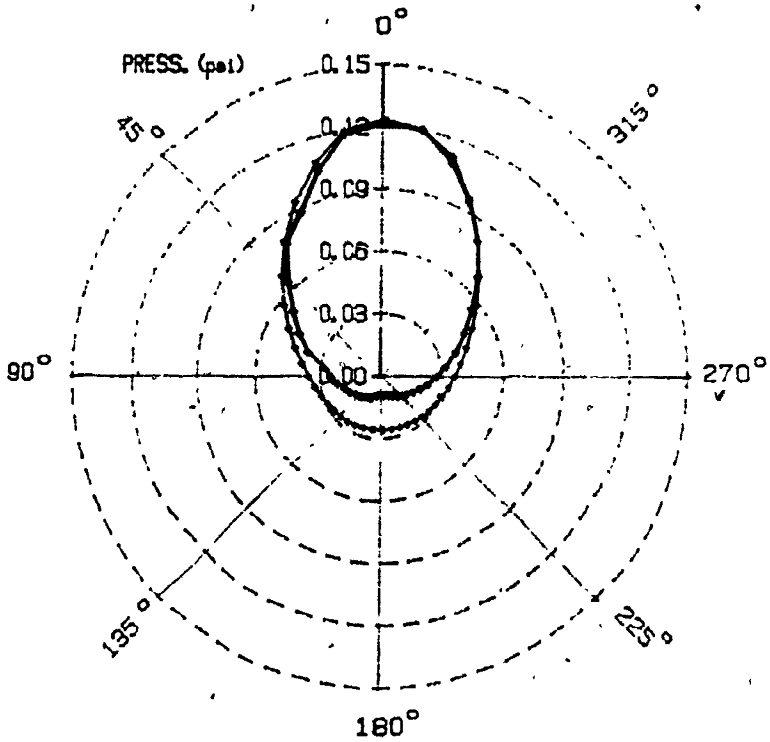

(a)

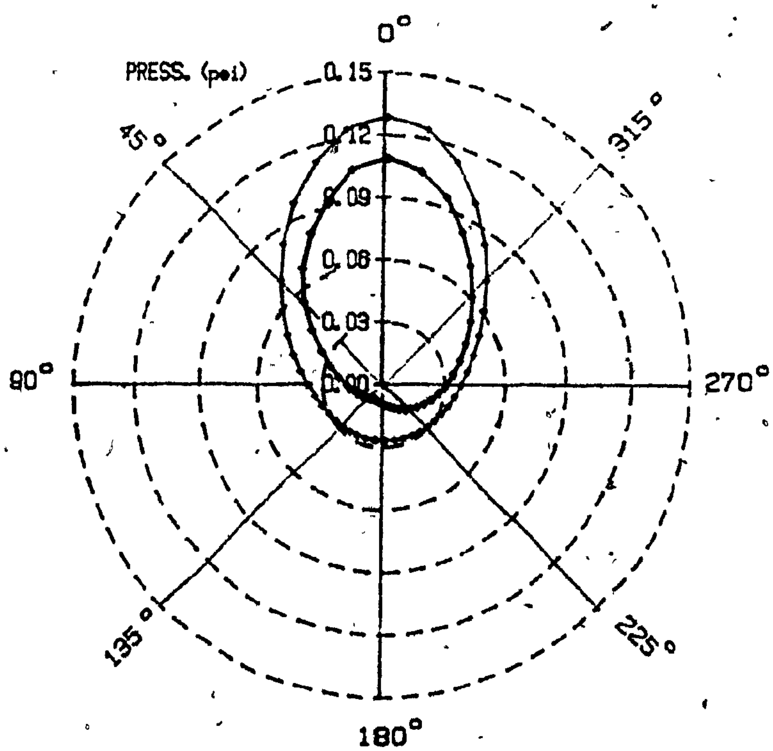

(b)

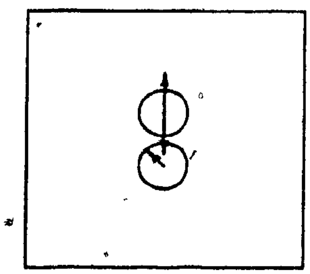

(Configuration of Fig. 4.5a)

Fig. 6.24: Theoretical (black) and measured pressure profiles (red) of the stationary cylinder (with inner arrow). Profile in (b) was taken from the tests done after the experimental setup was modified, as described in Section 6.2. (a) Freq. = 100 Hz, Ac = 2.18 g; (b) Freq. = 200 Hz, Ac = 2.27 g.

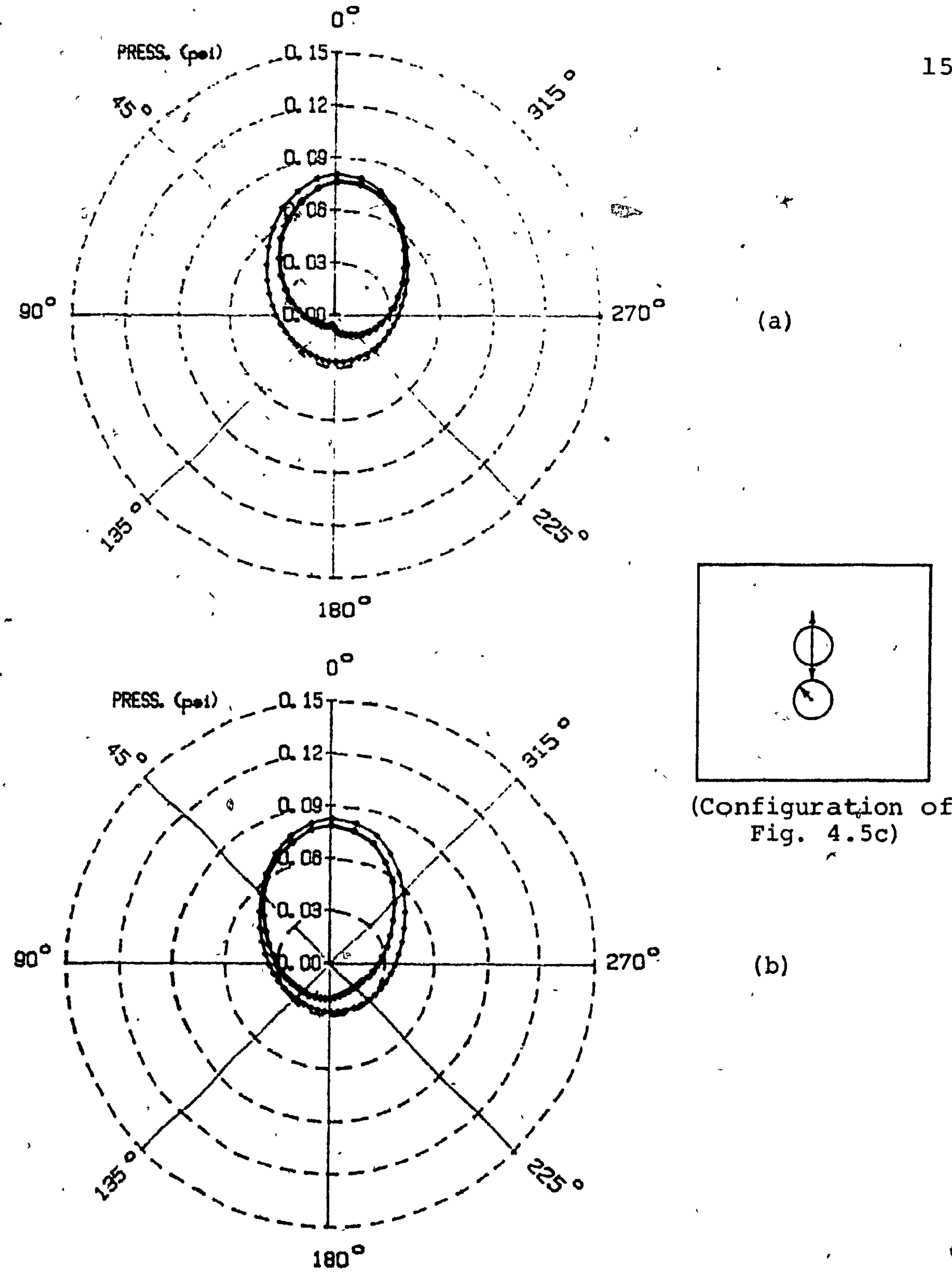

Fig. 6.25: Theoretical (black) and measured pressure profiles (red) of the stationary cylinder (with inner arrow). Tests were done after the experimental setup was modified, as described in Section 6.2. (a) Freq. = 170 Hz, Ac = 2.22 g; (b) Freq. = 200 Hz, Ac = 2.29 g.

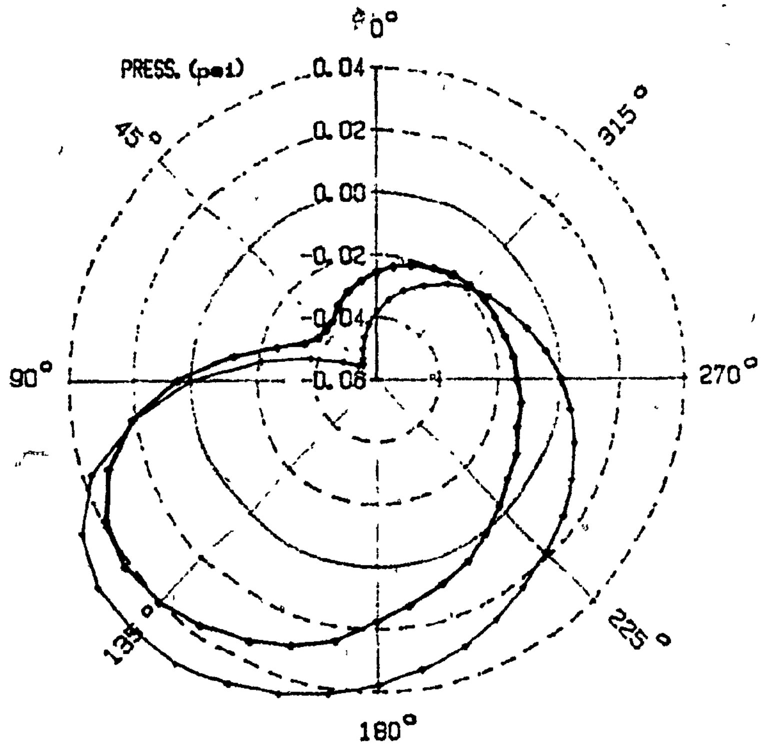

(a)

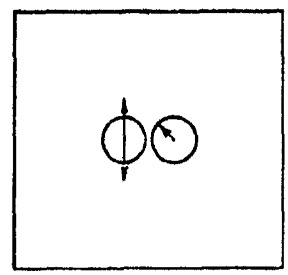

(Configuration of Fig. 4.5b)

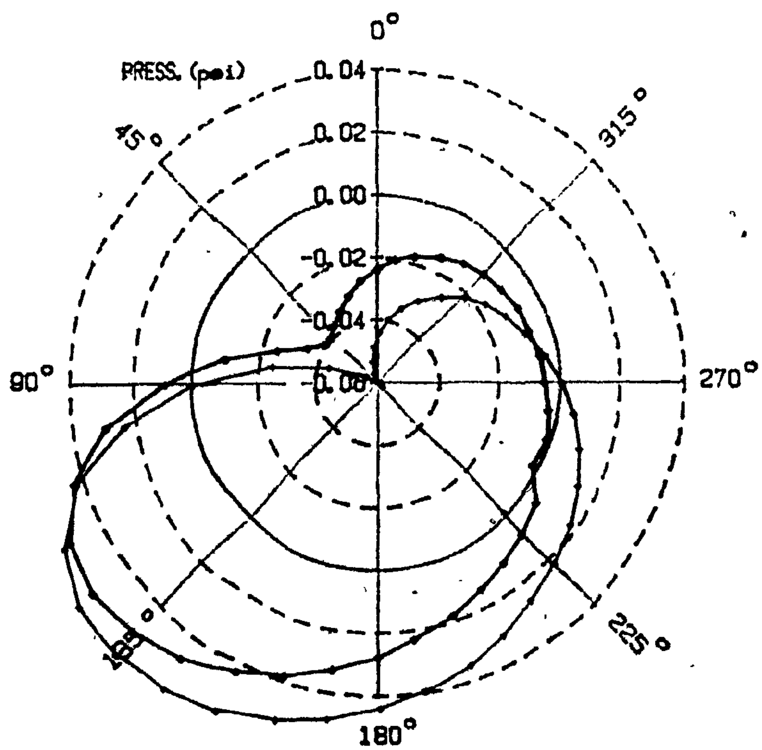

(b)

Fig. 6.26: Theoretical (black) and measured pressure profiles (red) of the stationary cylinder (with inner arrow). Measured profiles were obtained from the tests done after the experimental setup was modified, as described in Section 6.2. (a) Freq. = 100 Hz, Ac = 2.06 g; (b) Freq. = 230 Hz, Ac = 2.38 g.

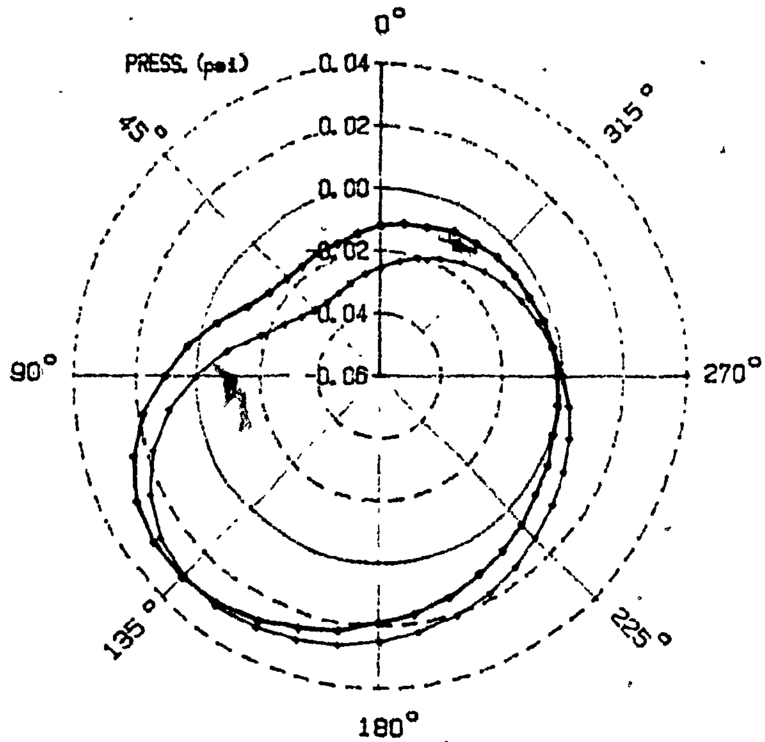

(a)

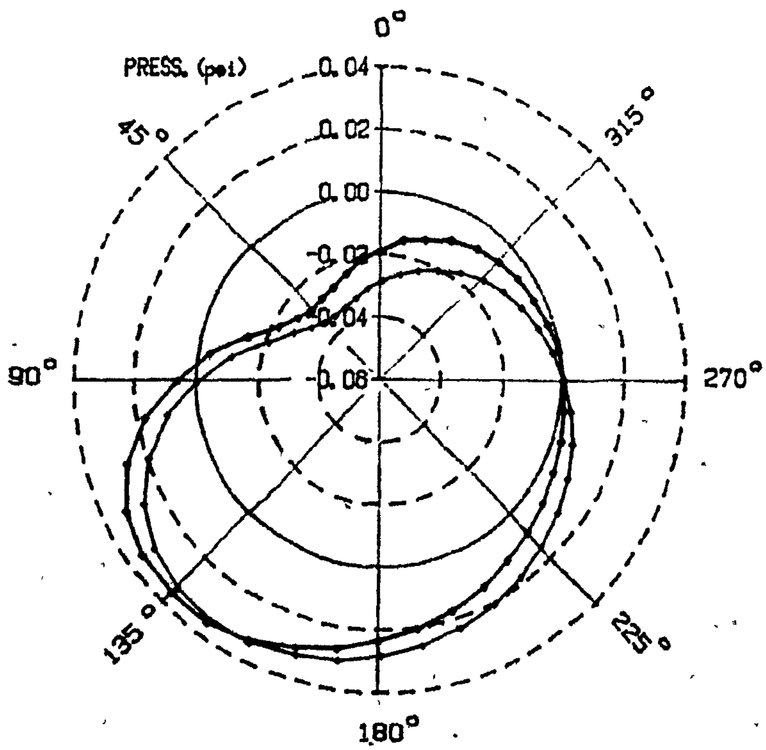

(b)

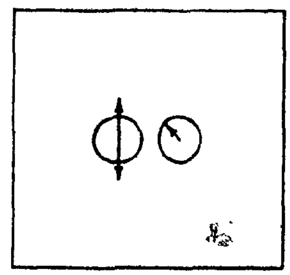

(Configuration of Fig. 4.5d)

<u>Fig. 6.27:</u> Theoretical (black) and measured pressure profiles (red) of the stationary cylinder (with inner arrow). Measured profiles were obtained from the tests done after the experimental setup was modified, as described in Section 6.2. (a) Freq. = 180 Hz, Ac = 1.98 g; (b) Freq. = 150 Hz, Ac = 2.21 g.

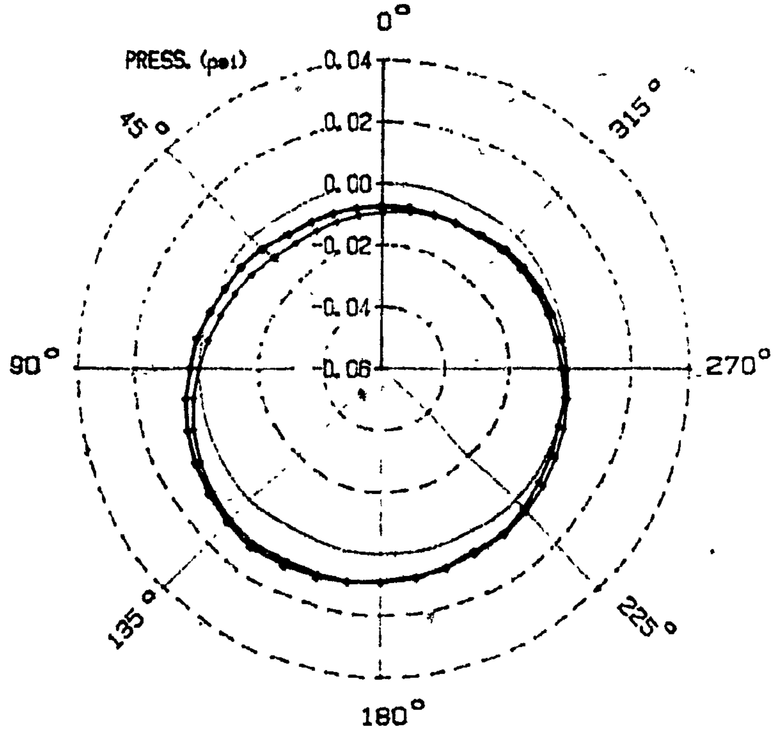

(a)

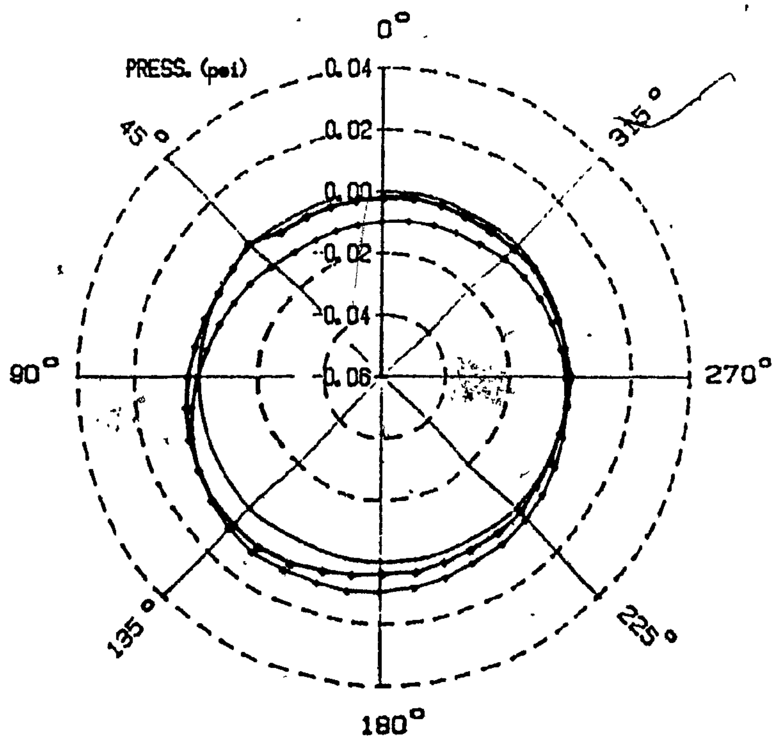

(b)

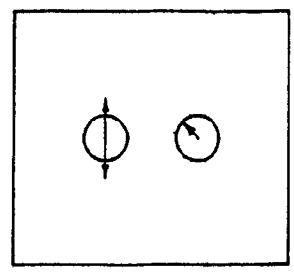

(Configuration of Fig. 4.5f)

Fig. 6.28: Theoretical (black) and measured pressure profiles (red) of the stationary cylinder (with inner arrow). (a) Freq. = 90 Hz, Ac = 1.30 g; (b) Freq. = 180 Hz, Ac = 1.40 g.

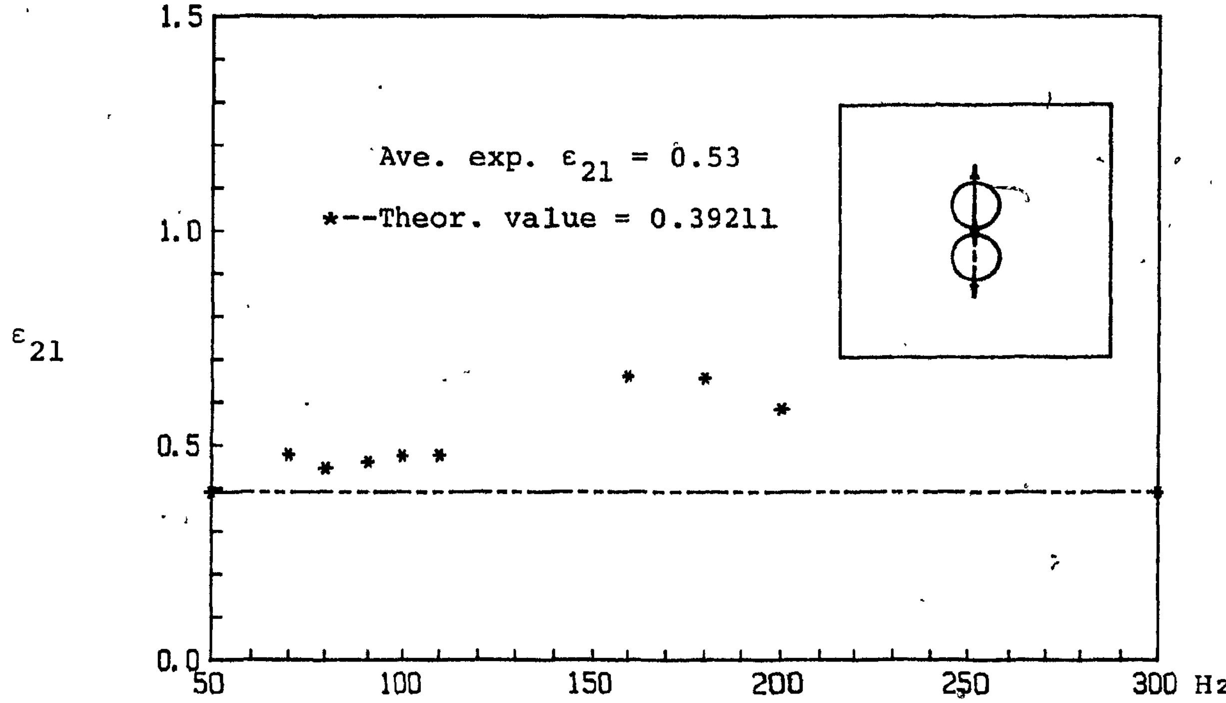

(a)

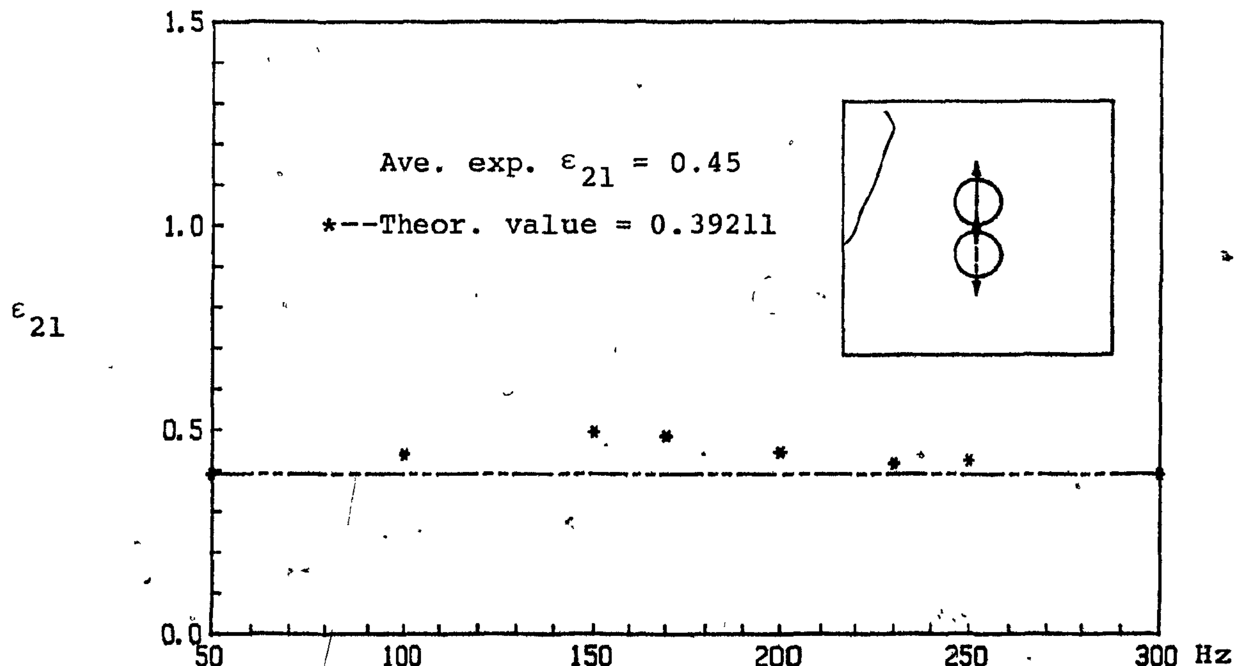

(b)

<u>Fig. 6.29</u>: Experimental added mass coefficients *versus* frequency, compared with theoretical values. Average discrepancy: for (a) 15.34%; for (b) 5.38% Results in (b) were obtained from the tests done after the experimental setup was modified.

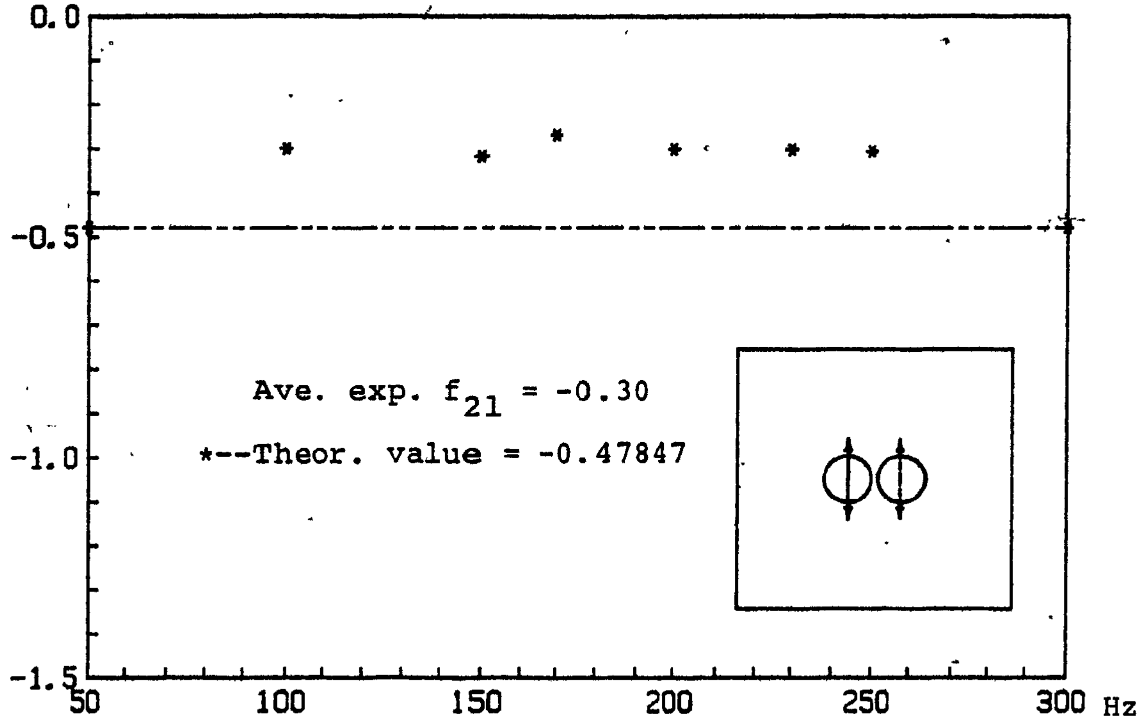

(a)

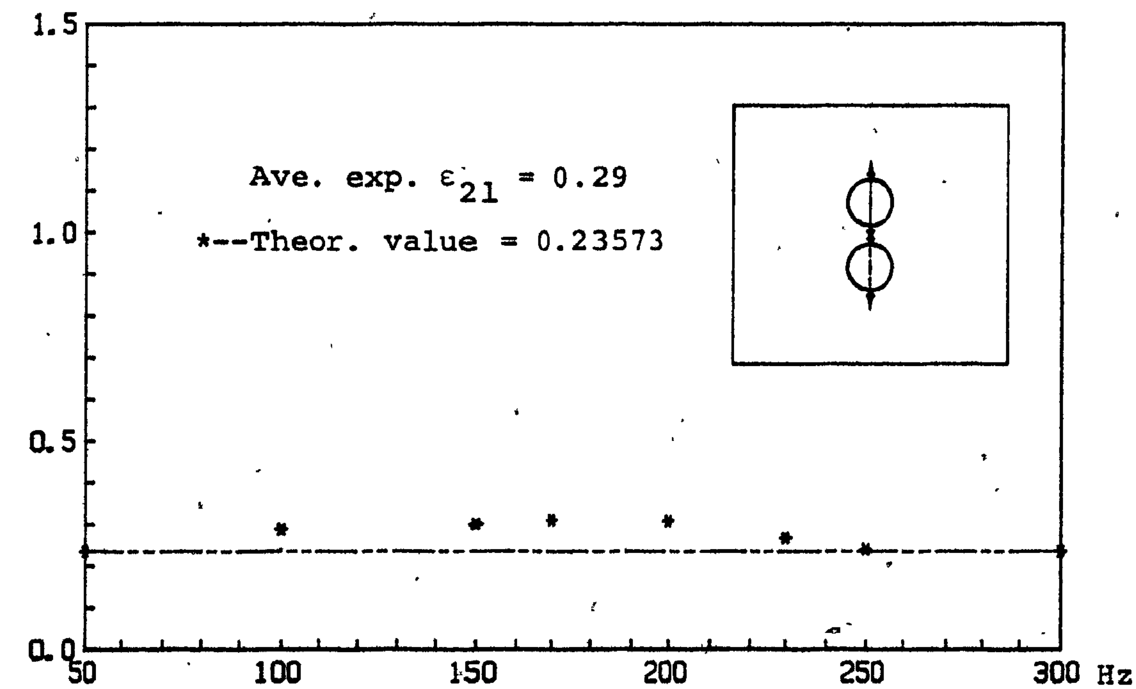

(b)

<u>Fig. 6.30</u>: Experimental added mass coefficients *versus* frequency, compared with theoretical values. Average discrepancy: for (a) -37.73; for (b) 21.56%. Both results were obtained from the tests after the experimental setup was modified.

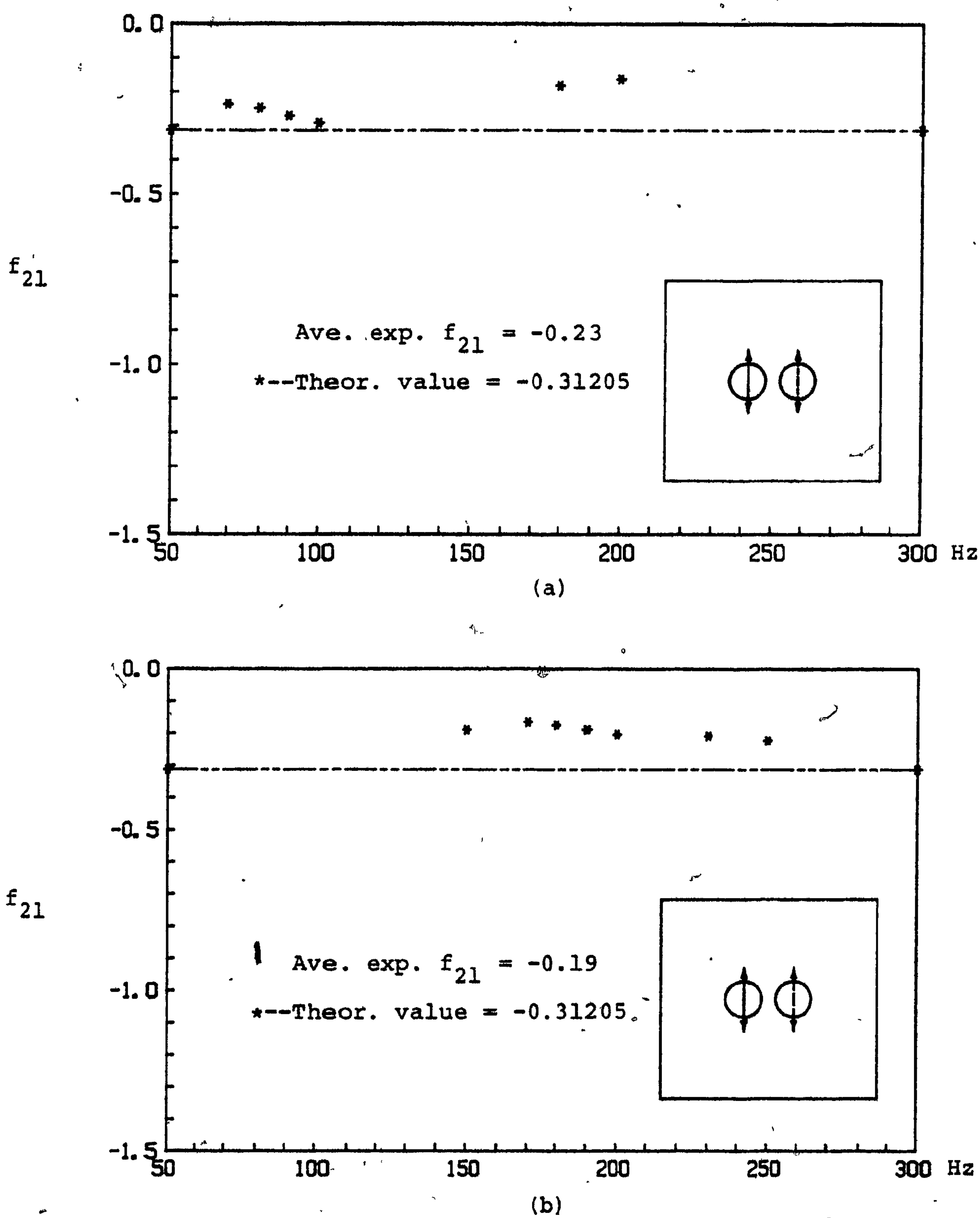

Fig. 6.31: Experimental added mass coefficients *versus* frequency, compared with theoretical values. Average discrepancy: for (a) -26.07%; for (b) -38.33%. Results in (b) were obtained from the tests done after the experimental setup was modified.

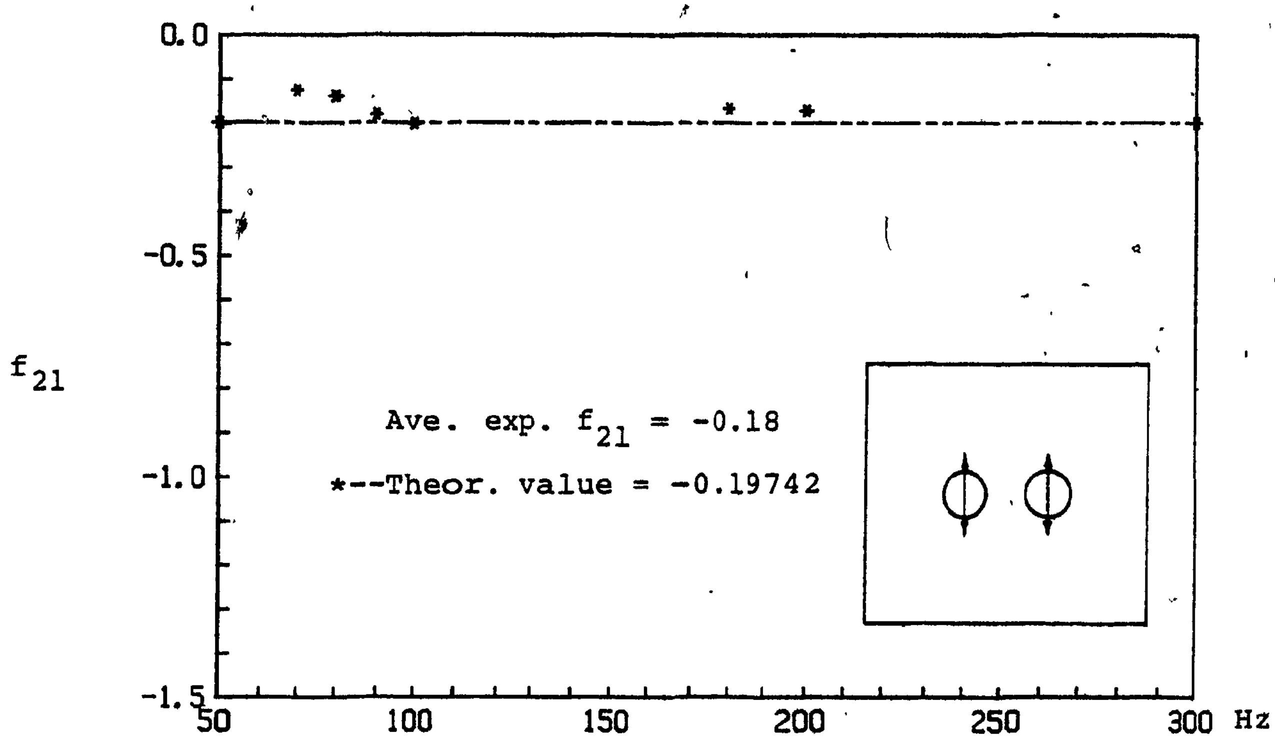

(a)

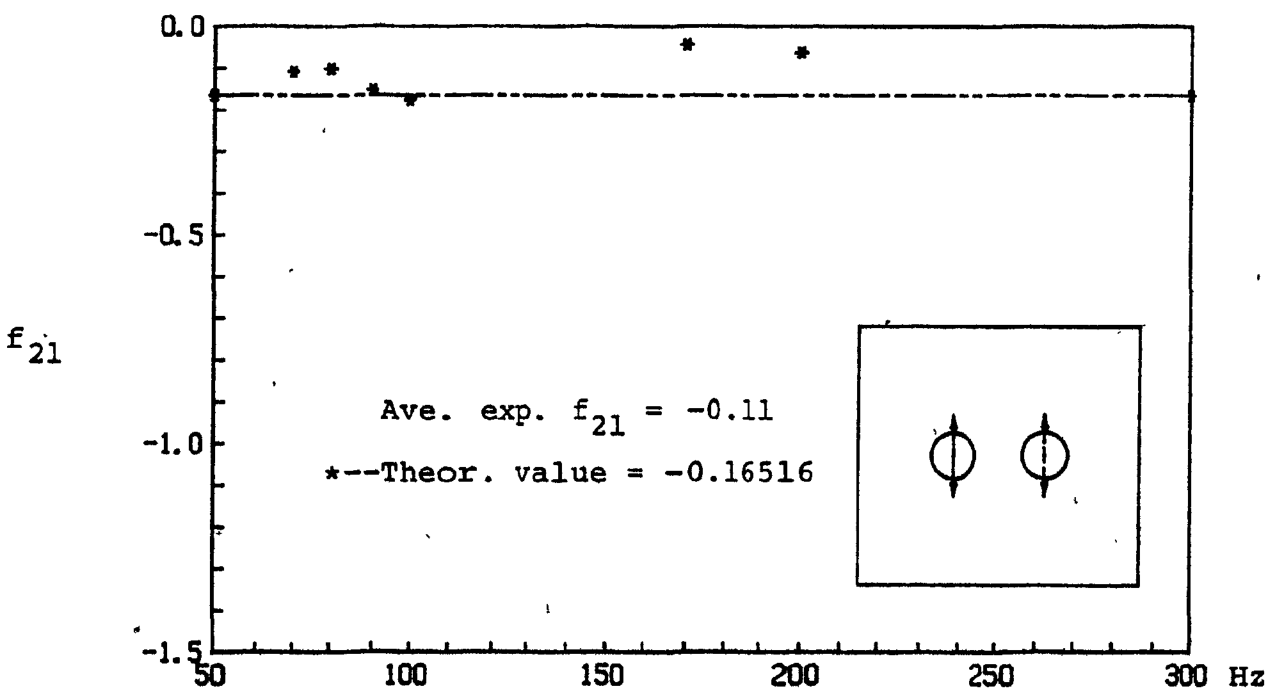

(b)

Fig. 6.32: Experimental added mass coefficients *versus* frequency, compared with theoretical values. Average discrepancy: for (a) -6.96%; for (b) -35.12%. Results in (b) were obtained from the tests done after the experimental setup was modified.

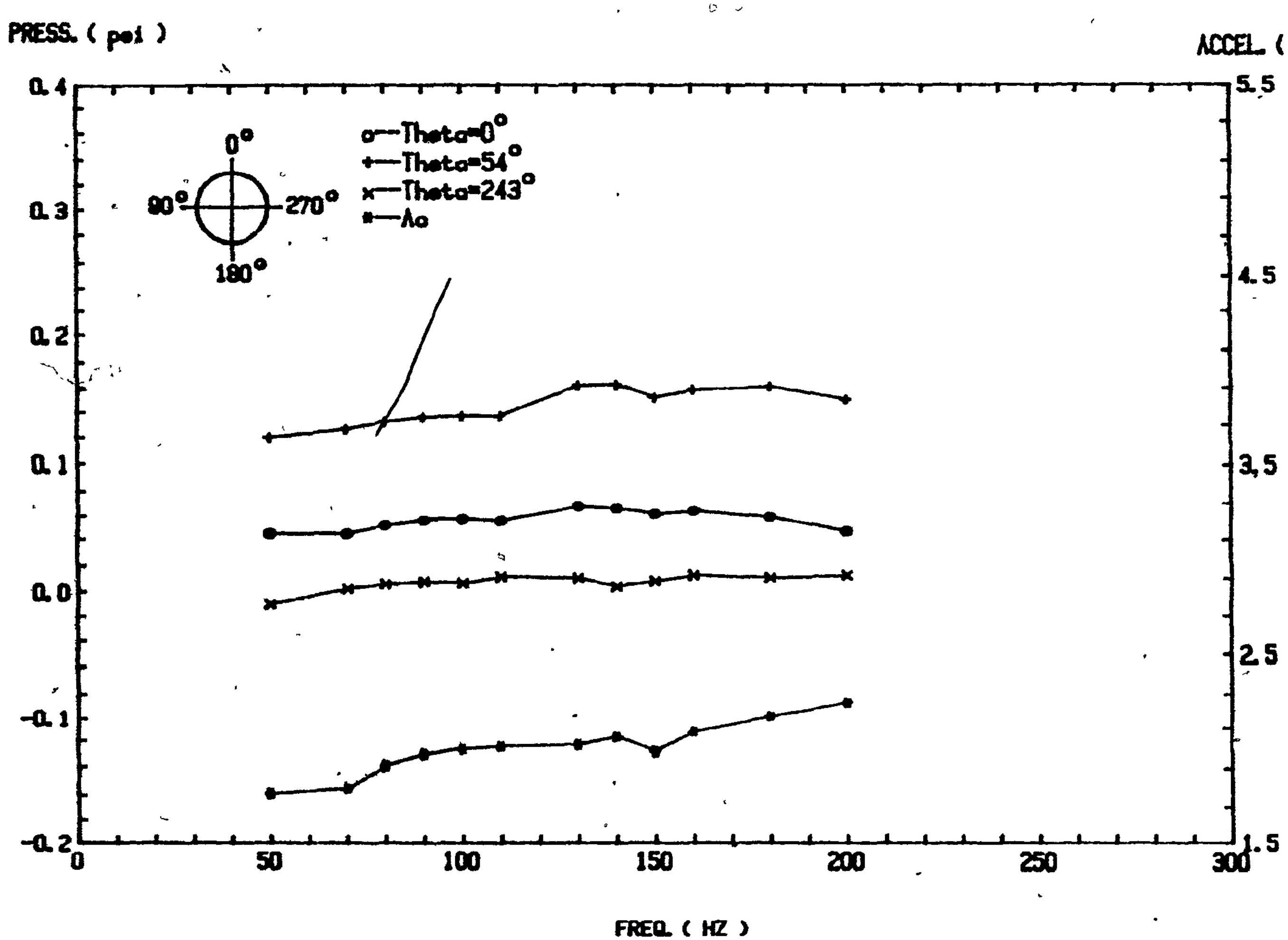

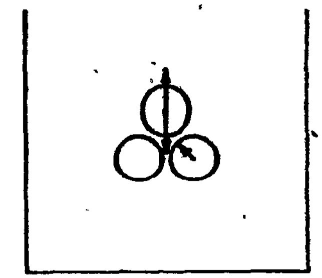

(Configuration of Fig. 4.6a)

<u>Fig. 6.33</u>: Pressure *versus* frequency curves measured on the stationary cylinder (with small inner arrow) for various θ.

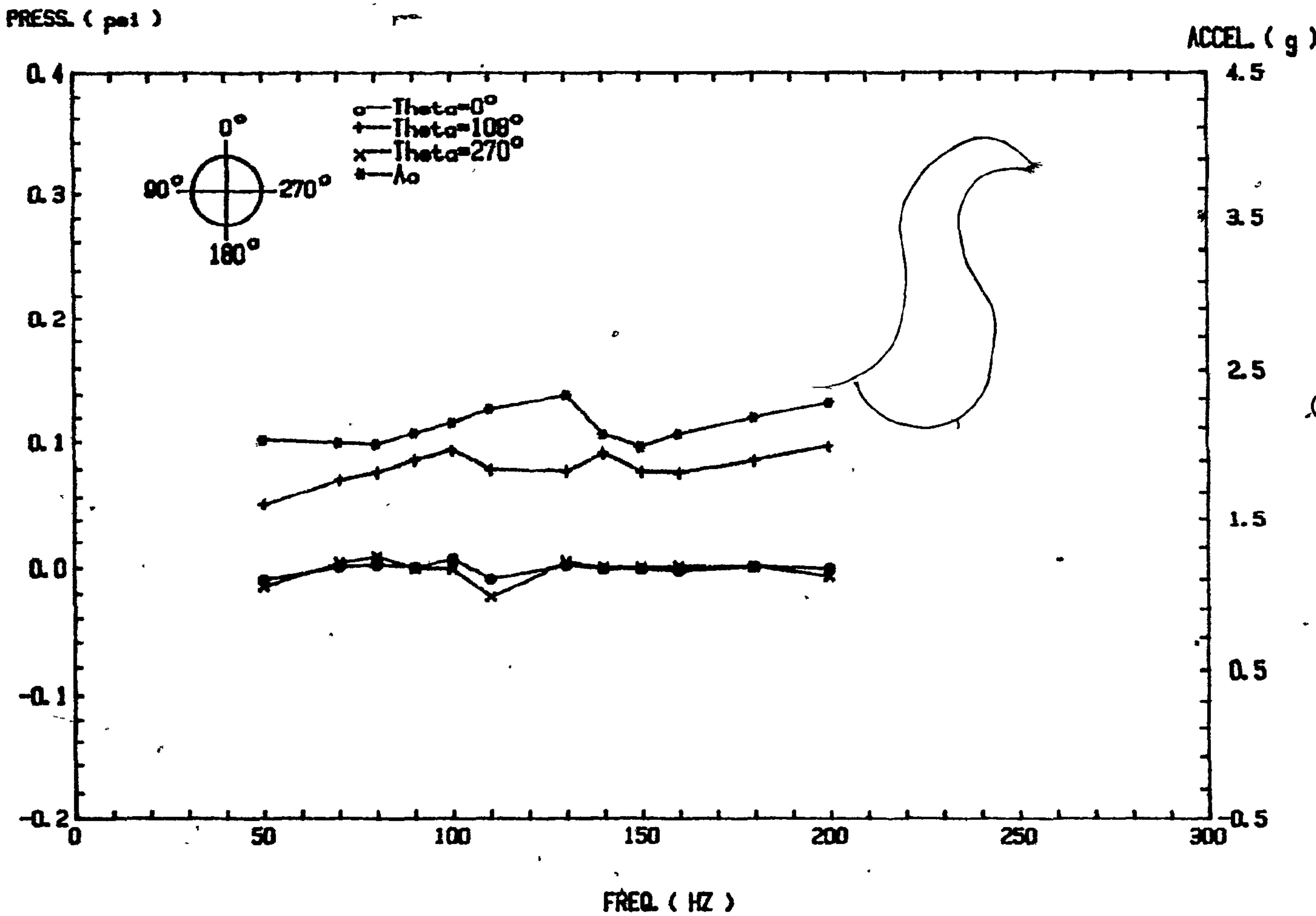

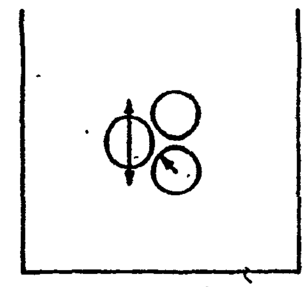

(Configuration of Fig. 4.6b)

<u>Fig. 6.34</u>: Pressure *versus* frequency curves measured on the stationary cylinder (with small inner arrow) for various θ.

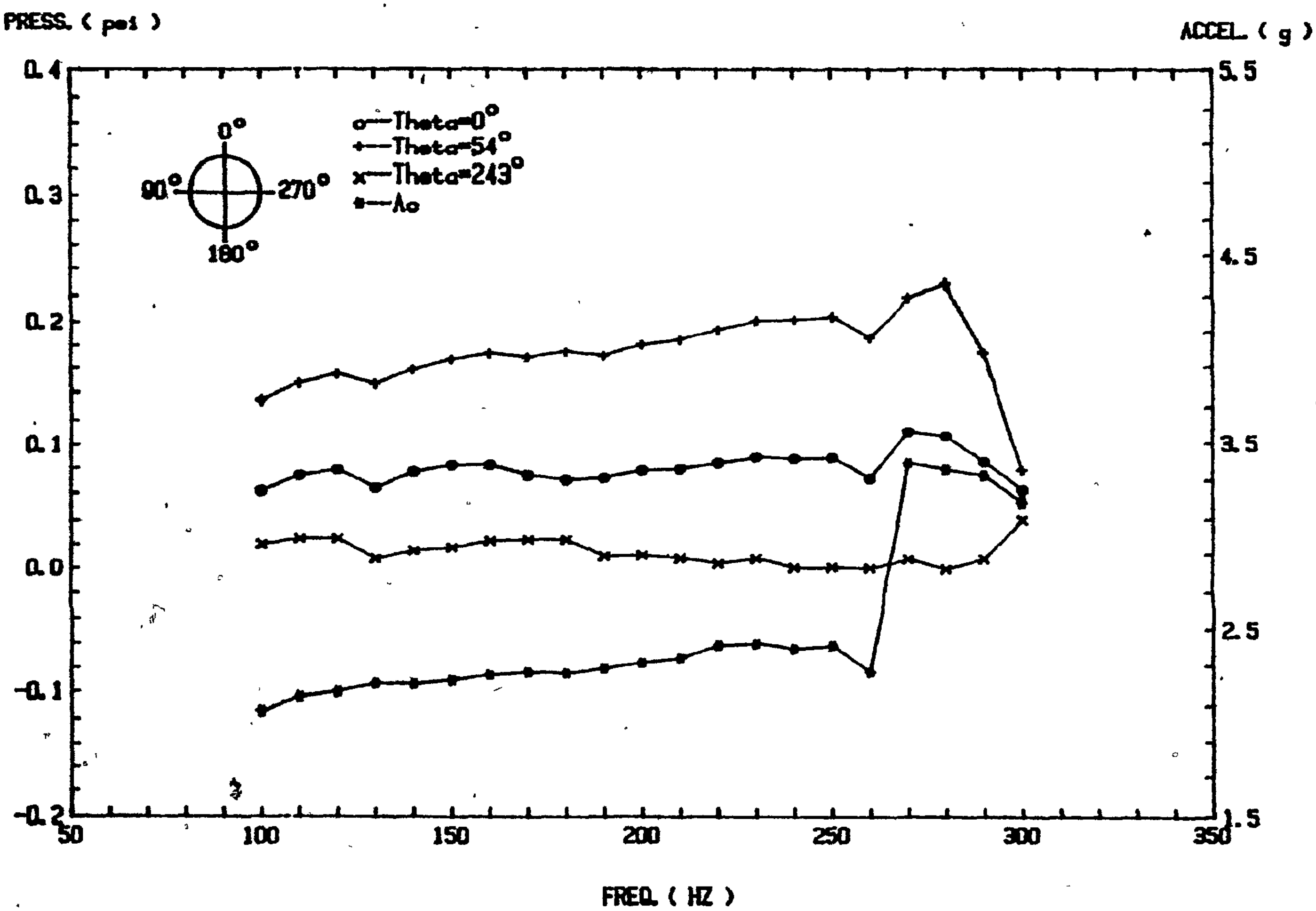

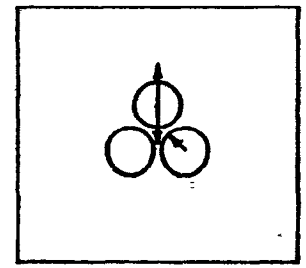

(Configuration of Fig. 4.6c)

Fig. 6.35: Pressure *versus* frequency curves measured on the cylinder shown (with inner arrow) for various θ. The test was done after the modification of the experimental setup, as described in Section 6.2.

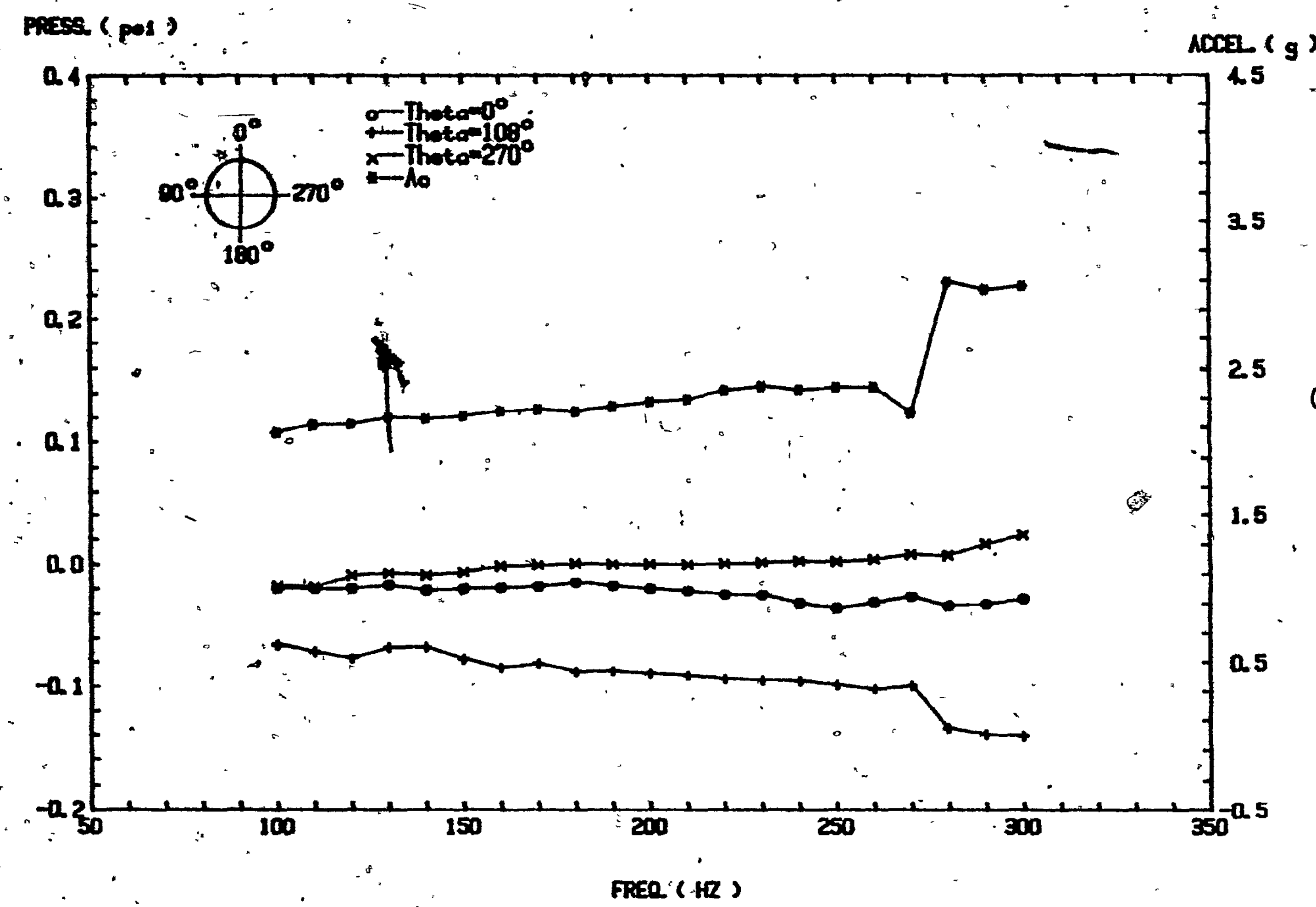

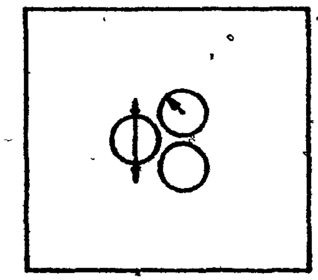

(Configuration of Fig. 4.6d)

<u>Fig. 6.36:</u> Pressure *versus* frequency curves measured on the cylinder shown (with inner arrow) for various θ. The test was done after the modification of the experimental setup, as described in Section 6.2.

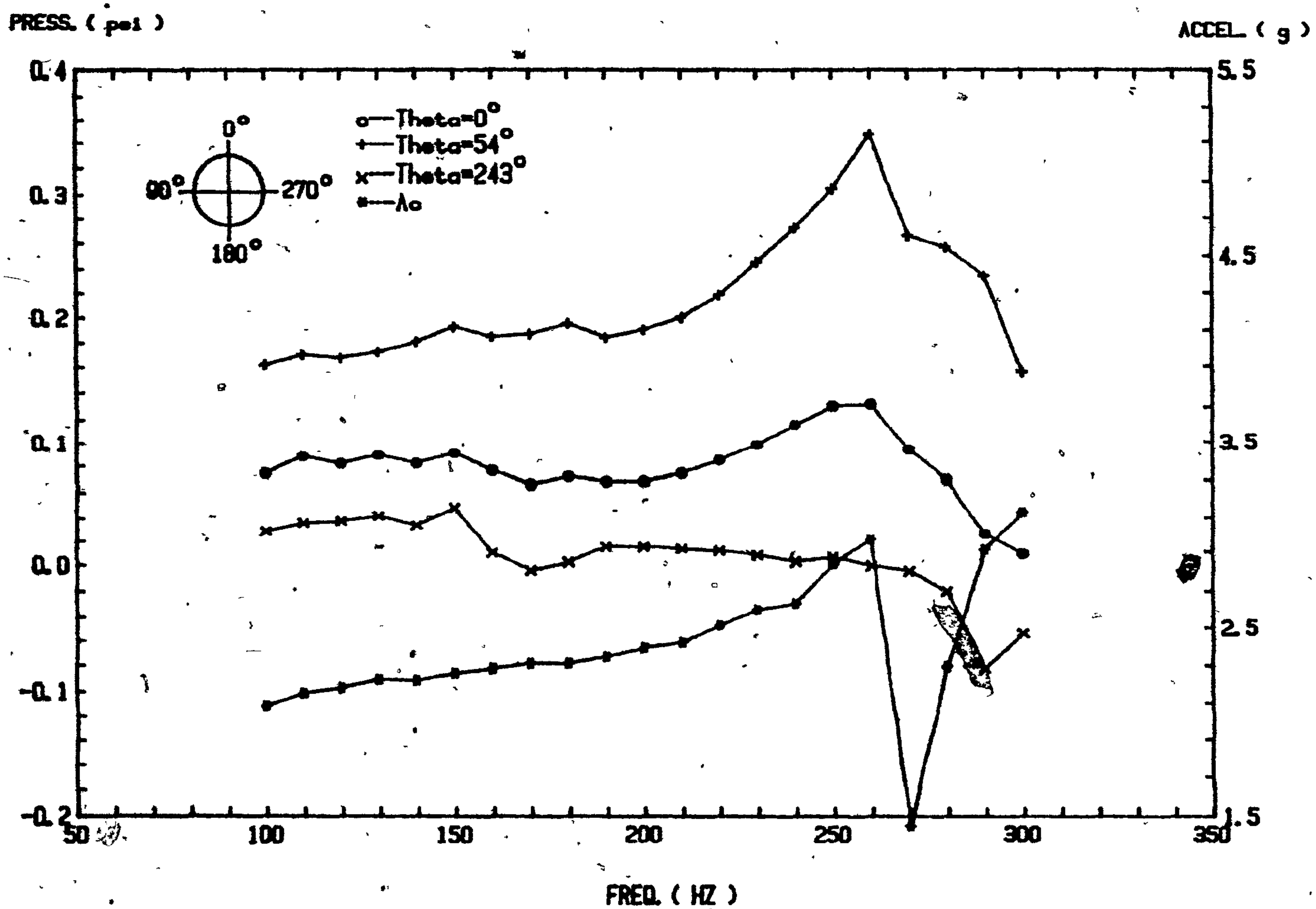

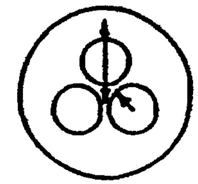

(Configuration of Fig. 4.6e)

Fig. 6.37: Pressure *versus* frequency curves measured on the cylinder (with inner arrow) for various θ. The test was done with water after the modification of the experimental setup, as described in Section 6.2.

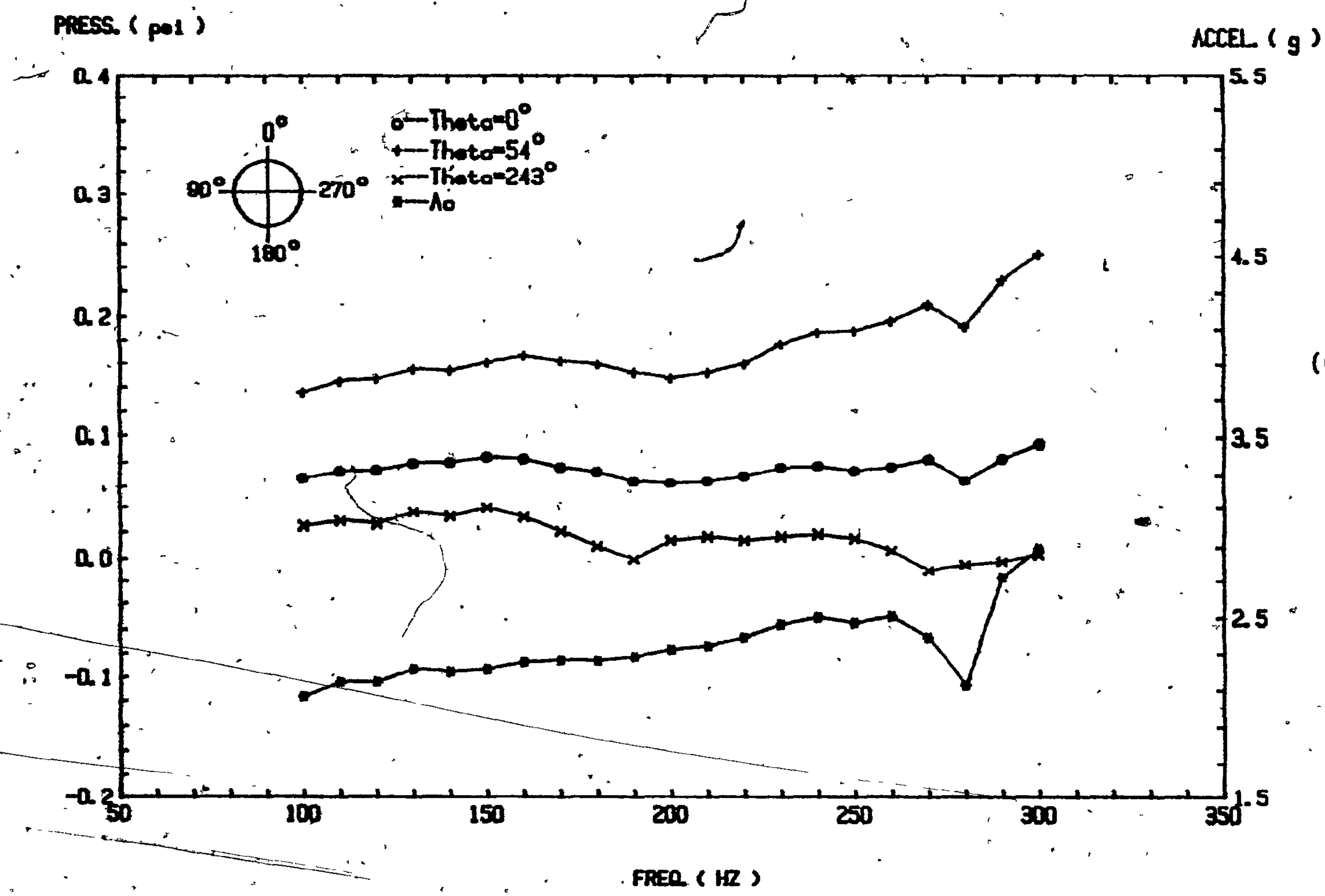

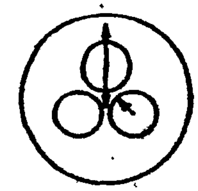

(Configuration of Fig. 4.6e)

<u>Fig. 6.38:</u> Pressure *versus* frequency curves measured on the cylinder (with inner arrow) for various θ. The test was done with lubricating oil after the modification of the experimental setup, as described in Section 6.2.

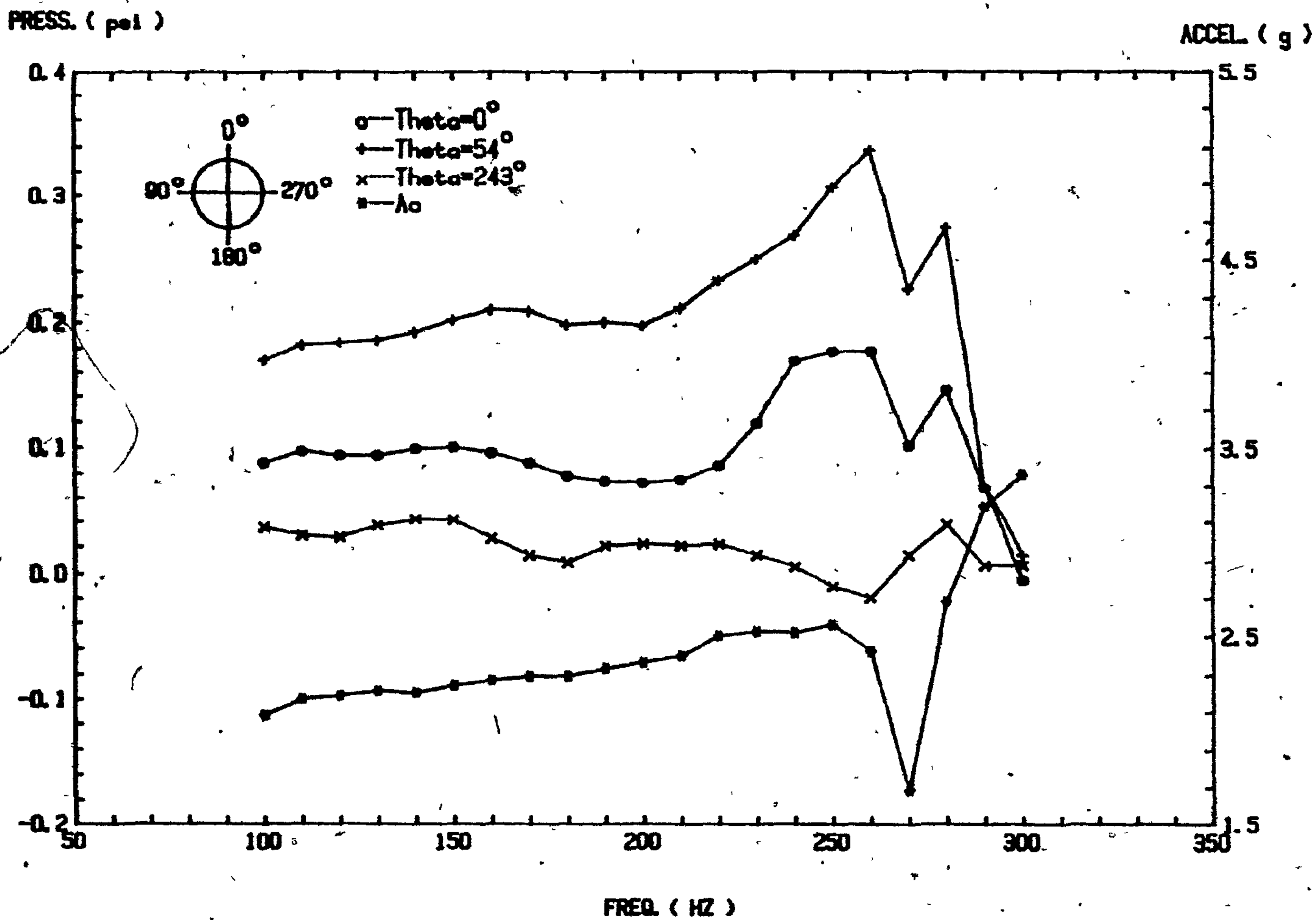

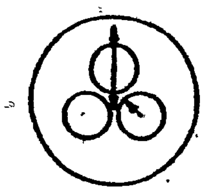

(Configuration of Fig. 4.6e)

Fig. 6.39: Pressure *versus* frequency curves measured on the cylinder (with inner arrow) for various θ. The test was done with ethylene glycol after the modification of the experimental setup, as described in Section 6.2.

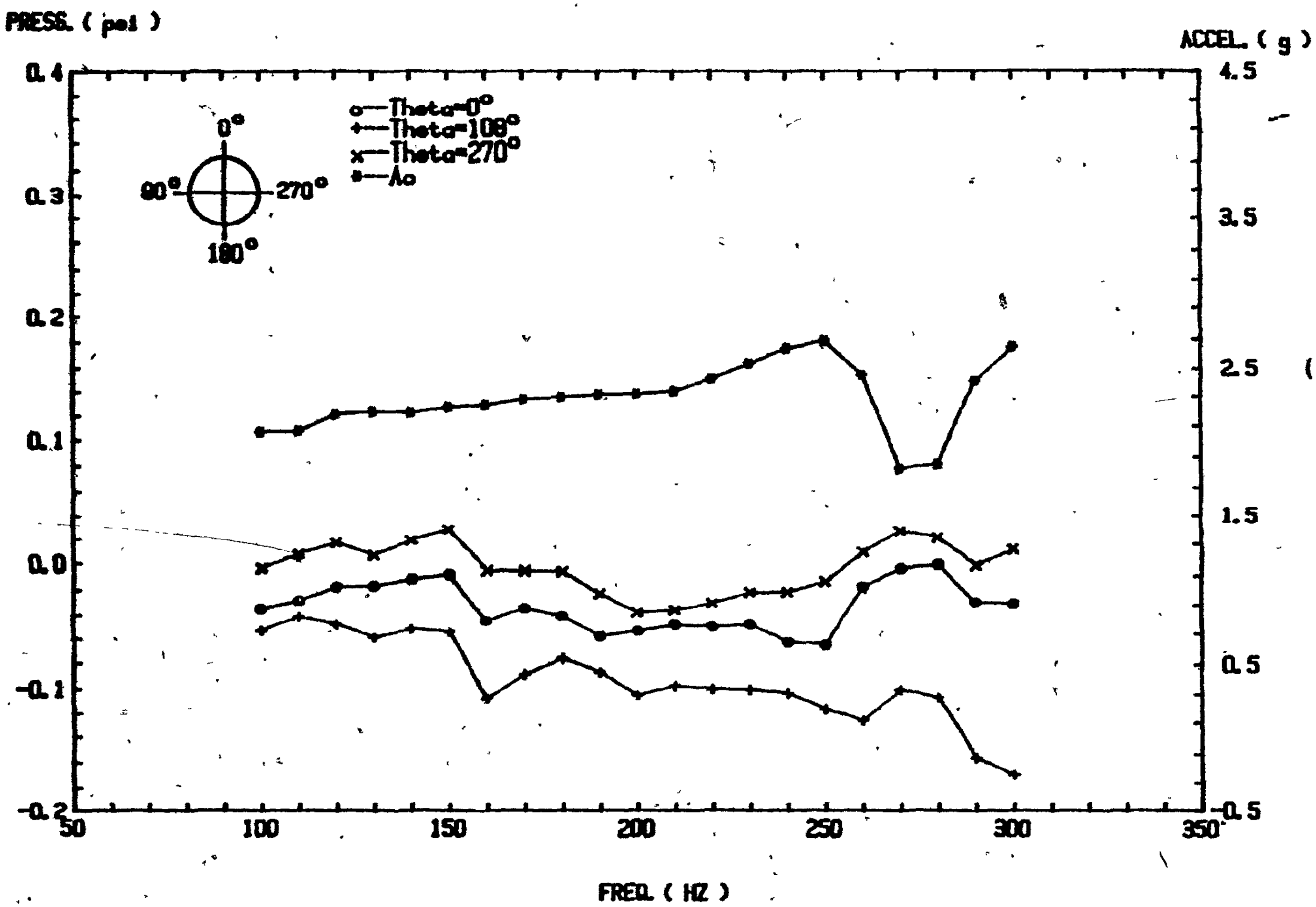

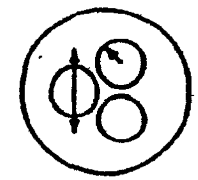

(Configuration of Fig. 4.6f)

Fig. 6.40: Pressure *versus* frequency curves measured on the cylinder (with inner arrow) for various θ. The test was done with water after the modification of the experimental setup, as described in Section 6.2.

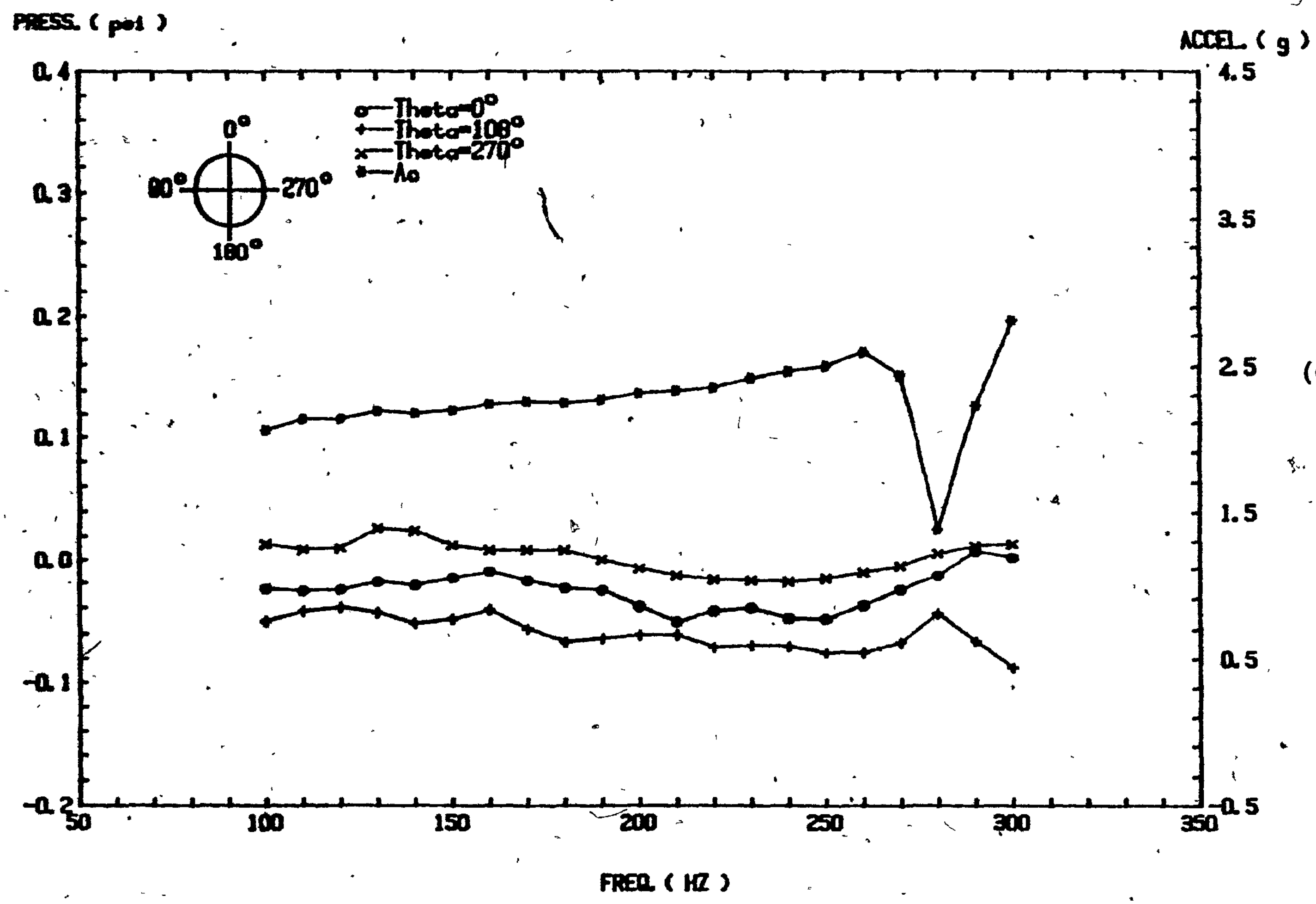

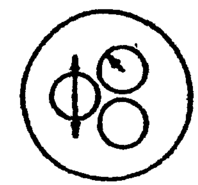

(Configuration of
Fig. 4.6f)

<u>Fig. 6.41</u>: Pressure *versus* frequency curves measured on the cylinder (with inner arrow) for various θ. The test was done with lubricating oil after the modification of the experimental setup, as described in Section 6.2.

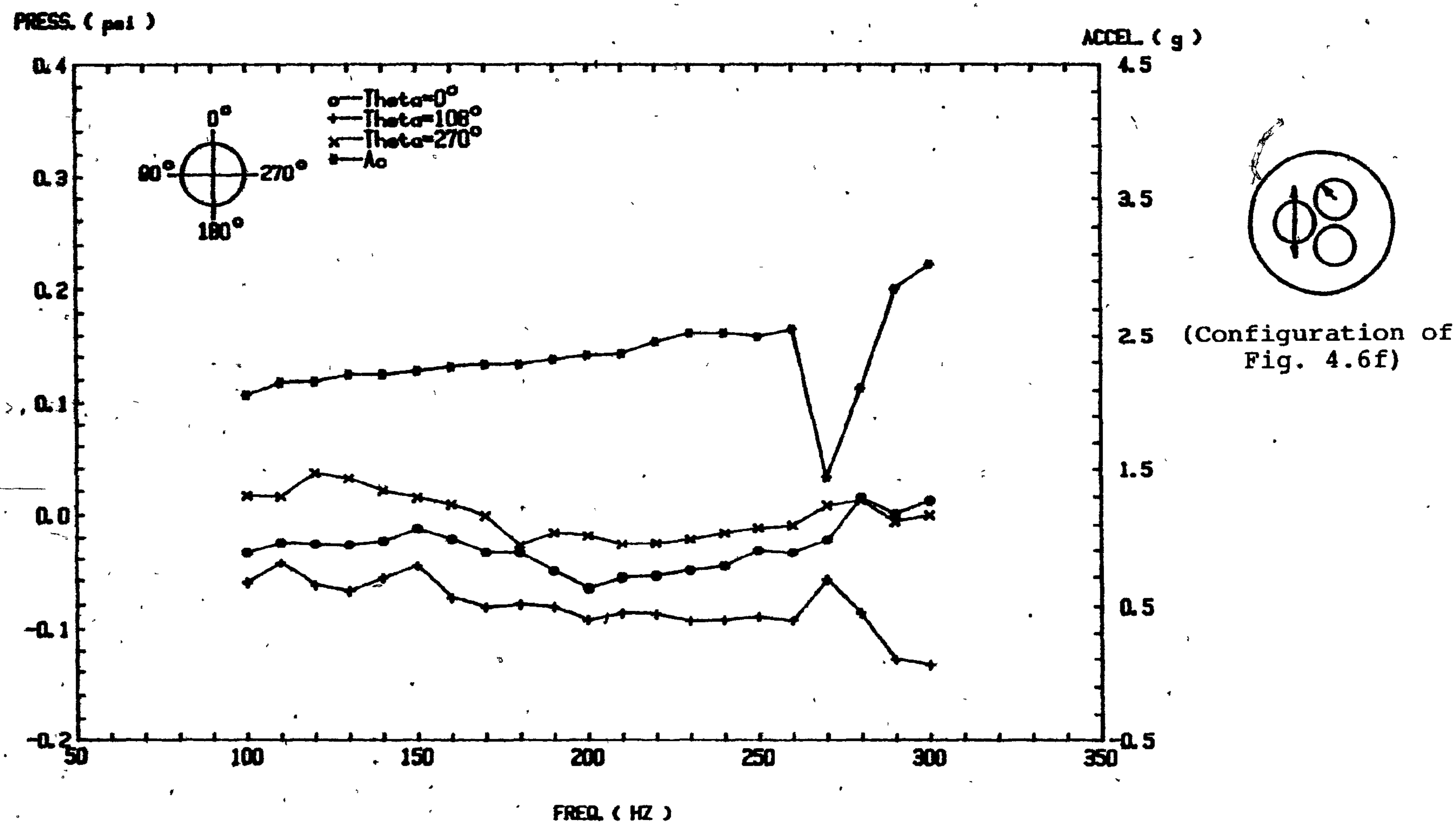

Fig. 6.42: Pressure *versus* frequency curves measured on the cylinder (with inner arrow) for various θ. The test was done with ethylene glycol after the modification of the experimental setup, as described in Section 6.2.

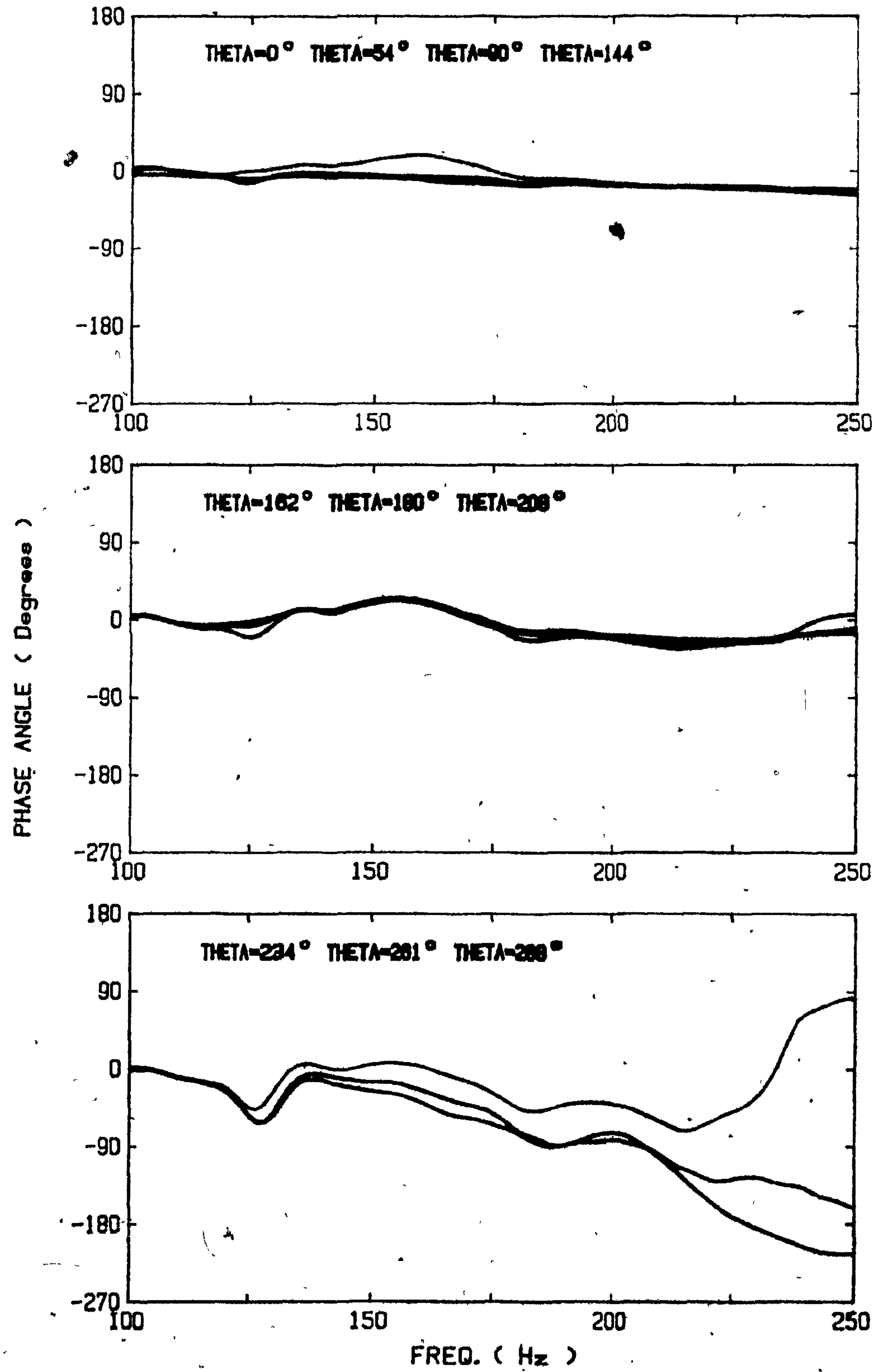

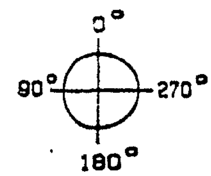

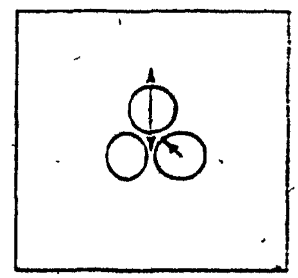

(Fig. 4.6c)

<u>Fig. 6.43:</u> Phase angle *versus* frequency diagrams for tests with water.

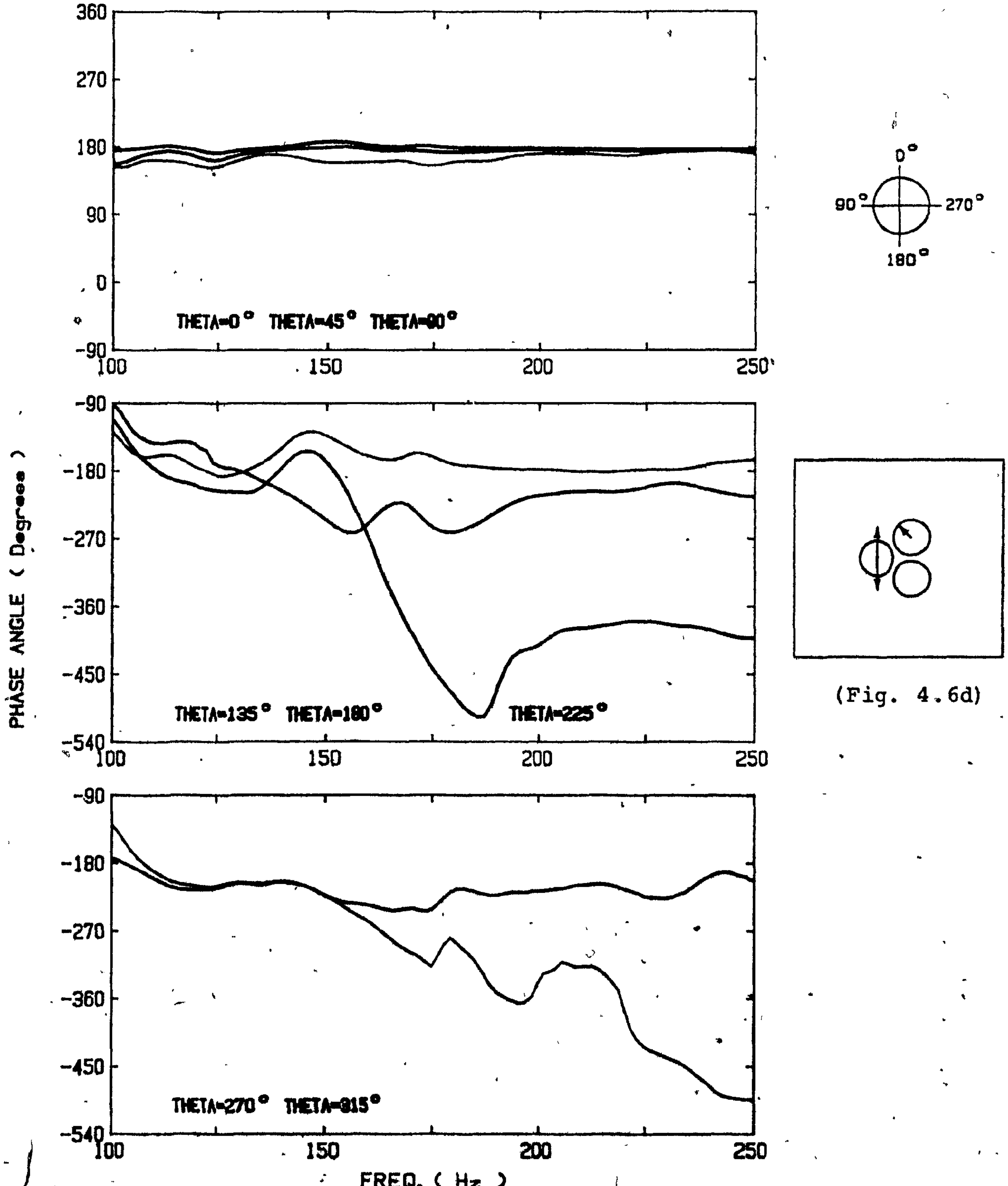

(Fig. 4.6d)

Fig. 6.44: Phase angle *versus* frequency diagrams for tests with water.

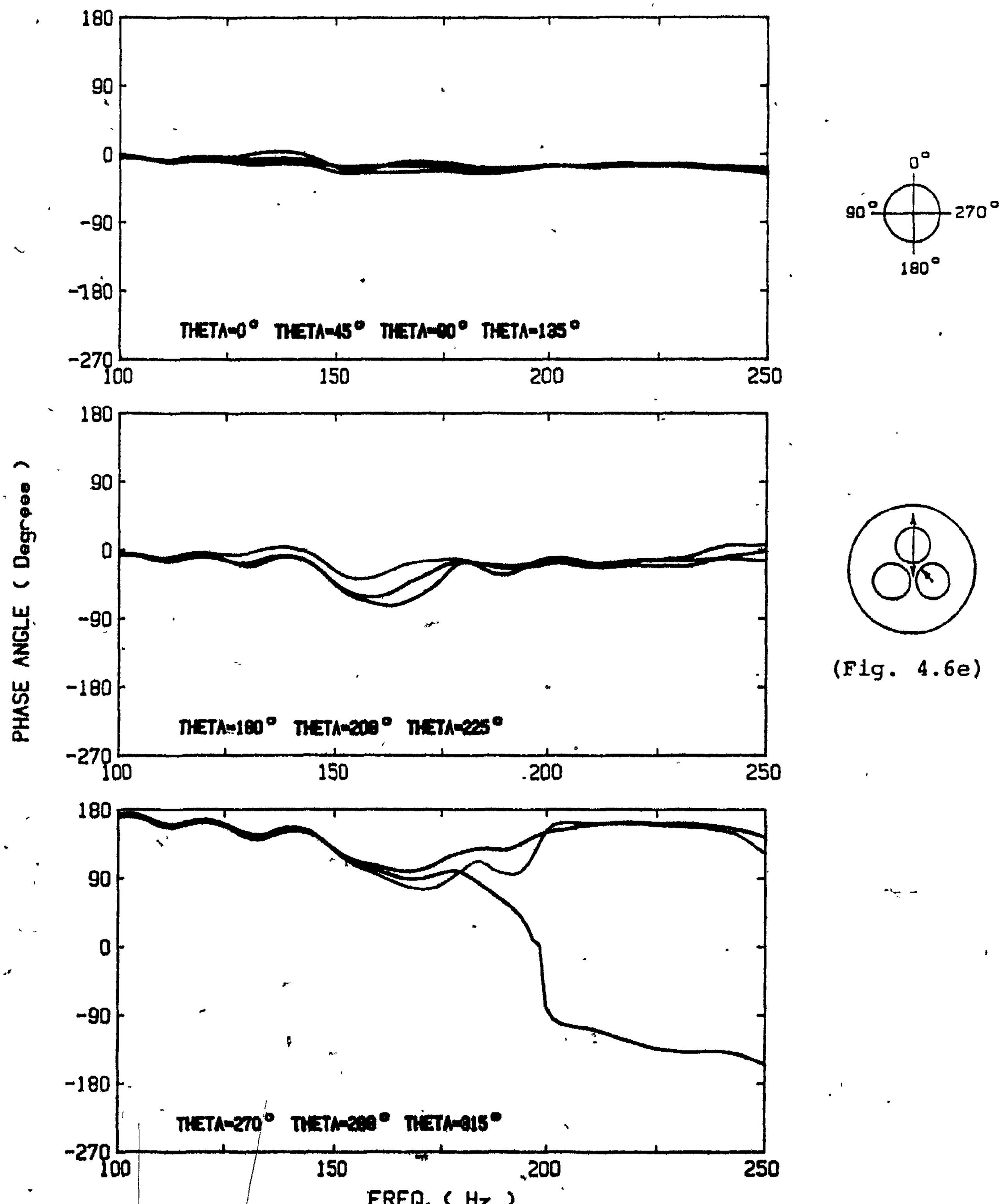

Fig. 6.45: Phase angle *versus* frequency diagrams for tests with water.

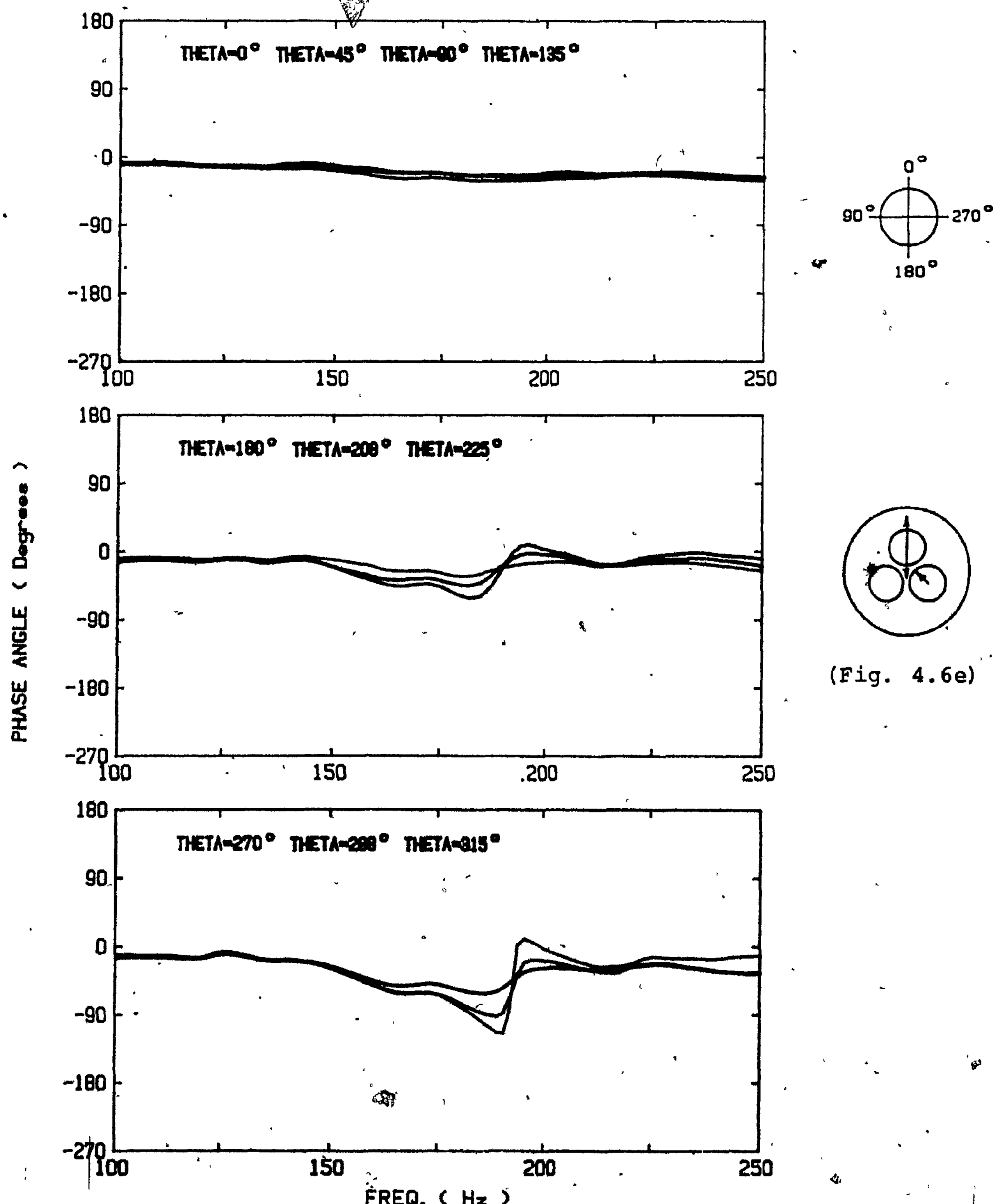

Fig. 6.46: Phase angle *versus* frequency diagrams for tests with lubricating oil.

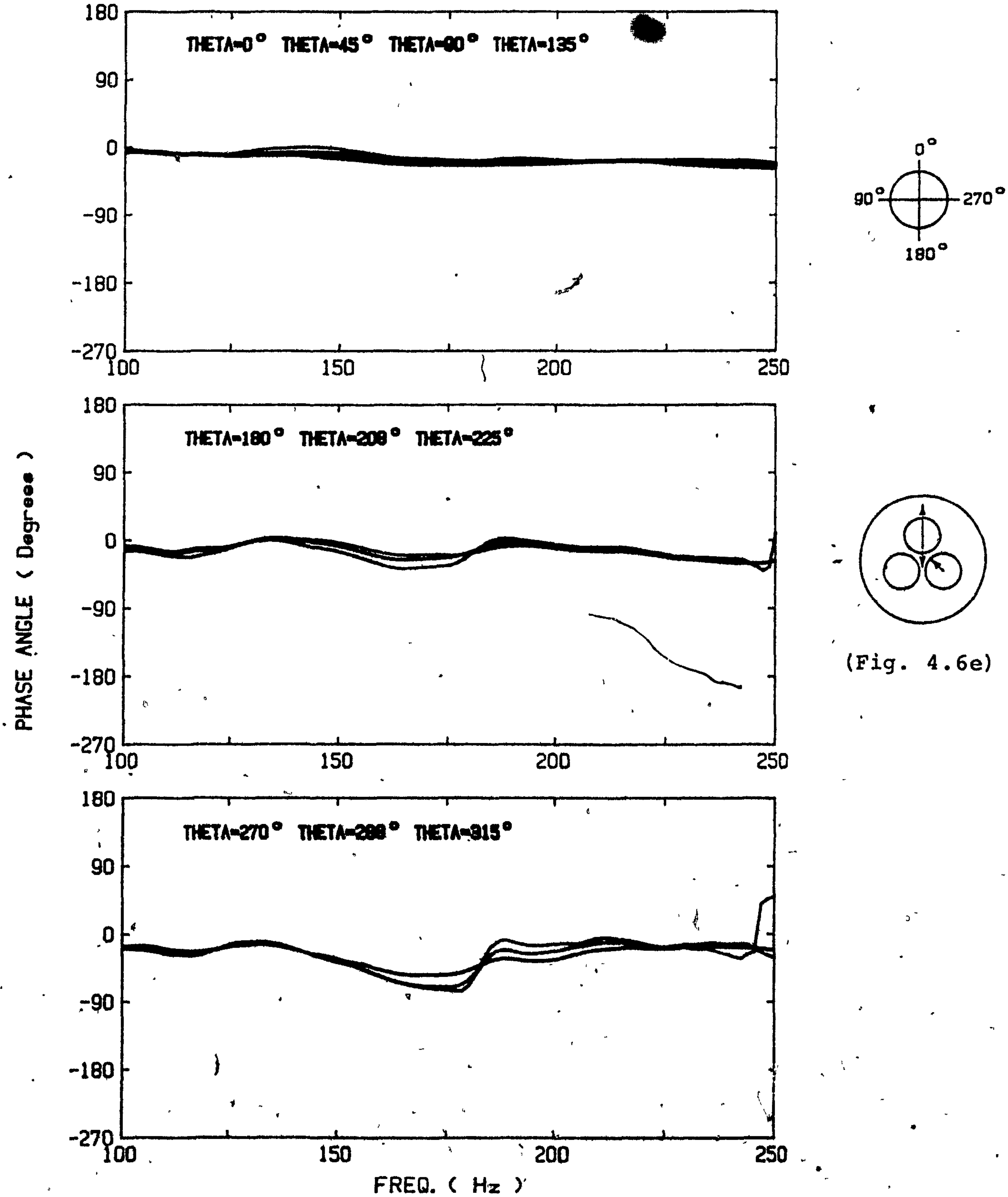

<u>Fig. 6.47</u>: Phase angle *versus* frequency diagrams for tests with ethylene glycol.

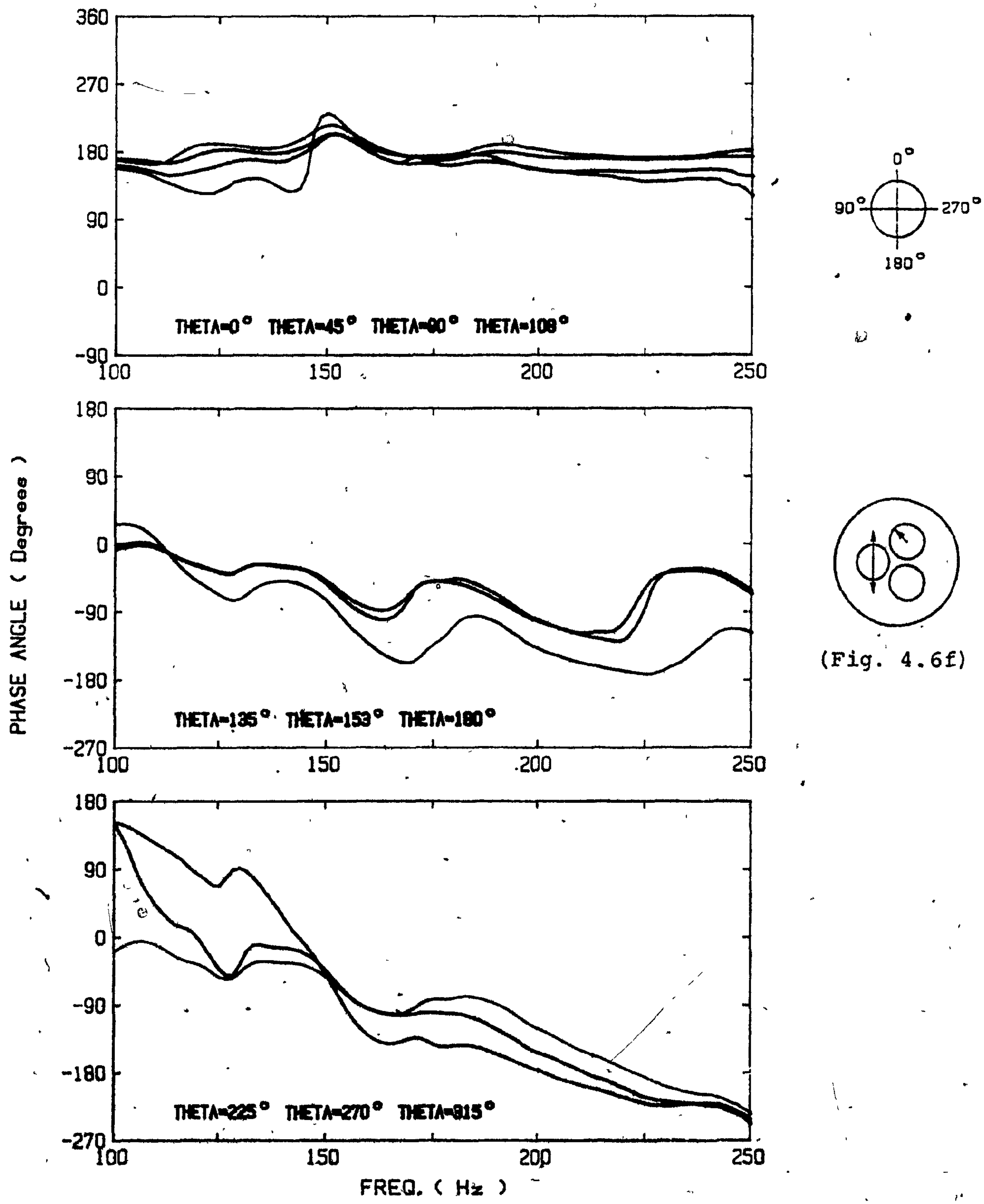

Fig. 6.48: Phase angle *versus* frequency diagrams for tests with water.

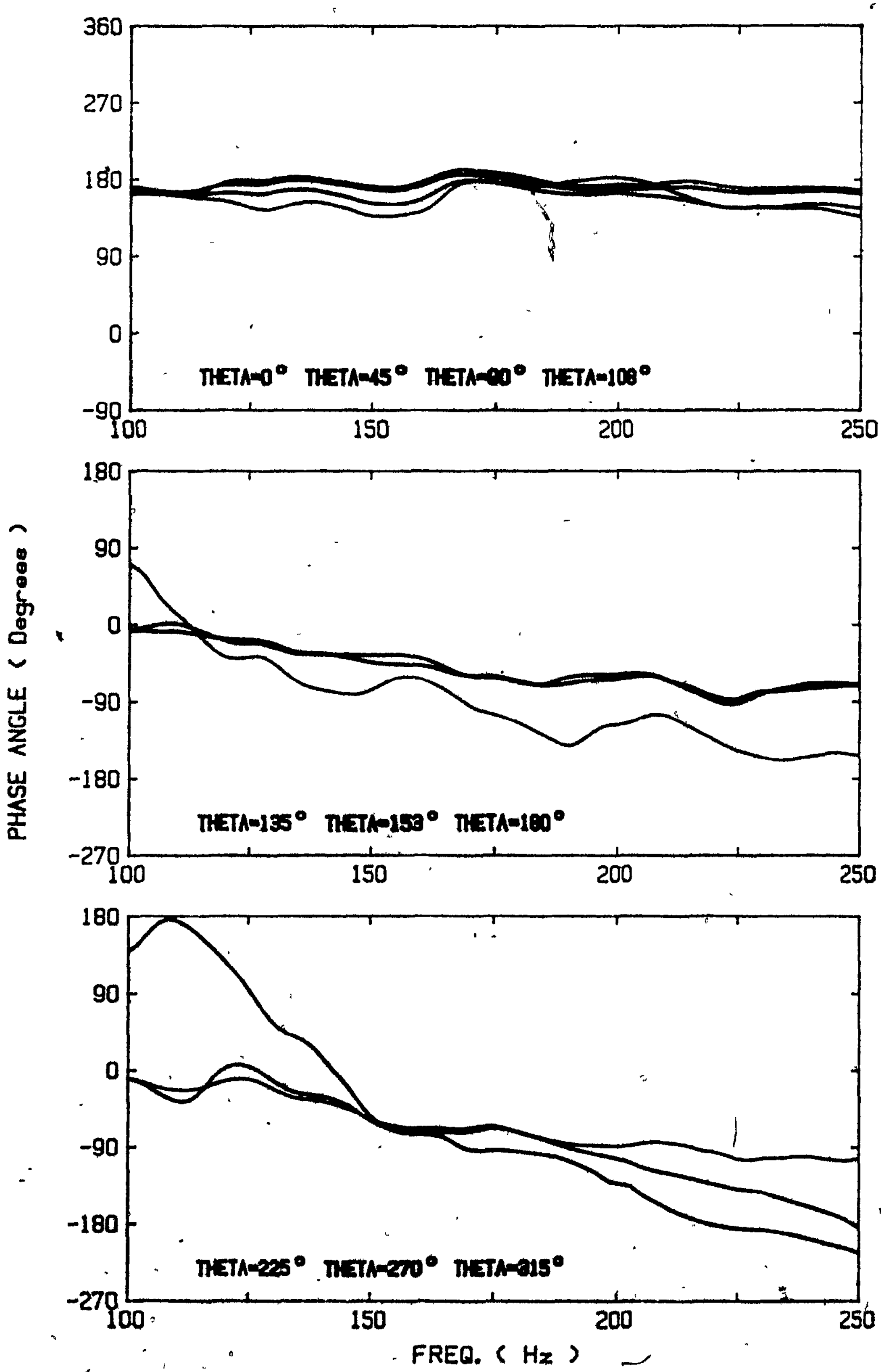

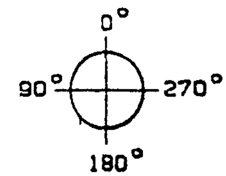

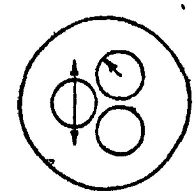

(Fig. 4.6f)

Fig. 6.49: Phase angle *versus* frequency diagrams for tests with lubricating oil.

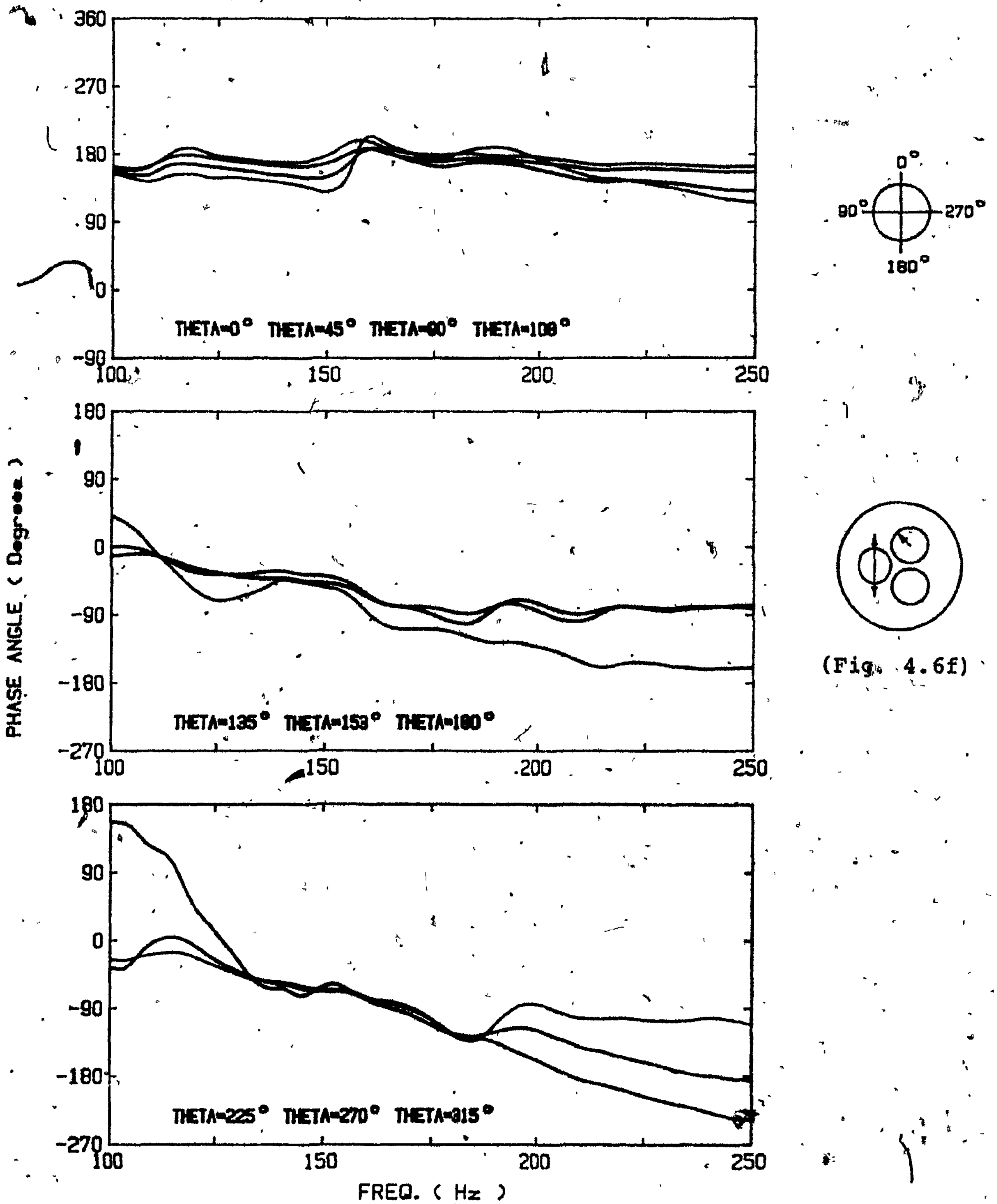

Fig. 6.50: Phase angle *versus* frequency diagrams for tests with ethylene glycol.

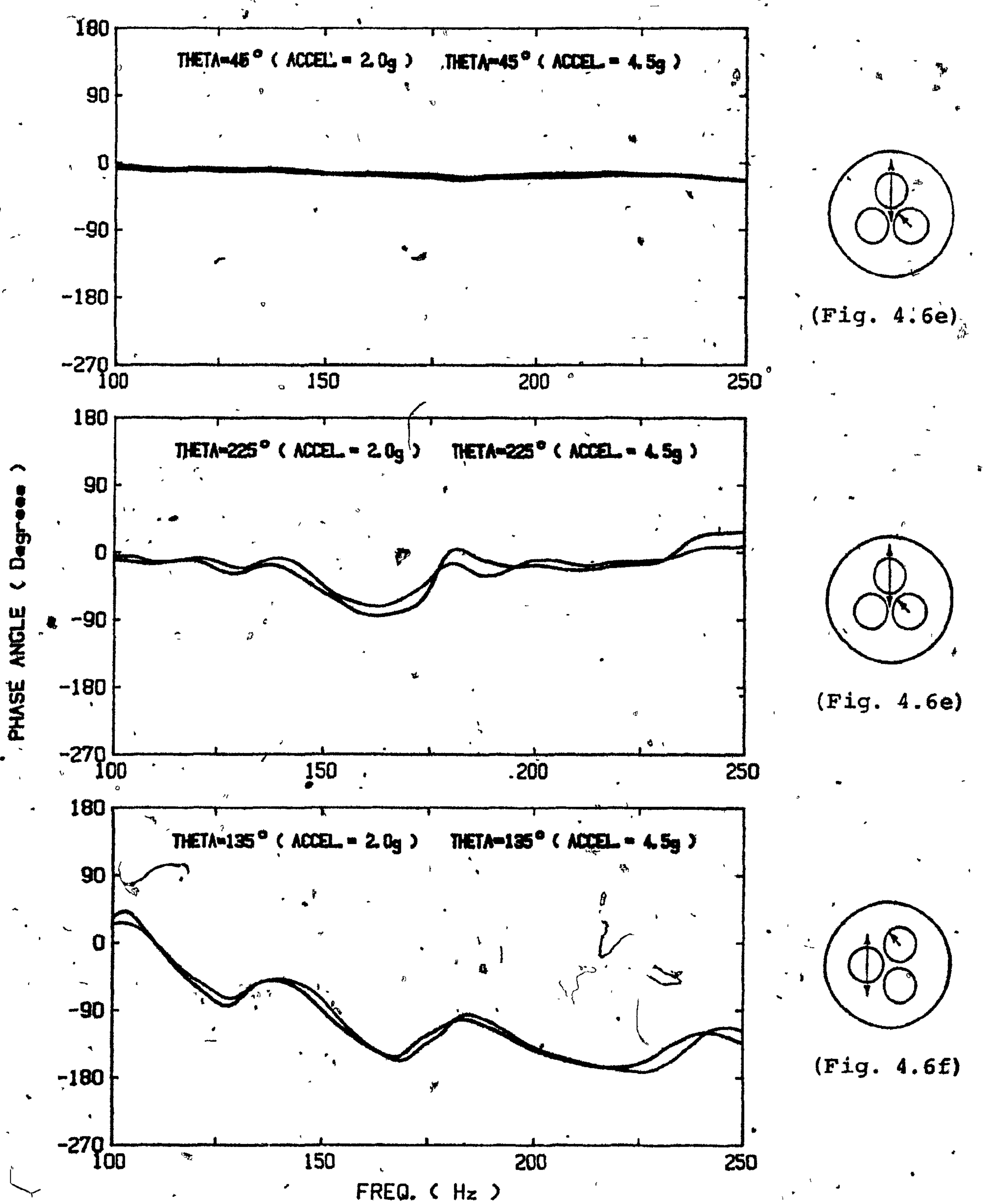

<u>Fig. 6.51</u>: Phase angle *versus* frequency diagrams for tests in water. The tests were done with different θ, Ac and configurations as shown

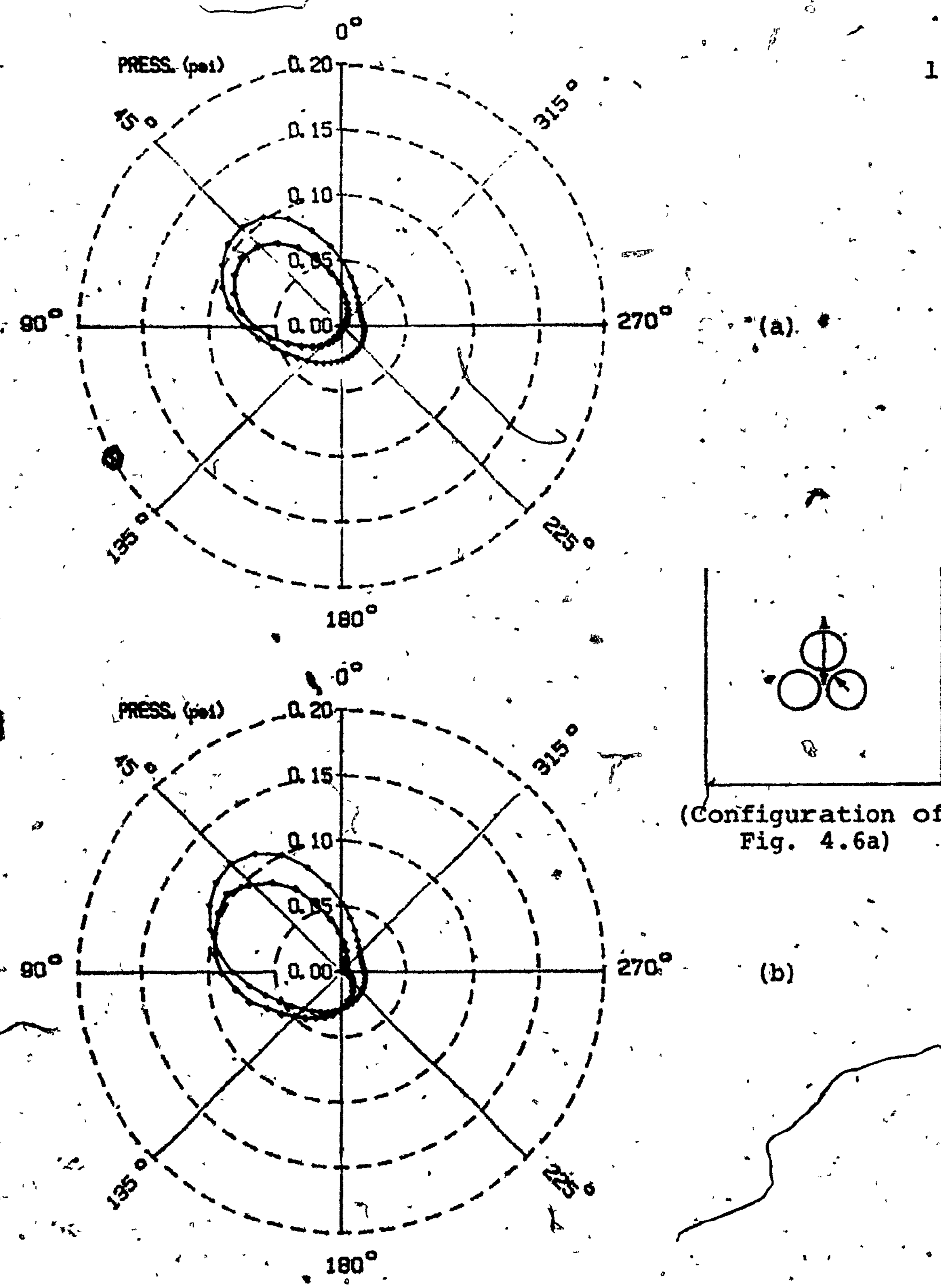

Fig. 6.52: Theoretical (black) and measured pressure profiles (red) of the stationary cylinder (with inner arrow). (a) Freq. = 80 Hz, Ac = 1.42 g; (b) Freq. = 200 Hz, Ac = 1.55 g.

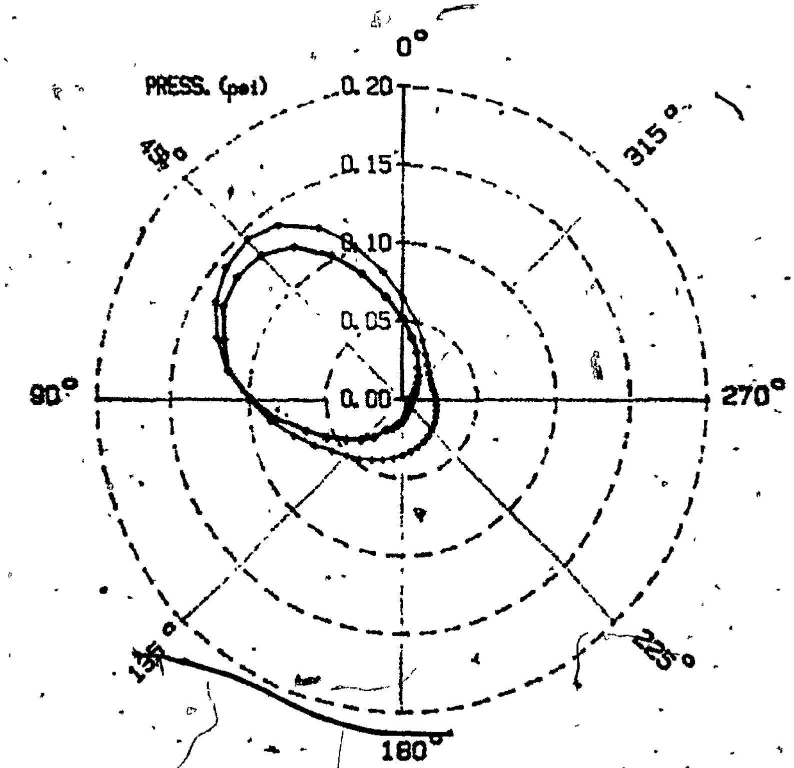

(a)

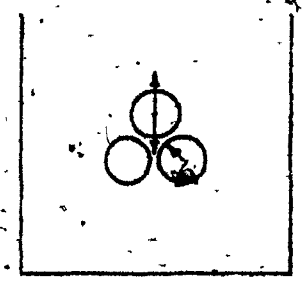

(Configuration of Fig. 4.6a)

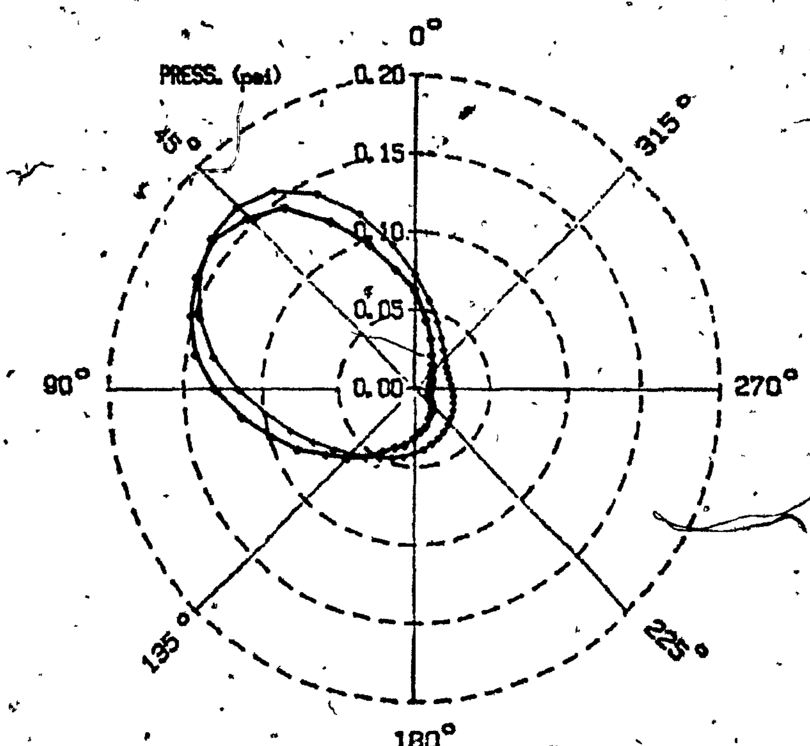

(b)

Fig. 6.53: Theoretical (black) and measured pressure profiles (red) of the stationary cylinder (with inner arrow). (a) Freq. = 100 Hz, Ac = 1.91 g; (b) Freq. = 180 Hz, Ac = 2.18 g.

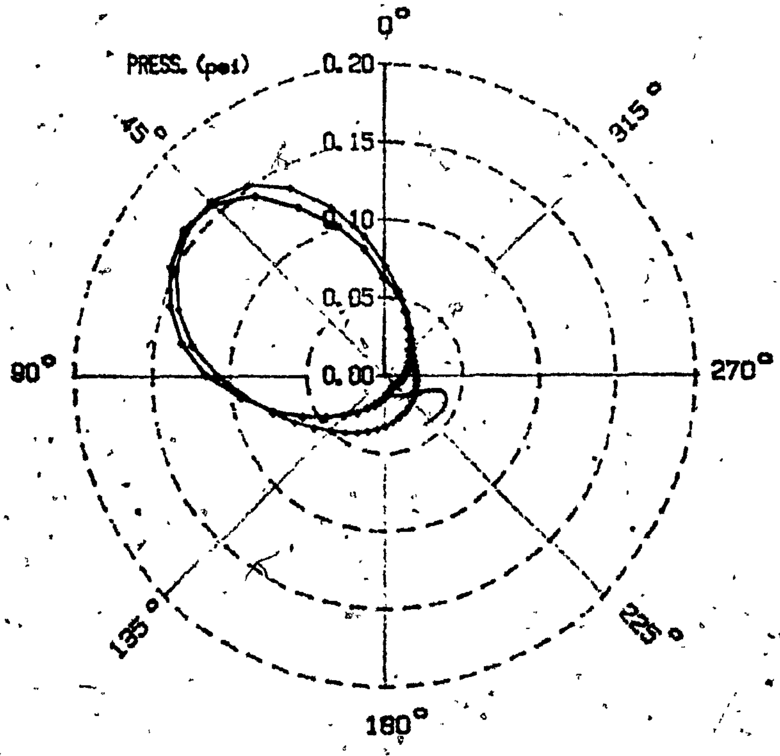

(a)

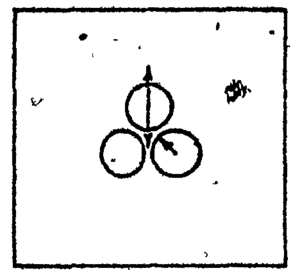

(Configuration of Fig. 4.6c)

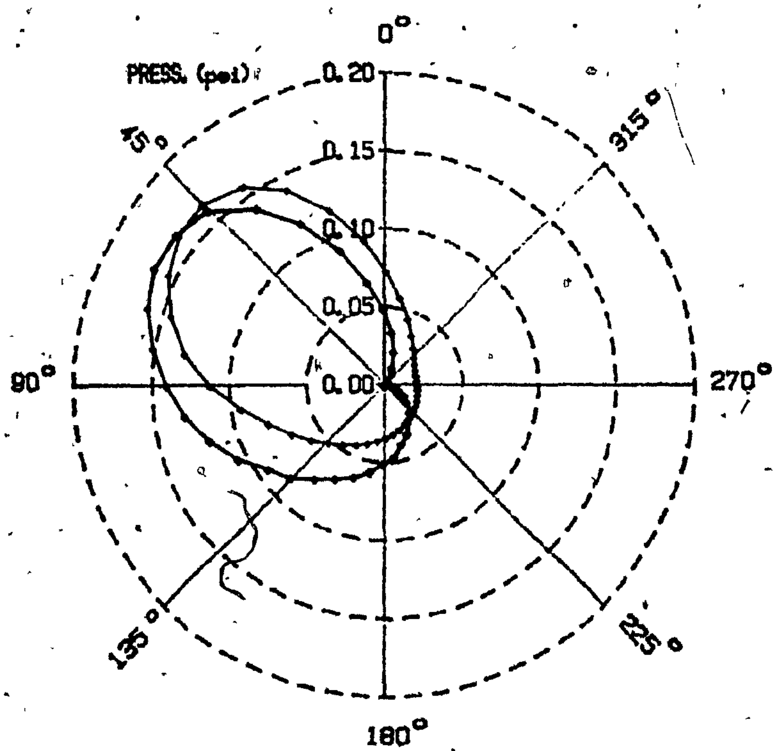

(b)

<u>Fig. 6.54</u>: Theoretical (black) and measured pressure profiles (red) of the stationary cylinder (with inner arrow). (a) Freq. = 100 Hz, Ac = 2.14 g; (b) Freq. = 200 Hz, Ac = 2.23 g.

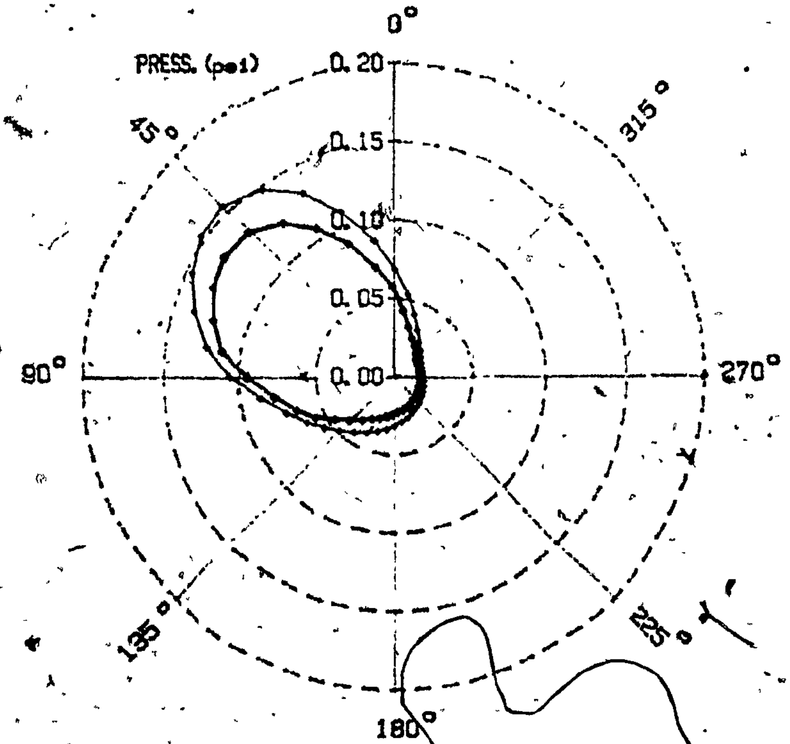

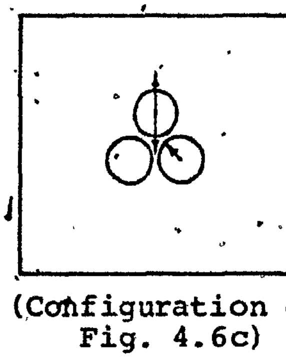

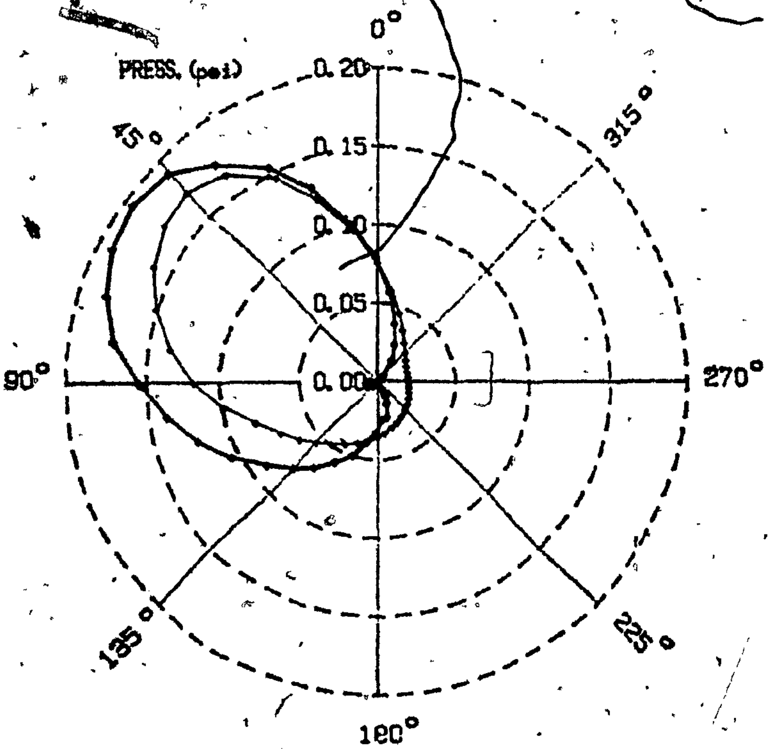

Fig. 6.55: Theoretical (black) and measured pressure profiles (red) of the stationary cylinder (with inner arrow). Measured profiles were obtained from the tests done after the experimental setup was modified, as described in Section 6.2. (a) Freq. = 100 Hz, Ac = 2.08 g; (b) Freq. = 250 Hz, Ac = 2.32 g.

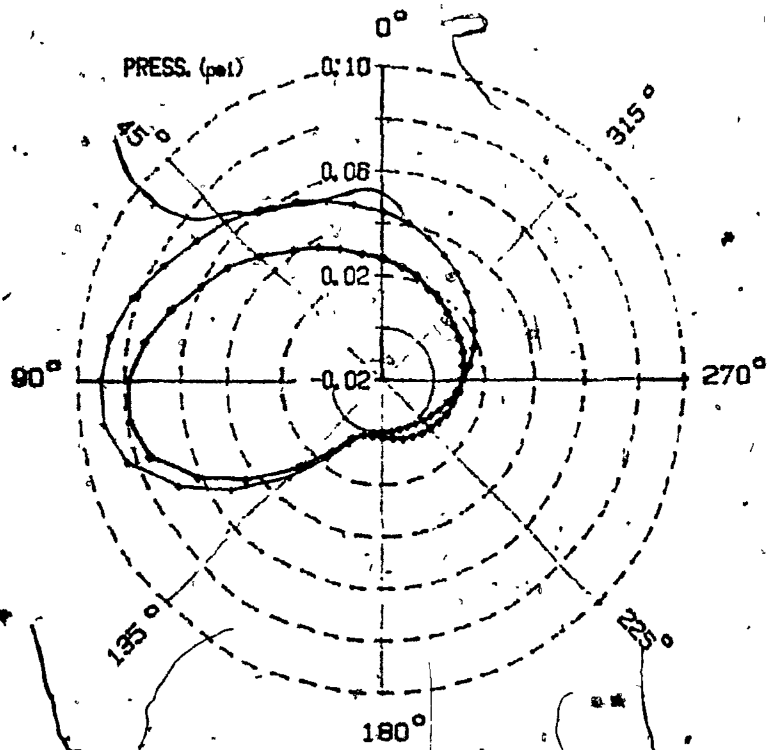

(a)

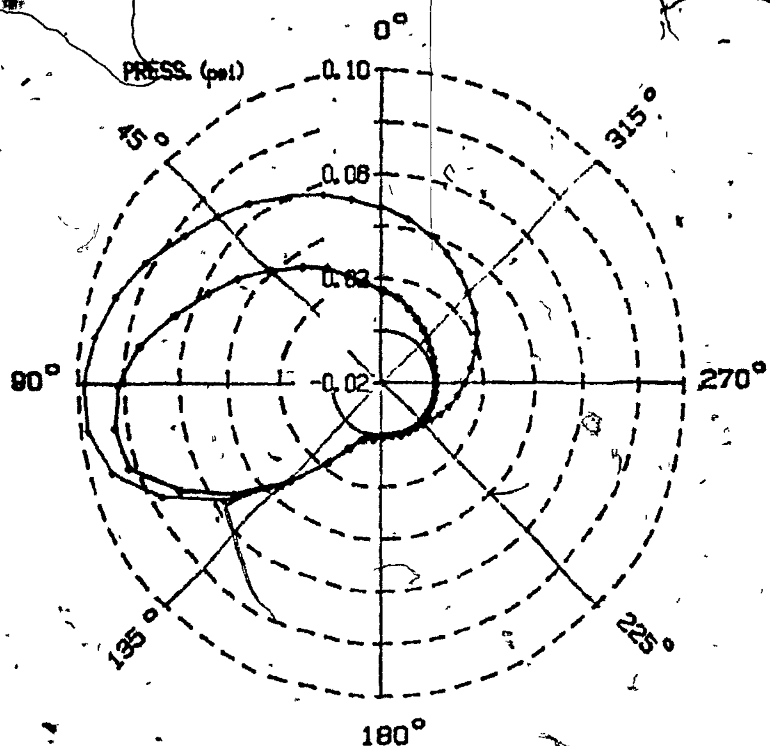

(b)

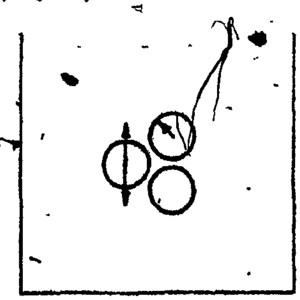

(Configuration of Fig. 4.6b)

Fig. 6.56: Theoretical (black) and measured pressure profiles (red) of the stationary cylinder (with inner arrow). (a) Freq. = 50 Hz, Ac = 1.99 g; (b) Freq. = 180 Hz, Ac = 2.15 g.

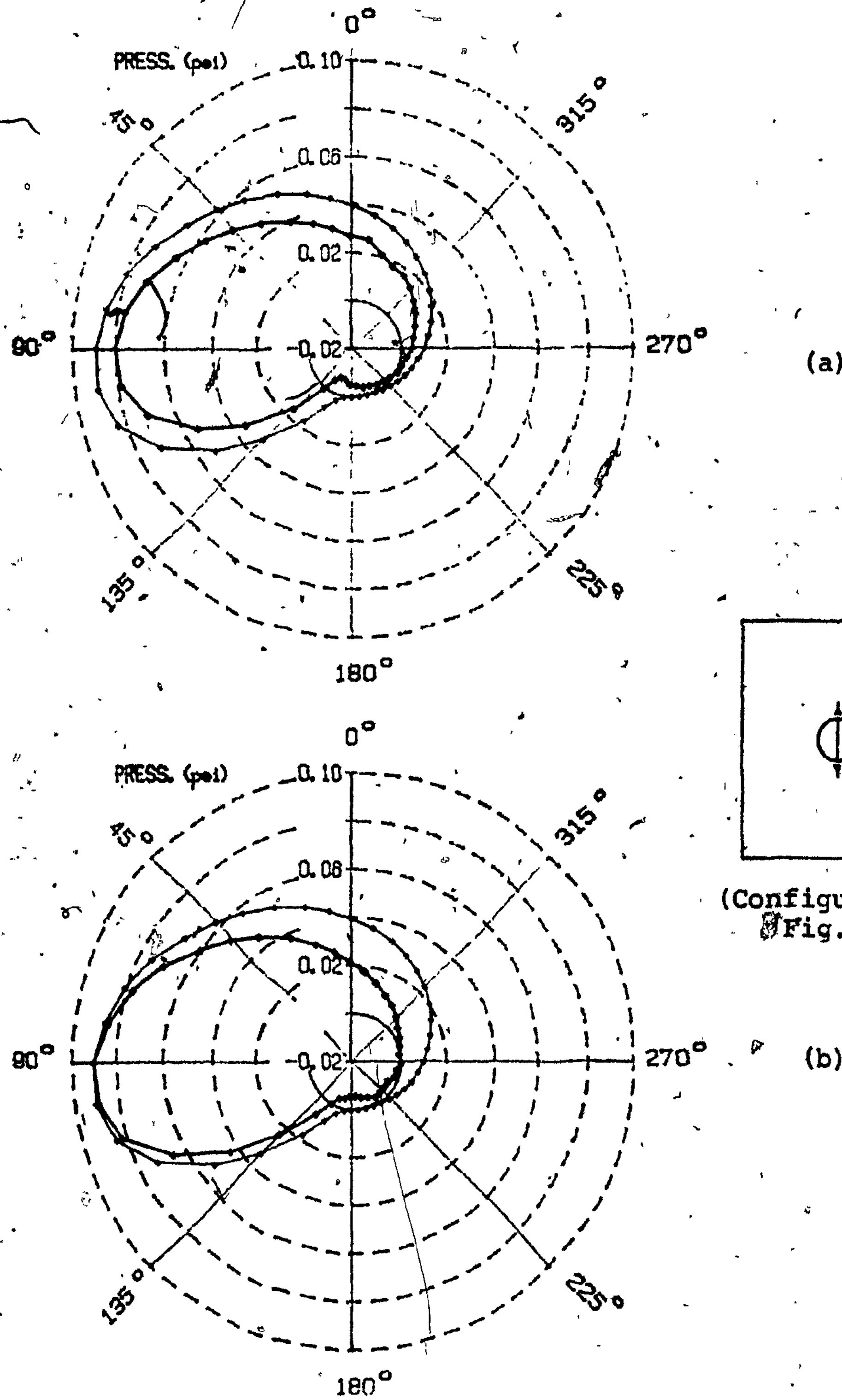

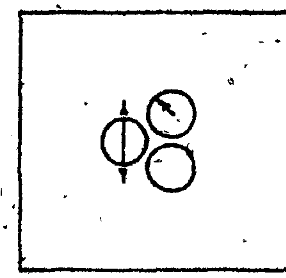

(Configuration of Fig. 4.6d)

Fig. 6.57: Theoretical (black) and measured pressure profiles (red) of the stationary cylinder (with inner arrow). (a) Freq. = 90 Hz, Ac = 2.09 g; (b) Freq. = 180 Hz, Ac = 2.11 g.

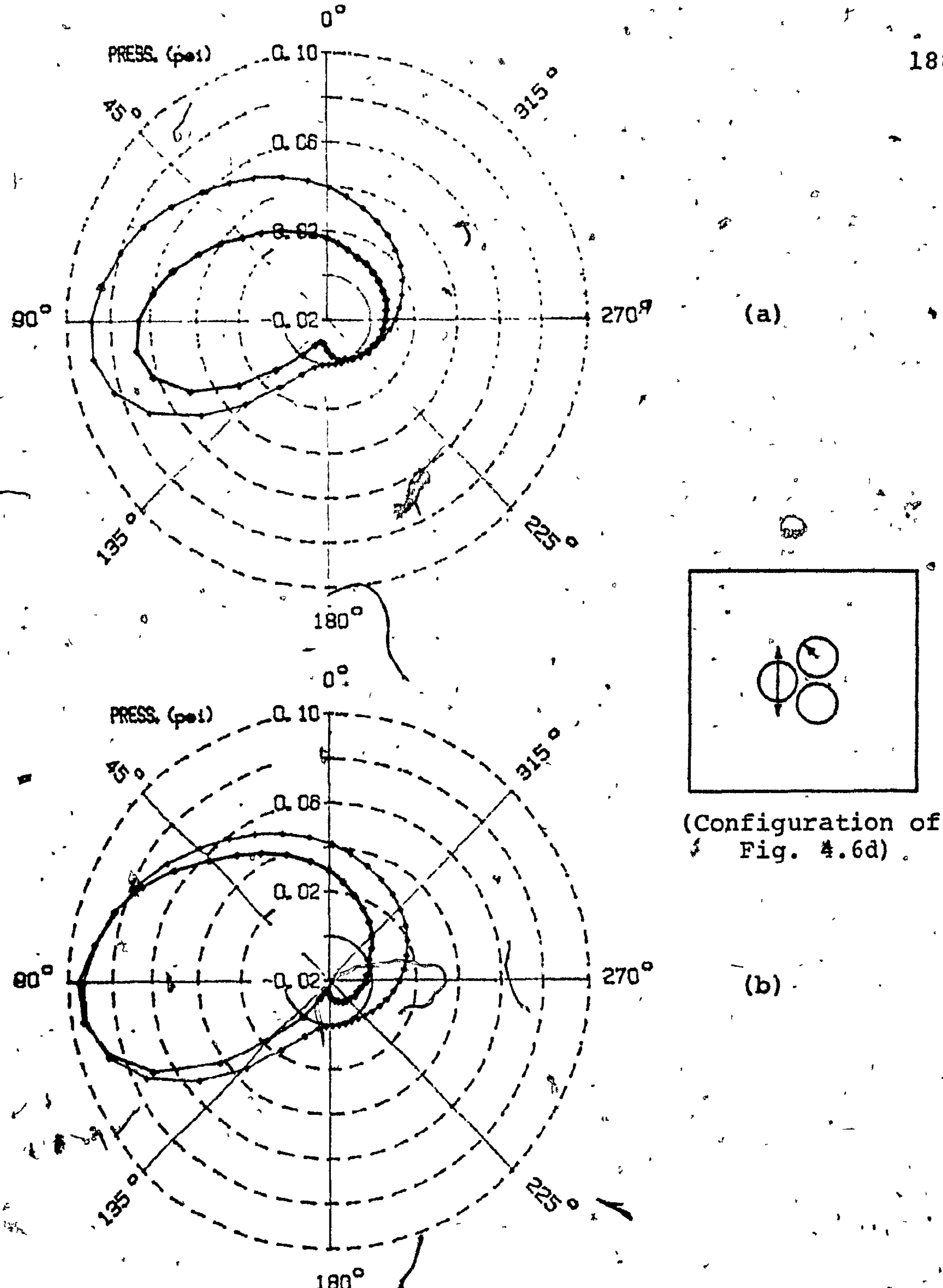

Fig. 6.58: Theoretical (black) and measured pressure profiles (red) of the stationary cylinder (with inner arrow). Measured profiles were obtained from the tests done after the experimental setup was modified, as described in Section 6.2. (a) Freq. = 130 Hz, Ac = 2.09 g; (b) Freq. = 250 Hz, Ac = 2.28 g.

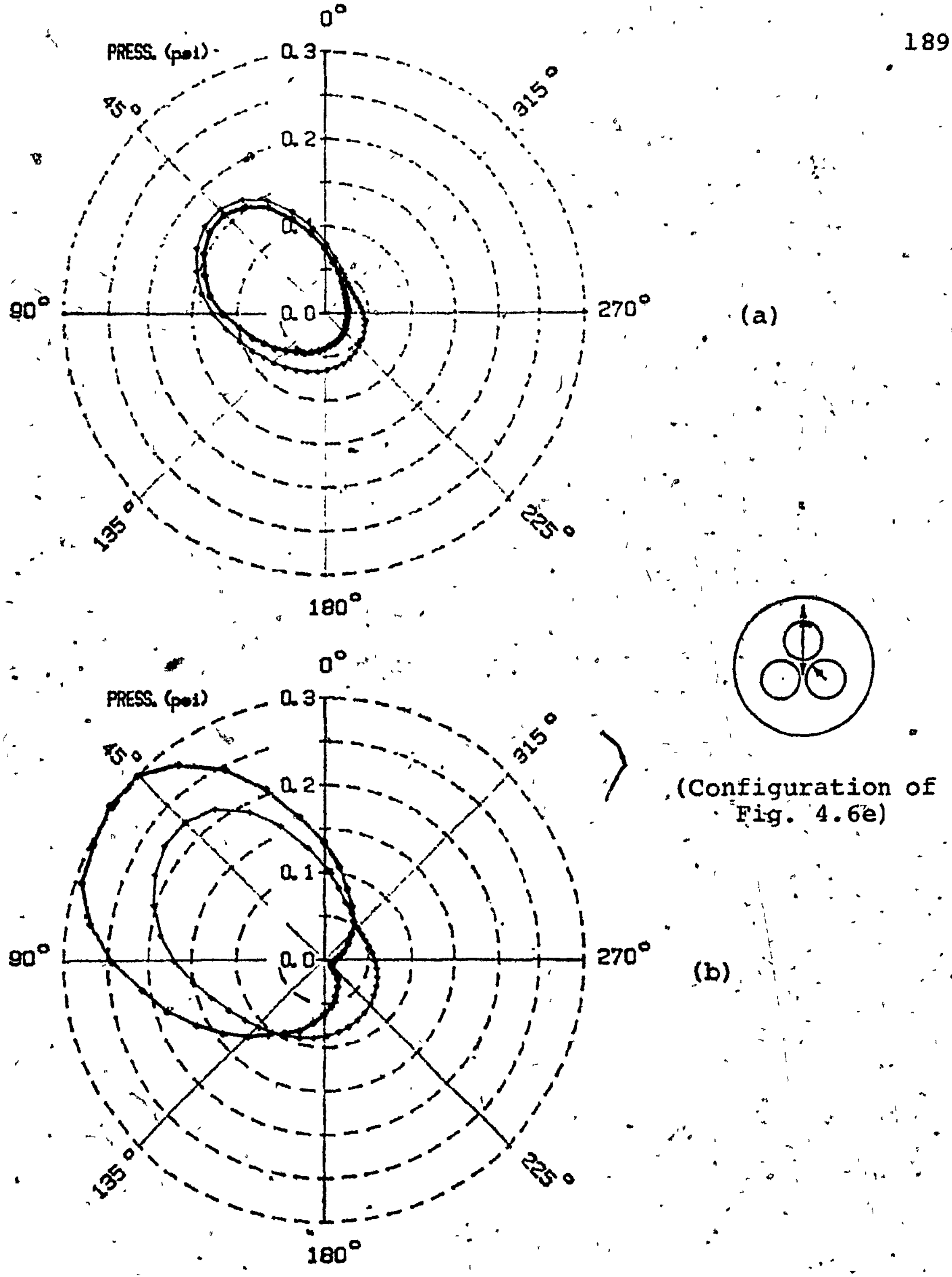

Fig. 6.59: Theoretical (black) and measured pressure profiles (red) of the stationary cylinder (with inner arrow). Measured profiles were obtained from the tests done with water after the modification, as described in Section 6.2. (a) Freq. = 100 Hz, Ac = 2.09 g; (b) Freq. = 250 Hz, Ac = 2.77 g.

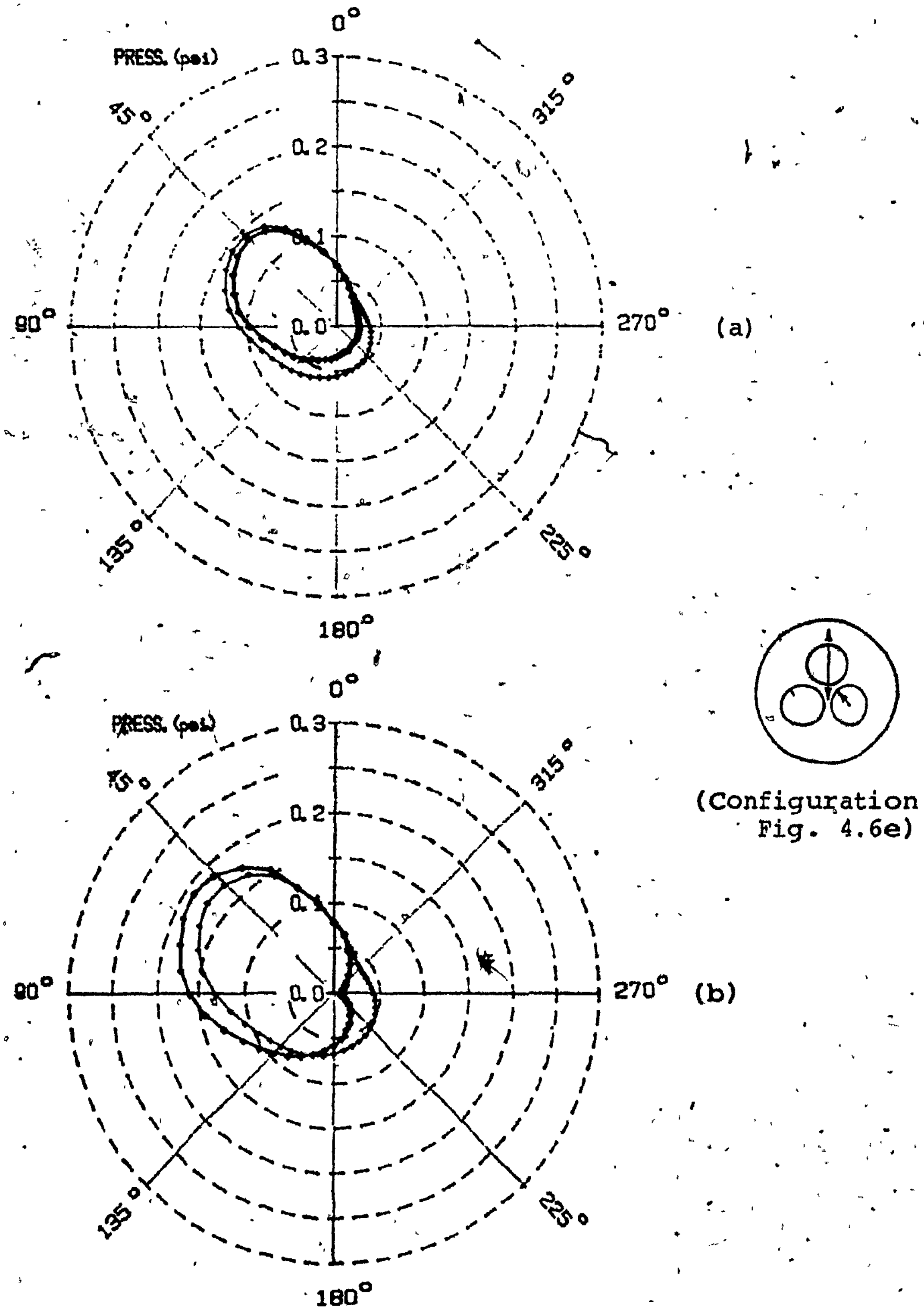

Fig. 6.60: Theoretical (black) and measured pressure profiles (red) of the stationary cylinder (with inner arrow). Measured profiles were obtained from the tests done with oil after the modification, as described in Section 6.2. (a) Freq. = 100 Hz, Ac = 2.06 g; (b) Freq. = 250 Hz, Ac = 2.47 g.

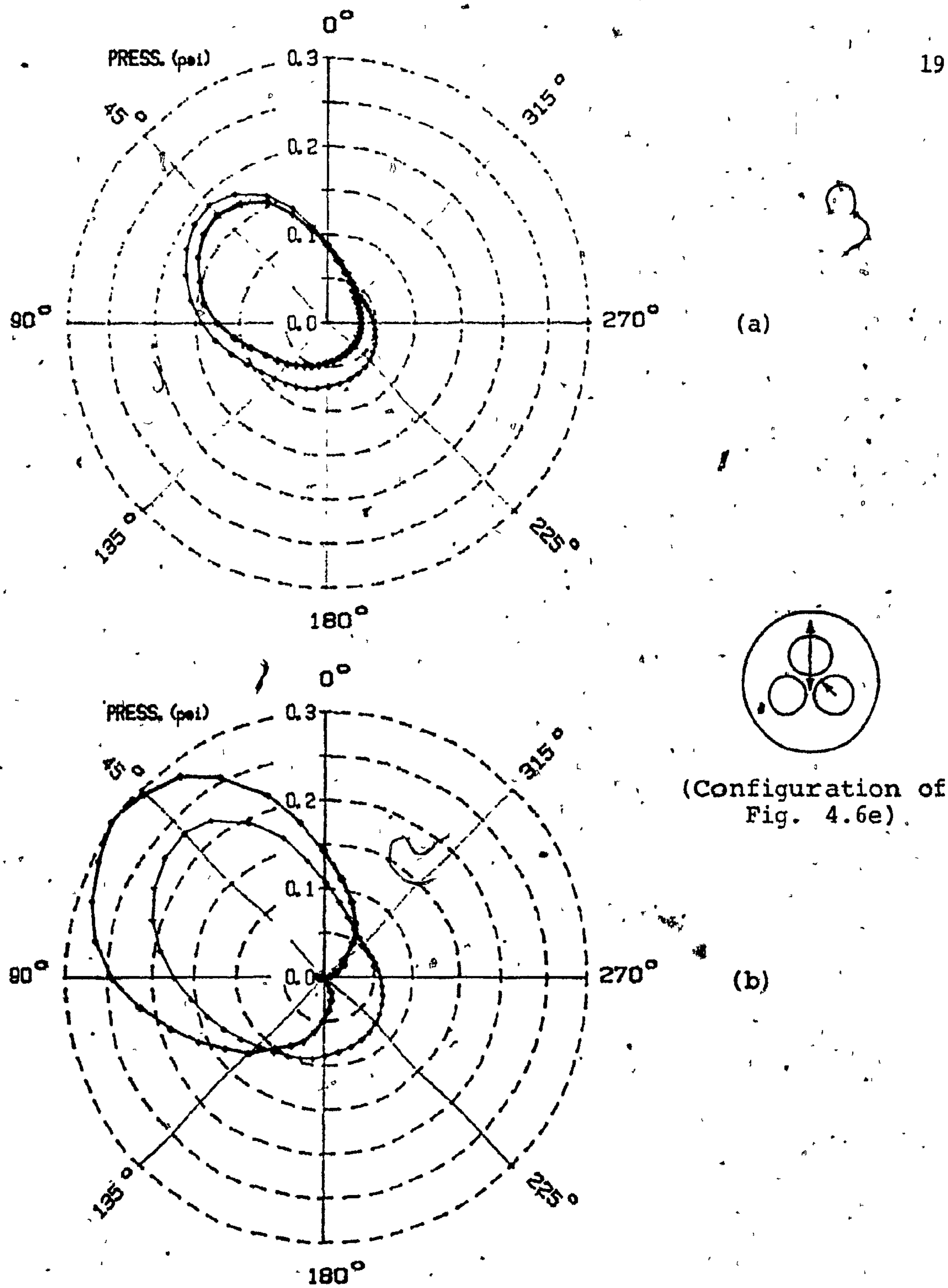

<u>**Fig. 6.61**</u>: Theoretical (black) and measured pressure profiles (red) of the stationary cylinder (with inner arrow). Measured profiles were obtained from the tests done with ethylene glycol after the modification, as described in Section 6.2. (a) Freq. = 100 Hz, Ac = 2.09 g; (b) Freq. = 250 Hz, Ac = 2.56 g.

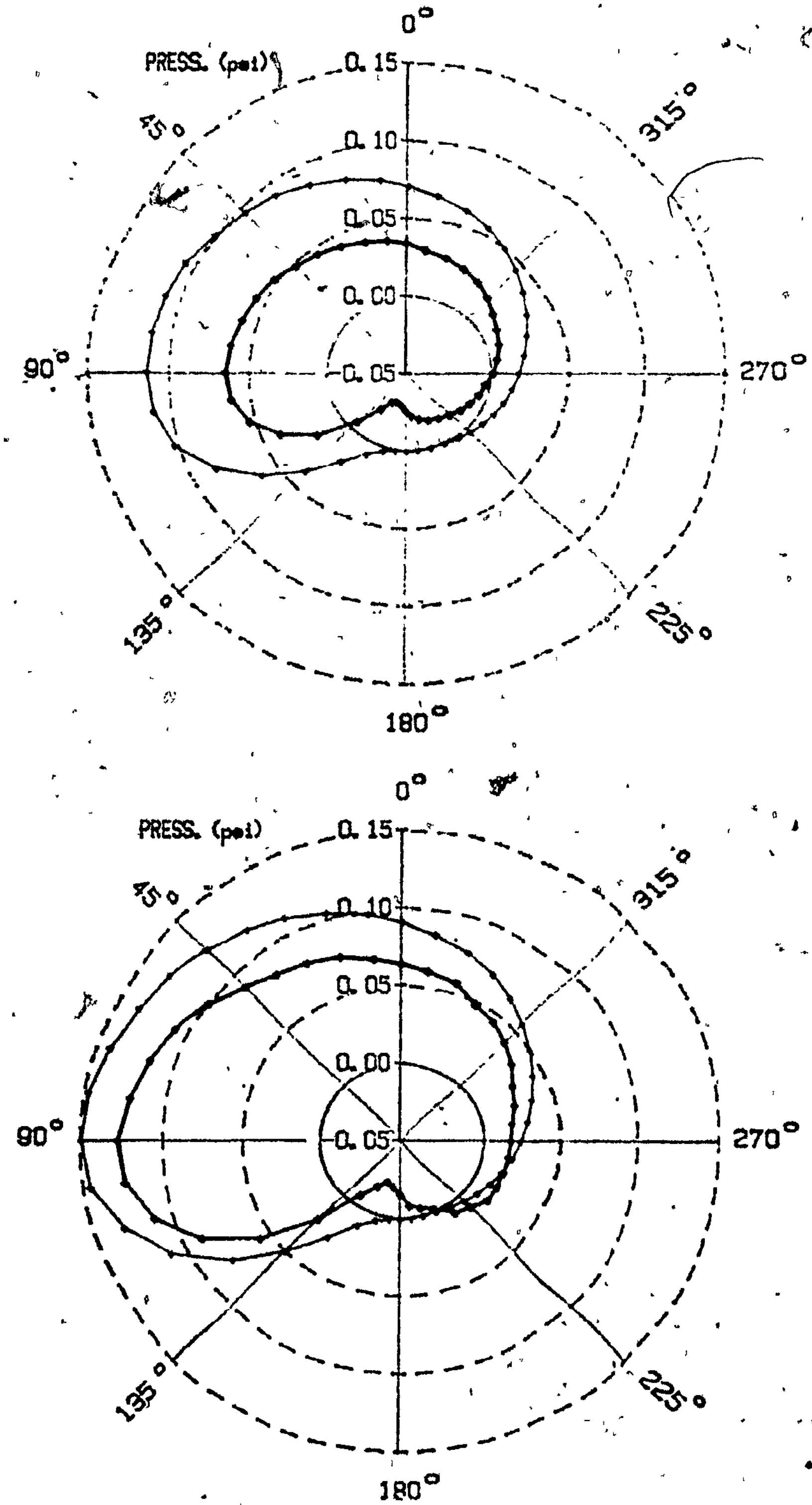

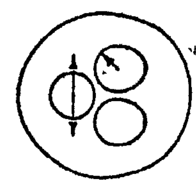

(Configuration of Fig. 4.6f)

<u>Fig. 6.62:</u> Theoretical (black) and measured pressure profiles (red) of the stationary cylinder (with inner arrow). Measured profiles were obtained from the tests done with water after the modification, as described in Section 6.2. (a) Freq. = 100 Hz, Ac = 2.05 g; (b) Freq. = 250 Hz, Ac = 2.65 g.

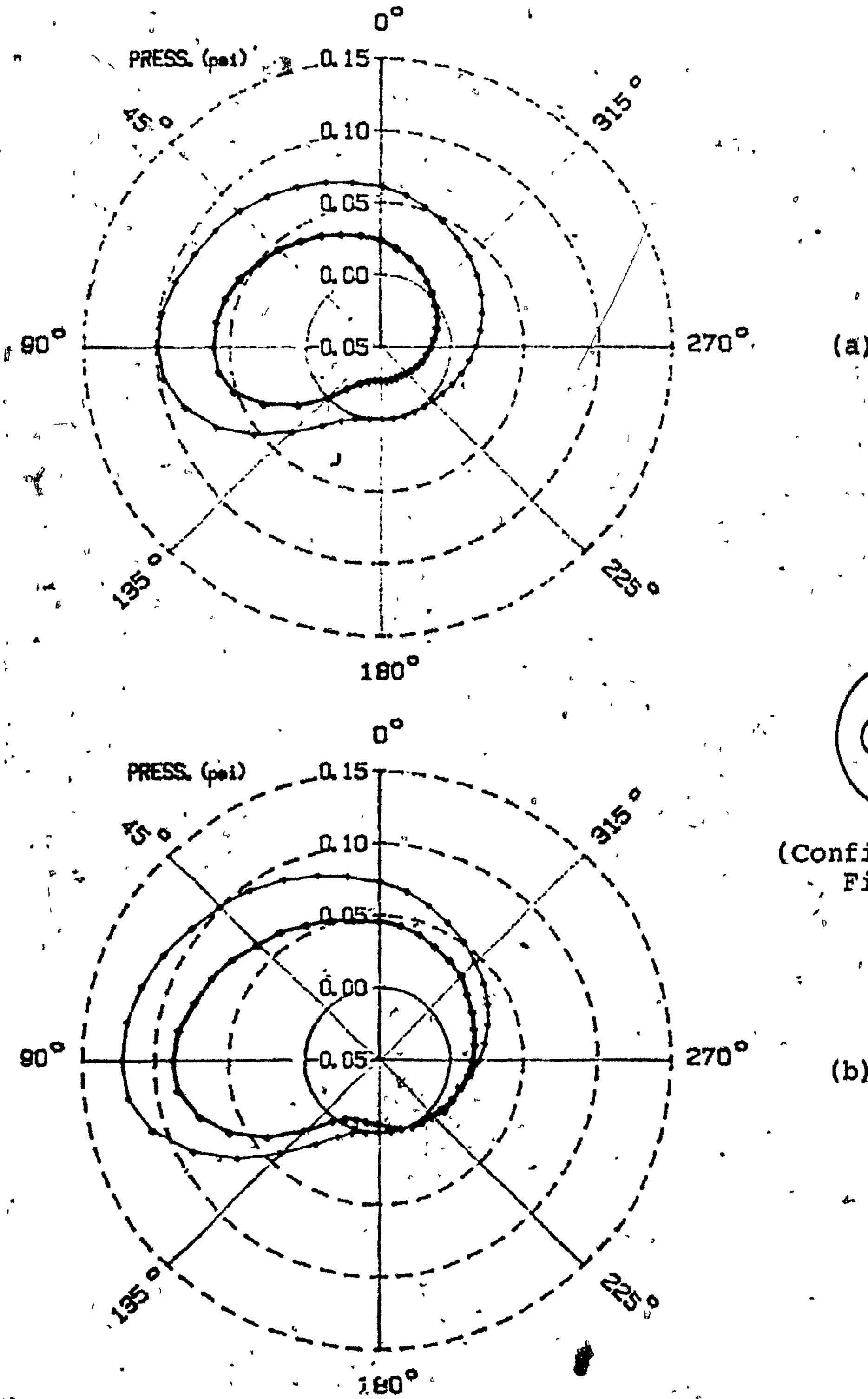

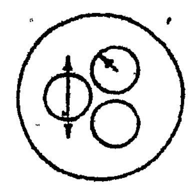

(Configuration of Fig. 4.6f)

Fig. 6.63: Theoretical (black) and measured pressure profiles (red) of the stationary cylinder (with inner arrow). Measured profiles were obtained from the tests done with oil after the modification, as described in Section 6.2. (a) Freq. = 100 Hz, Ac = 2.05 g; (b) Freq. = 250 Hz, Ac = 2.50 g.

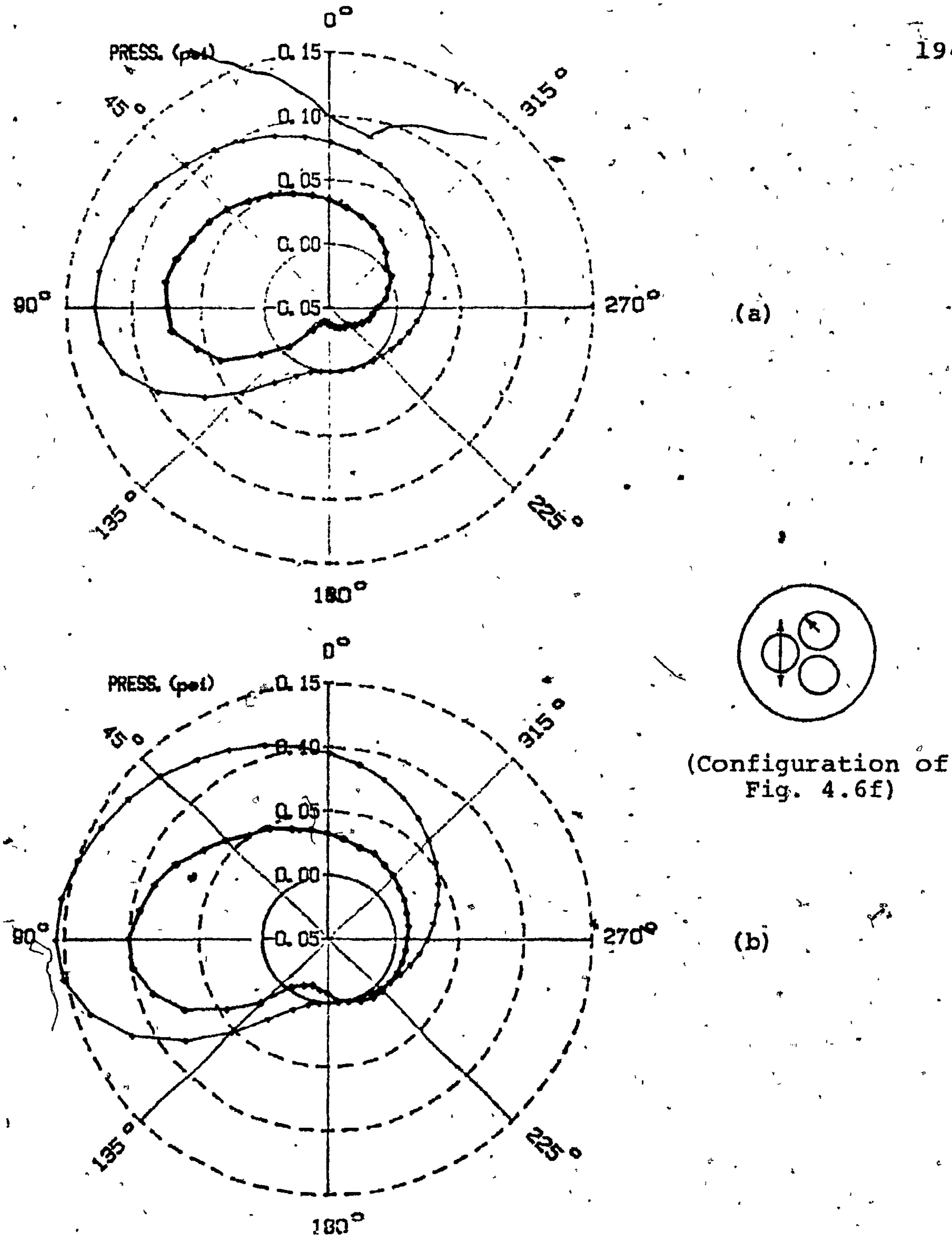

<u>Fig. 6.64:</u> Theoretical (black) and measured pressure profiles (red) of the stationary cylinder (with inner arrow). Measured profiles were obtained from the tests done with ethylene glycol after the modification, as described in Section 6.2. (a) Freq. = 100 Hz, Ac = 2.07 g; (b) Freq. = 250 Hz, Ac = 2.50 g.

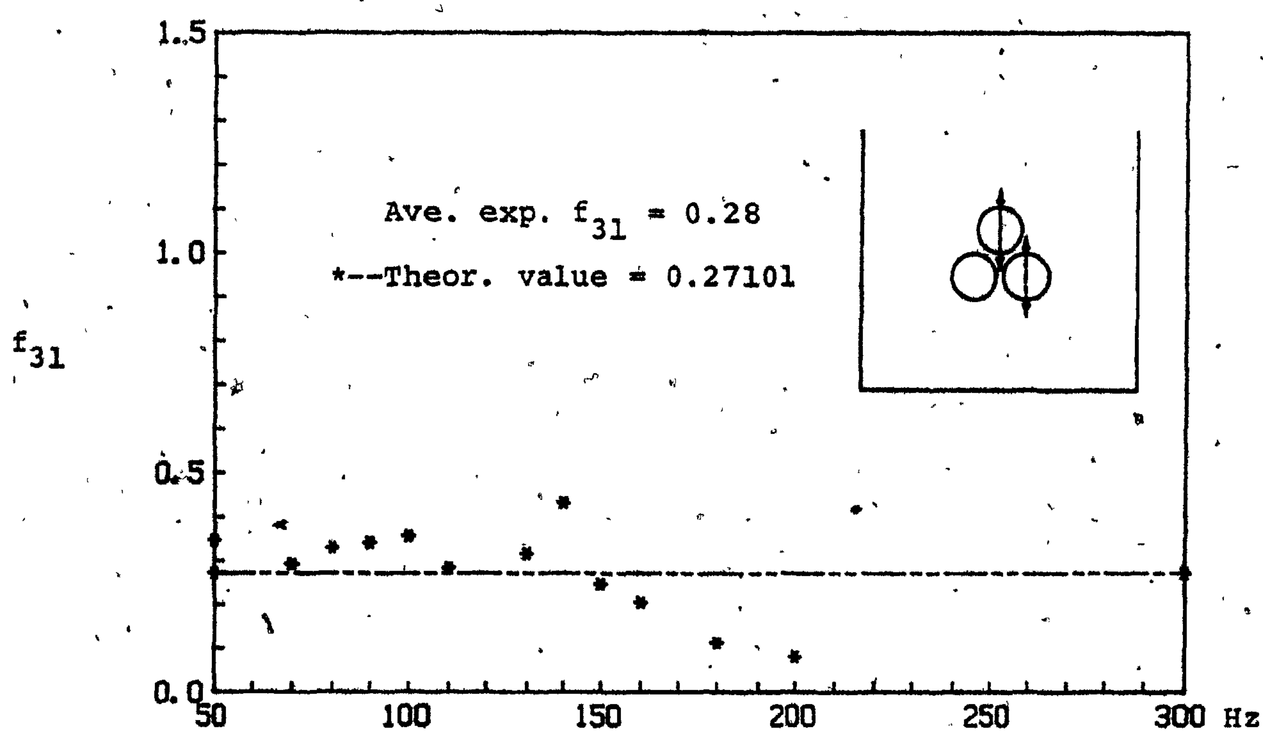

(a)

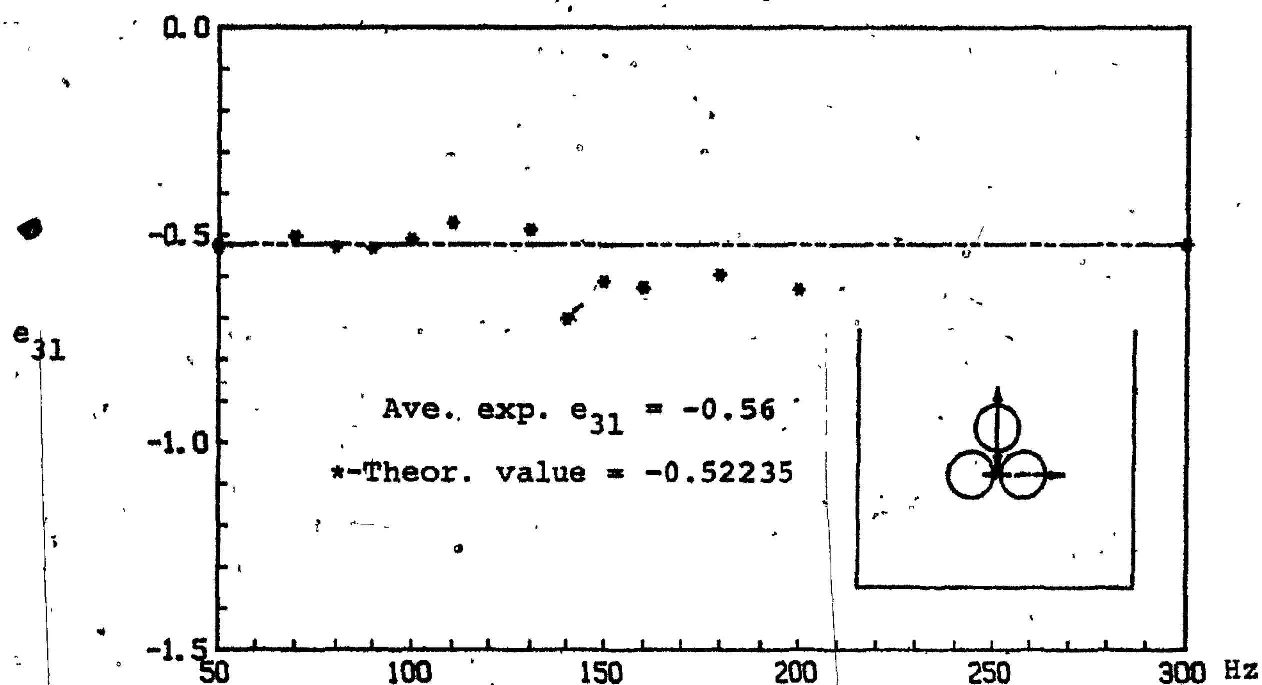

(b)

Fig. 6.65: Experimental added mass coefficients *versus* frequency, compared with theoretical values. The tests were done with the acceleration of the shaker (As) kept at 1.5 g. Average discrepancy: for (a) 2.79%; for (b) 7.26%.

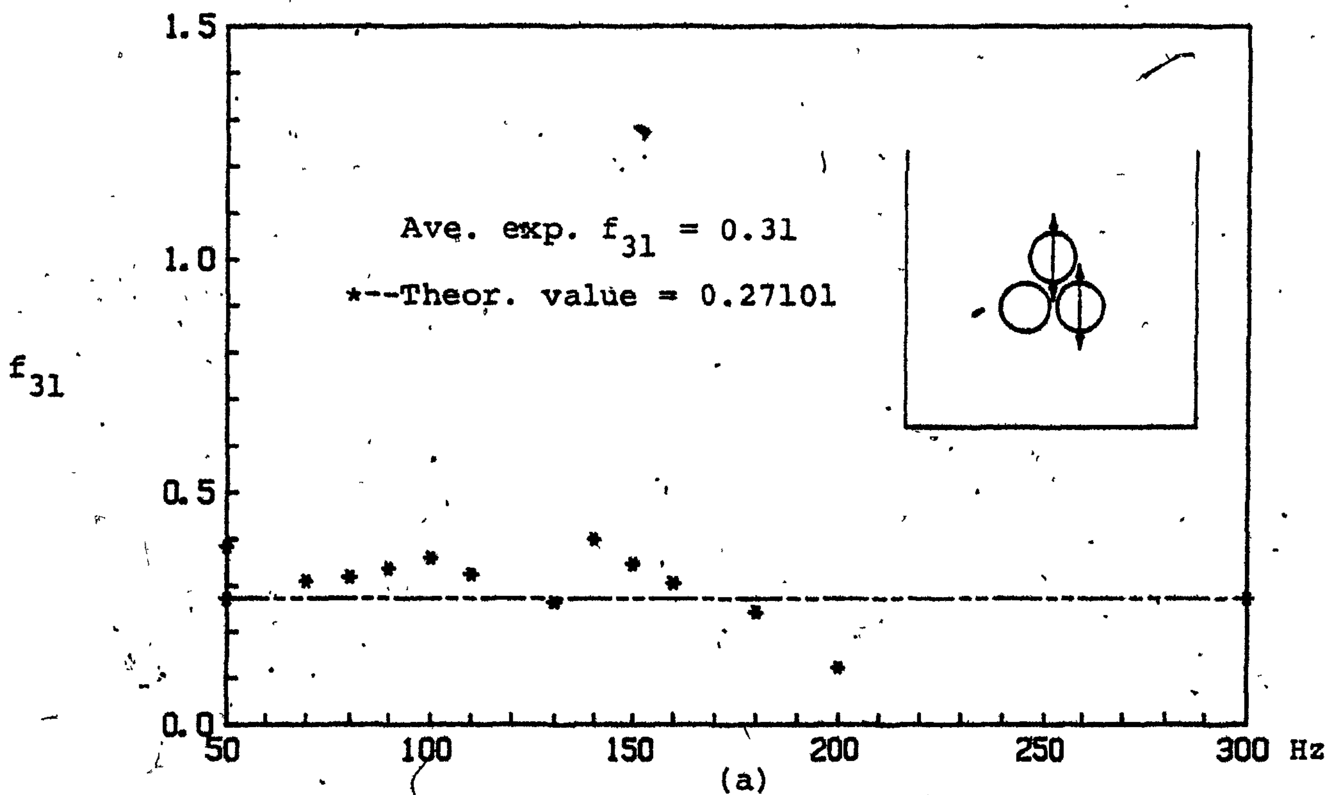

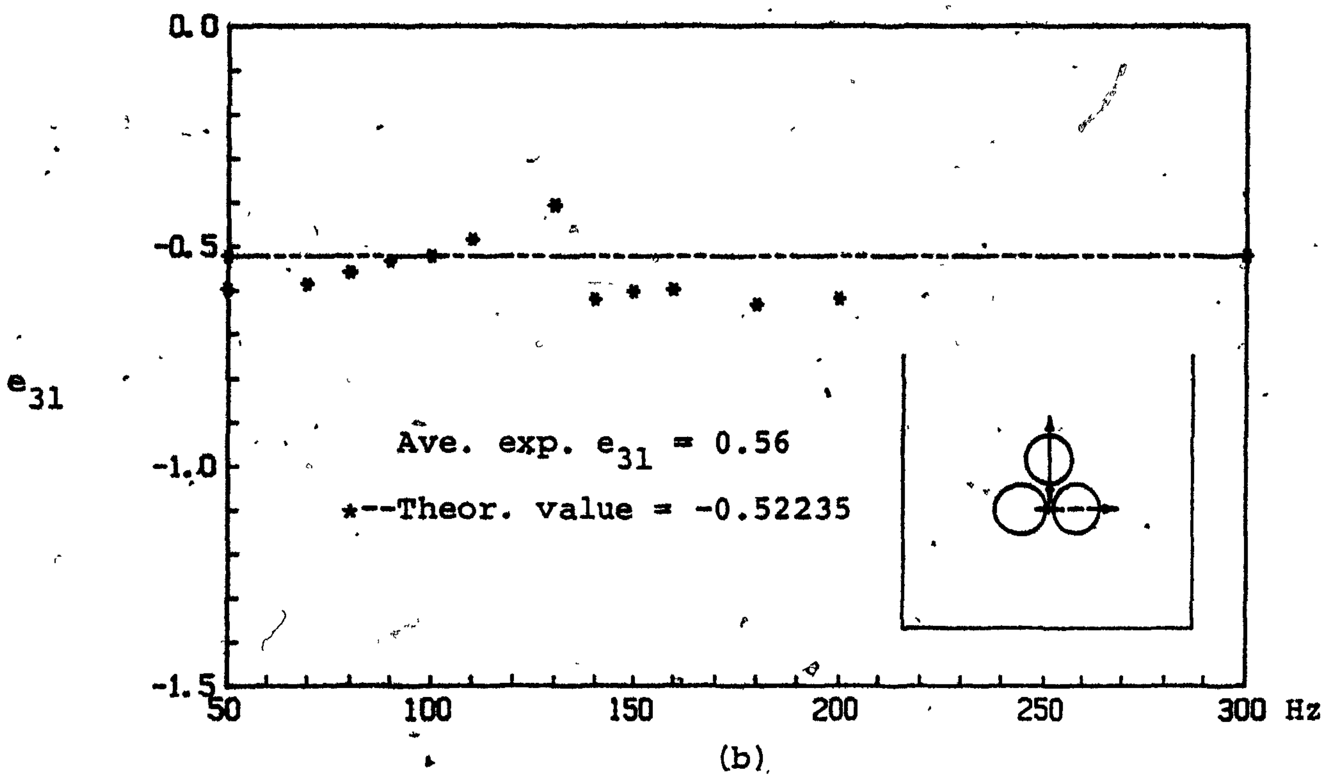

Fig. 6.66: Experimental added mass coefficients *versus* frequency, compared with theoretical values. The tests were done with the acceleration of the shaker (As) kept at 2.0 g. Average discrepancy: for (a) 14.03%; for (b) 7.77%.

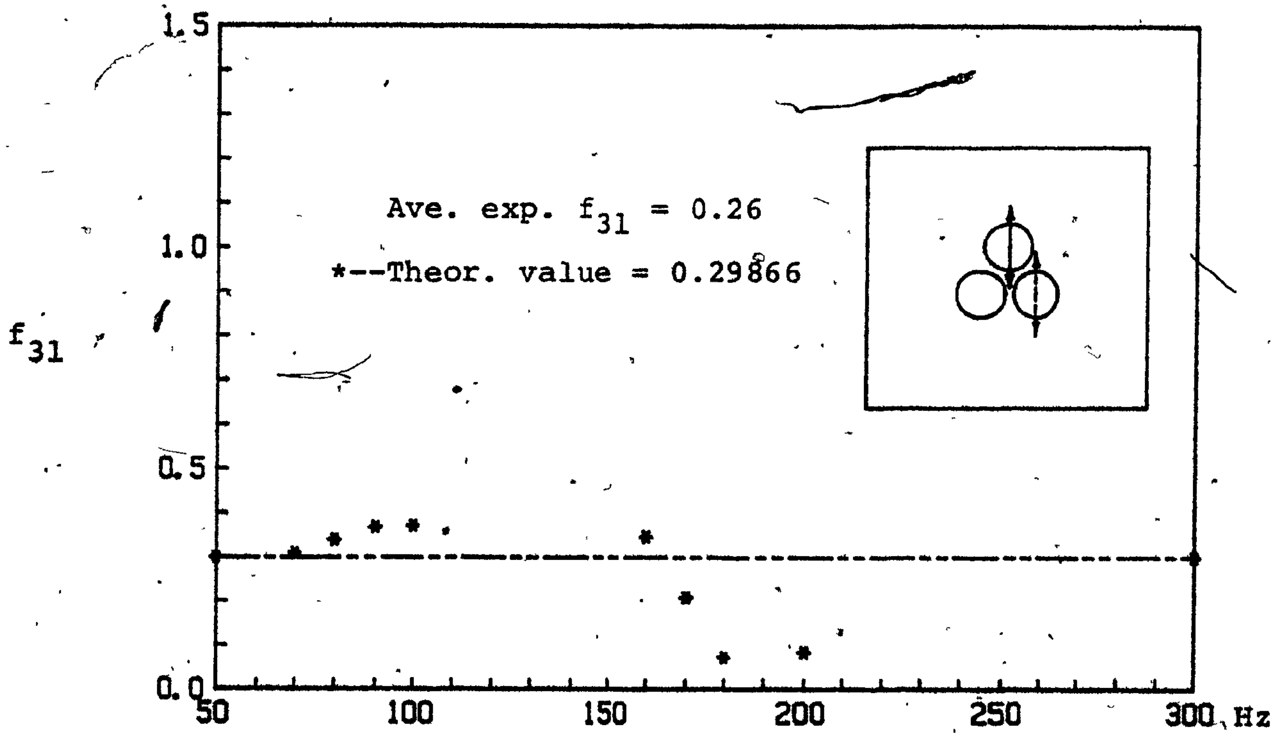

(a)

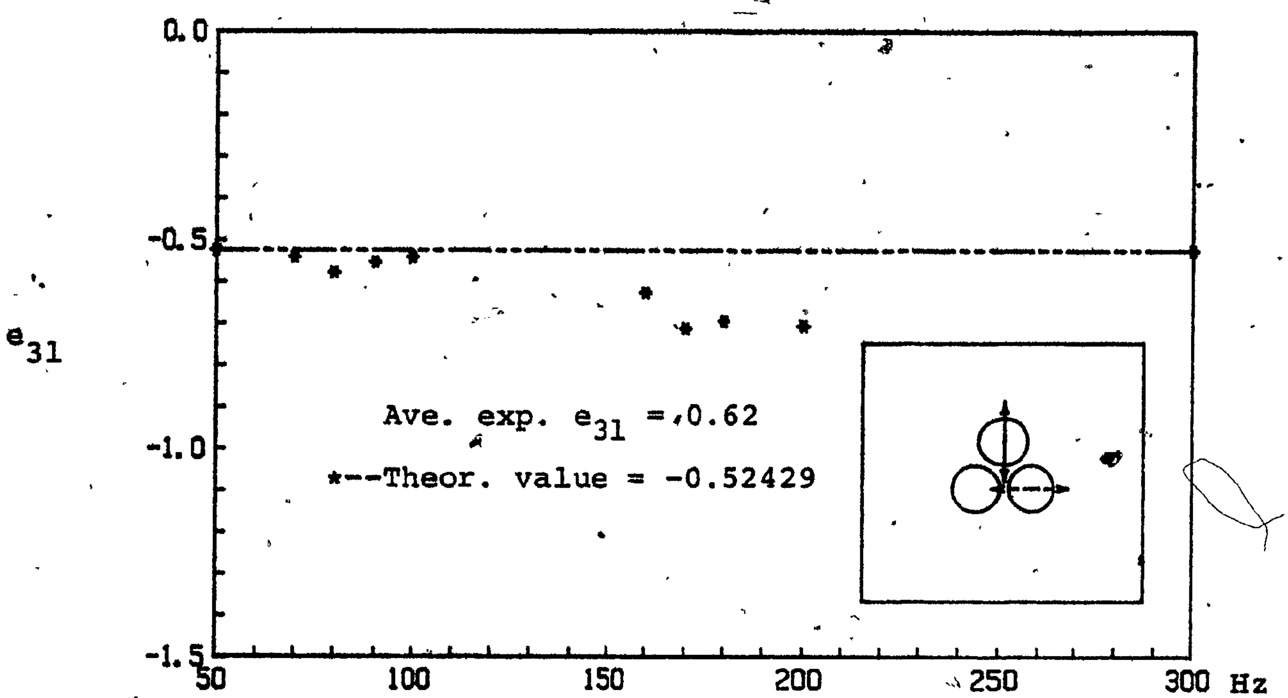

(b)

Fig. 6.67: Experimental added mass coefficients *versus* frequency, compared with theoretical values. Average discrepancy: for (a) 12.30%; for (b) 17.90%.

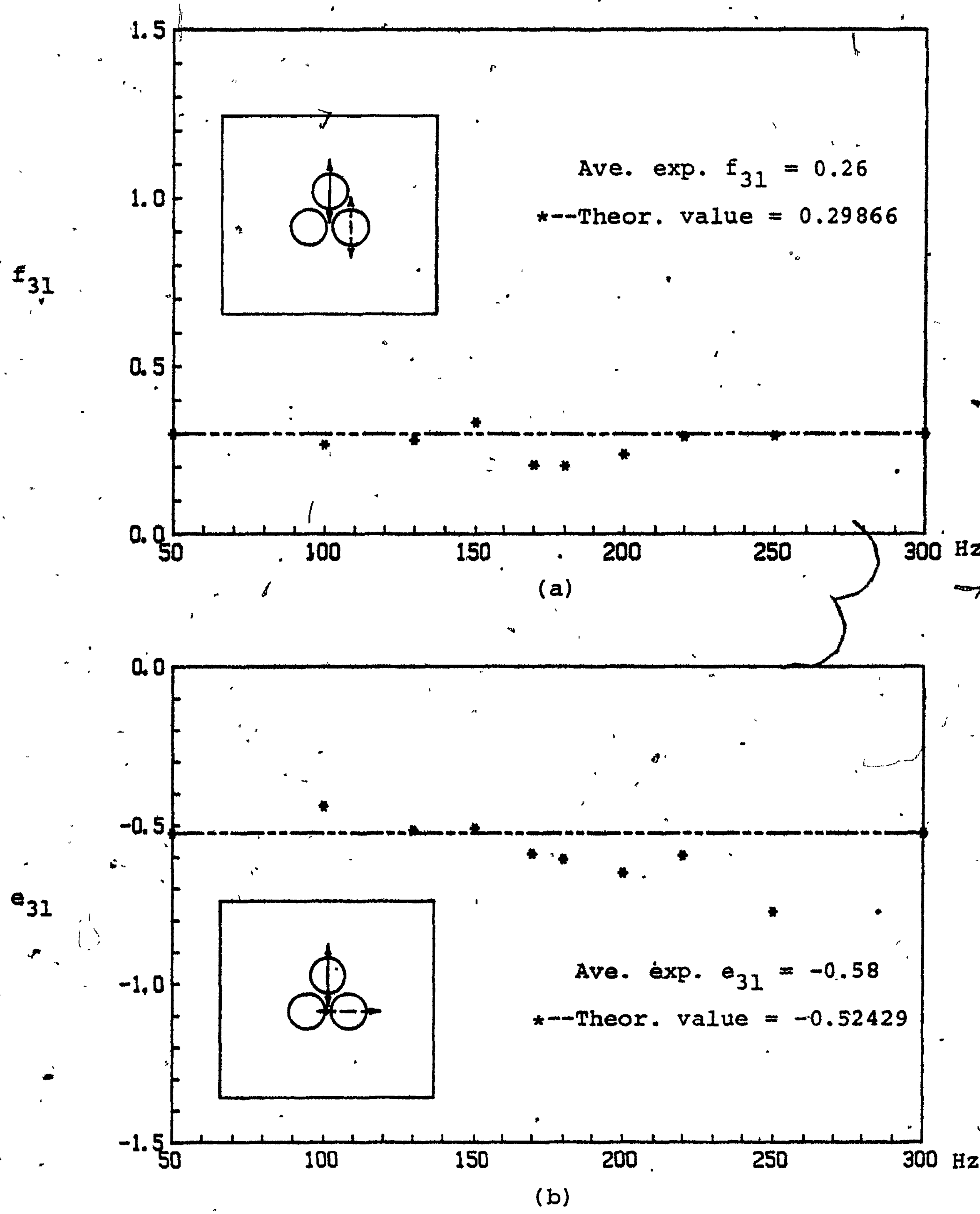

<u>Fig. 6.68</u>: Experimental added mass coefficients *versus* frequency, compared with theoretical values. Average discrepancy: for (a) -11.62%; for (b) 11.45%. The tests were done after the experimental setup was modified.

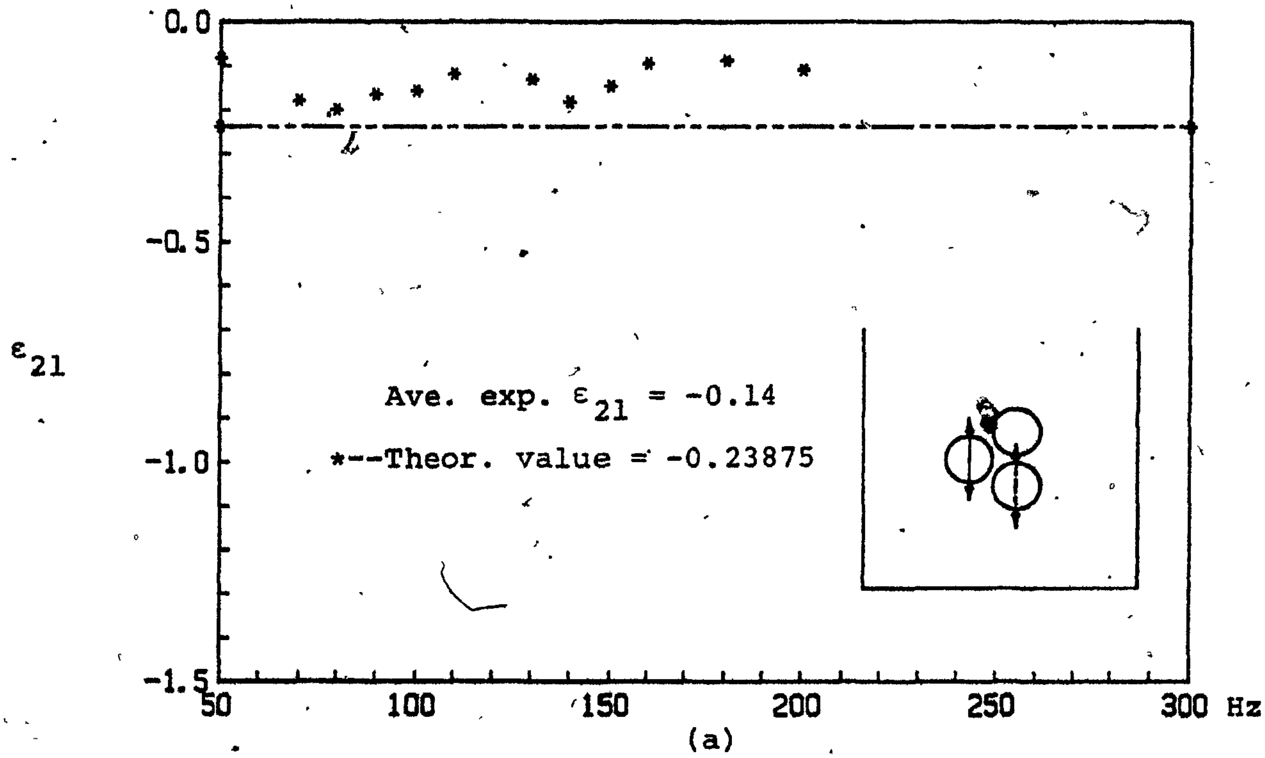

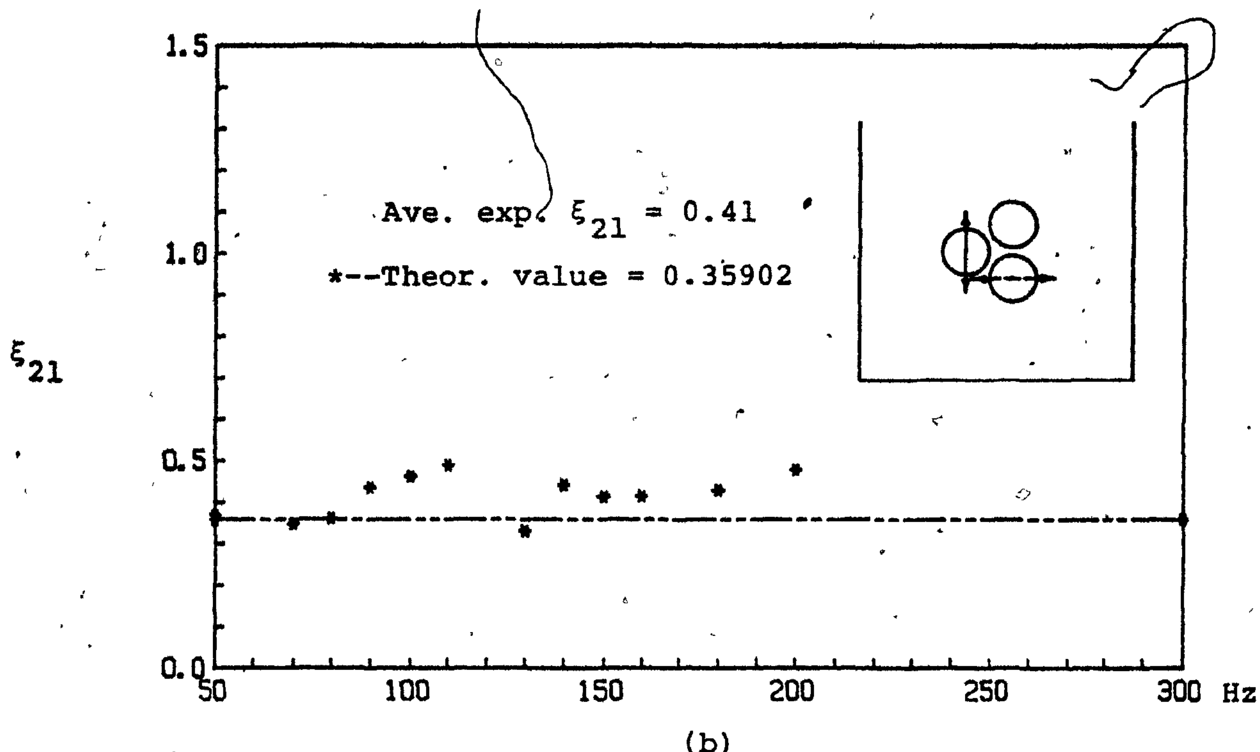

Fig. 6.69: Experimental added mass coefficients *versus* frequency, compared with theoretical values. Average discrepancy: for (a) -42.46%; for (b) 18.19%.

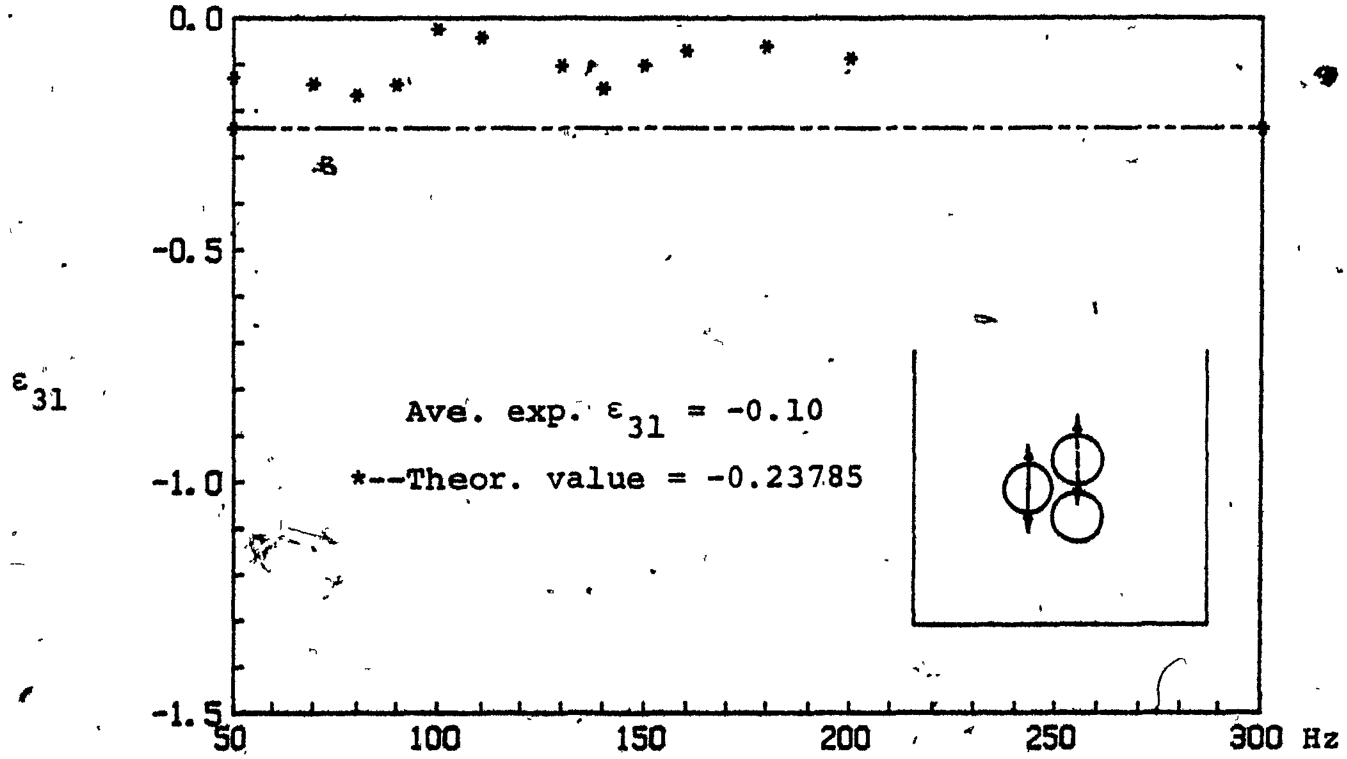

(a)

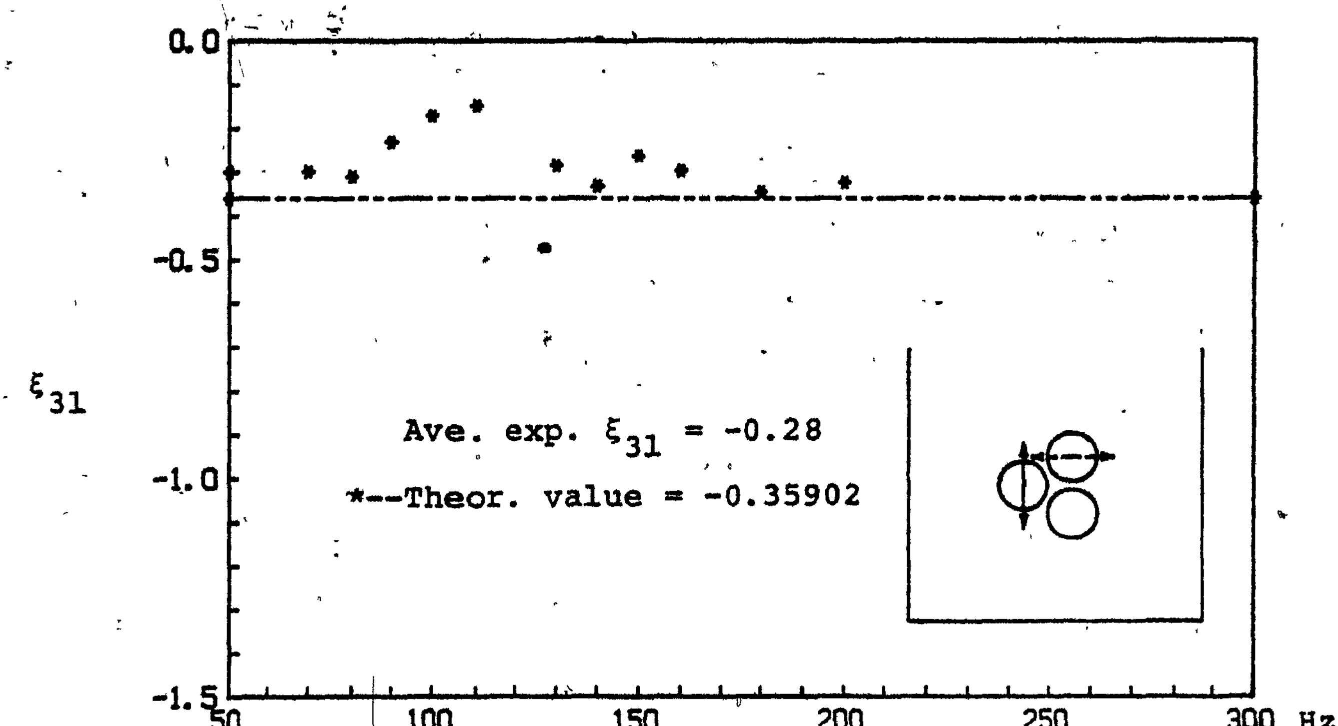

(b)

<u>Fig. 6.70</u>: Experimental added mass coefficients *versus* frequency, compared with theoretical values. Average discrepancy: for (a) -42.37%; for (b) -21.67%.

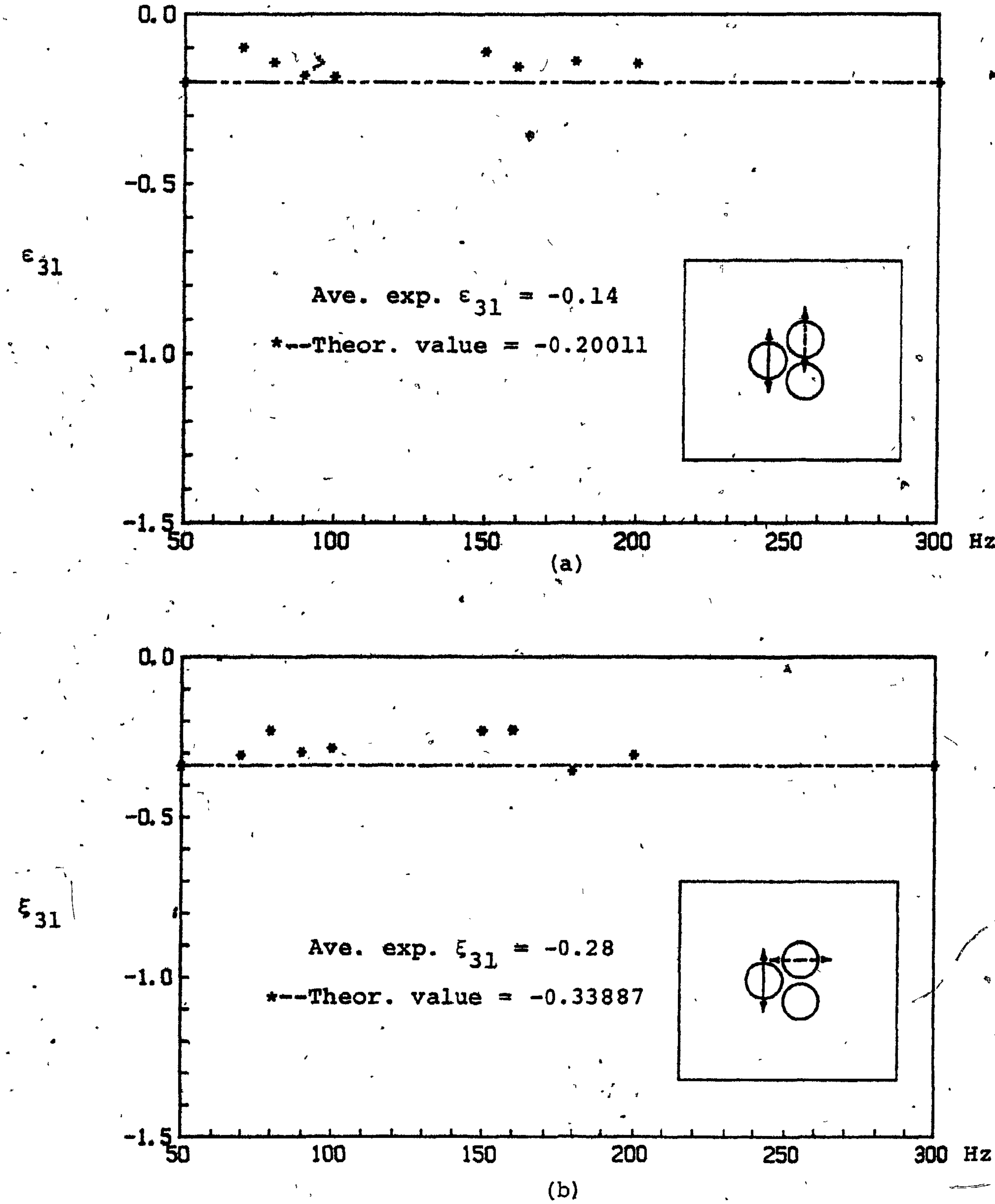

<u>Fig. 6.71</u>: Experimental added mass coefficients *versus* frequency, compared with theoretical values. Average discrepancy: for (a) -28.48%; for (b) -17.67%.

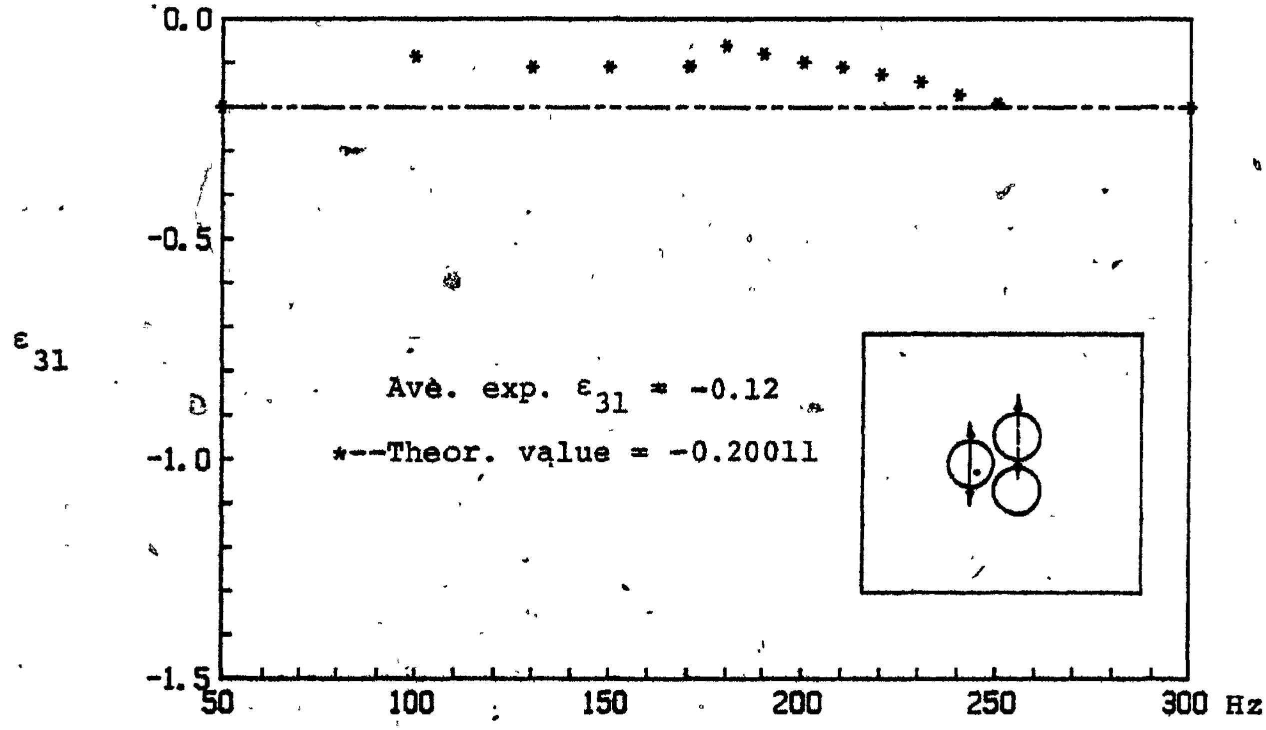

(a)

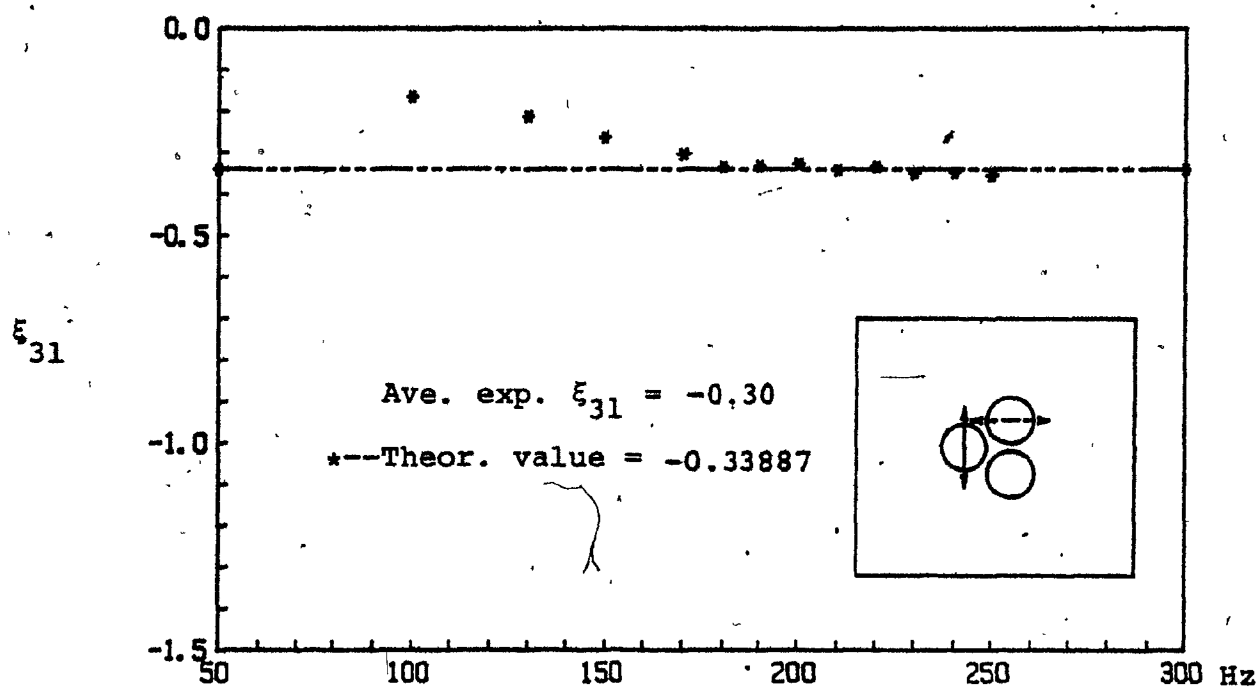

(b)

Fig. 6.72: Experimental added mass coefficients *versus* frequency, compared with theoretical values. Average discrepancy: for (a) -42.31%; for (b) -10.21%. The tests were done after the experimental setup was modified.

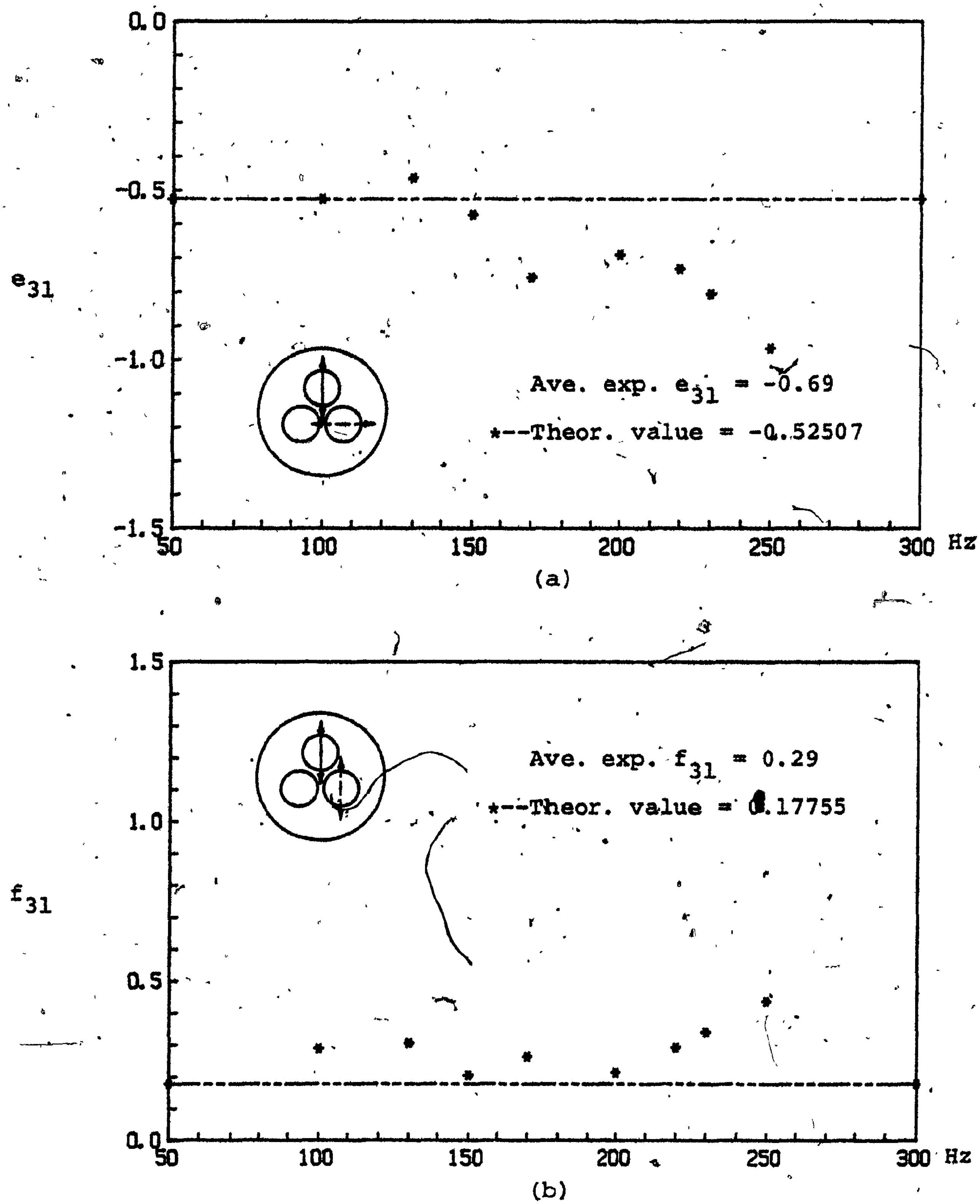

Fig. 6.73: Experimental added mass coefficients *versus* frequency, compared with theoretical values. Average discrepancy: for (a) 31.02%; for (b) 65.28%. The tests were done with water after the modification.

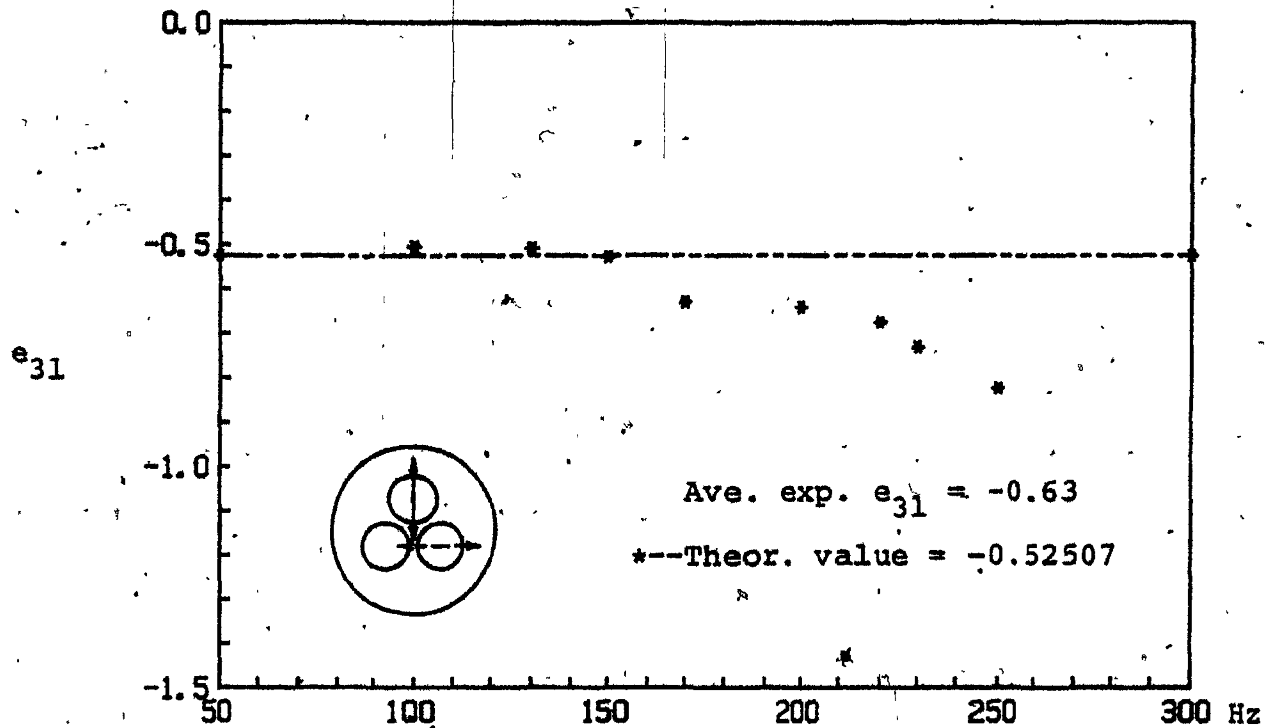

(a)

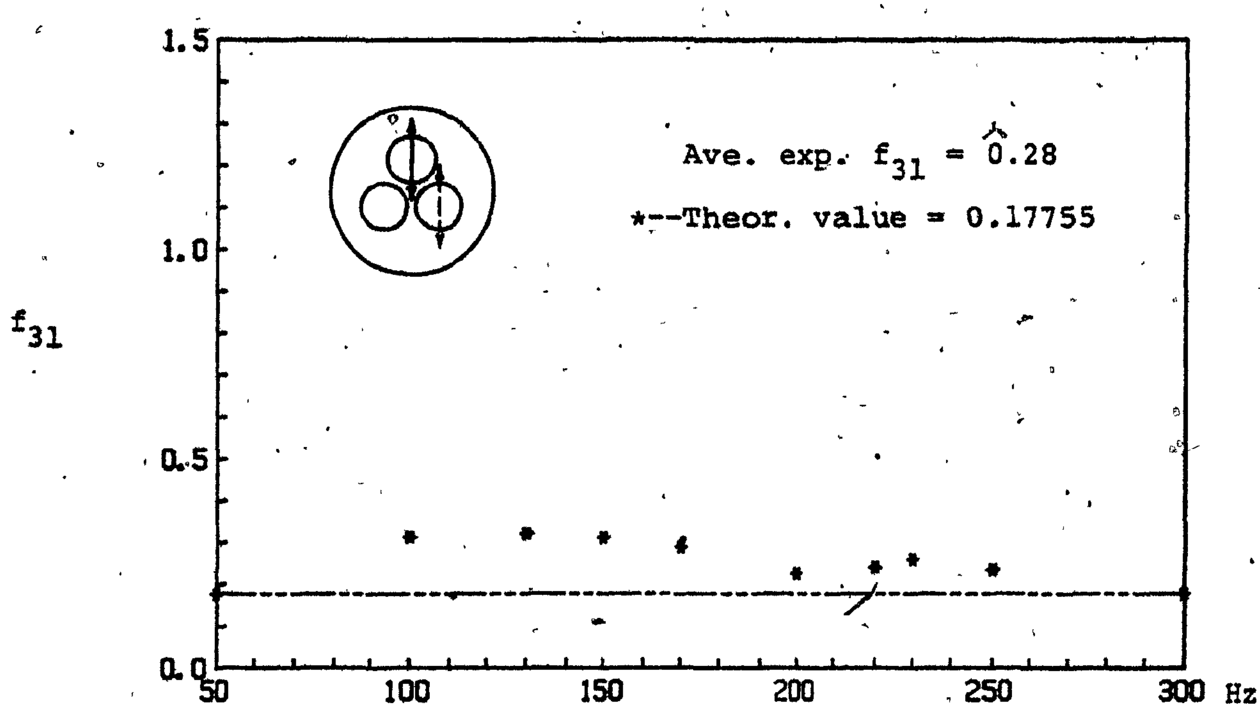

(b)

<u>Fig. 6.74</u>: Experimental added mass coefficients *versus* frequency, compared with theoretical values. Average discrepancy: for (a) 20.00%; for (b) 55.09%. The tests were done with oil after the modification.

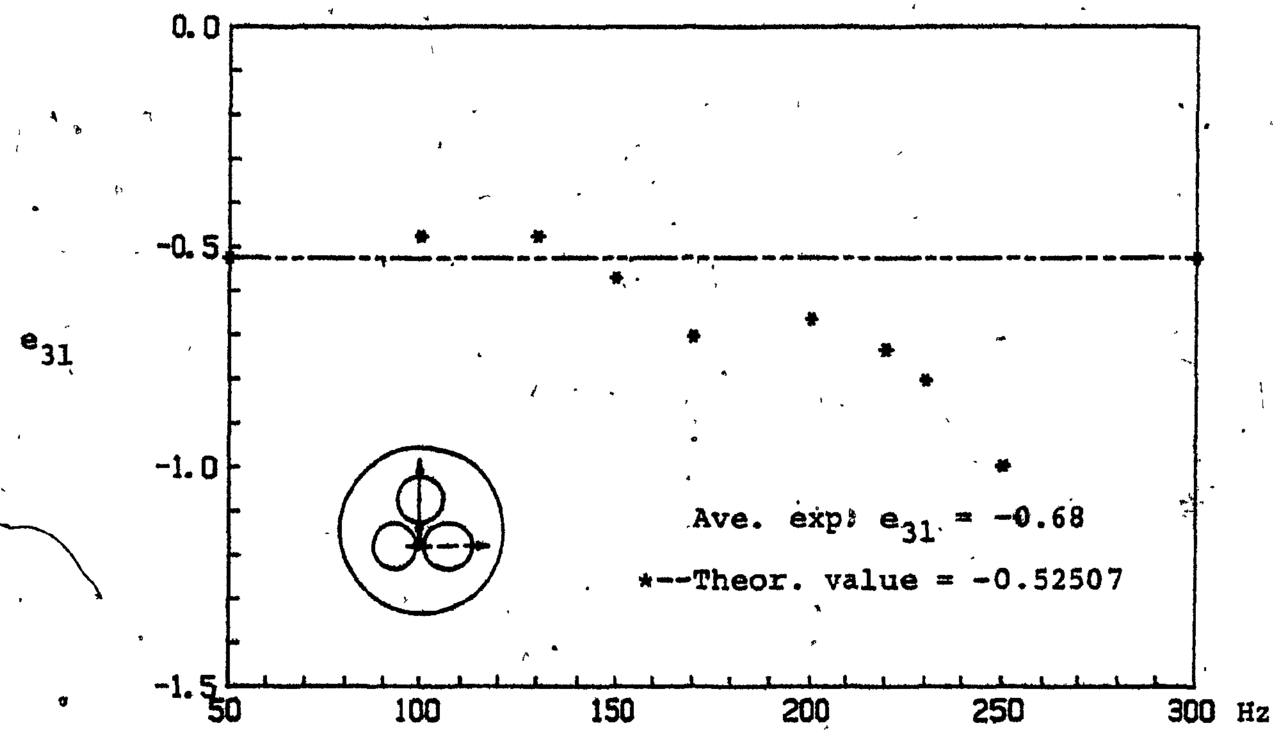

(a)

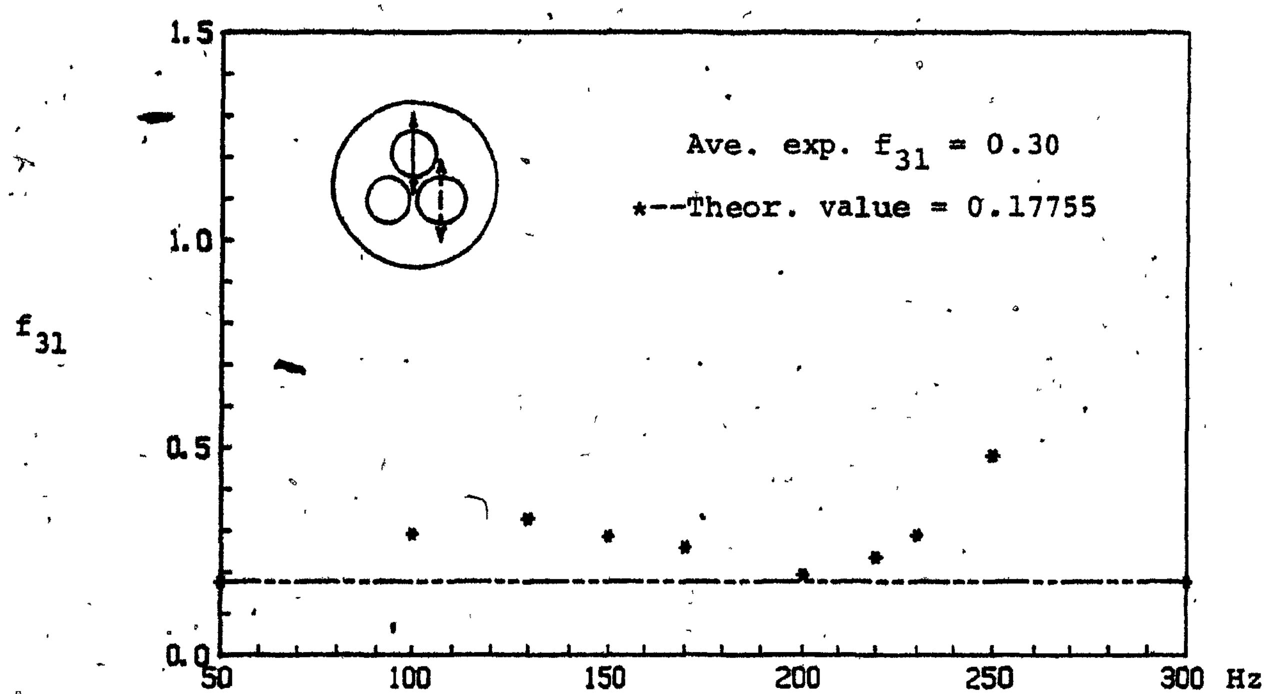

(b)

Fig. 6.75: Experimental added mass coefficients *versus* frequency, compared with theoretical values. Average discrepancy: for (a) 28.94%; for (b) 66.89%. The tests were done with ethylene glycol after the modification.

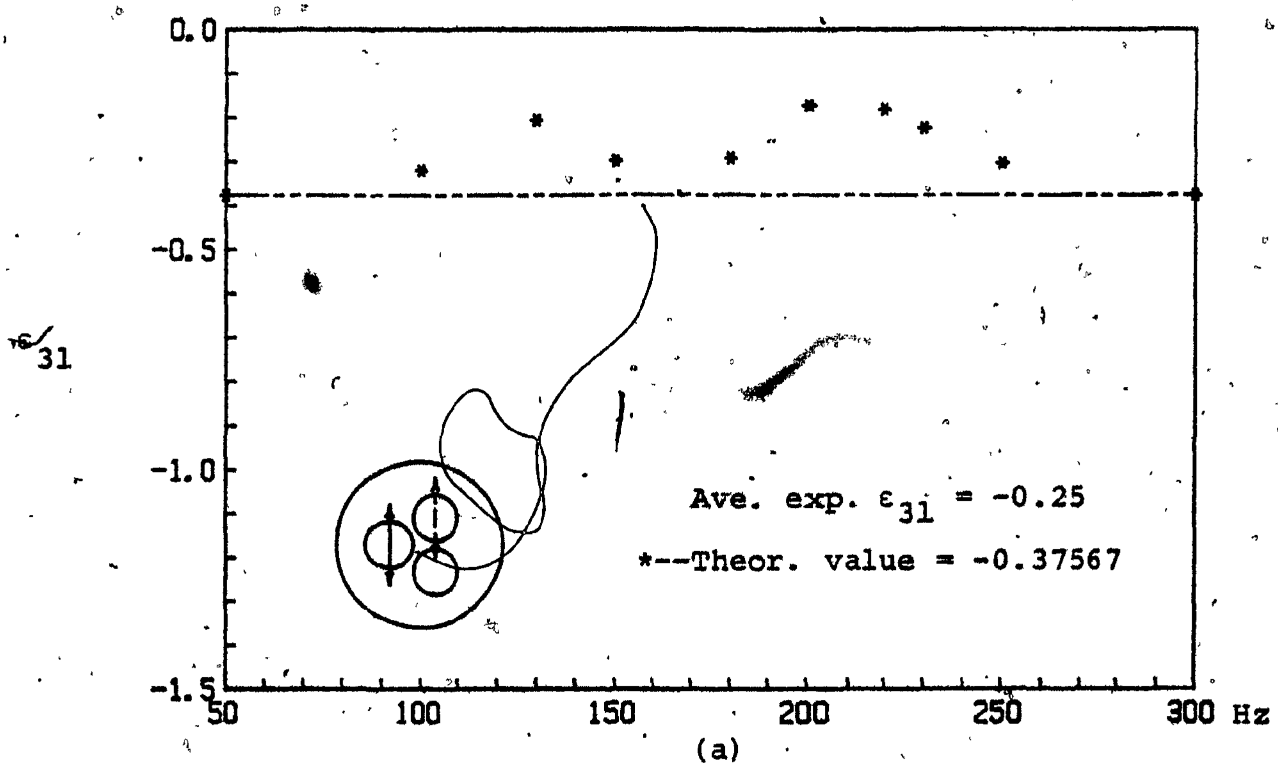

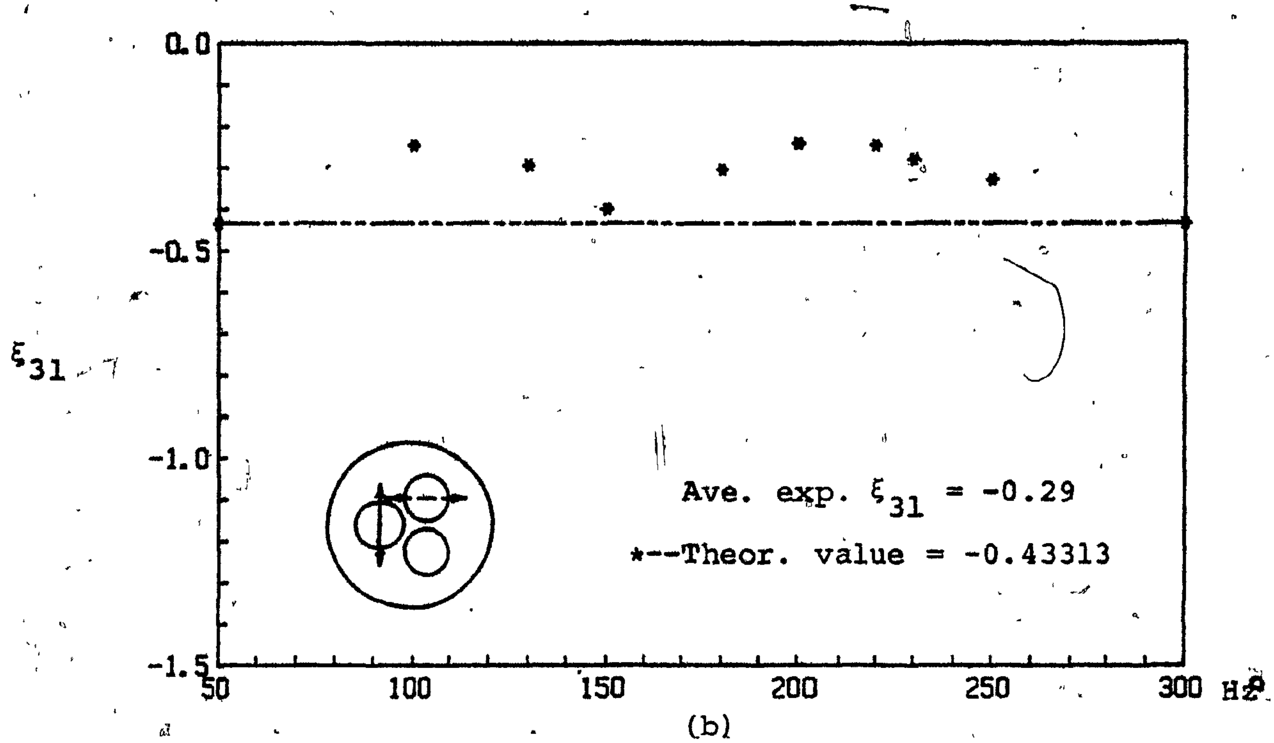

Fig. 6.76: Experimental added mass coefficients *versus* frequency, compared with theoretical values. Average discrepancy: for (a) 33.96%; for (b) -32.69%. The tests were done with water after the modification.

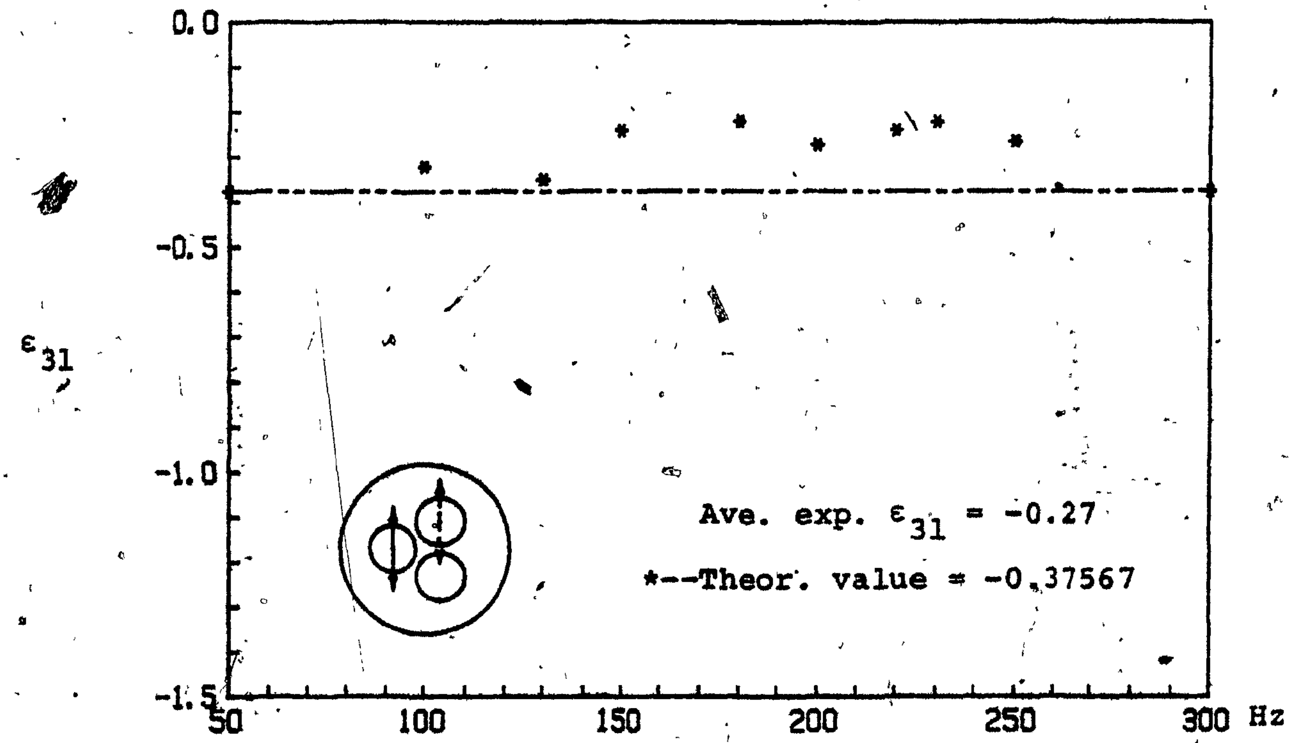

(a)

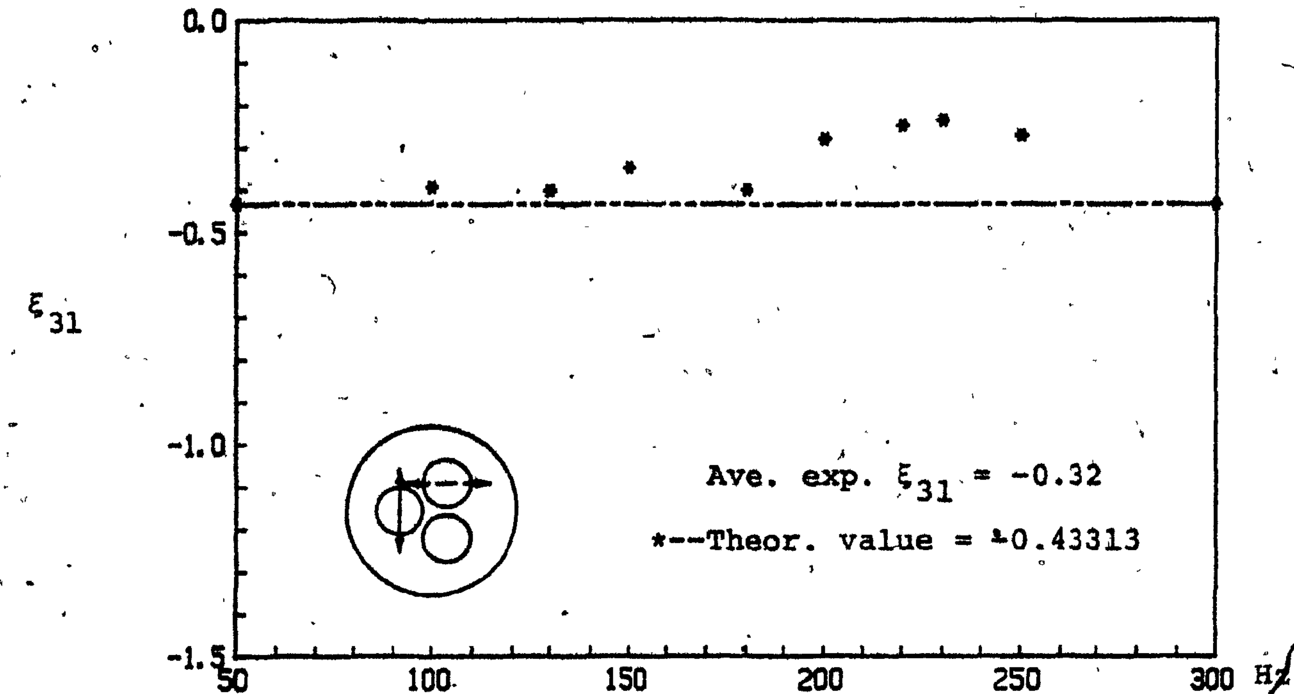

(b)

<u>Fig. 6.77:</u> Experimental added mass coefficients *versus* frequency, compared with theoretical values. Average discrepancy: for (a) -29.24%; for (b) -25.79%. The tests were done with oil after the modification.

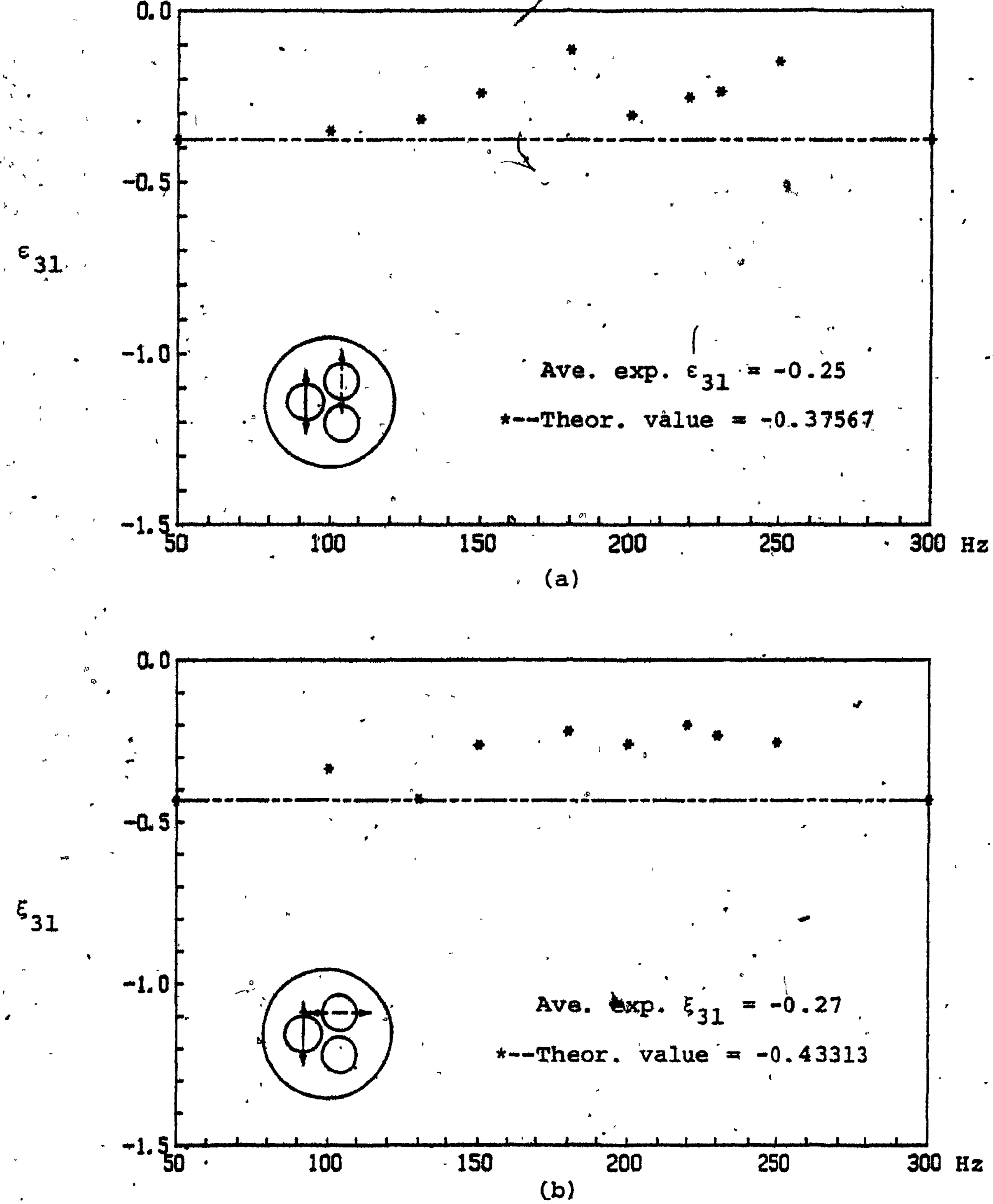

Fig. 6.78: Experimental added mass coefficients *versus* frequency, compared with theoretical values. Average discrepancy: for (a) -34.74%; for (b) -36.82%. The tests were done with ethylene glycol after the modification.

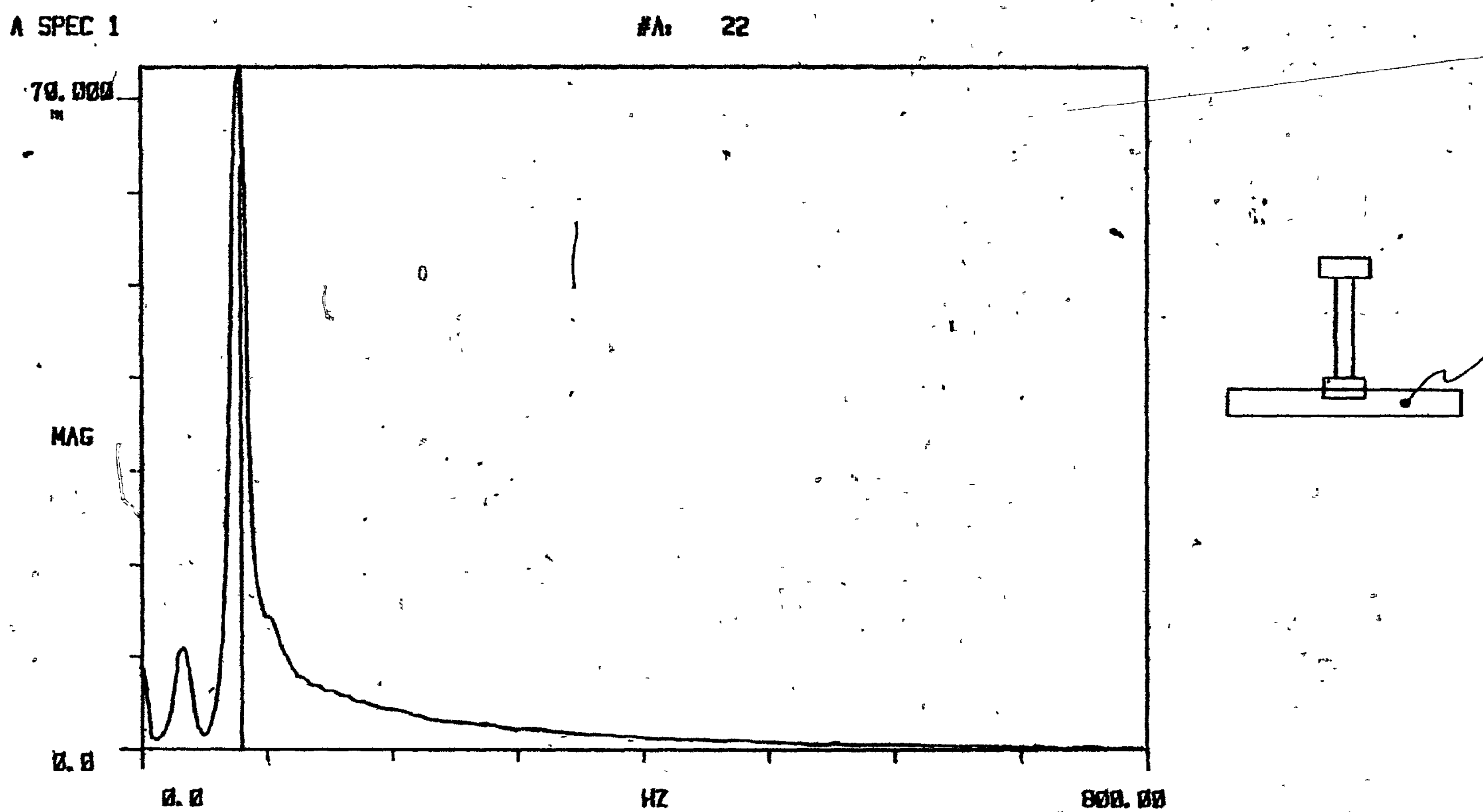

<u>Fig. 7.1</u>: The vibration spectrum of the oscillating cylinder in the horizontal direction. Oscillating frequency is indicated by the vertical cursor.

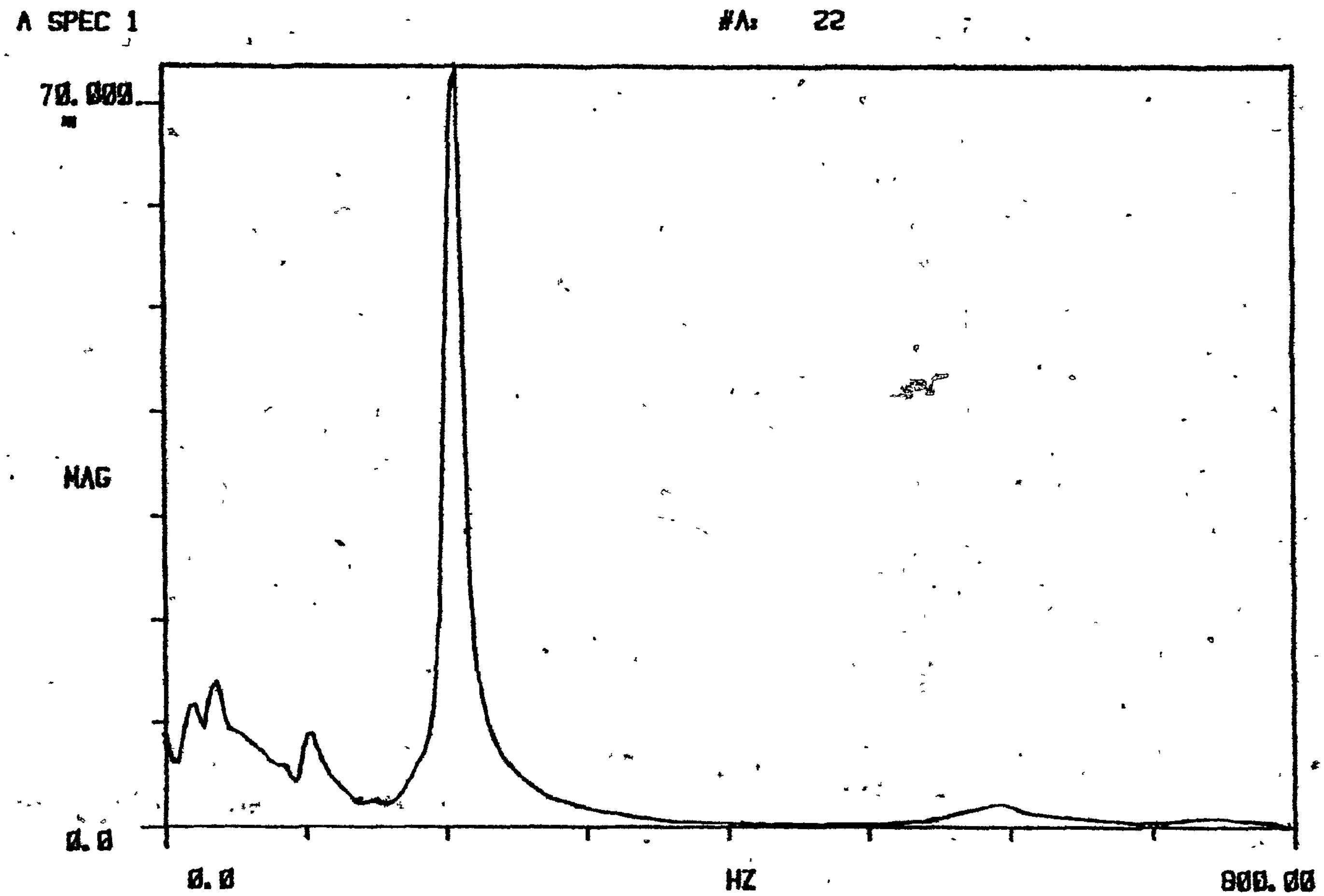

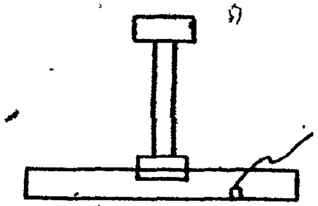

<u>Fig. 7.2</u>: The vibration spectrum of the oscillating cylinder in the vertical direction. Oscillating frequency corresponds to the largest peak.

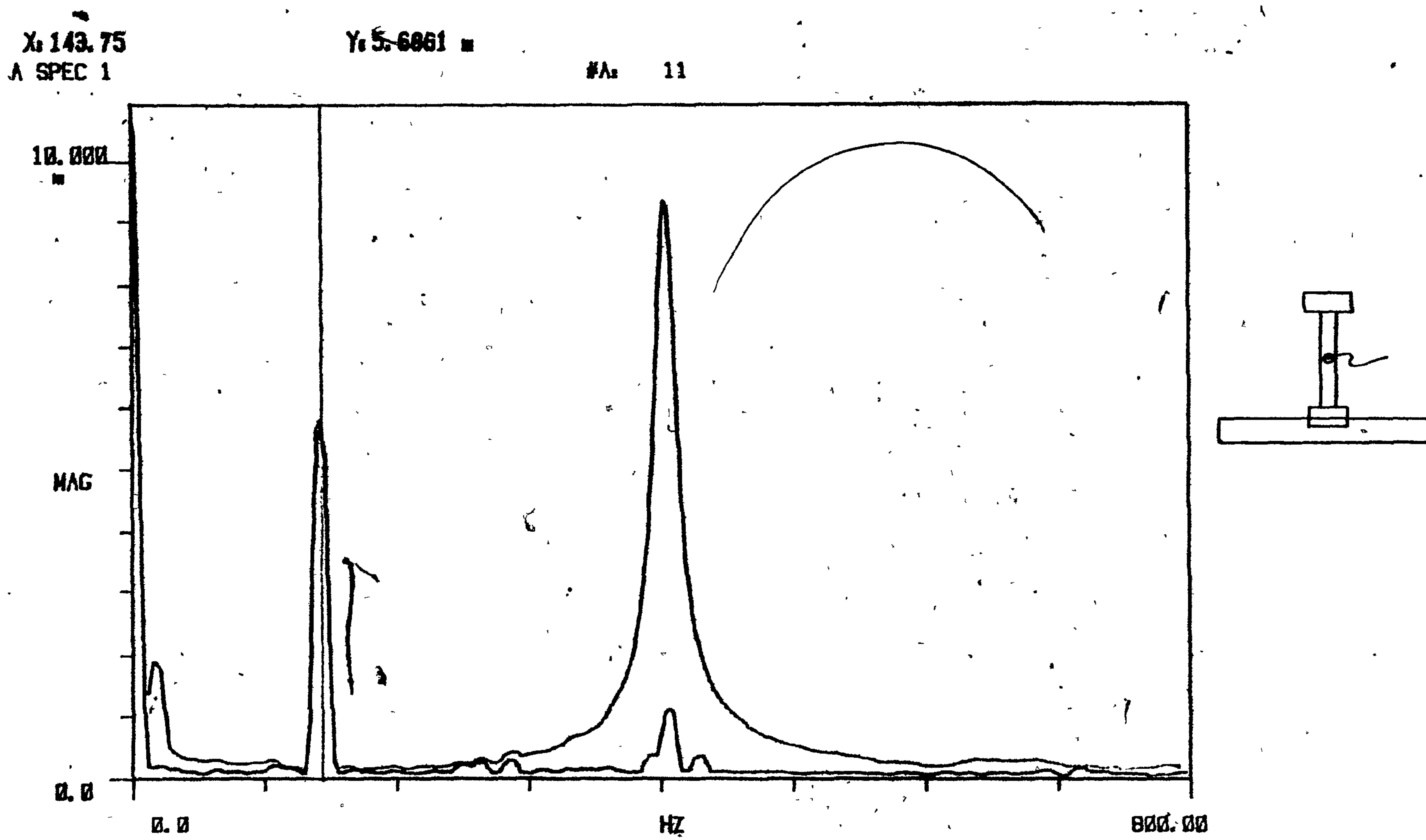

<u>Fig. 7.3</u>: The vibration spectrum (bottom curve) measured at the tube in the direction normal to the axis of the oscillating cylinder. The top curve represents the one measured when a small excitation force was added.

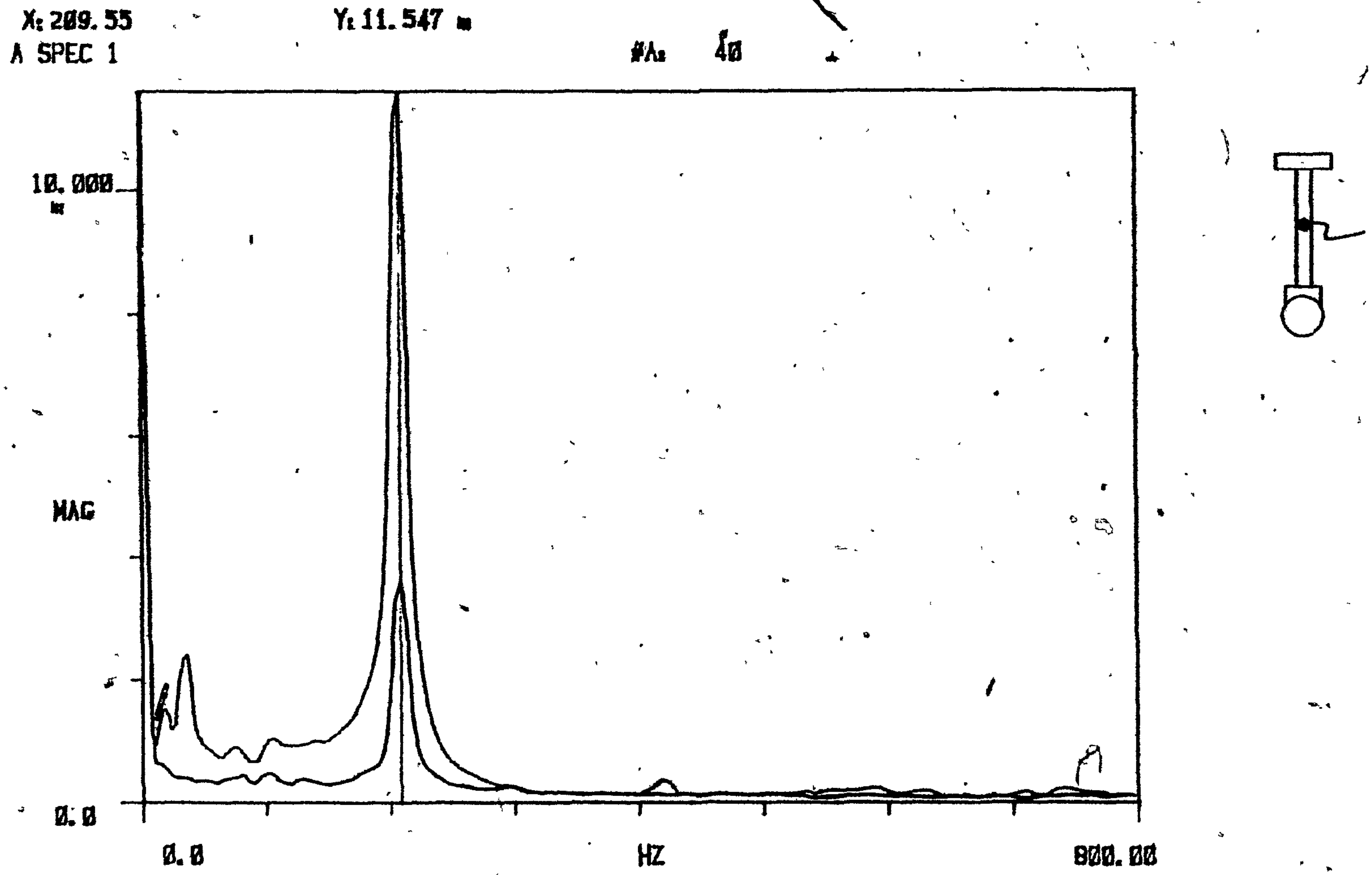

Fig. 7.4: The vibration spectrum (bottom curve) measured at the tube in the axial direction of the oscillating cylinder. The top curve represents the one measured when a small excitation force was added.

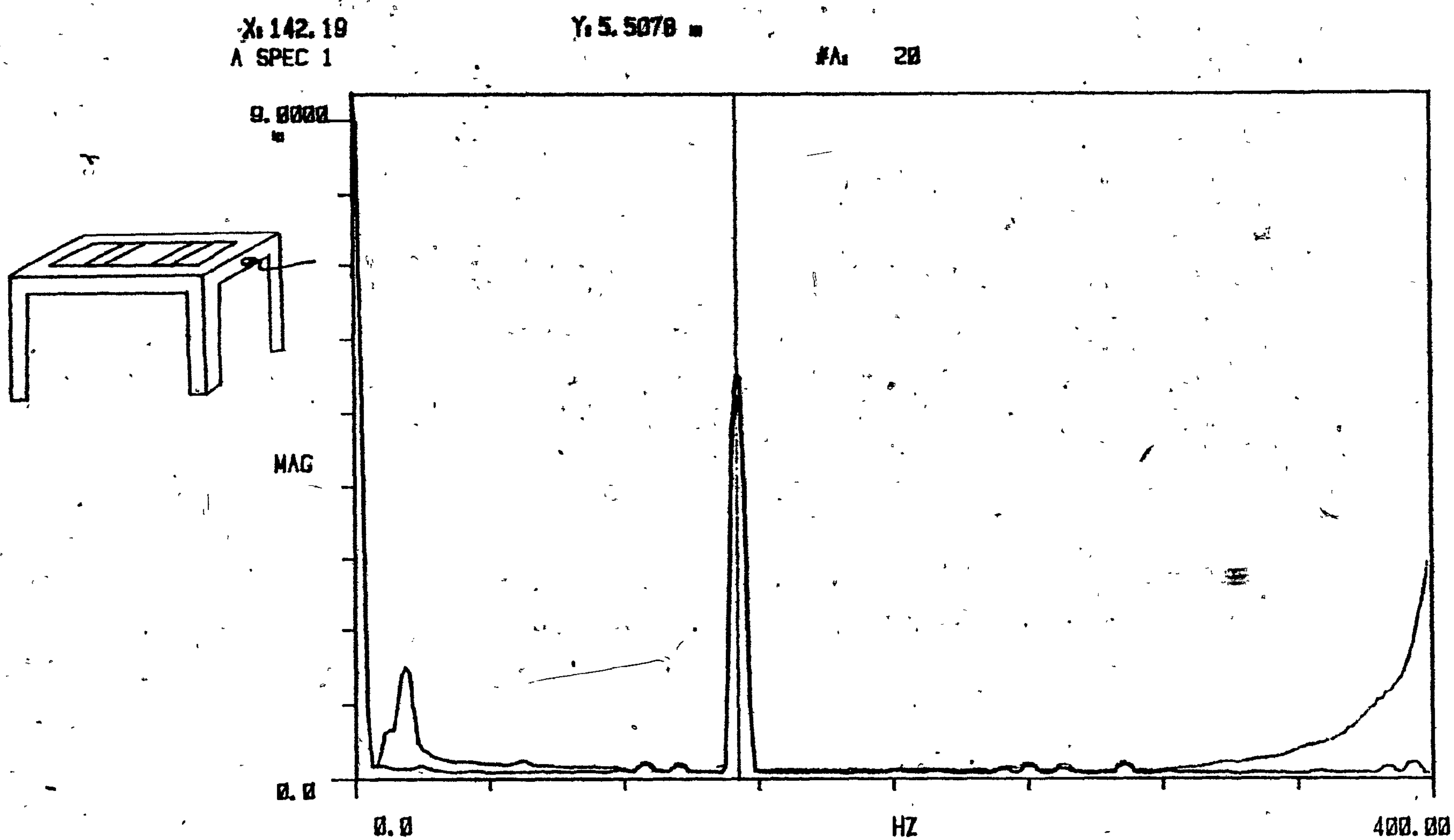

<u>Fig. 7.5</u>: The vibration spectrum (bottom curve) measured at the support of the shaker in the axial direction of the oscillating cylinder. The top curve represents the one measured when a small excitation force was added.

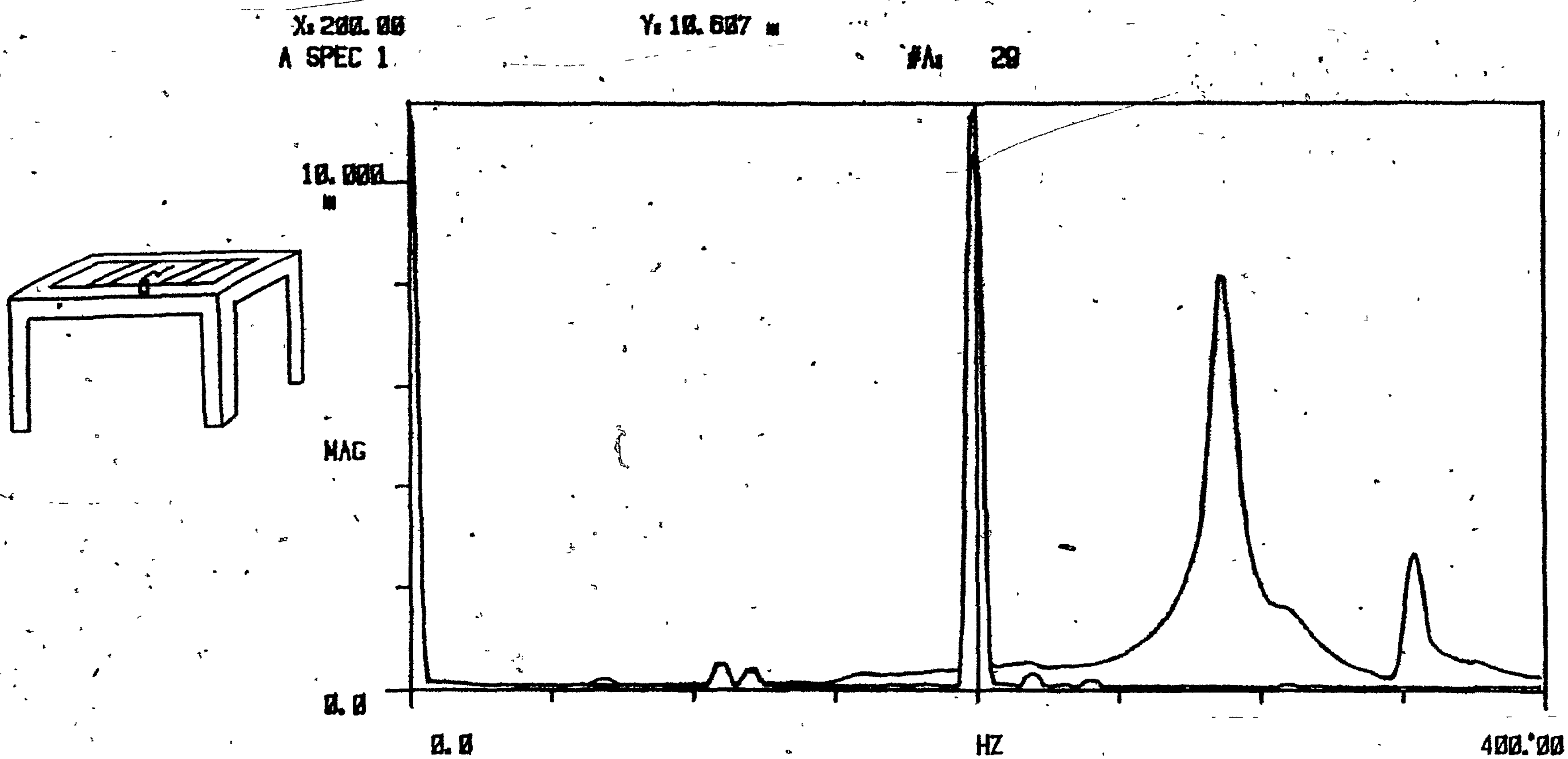

<u>Fig. 7.6</u>: The vibration spectrum (bottom curve) measured at the support of the shaker in the vertical direction of the oscillating cylinder. The top curve represents the one measured when a small excitation force was added.

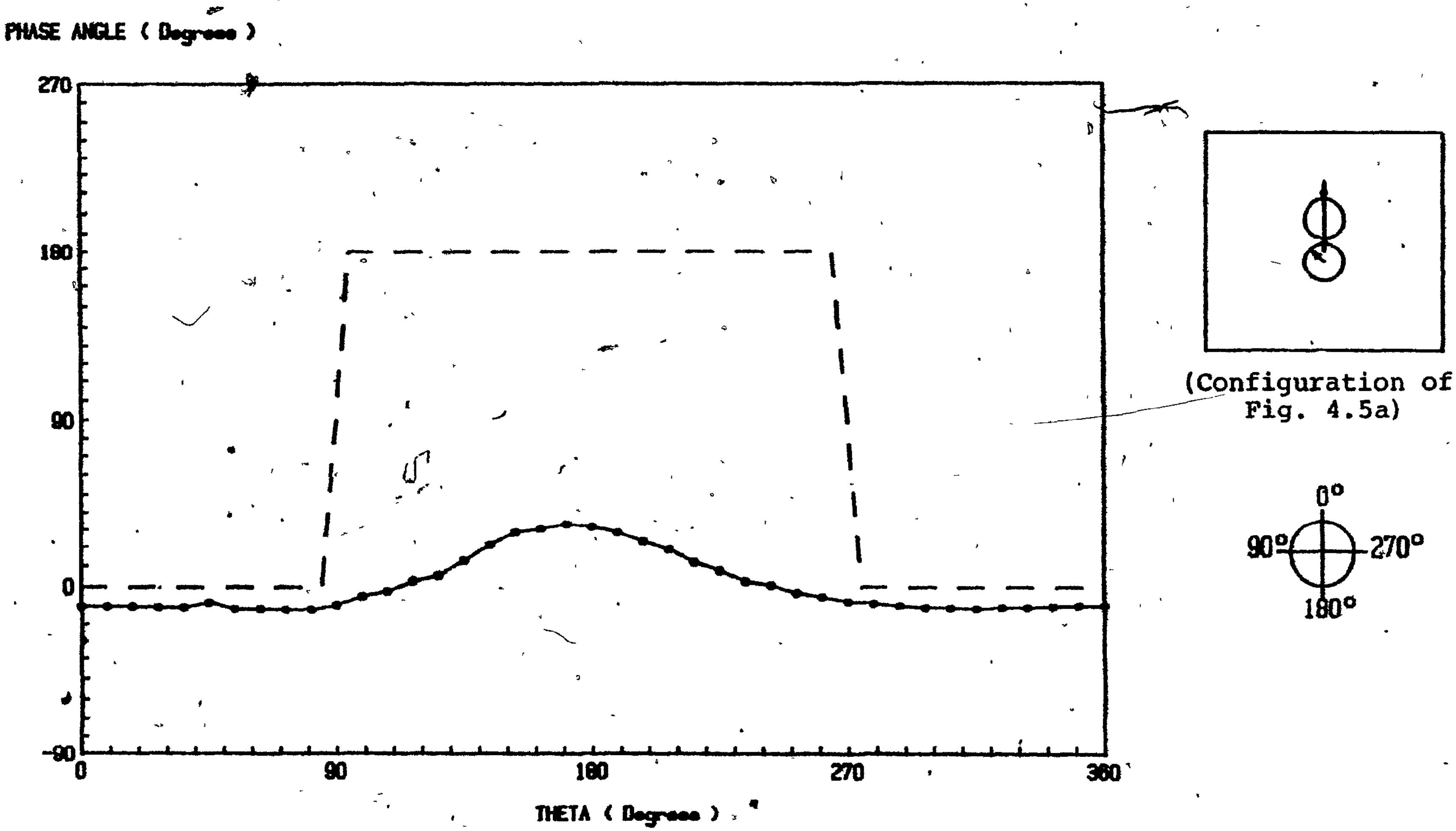

Fig. 7.7: The experimental distribution of phase angles measured on the stationary cylinder (with inner arrow) is shown by the solid line, whereas the dashed line represents the distribution predicted by the Inviscid Theory.

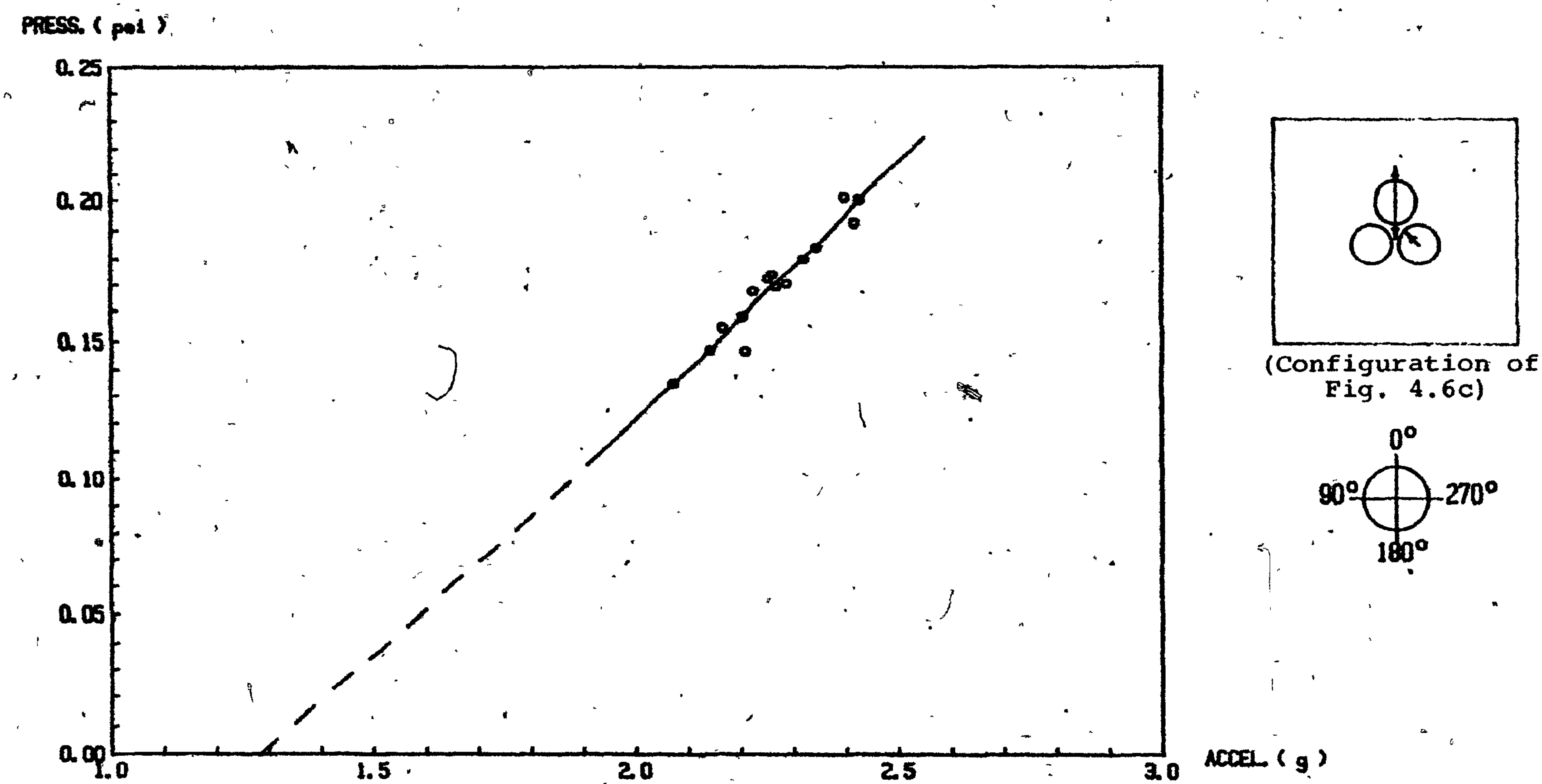

Fig. 7.8: Pressure *versus* acceleration graph with pressure readings taken at θ = 54° for the configuration shown.

PHOTOGRAPHS

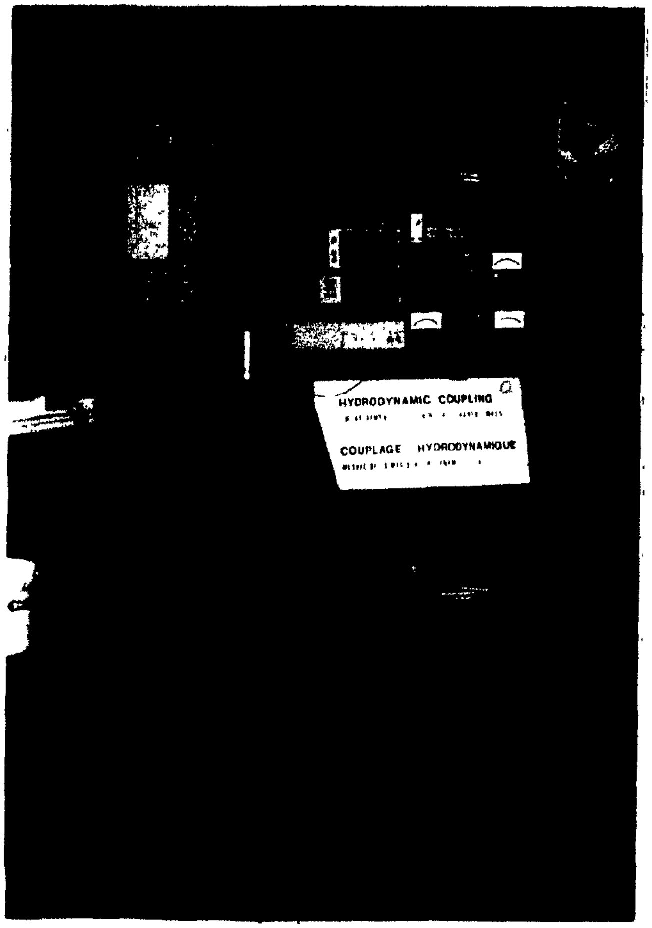

Picture 1: Overall view of the experimental setup.

Picture 2: The water tank sits on the wooden base of the steel frame with leveling screws at the four corners.

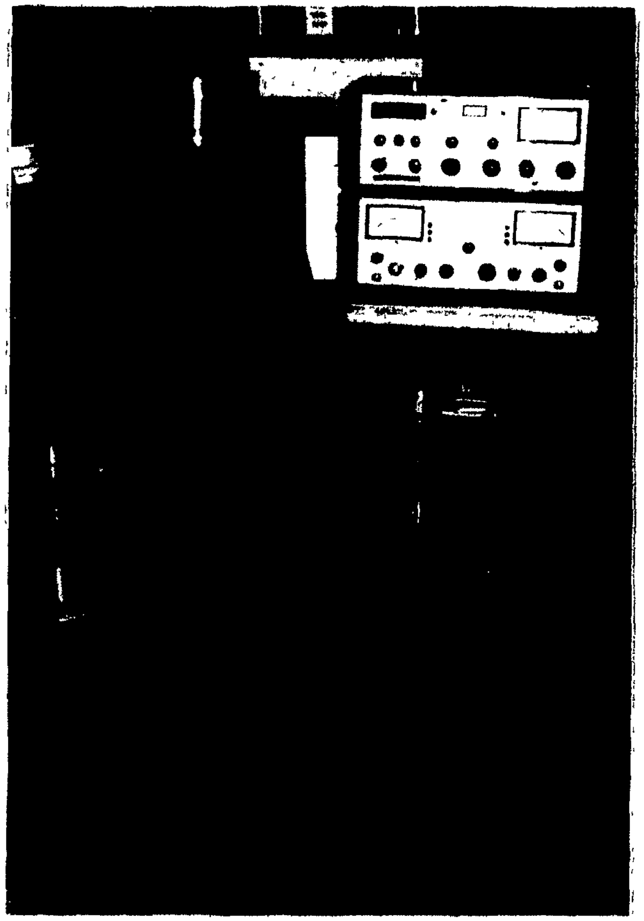

Picture 3: The shaker with support (left), the exciter control (top right), and the power amplifier (bottom right).

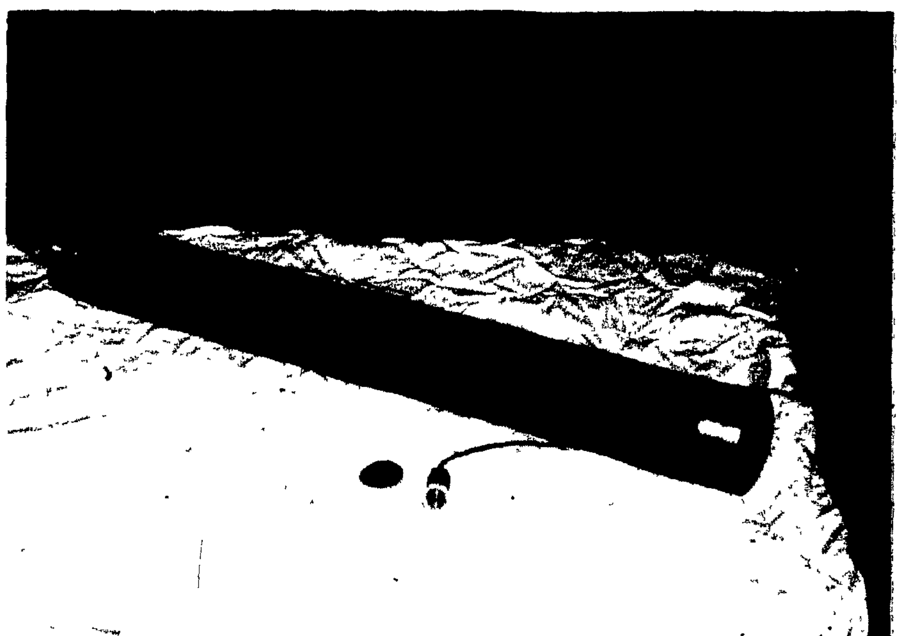

Picture 4: The pressure transducer bearing cylinder.

Picture 5: Supports for the stationary cylinders where the rectangular pieces stand vertically on the I-shaped supports. (on the left-hand side shown was the oscillating cylinder).

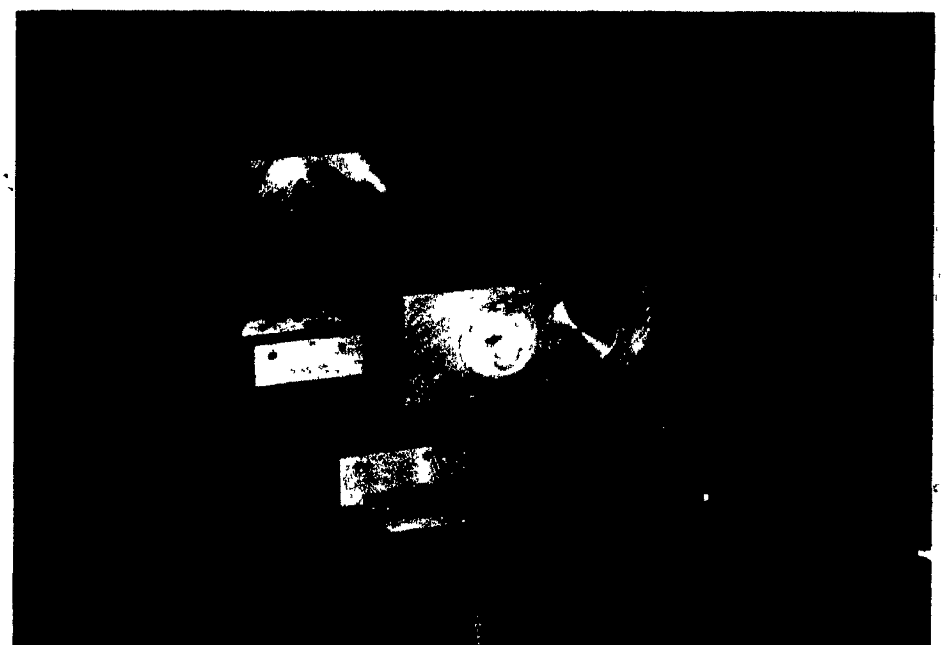

Picture 6: Supports for the stationary cylinders where the rectangular pieces lie horizontally on the I-shaped supports.

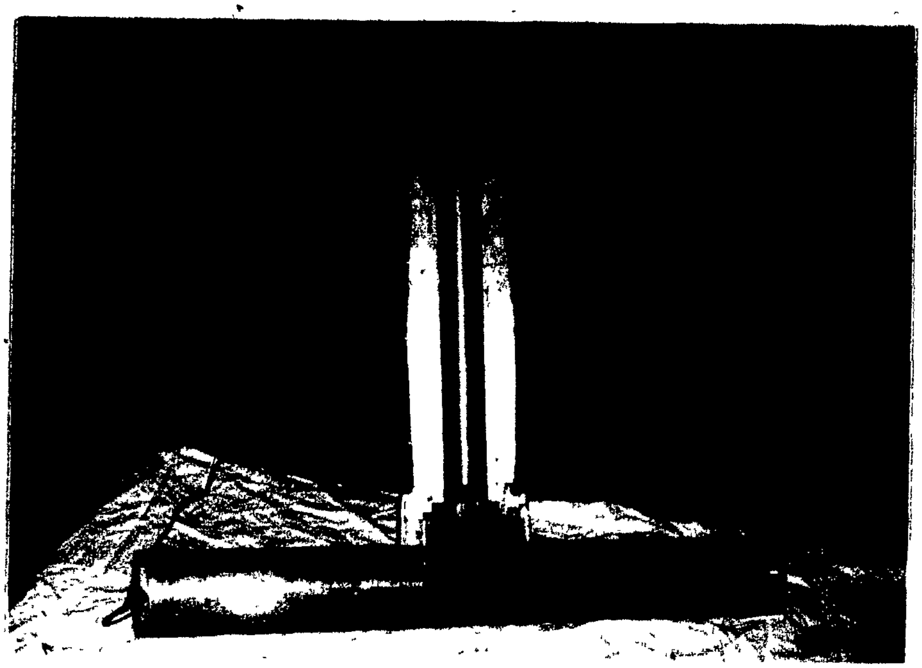

Picture 7: Oscillating cylinder with the tube components.
(Note that the fins on two sides of the blue tube were added to increase the stiffness of the tube. This was done in the later experiment).

Picture 8: The components joining the oscillating cylinder and the tube (left) used for experiments with a single cylinder. The triangular pieces for alignment purposes (right).

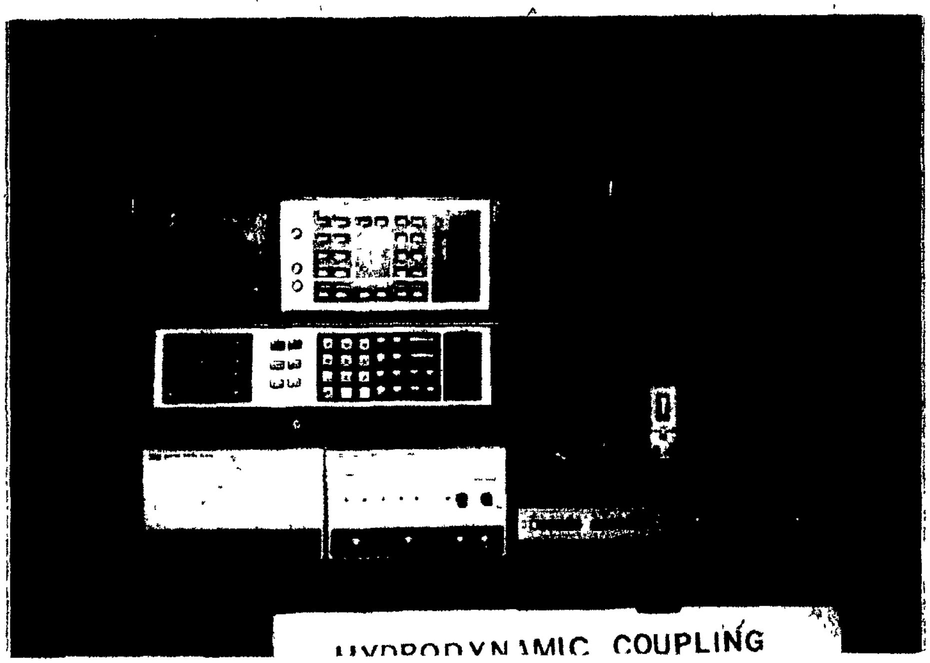

Picture 9: Measurement equipment.

Picture 10: The boundary channel with Plexiglas supports.

Picture 11: A view of the cluster of cylinders, arranged in the center of the boundary channel, at the pressure measuring side.

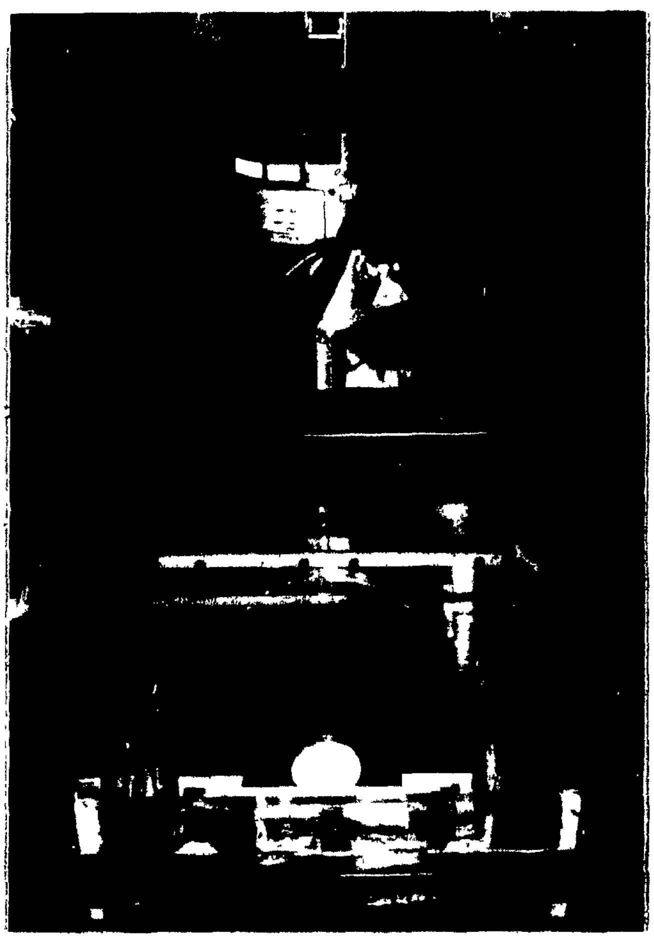

Picture 12: A view of the cluster of cylinders considered from the other side of the tank.

APPENDICES

The appendices in this thesis include three parts:

(A) Listings of the computer programs:

- A.1 "COUPRESS"
- A.2 "SSCHEN"
- A.3 "MAZUR"
- A.4 "EXPAMC"

(B) Algorithm for the computer program "COUPRESS".

(C) Typical outputs of the computer programs:

- C.1 "COUPRESS" with pressure distribution
- C.2 "COUPRESS" using $R_o = 9.2$ in.
- C.3 "COUPRESS" using $R_o = 10{,}000$ in.
- C.4 "EXPAMC for the case of three cylinders with configuration of Fig. 4.6c using water.

"COUPRESS": A computer program for calculating the added mass coefficient matrix for a cluster of cylinders vibrating in fluid based on S. Suss' theory. This program also gives us the pressure distribution on the surface of any cylinder in the system. A listing of the subroutines used in this program, except Subroutine Press, can be found in S. Suss (1977a).

<u>"SSCHEN"</u>: A computer program for calculating the unknown H in S.S. Chen's "viscous" mathematical model for an infinitely long cylinder oscillating in viscious fluid confined by a cylindrical annulus, of which the real part (Re(H)) is the added mass coefficient.

<u>"MAZUR"</u>: A computer program for calculating the added mass coefficients according to Mazur's theory, especially written for the case of the cylinders having the same radius as well as the same magnitude of acceleration.

<u>"EXPAMC"</u>: A computer program for obtaining the added mass coefficients from the experimental data, also based on S. Suss' theory.

APPENDIX A.1

PROGRAM "COUPRESS"

```
      IMPLICIT REAL*8(A-H,O-Z)
C      *******************************************************************
C      * K IS THE NUMBER OF CYLINDERS                                    *
C      * MN=NUMBER OF CYLINDER AT CENTER OF ARRAY                        *
C      * RO=RADIUS OF ENCLOSING CYLINDER                                 *
C      * C1(I)=CH(0,I) ,  RA(I)=R(0,I),  RI(I)=RADIUS OF CYLINDER I      *
C      * DIMENSION A(MM,MM,K),B(MM,MM,K),W1(MM,MM),W2(MM,MM),W3(MM,MM),W4(MM,MM)
C      * DIMENSION S(2MM+1),CO(2MM+1),F(2MM),R1(2MM+2),R2(2MM+2),R3(2MM+1)  *
C      * DIMENSION G(2MPK,2MPK),W5(2MPK,2K),W6(2MPK),VC(2K,2K)          *
C      * DIMENSION CH(K,K),R(K,K),RI(K),RA(K),C1(K)                     *
C      * DIMENSION A1(MM),A2(MM),A3(2,2MP(K-1)),A4(2,2(K-1))            *
C      * DIMENSION VC(2K,25),AM(2*(K+1),2*(K+1))                        *
C      *******************************************************************
      DIMENSION A(15,15,3),B(15,15,3)
      DIMENSION W1(15,15),W2(15,15),W3(15,15),W4(15,15)
      DIMENSION G(66,66),W5(66,6),W6(66)
      DIMENSION VC(6,6)
      DIMENSION AM(8,8)
      DIMENSION CH(3,3),R(3,3),RI(3),RA(3),C1(3)
      DIMENSION A1(25),A2(25),A3(2,44),A4(2,4)
      DIMENSION S(50),CO(50),F(50),R1(50),R2(50),R3(50)
      DIMENSION AA(3,3),BB(3,3)
      READ 99,K,MN
      READ 99,MM,MP
      PRINT 109,K,MM,MN,MP
      READ 99,IDEA,IPUNCH
C        READ CH(I,J) AND C1(I) IN DEGREES
      READ200, ((CH(I,J),R(I,J),J=1,K),I=1,K)
      PRINT 110
      PRINT 102,((CH(I,J),J=1,K),I=1,K)
      PRINT 111
      PRINT 102,((R(I,J),J=1,K),I=1,K)
C        READ R(I,J),RI(I),RA(I),RO IN THE SAME UNITS OF LENGTH
      READ 201,(RI(I),C1(I),RA(I),I=1,K)
      PRINT 107
      PRINT 108,(I,RI(I),RA(I),C1(I),I=1,K)
      READ 202,RO
```

```
C
C     ------------- IF PRESSURE PROFILE IS PRINTED ( IPRESS=1 )
C
      READ (5,*) IPRESS
      FF=3.14159265358980D0/180.D0
C        DEGREES TO RADIANS
      DO 301 I=1,K
      C1(I)=C1(I)*FF
      DO 301 J=1,K
  301 CH(I,J)=CH(I,J)*FF
      CALL FACT(MM,MP,F)
      M1=2*MP*K
      CALL FIXUP(MM,K,A,B,W1,W2,W3,W4,RO,MN,R1,R2,R3,RI,RA,C1,S,CO,F)
      IF(IDEA.EQ.0)GOTO 477
      DO 1 IDEA=1,K
      KK=2*(K-1)
      CALL FIXUP2(MM,MP,K,KK,M1,A,B,W1,W2,W3,W4,CH,R,RI,R1,R2,R3,S,CO,F,
     *G,W5,W6,IDEA)
      CALL VISCOU(MP,MM,K,IDEA,M1,S,CO,R,CH,R1,RI,A1,A2,A3,A4,W5,A,B)
      IX=IDEA+K
      JX=0
      KK=2*K
      DO 2 J=1,KK
      IF(J.EQ.IDEA.OR.J.EQ.IX)GOTO 2
      JX=JX+1
      VC(IDEA,J)=-A4(1,JX)
      VC(IX,J)=-A4(2,JX)
  2   CONTINUE
      VC(IDEA,IDEA)=1.D0
      VC(IX,IX)=1.D0
      VC(IDEA,IX)=0.D0
      VC(IX,IDEA)=0.D0
  1   CONTINUE
      PRINT 105,RO
      PRINT 102,((VC(I,J),J=1,K),I=1,KK)
      K1=K+1
      PRINT 105,RO
      PRINT 102,((VC(I,J),J=K1,KK),I=1,KK)
      IDEA=0
  477 KK=2*K
      CALL FIXUP2(MM,MP,K,KK,M1,A,B,W1,W2,W3,W4,CH,R,RI,R1,R2,R3,S,CO,F,
     *G,W5,W6,IDEA)
      IF(IPRESS.GT.1) GOTO 222
      DO 90 II=1,40
      THETA=(II-1)*9.0D0
      PRINT 114,THETA
      THETA=THETA*FF
      CALL PRESS(MP,MM,M1,K,S,CO,R,CH,RI,W5,A,B,R1,AA,BB,A1,A2,THETA)
      PRINT 115
      PRINT 116,((AA(I,J),J=1,K),I=1,K)
      PRINT 117
      PRINT 116,((BB(I,J),J=1,K),I=1,K)
   90 CONTINUE
```

```
 222 IX=1
     K2=K+2
     DO 81 I=1,M1,MP
     IX=IX+1
     DO 82 J=1,KK
     JX=J+1
     IF(J.GT.K)JX=J+2
     IF(IX.EQ.K2)IX=IX+1
     AM(IX,JX)=2.D0*W5(I,J)
  82 W5(I,J)=2.0D0*W5(I,J)
     J=(I-1+MP)/MP
     AM(IX,IX)=1.0D0+AM(IX,IX)
     W5(I,J)=1.0D0+W5(I,J)
  81 CONTINUE
     K1=K+2
     AM(1,1)=-1.0D0
     AM(1,K1)=0.0D0
     AM(K1,1)=0.0D0
     AM(K1,K1)=-1.0D0
     DO 83 J=1,K
     JX=J+1
     JP=JX+K+1
     FF=(RI(J)/RO)**2
     AM(1,JX)=FF
     AM(1,JP)=0.0D0
     AM(K1,JX)=0.0D0
     AM(K1,JP)=FF
     AM(JX,1)=1.0D0
     AM(JP,1)=0.0D0
     AM(JX,K1)=0.0D0
     AM(JP,K1)=1.0D0
     DO 84 I=1,K
     IX=I+1
     IP=IX+K+1
     FG=(RI(I)/RO)**2
     AM(1,JX)=AM(1,JX)-FG*AM(IX,JX)
     AM(1,JP)=AM(1,JP)-FG*AM(IX,JP)
     AM(K1,JX)=AM(K1,JX)-FG*AM(IP,JX)
     AM(K1,JP)=AM(K1,JP)-FG*AM(IP,JP)
     AM(JX,1)=AM(JX,1)-AM(JX,IX)
     AM(JP,1)=AM(JP,1)-AM(JP,IX)
     AM(JX,K1)=AM(JX,K1)-AM(JX,IP)
     AM(JP,K1)=AM(JP,K1)-AM(JP,IP)
  84 CONTINUE
```

```
      AM(1,1)=AM(1,1)-AM(1,JX)
      AM(1,K1)=AM(1,K1)-AM(1,JP)
      AM(K1,1)=AM(K1,1)-AM(K1,JX)
      AM(K1,K1)=AM(K1,K1)-AM(K1,JP)
 83   CONTINUE
      K1=KK+2
      PRINT 103,RO
      PRINT 106,((AM(I,J),J=1,K1),I=1,K1)
      PRINT 98, AM(4,2),AM(8,2),AM(4,6),AM(8,6)
      IX=0
      IF(IPUNCH.EQ.0) GOTO 629
      DO 529 I=1,M1,MP
      IX=IX+1
 529  PUNCH 200,(W5(I,J),VC(IX,J),J=1,KK)
 629  STOP
  98  FORMAT(//'0',2X,'EPSILON(3,1) = ',F12.5,/,3X,'XSI(3,1) = ',F12.5,/
     *3X,'E(3,1) = ',F12.5,/3X,'F(3,1) = ',F12.5)
 99   FORMAT(2I3)
 102  FORMAT('0',3F12.5)
 106  FORMAT('0',8D12.5)
 103  FORMAT(///,10X,'THE MATRIX OF ADDED MASS COEFFICIENTS WITH THE ENC
     *LOSING CYLINDER AT RO=',F10.1,//)
 104  FORMAT('1')
 105  FORMAT(///,10X,'THE VISCOUS COUPLING MATRIX WITH ENCLOSING CYLINDE
     *R AT RO=',F10.1,//)
 107  FORMAT(///,'0',12X,'I',7X,'R(I)',10X,'R(O,I)',9X,'CH(O,I) IN DEG')
 108  FORMAT('0',10X,I3,3F14.7)
 109  FORMAT('1',5X,'K=',I2,'  MM=',I2,'  CYLINDER AT CENTRE OF ARRAY',I
     *2,'  MP=',I2,//)
 110  FORMAT('0  THE MATRIX DEFINING CH(I,J) IN DEGREES')
 111  FORMAT(///,'0  THE MATRIX DEFINING R(I,J)')
 114  FORMAT(///,8X,'  ** THETA=',F5.1,'  **')
 115  FORMAT(/,1X,'MOTION IN Z DIRECTION OF CYLINDER          (1)
     *    (2)          (3)')
 116  FORMAT(/1X,'PRESSURE ON CYLINDER (1)',14X,3F12.5,/1X,'PRESSURE ON
     *CYLINDER (2)',14X,3F12.5/1X,'PRESSURE ON CYLINDER (3)',14X,3F12.5)
 117  FORMAT(/,1X,'MOTION IN Y DIRECTION OF CYLINDER          (1)
     *    (2)          (3)')
 200  FORMAT(2F10.5)
 201  FORMAT(3F10.5)
 202  FORMAT(F10.5)
      END
```

```
      SUBROUTINE PRESS(MP,MM,M1,K,S,C,R,CH,RI,W5,A,B,R1,AA,BB,A1,A2,TH)
      IMPLICIT REAL*8(A-H,O-Z)
      DIMENSION R(K,1),CH(K,1),W5(M1,1),A(MM,MM,K),B(MM,MM,K)
      DIMENSION RI(1),R1(1),S(1),C(1),AA(K,1),BB(K,1),A1(1),A2(1)
      M2=MM+1
      DO 20 I=1,K
      DO 15 L=1,K
      AA(I,L)=0.0D0
   15 BB(I,L)=0.0D0
      AA(I,I)=DCOS(TH)
      BB(I,I)=DSIN(TH)
      DO 30 J=1,K
      IF(J.EQ.I) GOTO 30
      R4=R(I,J)/RI(J)
      CALL CONT(R4,M2,R1)
      CALL GEN(CH(I,J),M2,S,C)
      DO 40 M=1,MM
      MG=M+1
      A1(M)=(-1.0D0)**M*C(MG)*R1(MG)
   40 A2(M)=(-1.0D0)**M*S(MG)*R1(MG)
      DO 50 M=1,MP
      R4=0.0D0
      R5=0.0D0
      DO 60 MH=1,MM
      R4=R4+A1(MH)*A(MH,M,J)-A2(MH)*B(MH,M,J)
   60 R5=R5+A1(MH)*B(MH,M,J)+A2(MH)*A(MH,M,J)
      MG=M+1
      R4=R4+(-1.0D0)**M*C(MG)/R1(MG)
      R5=R5+(-1.0D0)**M*S(MG)/R1(MG)
      IP=(J-1)*MP+M
      IPP=MP*K+IP
      DO 70 L=1,K
      LL=L+K
      AA(I,L)=AA(I,L)+(R4*W5(IP,L)+R5*W5(IPP,L))*RI(J)/RI(I)
   70 BB(I,L)=BB(I,L)+(R4*W5(IP,LL)+R5*W5(IPP,LL))*RI(J)/RI(I)
   50 CONTINUE
   30 CONTINUE
      DO 90 L=1,K
      LL=L+K
      DO 80 M=1,MP
      IP=(I-1)*MP+M
      IPP=MP*K+IP
      GM=M*TH
      AA(I,L)=AA(I,L)+2.0D0*DCOS(GM)*W5(IP,L)+2.0D0*DSIN(GM)*W5(IPP,L)
   80 BB(I,L)=BB(I,L)+2.0D0*DCOS(GM)*W5(IP,LL)+2.0D0*DSIN(GM)*W5(IPP,LL)
      AA(I,L)=AA(I,L)*RI(I)
   90 BB(I,L)=BB(I,L)*RI(I)
   20 CONTINUE
      RETURN
      END
```

APPENDIX A.2

PROGRAM "SSCHEN"

```
C
C   *******************************************************************
C   *                                                                 *
C   * PROGRAM FOR SOLVING THE COEFFICIENT 'H' FROM S.S.CHEN'S THEORY *
C   *                                                                 *
C   *******************************************************************
C
      COMPLEX A,B,C,D,W,X,Y,Z,H,ALFA,BETA,CONST,ARG
       COMPLEX CONST1,CONST2
      DIMENSION FREQ(16)
      DATA XMU/1.059E-5/,R/1.25/,RO/9.2/
      CONST=CMPLX(1.0,1.0)
      READ (5,10)FREQ
   10 FORMAT(6F10.4)
      GAMA=R/RO
      DO 20 I=1,16
      WRITE(6,15)FREQ(I)
   15 FORMAT(//3X,'FREQ= ',F10.2)
      OMEGA=2.0*3.1415927*FREQ(I)
      TR=(RO-R)*SQRT(OMEGA/(2.0*XMU*144.0))*3.1415927/180.0
      ALFA=CONST*SQRT(OMEGA/(XMU*144.0*2.0))*R
      BETA=CONST*SQRT(OMEGA/(XMU*144.0*2.0))*RO
      E=SINH(TR)*COS(TR)
      F=COSH(TR)*SIN(TR)
      T=COSH(TR)*COS(TR)
      U=SINH(TR)*SIN(TR)
      CONST1=CMPLX(E,F)
      CONST2=CMPLX(T,U)
      A=(ALFA**2*(1.0+GAMA**2)-8*GAMA)*CONST1
      B=2.0*ALFA*(2.0-GAMA+GAMA**2)*CONST2
      C=2.0*GAMA**2*CSQRT(ALFA*BETA)
      D=2.0*CSQRT(ALFA/BETA)*ALFA
      W=ALFA**2*(1.0-GAMA**2)*CONST1
      X=2.0*ALFA*GAMA*(1.0+GAMA)*CONST2
      Y=2.0*GAMA**2*CSQRT(ALFA*BETA)
      Z=2.0*ALFA*CSQRT(ALFA/BETA)
      H=(A+B-C-D)/(W-X+Y+Z)
      WRITE(6,14)H
   14 FORMAT(/3X,'RE(H)= ',F12.6/3X,'IM(H)= ',F12.6)
   20 CONTINUE
      STOP
      END
$DATA
30.0      40.0      50.0      70.0      80.0      90.0
100.0     110.0     130.0     140.0     150.0     160.0
170.0     180.0     190.0     200.0
//
```

Results:

FREQ=	30.00		
RE(H)=	-1.044312	IM(H)=	0.006698
FREQ=	40.00		
RE(H)=	-1.043414	IM(H)=	0.005800
FREQ=	50.00		
RE(H)=	-1.042802	IM(H)=	0.005188
FREQ=	70.00		
RE(H)=	-1.041999	IM(H)=	0.004385
FREQ=	80.00		
RE(H)=	-1.041716	IM(H)=	0.004102
FREQ=	90.00		
RE(H)=	-1.041480	IM(H)=	0.003867
FREQ=	100.00		
RE(H)=	-1.041282	IM(H)=	0.003668
FREQ=	110.00		
RE(H)=	-1.041112	IM(H)=	0.003498
FREQ=	130.00		
RE(H)=	-1.040832	IM(H)=	0.003217
FREQ=	140.00		
RE(H)=	-1.040714	IM(H)=	0.003100
FREQ=	150.00		
RE(H)=	-1.040610	IM(H)=	0.002995
FREQ=	160.00		
RE(H)=	-1.040514	IM(H)=	0.002900
FREQ=	170.00		
RE(H)=	-1.040427	IM(H)=	0.002814
FREQ=	180.00		
RE(H)=	-1.040349	IM(H)=	0.002734
FREQ=	190.00		
RE(H)=	-1.040276	IM(H)=	0.002661
FREQ=	200.00		
RE(H)=	-1.040209	IM(H)=	0.002594

APPENDIX A.3

PROGRAM "MAZUR"

```
0: dsp " Program
 for solving
 Mazur's A.M.C."
1: fmt 1,"Cylind
 er centers",/,
 "distance =",
 f6.3,/,"K=",
 f2.0
2: fmt 2,"Epsln1
 1=",f8.5,/,"Eps
 ln12=",f8.5,/,/
3: 1.25→r1
4: ent r0
5: (r0↑2-2*r1↑2)
 /(2*r1↑2)→r2
6: r0/(2*r1)→r5
7: ln(r2+√(r2↑2-
 1))→r3
8: 2*ln(r5+√(r5↑
 2-1))→r4
9: 0→C→D
10: K+1→K
11: (exp(K*r3)-
 exp(-K*r3))/
 2→r6
12: (exp(K*r3)+
 exp(-K*r3))/
 (exp(K*r3)-exp(
 -K*r3))→r7
13: K*exp(-K*
 (r3+r4))/r6+C→C
14: K*r7*exp(-2*
 K*r3)+D→D
15: 1+(r0↑4-4*
 r0↑2*r1↑2)/(r0↑
 2*r1↑2)*C→A
16: (1+(r0↑4-4*
 r0↑2*r1↑2)/r1↑4
 *D)*r1↑2/r0↑2→B
17: if K=1;A→X;
 B→Y;gto 10
18: if A-X>10↑(-
 6);A→X;gto 10
19: if B-Y>10↑(-
 6);B→Y;gto 10
20: wrt 16.1,r0,
 K
21: X*-1→X;Y*-
 1→Y
22: wrt 16.2,X,Y
23: end
```

r_o: Cylinder centers distance.

r_1: Radius of the oscillating cylinder.

r_3: h

r_4: h_1

r_6: *sinh* (kh)

r_7: *coth* (kh)

X: ε_{11}

Y: ε_{12}

K: No. of terms taken for solving the equation.

Note: This program is only good for the case where the cylinders have same radius and same acceleration

Results:

```
Cylinder centers
distance = 4.500
K= 4
Epsln11=-1.01410
Epsln12=-0.15562
```

```
Cylinder centers
distance = 2.675
K= 8
Epsln11=-1.13180
Epsln12=-0.41742
```

```
Cylinder centers
distance = 5.000
K= 4
Epsln11=-1.00893
Epsln12=-0.12564
```

```
Cylinder centers
distance = 3.500
K= 5
Epsln11=-1.04411
Epsln12=-0.26282
```

APPENDIX A.4

PROGRAM "EXPAMC"

```
C
C
C     *****************************************************************
C     *                                                               *
C     *    PROGRAM FOR CALCULATING THE ADDED MASS COEFFICIENTS FROM   *
C     *                  THE EXPERIMENTAL DATA                        *
C     *                                                               *
C     *****************************************************************
      DIMENSION PRESS(40)
      DIMENSION XPRESS(40),PHASE(40)
      DATA PI/3.1415927/,R/1.25/
      CONST=PI*10.0/180.0
      RHO=62.37/(12**3)
      DO 99 MN=1,8
      READ(5,50)ACCEL,FREQ
   50 FORMAT(2F10.4)
      READ(5,*)(XPRESS(I),PHASE(I),I=1,40)
      DO 22 I=1,40
      PHI=PI*PHASE(I)/180.0
      PRESS(I)=XPRESS(I)*1.414213562*COS(PHI)/257.7
   22 CONTINUE
      WRITE(6,12)
   12 FORMAT(//////8X,'@  DERIVATION OF THE VIRTUAL MASS COEFFICIENTS FR
     *OM EXPERIMENTAL DATA  @'///)
      WRITE(6,13)FREQ,ACCEL
   13 FORMAT(//5X,'FREQUENCY = ',9X,F10.2,1X,'HZ',/5X,'ACCEL.(Z DIRECTIO
     *N) = ',F10.4,1X,'G')
      WRITE(6,15)
   15 FORMAT(/5X,'PRESSURES MEASURED AT PEAK ACCELERATION',//35X,'ANGLE'
     *,5X,'PRESSURE',15X,'PHASE DIFFERENCE'/)
      DO 16 I=1,40
      IANG=9*(I-1)
      WRITE(6,17)IANG,PRESS(I),PHASE(I)
   17 FORMAT(36X,I3,6X,F10.4,1X,'PSI',13X,F6.1)
   16 CONTINUE
```

```
C
C      ***************************************************
C       INTEGRATION USING '' SIMPSON'S RULE ''
C      ***************************************************
C
       FZ=2.0*PRESS(1)*1.0
       FY=2.0*PRESS(1)*0.0
       DO 51 N=2,40
       THETA=CONST*(N-1)
       IF(N/2*2.EQ.N) GO TO 23
       COSINE=2.0*COS(THETA)
       SINE=2.0*SIN(THETA)
       GO TO 24
    23 COSINE=4.0*COS(THETA)
       SINE=4.0*SIN(THETA)
    24 FZ=FZ+PRESS(N)*COSINE
       FY=FY+PRESS(N)*SINE
    51 CONTINUE
       FZ=CONST/3*R*FZ
       FY=CONST/3*R*FY
       WRITE(6,18)FZ,FY
    18 FORMAT(//5X,'FORCE IN Z DIRECTION = ',F10.6,1X,'PSI',/5X,'FORCE IN
      * Y DIRECTION = ',F10.6,1X,'PSI'/)
       EXPTCZ=FZ/(RHO*PI*R**2*ACCEL)
       EXPTCY=FY/(RHO*PI*R**2*ACCEL)
       WRITE(6,19)EXPTCZ,EXPTCY
    19 FORMAT(/5X,'COEFFICIENT IN Z DIRECTION = ',F10.6,7X,/5X,'COEFFICIE
      *NT IN Y DIRECTION = ',F10.6////)
    99 CONTINUE
       STOP
       END
```

APPENDIX B

ALGORITHM USED IN THE "COUPRESS" PROGRAM

B.1 THE ADDED MASS COEFFICIENTS

This program is a modified version of Suss' "COUPLING" computer program (S. Suss' Master Thesis 1977a), where an extra part was added to predict the pressure distribution around the surface of a particular cylinder in the system.

The main job of this program is to solve equations (2.16) to (2.27) for $\alpha_{nj\ell}$, $\beta_{nj\ell}$, $\gamma_{nj\ell}$, $\delta_{nj\ell}$, $a_{nj\ell}$, $b_{nj\ell}$, $c_{nj\ell}$, $d_{nj\ell}$. The entire system of these equations may be written as the single matrix equation

$$[C]\ [W] = [T], \tag{B.1}$$

with

$$[C] = \begin{bmatrix} [\Gamma^{ij}], & [\Lambda^{ij}], & [\Omega^{\ell j}], & [\kappa^{ij}] \\ -[\Lambda^{ij}], & [\Gamma^{ij}], & [\kappa^{ij}], & -[\Omega^{*ij}] \\ [A^j], & [B^j], & [C^j], & [D^j] \\ [B^j], & -[A^j], & [D^j], & -[C^j] \end{bmatrix},$$

$$[W] = \begin{bmatrix} \{\alpha\}_1\{\alpha\}_2\ldots\{\alpha\}_k\{a\}_1\{a\}_2\ldots\{a\}_k \\ \{\beta\}_1\{\beta\}_2\ldots\{\beta\}_k\{b\}_1\{b\}_2\ldots\{b\}_k \\ \{\gamma\}_1\{\gamma\}_2\ldots\{\gamma\}_k\{c\}_1\{c\}_2\ldots\{c\}_k \\ \{\delta\}_1\{\delta\}_2\ldots\{\delta\}_k\{d\}_1\{d\}_2\ldots\{d\}_k \end{bmatrix},$$

$$[T] = \begin{bmatrix} \{\delta_{1m}\}_1\{\delta_{1m}\}_2\ldots\{\delta_{1m}\}_k\{\ 0\ \}_1\{\ 0\ \}_2\ldots\{\ 0\ \}_k \\ \{\ 0\ \}_1\{\ 0\ \}_2\ldots\{\ 0\ \}_k\{\delta_{1m}\}_1\{\delta_{1m}\}_2\ldots\{\delta_{1m}\}_k \\ \{\ 0\ \}_1\{\ 0\ \}_2\ldots\{\ 0\ \}_k\{\ 0\ \}_1\{\ 0\ \}_2\ldots\{\ 0\ \}_k \\ \{\ 0\ \}_1\{\ 0\ \}_2\ldots\{\ 0\ \}_k\{\ 0\ \}_1\{\ 0\ \}_2\ldots\{\ 0\ \}_k \end{bmatrix}$$

where [W] is a (4*MM*k) x (2*k) matrix of all the unknowns, [T] is a (4*MM*k) x (2*k) matrix of the right-hand side of equations (2.16) to (2.27), and [C] is a (4*MM*k) x (4*MM*k) matrix of the coefficients common to each column of [W]; δ_{1m} is Kronecker's delta; the sub-matrices in [C] will be defined later in this appendix.

The solution of this matrix equation is straightforward. However, it is found that for obtaining an accuracy up to three digits, the values (MM) of the indices, m,n in equations (2.16) to (2.27) may have to be as great as ten. For a modest system of three cylinders, with the unknowns being 8*MM*k, seven hundred and twenty unknowns have to be determined. Hence, a saving in computation to solve this problem is particularly desirable. Fortunately, the equations for the unknowns $\alpha_{nj\ell}$ to $\delta_{nj\ell}$ and $a_{nj\ell}$ to $d_{nj\ell}$ are not coupled. Thus, we can solve them separately. Also, the coefficients of the $\alpha_{nj\ell}$ to $\delta_{nj\ell}$ are independent of ℓ and are identical in corresponding equations to those of the $a_{nj\ell}$ to $d_{nj\ell}$. These will be proved later in the appendix.

An attempt to simplify the solution of equation (B.1) was made by utilizing some of the properties of matrix [C]. Let us consider the relation (A.1) for just one column of [W].

$$[C]\begin{Bmatrix}\{\alpha\}_\ell\\ \{\beta\}_\ell\\ \{\gamma\}_\ell\\ \{\delta\}_\ell\end{Bmatrix} = \begin{Bmatrix}\{\delta_{1m}\}\\ \{\ 0\ \}\\ \{\ 0\ \}\\ \{\ 0\ \}\end{Bmatrix}. \qquad (B.2)$$

The elements of the lower 2*MM*k rows of [C] are the coefficients of the α's, β's, γ's and δ's in equation (2.20) and equation (2.22). Coefficients in equations (2.24) and (2.26) must also be included if there is a cylinder in the center of the array.

In terms of sub-matrices, equation (B.2) can be expressed as:

$$[A^j]\{\alpha\}_{j\ell} + [B^j]\{\beta\}_{j\ell} + [C^j]\{\gamma\}_{j\ell} + [D^j]\{\delta\}_{j\ell} = \{0\} \qquad (B.3)$$

$$[B^j]\{\alpha\}_{j\ell} - [A^j]\{\beta\}_{j\ell} + [D^j]\{\gamma\}_{j\ell} - [C^j]\{\delta\}_{j\ell} = \{0\} \qquad (B.4)$$

where,

$$A^j_{mn} = \frac{(-1)^{n-m}n!}{(m-1)!(n-m)!}\ \frac{R_{oj}^{n-m}\ R_o^{m-1}}{R_j^{n-1}}\cos(n-m)\psi_{oj} \quad \text{for } n \geq m$$

$$= 0 \quad \text{for } n < m \qquad (B.5)$$

$$B^j_{mn} = \frac{(-1)^{n-m} n!}{(m-1)!(n-m)!} \frac{R_{oj}^{n-m} R_o^{m-1}}{R_j^{n-1}} \sin(n-m)\psi_{oj} \quad \text{for } n \geq m$$

$$= 0. \quad \text{for } n < m \quad \text{(B.6)}$$

$$C^j_{mn} = \frac{-m! R_{oj}^{m-n} R_j^{n+1}}{(n-1)!(m-n)! R_o^{m+1}} \cos(m-n)\psi_{oj} \quad \text{for } n \leq m$$

$$= 0 \quad \text{for } n > m \quad \text{(B.7)}$$

$$D^j_{mn} = \frac{m! R_{oj}^{m-n} R_j^{n+1}}{(n-1)!(m-n)! R_o^{m+1}} \sin(m-n)\psi_{oj} \quad \text{for } n \leq m$$

$$= 0 \quad \text{for } n > m \quad \text{(B.8)}$$

$$j = 1,2,3\ldots k; \; j \neq q.$$

If $j = q$, we have from equations (2.24) and (2.26) that,

$$A^q_{mn} = \left(\frac{R_o}{R_q}\right)^{n-1} \quad \text{for } n = m$$

$$= 0 \quad \text{(B.9)}$$

otherwise,

$$B^q_{mn} = 0 \quad \text{for all } m, n, \quad \text{(B.10)}$$

$$C^q_{mn} = -\left(\frac{R_q}{R_o}\right)^{n+1} \quad \text{for } n = m$$

$$= 0 \quad \text{(B.11)}$$

otherwise,

$$D^q_{mn} = 0 \quad \text{for all } m, n, \tag{B.12}$$

It can be seen from equations (A.3) and (A.4) that $\{\alpha\}_{j\ell}$ and $\{\beta\}_{j\ell}$ may be expressed in terms of the corresponding $\{\gamma\}_{j\ell}$ and $\{\delta\}_{j\ell}$ as,

$$\{\alpha\}_{j\ell} = [X^j]\{\gamma\}_{j\ell} + [Y^j]\{\delta\}_{j\ell}, \tag{B.13}$$

$$\{\beta\}_{j\ell} = -[Y^j]\{\gamma\}_{j\ell} + [X^j]\{\delta\}_{j\ell}, \tag{B.14}$$

where,

$$[X^j] = -([B^j][A^j]^{-1}[B^j] + [A^j])^{-1}([B^j][A^j]^{-1}[D^j] + [C^j]) \tag{B.15}$$

$$[Y^j] = ([B^j][A^j]^{-1}[B^j] + [A^j]^{-1})([B^j][A^j]^{-1}[C^j] - [D^j]) \tag{B.16}$$

Now attention is centered on the upper part of matrix [C]. The elements of the upper 2*MM*k rows of [C] are the coefficients of the $\alpha_{nj\ell}$ to $\delta_{nj\ell}$ in equations (2.16) and (2.18). Similarly, these matrix equations may be written,

$$\sum_{j=1}^{k} [\Gamma^{ij}]\{\alpha\}_{j\ell} + \sum_{j=1}^{k} [\Lambda^{ij}]\{\beta\}_{j\ell} + \sum_{j=1}^{k} [\Omega^{ij}]\{\gamma\}_{j\ell}$$

$$+ \sum_{j=1}^{k} [\kappa^{ij}]\{\delta\}_{j\ell} = \{\delta_{1m}\}_{i\ell}, \tag{B.17}$$

$$-\sum_{j=1}^{k}[\Lambda^{ij}]\{\alpha\}_{j\ell}+\sum_{j=1}^{k}[\Gamma^{ij}]\{\beta\}_{j\ell}+\sum_{j=1}^{k}[\kappa^{ij}]\{\gamma\}_{j\ell}$$

$$-\sum_{j=1}^{k}[\Omega^{*ij}]\{\delta\}_{j\ell}=\{0\}_{i\ell}, \qquad (B.18)$$

$$i = 1,2,3\ldots k,$$

where k is the number of cylinders in the system, and

$$\Gamma^{ij}_{mn}=\frac{(-1)^{n-m}n!R_{ij}^{n-m}R_i^{m-1}}{(m-1)!(n-m)\;R_j^{n-1}}\cos(n-m)\psi_{ij} \quad \text{for } i\neq j,\ n\geq m$$

$$= 0 \qquad \text{for } n<m,\ i\neq j$$

$$= m \qquad \text{for } n=m,\ i=j$$

$$= 0 \qquad \text{for } n\neq m,\ i=j\ , \qquad (B.19)$$

$$\Lambda^{ij}_{mn}=\frac{(-1)^{n-m}n!R_{ij}^{n-m}R_i^{m-1}}{(m-1)!(n-m)!\;R_j^{n-1}}\sin(n-m)\psi_{ij} \quad \text{for } i\neq j,\ n\geq m$$

$$= 0 \qquad \text{for } n<m \text{ or } i=j, \qquad (B.20)$$

$$\Omega^{ij}_{mn}=\frac{(-1)^{n}(n+m-1)!R_i^{m-1}R_j^{n+1}}{(m-1)!(n-1)!R_{ij}^{n+m}}\cos(n+m)\psi_{ij} \quad \text{for } i\neq j$$

$$\Omega_{mn}^{ij} = -m \qquad \text{for } i = j,\ n = m$$

$$= 0 \qquad \text{for } i = j,\ n \neq m, \tag{B.21}$$

$$\Omega_{mn}^{*ij} = \Omega_{mn}^{ij} \qquad \text{for } i \neq j,$$

$$= -\Omega_{mn}^{ij} \qquad \text{for } i = j, \tag{B.22}$$

$$\kappa_{mn}^{ij} = \frac{(-1)^n (n+m-1)!\, R_i^{m-1} R_j^{n+1}}{(m-1)!\,(n-1)!\,R_{ij}^{n+m}} \sin(n+m)\psi_{ij} \qquad \text{for } i \neq j$$

$$= 0 \qquad \text{for } i = j. \tag{B.23}$$

Replacing $\{\alpha\}_{j\ell}$ and $\{\beta\}_{j\ell}$ in equations (B.17) and (B.18) by $\{\gamma\}_{j\ell}$ and $\{\delta\}_{j\ell}$, we obtain,

$$[G]\{\gamma\}_{j\ell} + [H]\{\delta\}_{j\ell} = \{\delta_{1m}\}_{i\ell}, \tag{B.24}$$

$$[P]\{\gamma\}_{j\ell} + [Q]\{\delta\}_{j\ell} = \{0\} \tag{B.25}$$

where,

$$[G] = \sum_{j=1}^{k} ([\Gamma^{ij}][X^j] - [\Lambda^{ij}][Y^j] + [\Omega^{ij}]) \tag{B.26}$$

$$[H] = \sum_{j=1}^{k} ([\Gamma^{ij}][Y^j] + [\Lambda^{ij}][X^j] + [\kappa^{ij}]) \tag{B.27}$$

$$[P] = \sum_{j=1}^{k} (-[\Gamma^{ij}][Y^j] - [\Lambda^{ij}][X^j] + [\kappa^{ij}]), \quad (B.28)$$

$$[Q] = \sum_{j=1}^{k} ([\Gamma^{ij}][X^j] - [\Lambda^{ij}][Y^j] - [\Omega^{*ij}]). \quad (B.29)$$

Similarly, the relation between $\{c\}_{j\ell}$ and $\{d\}_{j\ell}$ to equations (B.26) to (B.30) may be written as:

$$[G]\{c\}_{j\ell} + [H]\{d\}_{j\ell} = \{0\}, \quad (B.30)$$

$$[P]\{c\}_{j\ell} + [Q]\{d\}_{j\ell} = \{\delta_{1m}\}_{i\ell}. \quad (B.31)$$

Combining equations (B.24), (B.25), (B.30) and (B.31), we arrive at:

$$\begin{bmatrix} [G] & [H] \\ [P] & [Q] \end{bmatrix} \begin{bmatrix} [\gamma] & [c] \\ [\delta] & [d] \end{bmatrix} = \begin{bmatrix} [\delta_{1m}] & [\ 0\ ] \\ [\ 0\ ] & [\delta_{1m}] \end{bmatrix} . \quad (B.32)$$

With $\gamma_{1i\ell}$, $\delta_{1i\ell}$, $c_{1i\ell}$ and $d_{1i\ell}$ known from the above equation, the added mass coefficients can now be calculated, since:

$$\begin{Bmatrix} \varepsilon_{i\ell} \\ \xi_{i\ell} \\ e_{i\ell} \\ f_{i\ell} \end{Bmatrix} = \begin{Bmatrix} \delta_{i\ell} + 2\gamma_{1i\ell} \\ 2\delta_{1i\ell} \\ 2c_{1i\ell} \\ \delta_{i\ell} + 2d_{1i\ell} \end{Bmatrix}, \qquad i,\ell = 1,2,3....k \tag{B.33}$$

where $\delta_{i\ell}$ is the Kronecker's delta.

Comparing (B.32) with (B.1), it can easily be seen that we now only have to solve the upper half of (B.1) instead of solving the whole matrix equation in order to obtain the added mass coefficients.

For the case of the boundary channel free to move, the added mass coefficients for this channel are calculated by using the following equations.

$$\begin{Bmatrix} \varepsilon_{o\ell} \\ \xi_{o\ell} \\ e_{o\ell} \\ f_{o\ell} \end{Bmatrix} = \sum_{j=1}^{k} \left(\frac{R_j}{R_o}\right)^2 \begin{Bmatrix} \delta_{j\ell} - \varepsilon_{j\ell} \\ - \xi_{j\ell} \\ - e_{j\ell} \\ \delta_{j\ell} - f_{j\ell} \end{Bmatrix} \tag{B.34}$$

$$\begin{Bmatrix} \varepsilon_{oo} \\ \xi_{oo} \\ e_{oo} \\ f_{oo} \end{Bmatrix} = \sum_{\ell=1}^{k} \begin{Bmatrix} \varepsilon_{o\ell} & & 1 \\ \xi_{o\ell} & & 0 \\ e_{o\ell} & + & 0 \\ f_{o\ell} & & 1 \end{Bmatrix} \tag{B.35}$$

$$\begin{Bmatrix} \varepsilon_{io} \\ \xi_{io} \\ e_{io} \\ f_{io} \end{Bmatrix} = \sum_{\ell=1}^{k} \begin{Bmatrix} \varepsilon_{i\ell} - \delta_{i\ell} \\ \xi_{i\ell} \\ e_{i\ell} \\ f_{i\ell} - \delta_{i\ell} \end{Bmatrix} \tag{B.36}$$

Details of the derivation of these equations can be found in Appendix A of Suss' (1977a).

B.2 THE VISCOUS COUPLING COEFFICIENTS

To calculate the viscous coupling coefficients, we also have to determine γ's, δ's, c's, d's. The procedure is similar except that the system has only (K-1) cylinders, that means the system is considered as if the particular P^{th} cylinder were missing. In order to express this fact, these unknowns are superscripted with P as γ^P, δ^P, c^P and d^P.

Referring to Suss' (1977a), the viscous coupling coefficients may be written as follows:

$$\zeta_\ell^P = \sum_{j=1}^{k} \sum_{n=1}^{\infty} \left\{ (-1)^{n-1} n \left(\frac{R_{pj}}{R_j}\right)^{n-1} (\alpha_{nj\ell}^P \cos(n-1)\psi_{pj} + \beta_{nj\ell}^P \sin(n-1)\psi_{pj}) \right.$$

$$\left. + (-1)^n n \left(\frac{R_j}{R_{pj}}\right)^{n+1} (\gamma_{nj\ell}^P \cos(n+1)\psi_{pj} + \delta_{nj\ell}^P \sin(n+1)\psi_{pj}) \right\}, \tag{B.37}$$

$$\sigma_{\ell}^{P} = \sum_{j=1}^{k} \sum_{n=1}^{\infty} \left\{ (-1)^n n \left(\frac{R_{pj}}{R_j}\right)^{n-1} (a_{nj\ell}^{P} \cos(n-1)\psi_{pj} + b_{nj\ell}^{P} \sin(n-1)\psi_{pj}) \right.$$

$$\left. + (-1)^n n \left(\frac{R_j}{R_{pj}}\right)^{n+1} (c_{nj\ell}^{P} \cos(n+1)\psi_{pj} + d_{nj\ell}^{P} \sin(n+1)\psi_{pj}) \right\},$$

(B.38)

$$g_{\ell}^{P} = \sum_{j=1}^{k} \sum_{n=1}^{\infty} \left\{ (-1)^n n \left(\frac{R_{pj}}{R_j}\right)^{n-1} (-\alpha_{nj\ell}^{P} \sin(n-1)\psi_{pj} + \beta_{nj\ell}^{P} \cos(n-1)\psi_{pj}) \right.$$

$$\left. + (-1)^n n \left(\frac{R_j}{R_{pj}}\right)^{n+1} (\gamma_{nj\ell}^{P} \sin(n+1)\psi_{pj} - \delta_{nj\ell}^{P} \cos(n+1)\psi_{pj}) \right\},$$

(B.39)

$$\delta_{\ell}^{P} = \sum_{j=1}^{k} \sum_{n=1}^{\infty} \left\{ (-1)^n n \left(\frac{R_{pj}}{R_j}\right)^{n-1} (-a_{nj\ell}^{P} \sin(n-1)\psi_{pj} + b_{nj\ell}^{P} \cos(n-1)\psi_{pj}) \right.$$

$$\left. + (-1)^n n \left(\frac{R_j}{R_{pj}}\right)^{n+1} (c_{nj\ell}^{P} \sin(n+1)\psi_{pj} - d_{nj\ell}^{P} \cos(n+1)\psi_{pj}) \right\},$$

(B.40)

$$\ell, P = 1,2,3\ldots k;\ \ell \neq P.$$

As in matrix form, these equations become:

$$\zeta_{\ell}^{P} = \sum_{j=1}^{k} [\{\lambda^P\}_j^T\{\alpha\}_{j\ell}^P + \{\eta^P\}_j^T\{\beta\}_{j\ell}^P + \{\mu^P\}_j^T\{\gamma\}_{j\ell}^P + \{\nu^P\}_j^T\{\delta\}_{j\ell}^P],$$

(B.41)

$$\sigma_\ell^P = \sum_{j=1}^{k} [\{\lambda^P\}_j^T\{a\}_{j\ell}^P + \{\eta^P\}_j^T\{b\}_{j\ell}^P + \{\mu^P\}_j^T\{c\}_{j\ell}^P + \{\nu^P\}_j^T\{d\}_{j\ell}^P], \tag{B.42}$$

$$g_\ell^P = \sum_{j=1}^{k} [-\{\eta^P\}_j^T\{\alpha\}_{j\ell}^P + \{\lambda^P\}_j^T\{\beta\}_{j\ell}^P + \{\nu^P\}_j^T\{\gamma\}_{j\ell}^P + \{\mu^P\}_j^T\{\delta\}_{j\ell}^P], \tag{B.43}$$

$$s_\ell^P = \sum_{j=1}^{k} [-\{\eta^P\}_j^T\{a\}_{j\ell}^P + \{\lambda^P\}_j^T\{b\}_{j\ell}^P + \{\nu^P\}_j^T\{c\}_{j\ell}^P - \{\mu^P\}_j^T\{d\}_{j\ell}^P], \tag{B.44}$$

With,

$$(\{\lambda^P\}_j^T)_n = (-1)^{n-1} n \left(\frac{R_{pj}}{R_j}\right)^{n-1} \cos(n-1)\psi_{pj} , \tag{B.45}$$

$$(\{\eta^P\}_j^T)_n = (-1)^{n-1} n \left(\frac{R_{pj}}{R_j}\right)^{n-1} \sin(n-1)\psi_{pj} , \tag{B.46}$$

$$(\{\mu^P\}_j^T)_n = (-1)^{n} n \left(\frac{R_j}{R_{pj}}\right)^{n+1} \cos(n+1)\psi_{pj} , \tag{B.47}$$

$$(\{\nu^P\}_j^T)_n = (-1)^{n} n \left(\frac{R_j}{R_{pj}}\right)^{n+1} \sin(n+1)\psi_{pj} , \tag{B.48}$$

$$n = 1,2,3....MM.$$

Replacing $\{\alpha\}^P_{j\ell}$ and $\{\beta\}^P_{j\ell}$ by $\{\gamma\}^P_{j\ell}$ and $\{\delta\}^P_{j\ell}$, equations (B.41) to (B.44) may be written as:

$$\zeta^P_\ell = \{E^P\}^T\{\gamma\}^P_\ell + \{F^P\}^T\{\delta\}^P_\ell \,, \tag{B.49}$$

$$\sigma^P_\ell = \{E^P\}^T\{c\}^P_\ell + \{F^P\}^T\{d\}^P_\ell \,, \tag{B.50}$$

$$g^P_\ell = \{U^P\}^T\{\gamma\}^P_\ell + \{V^P\}^T\{\delta\}^P_\ell \,, \tag{B.51}$$

$$\delta^P_\ell = \{U^P\}^T\{c\}^P_\ell + \{V^P\}^T\{d\}^P_\ell \,, \tag{B.52}$$

where: $\{E^P\}^T = \left\{ \{E^P\}^T_1 \;\{E^P\}^T_2 \;\ldots.\; \{E^P\}^T_k \right\}$, such that

$$\{E^P\}^T_j = \{\lambda^P\}^T_j[X^j] - \{\eta^P\}^T_j[Y^j] + \{\mu^P\}^T_j \,, \tag{B.53}$$

$$\{F^P\}^T_j = \{\lambda^P\}^T_j[Y^j] + \{\eta^P\}^T_j[X^j] + \{\nu^P\}^T_j \,, \tag{B.54}$$

$$\{U^P\}^T_j = -\{\eta^P\}^T_j[X^j] - \{\lambda^P\}^T_j[Y^j] + \{\nu^P\}^T_j \,, \tag{B.55}$$

$$\{V^P\}^T_j = \{\lambda^P\}^T_j[X^j] - \{\eta^P\}^T_j[Y^j] - \{\mu^P\}^T_j \,. \tag{B.56}$$

Expressing equations (B.49) to (B.52) in matrix form, we arrive at:

$$\begin{bmatrix} \{\zeta^P\}^T\{\sigma^P\}^T \\ \{g^P\}^T\{s^P\}^T \end{bmatrix} = \begin{bmatrix} \{E^P\}^T\{F^P\}^T \\ \{U^P\}^T\{V^P\}^T \end{bmatrix} \begin{bmatrix} \{\gamma\}^P\{c\}^P \\ \{\delta\}^P\{d\}^P \end{bmatrix} \tag{B.57}$$

with $\{\zeta^P\}^T = \{\zeta_1^P, \zeta_2^P, \ldots \zeta_k^P\}$, and similarly for $\{\sigma^P\}^T$, $\{g^P\}^T$ and $\{s^P\}^T$.

Hence, the viscous coupling coefficients ζ, σ, g and s can be determined as soon as γ^P, δ^P, c^P and d^P are known.

B.3 CALCULATION OF THE PRESSURE

The pressure distribution around the surface of any cylinder in the system is calculated by making use of the values of $\alpha_{nj\ell}$ to $d_{nj\ell}$ obtained from the solution of equations (2.16) to (2.27) to determine the velocity potential of that particular cylinder. The pressure may then be evaluated from the relation:

$$p^i\Big|_{r_i=R_i} = -\rho\,\frac{\partial\phi^i}{\partial t} \quad . \tag{B.58}$$

Referring to Chapter 2, the total potential written in terms of coordinates centered on cylinder i can be expressed as:

$$\phi^i = \sum_{j=1}^{k}{}^{*}\ \phi_j^i + \phi_i \ , \tag{B.59}$$

where,

$$\phi^i_j(r_i,\theta_i) = \sum_{n=1}^{\infty}\sum_{m=0}^{n} \frac{(-1)^{n-m} n! r_i^m R_{ij}^{n-m}}{(m-1)!(n-m)!m} \Big\{ A_{nj}\cos[m\theta_i+(n-m)\psi_{ij}]$$

$$+ B_{nj}\sin[m\theta_i+(n-m)\psi_{ij}]\Big\} + \sum_{n=1}^{\infty}\sum_{m=0}^{\infty} \frac{(-1)^n (n+m-1)! r_i^m}{(n-1)!(m-1)!m R_{ij}^{n+m}}$$

$$\Big\{ C_{nj}\cos[m\theta_i-(n+m)\psi_{ij}] - D_{nj}\sin[m\theta_i-(n+m)\psi_{ij}]\Big\}, \tag{B.60}$$

$$\phi_i(r_i,\theta_i) = \sum_{n=1}^{\infty} \Big\{ A_{ni} r_i^n \cos n\theta_i + B_{ni} r_i^n \sin n\theta_i + \frac{C_{ni}}{r_i^n}\cos n\theta_i$$

$$+ \frac{D_{ni}}{r_i^n}\sin n\theta_i \Big\}, \tag{B.61}$$

and where the summation with the asterisk indicates that it excludes $i = j$.

In the above, A_{nj}, B_{nj}, C_{nj} and D_{nj} are defined as:

$$A_{nj} = \sum_{j=1}^{k} \frac{\alpha_{nj\ell}}{R_j^{n-1}}\left(\frac{\partial u_\ell}{\partial t}\right) + \frac{a_{nj\ell}}{R_j^{n-1}}\left(\frac{\partial v_\ell}{\partial t}\right), \tag{B.62}$$

$$B_{nj} = \sum_{j=1}^{k} \frac{\beta_{nj\ell}}{R_j^{n-1}}\left(\frac{\partial u_\ell}{\partial t}\right) + \frac{b_{nj\ell}}{R_j^{n-1}}\left(\frac{\partial v_\ell}{\partial t}\right), \tag{B.63}$$

$$C_{nj} = \sum_{j=1}^{k} \gamma_{nj\ell} R_j^{n+1} \left(\frac{\partial u_\ell}{\partial t}\right) + c_{nj\ell} R_j^{n+1} \left(\frac{\partial v_\ell}{\partial t}\right), \qquad (B.64)$$

$$D_{nj} = \sum_{j=1}^{k} \delta_{nj\ell} R_j^{n+1} \left(\frac{\partial u_\ell}{\partial t}\right) + d_{nj\ell} R_j^{n+1} \left(\frac{\partial v_\ell}{\partial t}\right), \qquad (B.65)$$

where: $\frac{\partial u_\ell}{\partial t}$ = acceleration of cylinder ℓ in z direction,

$\frac{\partial v_\ell}{\partial t}$ = acceleration of cylinder ℓ in y direction.

Since we consider the pressure profile of the particular cylinder due to the oscillation of cylinder ℓ in one direction at each time, say the z direction, then the A_{nj}, B_{nj}, C_{nj} and D_{nj} become:

$$A_{nj} = \sum_{j=1}^{k} \frac{\alpha_{nj\ell}}{R_j^{n-1}} \left(\frac{\partial u_\ell}{\partial t}\right), \qquad (B.66)$$

$$B_{nj} = \sum_{j=1}^{k} \frac{\beta_{nj\ell}}{R_j^{n-1}} \left(\frac{\partial u_\ell}{\partial t}\right), \qquad (B.67)$$

$$C_{nj} = \sum_{j=1}^{k} \gamma_{nj\ell} R_j^{n+1} \left(\frac{\partial u_\ell}{\partial t}\right), \qquad (B.68)$$

$$D_{nj} = \sum_{j=1}^{k} \delta_{nj\ell} R_j^{n+1} \left(\frac{\partial u_\ell}{\partial t}\right). \qquad (B.69)$$

In the program, subroutine FIXUP2 only gives us γ, δ, c and d; however, α and β can be replaced by γ and δ through the relation (B.13) and (B.14)

Substituting equations (B.66-69) into (B.60) and (B.61), ϕ^i is determined. Then, by taking the required derivative of ϕ^i, P^i can be calculated.

Subroutine PRESS in this "COUPRESS" program carries out all the above calculation. It should be noted that the pressure distribution obtained from this subroutine is normalized by the product of the acceleration of moving cylinder ℓ and the density of fluid.

FLOWCHART OF THE ALGORITHM USED IN "COUPRESS"

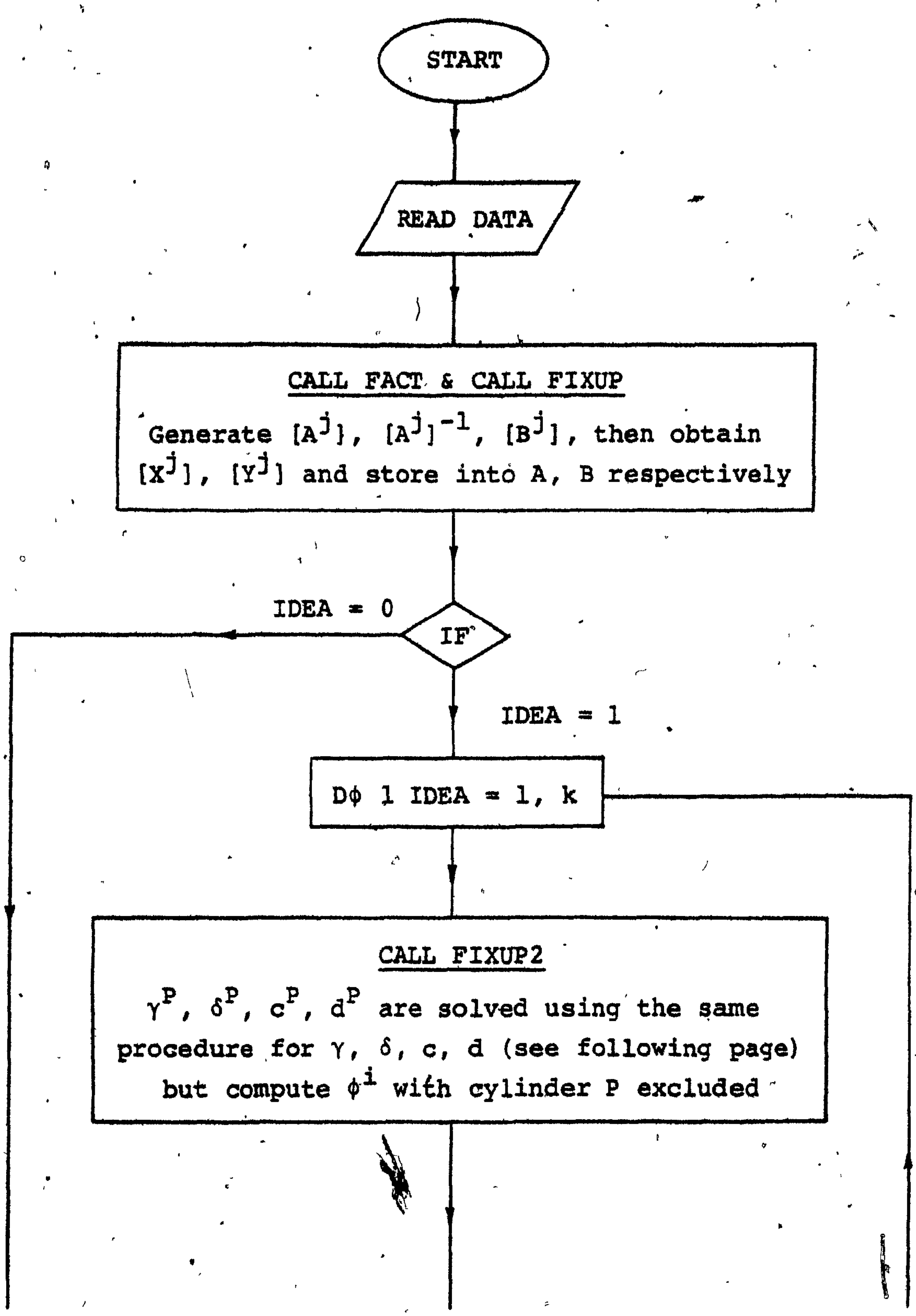

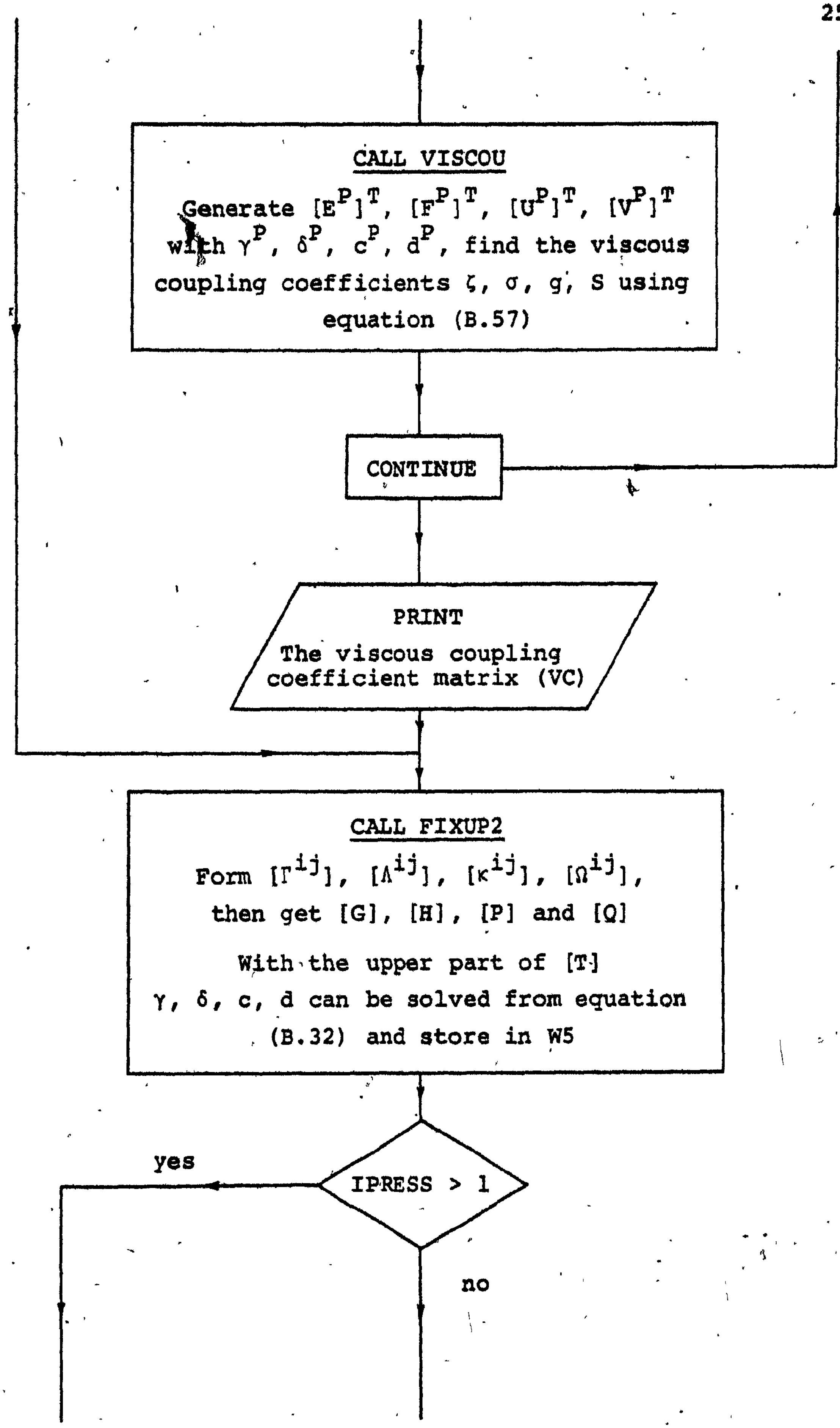
CALL VISCOU
Generate $[E^P]^T$, $[F^P]^T$, $[U^P]^T$, $[V^P]^T$ with γ^P, δ^P, c^P, d^P, find the viscous coupling coefficients ζ, σ, g, S using equation (B.57)
CONTINUE
PRINT
The viscous coupling coefficient matrix (VC)
CALL FIXUP2
Form $[\Gamma^{ij}]$, $[\Lambda^{ij}]$, $[\kappa^{ij}]$, $[\Omega^{ij}]$, then get [G], [H], [P] and [Q]
With the upper part of [T] γ, δ, c, d can be solved from equation (B.32) and store in W5
yes
IPRESS > 1
no

CALL PRESS

Use γ, δ, c, d to obtain ϕ^i, then evaluate the pressure from

$$p^i = -\rho \frac{\partial \phi^i}{\partial t}$$

PRINT

The pressure distribution around the surface of the cylinder

Dϕ 81

Calculate the added mass coefficients from the following equations

$$\varepsilon_{i\ell} = \delta_{i\ell} + 2\gamma_{1i\ell}$$
$$\xi_{i\ell} = 2\delta_{1i\ell}$$
$$e_{i\ell} = 2c_{1i\ell}$$
$$f_{i\ell} = \delta_{i\ell} + 2d_{1i\ell}$$

Then store in W5

Dϕ 83

Using equation (B.34-36) to calculate the added mass coefficients for the case of the boundary channel is free to move, then store in AM (includes W5)

B.21

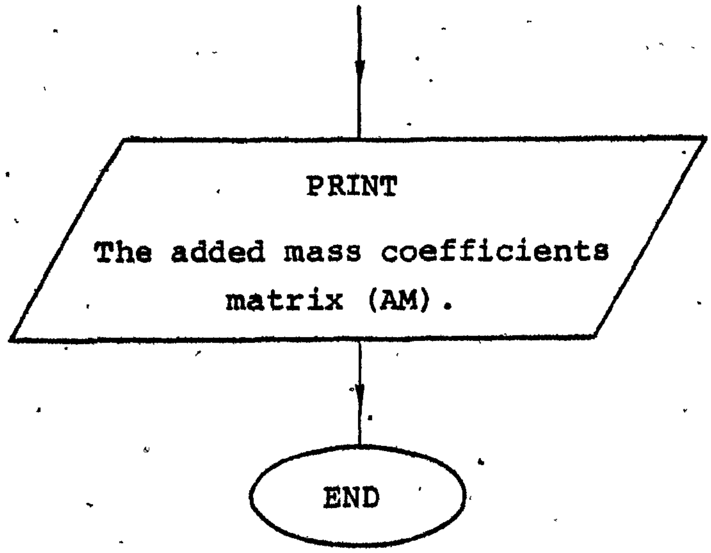

APPENDIX C.1

TYPICAL OUTPUT OF PROGRAM "COUPRESS"

K= 3 MM=15 CYLINDER AT CENTRE OF ARRAY 0 MP=11

THE MATRIX DEFINING CH(I,J) IN DEGREES

0.0	240.00000	300.00000
60.00000	0.0	360.00000
120.00000	180.00000	0.0

THE MATRIX DEFINING R(I,J)

0.0	2.87500	2.87500
2.87500	0.0	2.87500
2.87500	2.87500	0.0

I	R(I)	R(O,I)	CH(O,I) IN DEG
1	1.2500000	1.6598820	90.0000000
2	1.2500000	1.6598820	210.0000000
3	1.2500000	1.6598820	330.0000000

THE VISCOUS COUPLING MATRIX WITH ENCLOSING CYLINDER AT RO= 4.5

1.00000	0.14322	0.14322
0.13394	1.00000	-0.16774
0.13394	-0.16774	1.00000
0.0	-0.18942	0.18942
-0.16428	0.0	-0.02060
0.16428	0.02060	0.0

THE VISCOUS COUPLING MATRIX WITH ENCLOSING CYLINDER AT RO= 4.5

0.0	-0.15893	0.15893
-0.19478	0.0	0.00989
0.19478	-0.00989	0.0
1.00000	-0.07027	-0.07027
-0.06100	1.00000	0.24068
-0.06100	0.24068	1.00000

** THETA= 0.0 **

MOTION IN Z DIRECTION OF CYLINDER	(1)	(2)	(3)
PRESSURE ON CYLINDER (1)	-1.99188	-0.80581	-0.20377
PRESSURE ON CYLINDER (2)	0.00184	-2.45283	2.26799
PRESSURE ON CYLINDER (3)	-0.95569	-0.89627	-1.52397

MOTION IN Y DIRECTION OF CYLINDER	(1)	(2)	(3)
PRESSURE ON CYLINDER (1)	0.22883	-0.57874	-1.51106
PRESSURE ON CYLINDER (2)	1.71274	-0.09013	-0.08926
PRESSURE ON CYLINDER (3)	0.55973	0.03226	-0.23565

.   .   .   .

[Intermediate results for other values of THETA (increments of 9°) are not shown.]

.   .   .   .

** THETA=351.0 **

MOTION IN Z DIRECTION OF CYLINDER	(1)	(2)	(3)
PRESSURE ON CYLINDER (1)	-2.00549	-0.86692	-0.16477
PRESSURE ON CYLINDER (2)	0.00116	-2.35534	2.15852
PRESSURE ON CYLINDER (3)	-0.88422	-0.90445	-1.48707

MOTION IN Y DIRECTION OF CYLINDER	(1)	(2)	(3)
PRESSURE ON CYLINDER (1)	0.49432	-0.57311	-1.60835
PRESSURE ON CYLINDER (2)	1.52966	0.32325	0.28398
PRESSURE ON CYLINDER (3)	0.58687	0.10844	0.05845

THE MATRIX OF ADDED MASS COEFFICIENTS WITH THE ENCLOSING CYLINDER AT RO=   4.5

```
-0.16451D+01 0.26130D+00 0.19192D+00 0.19192D+00-0.16046D-14-0.29317D-15-0.40055D-01 0.40055D-0
 0.33865D+01-0.16351D+01-0.37567D+00-0.37567D+00 0.13142D-13 0.49106D-14 0.43313D+00-0.43313D+0
 0.24873D+01-0.37567D+00-0.15658D+01 0.45416D+00-0.51912D+00 0.52507D+00 0.40020D-01-0.45972D-0
 0.24873D+01-0.37567D+00 0.45416D+00-0.15658D+01 0.51912D+00-0.52507D+00 0.45972D-01-0.40020D-0
-0.13774D-14 0.72511D-15-0.40055D-01 0.40055D-01-0.16451D+01 0.16880D+00 0.23818D+00 0.23818D+0
 0.14780D-13-0.46962D-14 0.52507D+00-0.52507D+00 0.21876D+01-0.15427D+01 0.17755D+00 0.17755D+0
-0.51912D+00 0.43313D+00 0.40020D-01 0.45972D-01 0.30867D+01 0.17755D+00-0.16120D+01-0.65227D+0
 0.51912D+00-0.43313D+00-0.45972D-01-0.40020D-01 0.30867D+01 0.17755D+00-0.65227D+00-0.16120D+0
```

```
EPSILON(3,1) =      -0.37567
XSI(3,1) =      -0.43313
E(3,1) =      -0.52507
F(3,1) =       0.17755
```

APPENDIX C.2

TYPICAL OUTPUT OF PROGRAM "COUPRESS"

```
K= 2  MM=15  CYLINDER AT CENTRE OF ARRAY 0  MP=11


THE MATRIX DEFINING CH(I,J) IN DEGREES
   0.0           0.0
 180.00000       0.0


THE MATRIX DEFINING R(I,J)
   0.0           3.50000
   3.50000       0.0


             I         R(I)           R(0,I)          CH(0,I) IN DEG
             1       1.2500000      1.7500000     180.0000000
             2       1.2500000      1.7500000       0.0


         THE VISCOUS COUPLING MATRIX WITH ENCLOSING CYLINDER AT RO=        9.2


    1.00000     -0.11255
   -0.11255      1.00000
    0.0          0.0
    0.0          0.0


         THE VISCOUS COUPLING MATRIX WITH ENCLOSING CYLINDER AT RO=        9.2


    0.0          0.0
    0.0          0.0
    1.00000      0.14763
    0.14763      1.00000


         THE MATRIX OF ADDED MASS COEFFICIENTS WITH THE ENCLOSING CYLINDER AT RO=      9.2


-0.10680D+01 0.34007D-01 0.34007D-01 0.0          0.0          0.0
 0.18421D+01-0.10779D+01 0.23573D+00 0.0          0.0          0.0
 0.18421D+01 0.23573D+00-0.10779D+01 0.0          0.0          0.0
 0.0         0.0         0.0        -0.10890D+01 0.44488D-01 0.44488D-01
 0.0         0.0         0.0         0.24099D+01-0.10979D+01-0.31205D+00
 0.0         0.0         0.0         0.24099D+01-0.31205D+00-0.10979D+01


  EPSILON(2,1) =       0.23573
  XSI(2,1) =       0.0
  E(2,1) =      0.0
  F(2,1) =     -0.31205
```

APPENDIX C:3

TYPICAL OUTPUT OF PROGRAM "COUPRESS"

```
K= 2  MM=15  CYLINDER AT CENTRE OF ARRAY 0  MP=11

THE MATRIX DEFINING CH(I,J) IN DEGREES
   0.0            0.0
 180.00000        0.0


THE MATRIX DEFINING R(I,J)
   0.0            3.50000
   3.50000        0.0


        I        R(I)          R(0,I)          CH(0,I) IN DEG
        1      1.2500000     1.7500000     180.0000000
        2      1.2500000     1.7500000       0.0


     THE VISCOUS COUPLING MATRIX WITH ENCLOSING CYLINDER AT RO=   10000.0

   1.00000      -0.12755
  -0.12755       1.00000
   0.0           0.0
   0.0           0.0


     THE VISCOUS COUPLING MATRIX WITH ENCLOSING CYLINDER AT RO=   10000.0

   0.0           0.0
   0.0           0.0
   1.00000       0.12755
   0.12755       1.00000


     THE MATRIX OF ADDED MASS COEFFICIENTS WITH THE ENCLOSING CYLINDER AT RO=   10000.0

[illegible]10000D+01 0.27833D-07 0.27833D-07 0.0         0.0         0.0
[illegible]17813D+01-0.10441D+01 0.26282D+00 0.0         0.0         0.0
0.17813D+01 0.26282D+00-0.10441D+01 0.0         0.0         0.0
0.0         0.0         0.0        -0.10000D+01 0.36046D-07 0.36046D-07
0.0         0.0         0.0         0.23069D+01-0.10441D+01-0.26282D+00
0.0         0.0         0.0         0.23069D+01-0.26282D+00-0.10441D+01

 EPSILON(2,1) =       0.26282
 XSI(2,1) =        0.0
 E(2,1) =        0.0
 F(2,1) =       -0.26282
```

APPENDIX C.4

TYPICAL OUTPUT OF PROGRAM "EXPAMC"

DERIVATION OF THE VIRTUAL MASS COEFFICIENTS FROM EXPERIMENTAL DATA

FREQUENCY = 100.00 HZ
ACCEL.(Z DIRECTION) = 2.0858 G

PRESSURES MEASURED AT PEAK ACCELERATION

ANGLE	PRESSURE	PHASE DIFFERENCE
0	0.0763 PSI	-1.0
9	0.0933 PSI	-1.6
18	0.1146 PSI	-2.3
27	0.1371 PSI	-2.3
36	0.1524 PSI	-2.4
45	0.1612 PSI	-2.5
54	0.1601 PSI	-2.4
63	0.1524 PSI	-2.2
72	0.1425 PSI	-2.7
81	0.1311 PSI	-2.2
90	0.1152 PSI	-1.9
99	0.0971 PSI	-1.7
108	0.0856 PSI	-1.7
117	0.0752 PSI	-1.5
126	0.0669 PSI	-1.5
135	0.0592 PSI	-1.8
144	0.0532 PSI	-2.0
153	0.0499 PSI	-2.1
162	0.0455 PSI	-2.2
171	0.0422 PSI	-2.6
180	0.0395 PSI	-2.7
189	0.0367 PSI	-3.0
198	0.0351 PSI	-3.6
207	0.0334 PSI	-4.1
216	0.0317 PSI	-5.0
225	0.0306 PSI	-5.0
234	0.0295 PSI	-5.6
243	0.0278 PSI	-5.9
252	0.0268 PSI	-5.6
261	0.0274 PSI	-2.5
270	0.0262 PSI	-6.0
279	0.0280 PSI	-2.1
288	0.0274 PSI	-4.2
297	0.0285 PSI	-3.9
306	0.0307 PSI	-1.0
315	0.0329 PSI	-2.2
324	0.0368 PSI	-1.0
333	0.0417 PSI	-1.0
342	0.0494 PSI	-1.0
351	0.0592 PSI	-1.8

FORCE IN Z DIRECTION = -0.217996
FORCE IN Y DIRECTION = 0.101399

COEFFICIENT IN Z DIRECTION = -0.589895
COEFFICIENT IN Y DIRECTION = 0.274385